

Static and Dynamical Quantum Correlations
of Ultracold Bosonic Mixtures

Dissertation

zur Erlangung des Doktorgrades
an der Fakultät für Mathematik,
Informatik und Naturwissenschaften
der Universität Hamburg,
Fachbereich Physik

vorgelegt von

Kevin Keiler

geboren am 27. Dezember 1991 in Lüneburg

Hamburg

2021

Gutachter der Dissertation:

Prof. Dr. Peter Schmelcher
Prof. Dr. Michael Potthoff

Zusammensetzung der Prüfungskommission:

Prof. Dr. Daniela Pfannkuche
Prof. Dr. Peter Schmelcher
Prof. Dr. Michael Potthoff
Prof. Dr. Andreas Hemmerich
Dr. Thore Posske

Vorsitzende der Prüfungskommission:

Prof. Dr. Daniela Pfannkuche

Datum der Disputation:

25.10.2021

Vorsitzender des Fach-Promotionsausschusses PHYSIK:

Prof. Dr. Wolfgang Hansen

Leiter des Fachbereichs PHYSIK:

Prof. Dr. Günter H. W. Sigl

Dekan der Fakultät MIN:

Prof. Dr. Heinrich Graener

*Das schönste Glück des denkenden Menschen ist,
das Erforschliche erforscht zu haben
und das Unerforschliche ruhig zu verehren.*

Johann Wolfgang von Goethe

To my parents who taught me diligence

And to Janina who taught me to see beauty everywhere

Abstract

This cumulative dissertation deals with the stationary and dynamical properties of highly particle imbalanced atomic mixtures of bosons trapped in various one-dimensional confining potentials. The ground state properties are studied under variation of the system parameters, while a strong focus is given to the relation of the many-body wave function characteristics to the emerging correlations in the system. After preparing the system in its ground state the non-equilibrium dynamics are initiated by performing a quench of a parameter of the associated Hamiltonian. In order to obtain the ground state and to track the dynamical response of the system we employ the ab-initio Multi-Layer Multi-Configuration Time-Dependent Hartree method for atomic mixtures (ML-MCTDHX).

The first four works are dedicated to the investigation of lattice-trapped impurities and the impact of their coupling to a majority species. Varying the interspecies interaction strength and the lattice depth it is shown that the impurities tend to cluster in a single lattice site for large repulsive interspecies couplings. We attribute this to the emergence of an attractive induced interaction among the impurities due to the repulsive interaction with the majority species. In the second work, including the possible variation of the repulsive contact intraspecies interaction between the impurities we identify further localization configurations of the impurities, comprising e.g. a pairwise accumulation in adjacent sites. The selection of the boundary conditions represents an additional control parameter for manipulating the degeneracies of the many-body ground state. We then turn to the dynamical response of such engineered ground states in the third work, in particular focusing on a state featuring a pairwise accumulation of impurities in adjacent sites. Initializing the system in the latter way, the interspecies interaction strength is suddenly reduced in order to induce a tunneling of the impurity species. We observe tunneling of a single impurity out of the cluster to the adjacent site for a finite post-quench interaction strength. This impurity can be further transported to the next-neighboring site for even smaller post-quench coupling strengths, while for a quench to zero interaction the impurities remain localized in their initial configuration, being reminiscent of repulsively bound pairs. In the last of those works also the majority species is subject to a lattice potential, leading to the formation of a particle-hole pair for large coupling strengths, with the majority species atoms exhibiting a Mott insulator-like state. Quenching the interspecies coupling strength the particle-hole pair can be transported to the opposite outermost well. Its stability strongly depends on the post-quench interspecies interaction strength, requiring it also to be finite for a stable transport.

The next two publications deal with the collisional dynamics of impurities with a majority species which is trapped in a lattice geometry. The system is prepared in its ground state for a finite interspecies coupling strength, while the dynamics is initiated differently in each case. Starting with impurities trapped in a double well the tunneling dynamics is initiated by quenching the tilt of the double well. Due to the other species being trapped in a lattice geometry, the impurities experience an effective potential being formed by the double well and the material barrier comprised of the density maxima of the lattice-trapped species. For increasing repulsive coupling strengths it is shown that the material barrier tunneling to the opposite site of the double well can be delayed in time, while very large couplings even completely prohibit the transport to the other well. In the other work the impurities are initialized in a displaced harmonic oscillator and are forced to collide with a medium trapped in a double well by quenching the center of the harmonic confinement to the center of the double well. Varying the interspecies coupling strength from strongly attractive to strongly repulsive a multitude of dynamical response regimes can be recovered. On the attractive branch these include a strong binding of the impurities to the density of the medium and an effective tunneling of the impurity

between the density maxima of the host. For weak attractive and weak repulsive couplings a dissipative oscillatory motion of the impurity species takes place. In the case of intermediate and strong repulsive interactions the impurity species is pinned in the center of the double well and completely reflected from one of the density maxima of the medium, respectively. In both works the underlying microscopic processes can be uncovered by employing a time-averaged effective potential.

In our final work we go a significant step beyond the previous scenarios by introducing a third bosonic species into the system. Specifically, we investigate the polaronic properties of impurities immersed in a cumulative bath comprised of two hosts. Allowing for the impurities to couple either attractively or repulsively to the individual components it is possible to flexibly control the impurity residue and thereby also the polaronic character. As such the quasiparticle character can be maintained for larger interactions in case the impurity couples attractively to one medium and repulsively to the other one. In the case of two impurities the formation of a bipolaron is captured for sufficiently attractive couplings to one of the hosts. For strongly repulsive couplings to one of the hosts the impurity forms a shell structure whose width can be controlled by the interaction to the other medium.

Zusammenfassung

Diese kumulative Dissertation behandelt die stationären und dynamischen Eigenschaften von atomaren bosonischen Mixturen mit starkem Ungleichgewicht bezüglich der Teilchenzahl, welche in verschiedenen eindimensionalen Potentialen gefangen sind. Die Grundzustandseigenschaften werden unter Variation der Systemparameter studiert, wobei ein besonderer Fokus auf dem Verhältnis zwischen der Charakteristik der Vielteilchenwellenfunktion und den auftretenden Korrelationen liegt. Die Nichtgleichgewichtsdynamik wird initiiert, indem man das System im Grundzustand präpariert und anschließend einen Quench der Parameter des Hamiltonians durchführt. Zur Berechnung des Grundzustands und der Nachverfolgung der Dynamik verwenden wir die ab-initio Multi-Layer Multi-Configuration Time-Dependent Hartree Methode für atomare Mixturen (ML-MCTDHF).

Die ersten vier Arbeiten widmen sich dem Einfluss der Kopplung einer gittergefangenen Fremdteilchenspezies an eine bezüglich der Teilchenzahl größere Spezies auf die Verteilung der Fremdteilchen. Variiert man die Interspezieswechselwirkungsstärke sowie die Gittertiefe, lässt sich zeigen, dass die Fremdteilchen für große repulsive Interspezieskopplungen dazu tendieren sich in einem einzigen Gitterplatz anzuhäufen. Dies kann dem Auftreten einer attraktiven induzierten Wechselwirkung durch die repulsive Kopplung an die andere Spezies zugeschrieben werden. Durch Hinzufügen einer repulsiven Kontaktwechselwirkung zwischen den Fremdteilchen in der zweiten Arbeit identifizieren wir weitere Lokalisierungskonfigurationen der Fremdteilchen, zum Beispiel in der Form von paarweiser benachbarter Lokalisierung. Mit der möglichen Variation der Randbedingungen führen wir einen weiteren Kontrollparameter für die Manipulation der Entartung des Grundzustands ein. Anschließend befassen wir uns in der dritten Arbeit mit der dynamischen Antwort solcher arrangierter Grundzustände, wobei wir uns insbesondere auf solche fokussieren, die eine paarweise benachbarte Lokalisierung der Fremdteilchen aufweisen. Nachdem das System in einer solchen Konfiguration präpariert wurde, wird die Interspezieswechselwirkungsstärke plötzlich reduziert, um ein Tunneln der Fremdteilchen zu induzieren. Wir beobachten das Tunneln eines einzelnen Fremdteilchens aus dem Cluster zu dem nächstliegenden Gitterplatz für finite Post-Quench-Wechselwirkungsstärken. Dieses Fremdteilchen lässt sich für noch geringere Post-Quench-Wechselwirkungsstärken zum übernächsten Gitterplatz transportieren, wobei ein Quench zu einem nichtwechselwirkenden System dazu führt, dass die Fremdteilchen in ihrer initialen Konfiguration verbleiben, was repulsiv gebundenen Paaren ähnelt. In der letzten dieser Arbeiten ist auch die bezüglich der Teilchenzahl größere Spezies im Gitter gefangen, was bei starken repulsiven Kopplungen zur Entstehung von Teilchen-Loch-Paaren und einem Mott-Isolator ähnlichen Zustand für die letztere Spezies führt. Durch einen Quench der Interspezieswechselwirkungsstärke lässt sich das Teilchen-Loch-Paar zum gegenüberliegenden äußersten Gitterplatz transportieren. Die Stabilität des Paares hängt stark von der Post-Quench-Wechselwirkungsstärke ab, wobei es essentiell ist, dass diese endlich und nicht zu gering ist, um einen stabilen Transport zu garantieren.

Die beiden nächsten Publikationen behandeln die Kollisionsdynamik von Fremdteilchen mit einer bezüglich der Teilchenzahl größeren Spezies, welche in einem Gitter gefangen ist. Das System wird für finite repulsive Interspezieswechselwirkungsstärken im Grundzustand präpariert, während die Dynamik in jedem der Fälle unterschiedlich initiiert wird. Angefangen mit Fremdteilchen, die in einem Doppelpotential gefangen sind, wird die Tunneldynamik durch einen Quench der Neigung des Doppelpotentials generiert. Da die andere Spezies in einem Gitter gefangen ist, erfahren die Fremdteilchen nicht nur das Doppelpotential, sondern auch ein effektives Potential durch die Materialbarrieren in Form der Dichtemaxima der gittergefangenen Spezies. Für steigende repulsive Kopplungsstärken wird gezeigt, dass das Materialbarriere-Tunneln

zur gegenüberliegenden Seite des Doppeltopfs verzögert werden kann, bis hin zur vollständigen Unterdrückung des Tunnelns. In der anderen Arbeit werden die Fremdteilchen in einem verschobenen harmonischen Oszillator initialisiert und durch einen Quench der Verschiebung des Oszillators zum Zentrum des Doppeltopfs, in dem die andere Spezies gefangen ist, zur Kollision mit letzterer gezwungen. Unter Variation der Interspezieswechselwirkungsstärke von stark attraktiv zu stark repulsiv lässt sich eine Vielzahl von dynamischen Regimen realisieren. Auf dem attraktiven Ast beinhaltet das die starke Bindung der Fremdteilchen an die Dichte des Mediums sowie ein effektives Tunneln der Fremdteilchen zwischen den Dichtemaxima der anderen Spezies. Für schwache attraktive und schwache repulsive Wechselwirkungen findet eine dissipative, oszillatorische Bewegung der Fremdteilchen statt. Für mittlere und starke repulsive Kopplungen wird die Fremdteilchenspezies im Zentrum des Doppeltopfs gefangen bzw. komplett an dem Dichtemaximum des Mediums reflektiert. In beiden Arbeiten können die zugrundeliegenden mikroskopischen Prozesse mit Hilfe eines zeitlich gemittelten, effektiven Potentials beschrieben werden.

In unserer letzten Arbeit gehen wir verglichen mit den bisherigen Arbeiten einen bedeutenden Schritt weiter, indem wir eine dritte bosonische Spezies in das System einführen. Speziell untersuchen wir die polaronischen Eigenschaften von Fremdteilchen, die in ein kumulatives Medium, bestehend aus zwei Komponenten, eingebettet sind. Indem man den Fremdteilchen erlaubt jeweils attraktiv und repulsiv an die unterschiedlichen Komponenten zu koppeln, ist es möglich das Fremdteilchen-Residuum und damit den polaronischen Charakter flexibel zu kontrollieren. In diesem Sinne kann der Quasiteilchen-Charakter für größere Wechselwirkungsstärken aufrecht erhalten werden, falls das Fremdteilchen attraktiv an ein Medium und repulsiv an das andere koppelt. Im Falle von zwei Fremdteilchen lässt sich ein Bipolaron für genügend große attraktive Wechselwirkungen zu einer der Spezies identifizieren. Für starke repulsive Kopplungen an eines der Medien bildet das Fremdteilchen eine Schalenstruktur der Dichte, deren Breite durch die Wechselwirkung mit der anderen Spezies manipuliert werden kann.

Contents

Preface	1
1 Introduction	5
1.1 Atoms trapped in optical lattices	9
1.2 The Gross-Pitaevskii equation and mean-field approximations	11
1.3 Including correlations beyond the mean-field approximation	13
1.4 Methodological approach: ML-MCTDHX	14
1.4.1 Wave function ansatz for mixtures	14
1.4.2 Convergence and approximate limiting cases	15
1.5 Effective potentials and number state analysis	17
2 Outline of the scientific contributions	19
2.1 Lattice trapped impurities immersed in a Bose gas	19
2.2 Collisional dynamics of impurities with a lattice trapped bath	25
2.3 Highly imbalanced triple mixtures	28
3 Scientific contributions	31
3.1 Correlation induced localization of lattice trapped bosons coupled to a Bose-Einstein condensate	33
3.2 State engineering of impurities in a lattice by coupling to a Bose gas	47
3.3 Interaction-induced single-impurity tunneling in a binary mixture of trapped ultracold bosons	61
3.4 Doping a lattice-trapped bosonic species with impurities: from ground state properties to correlated tunneling dynamics	75
3.5 Entanglement-assisted tunneling dynamics of impurities in a double well immersed in a bath of lattice trapped bosons	95
3.6 Many-body collisional dynamics of impurities injected into a double-well trapped Bose-Einstein condensate	117
3.7 Polarons and their induced interactions in highly imbalanced triple mixtures	135
4 Conclusions and Outlook	147
Bibliography	153

Danksagungen	175
Eidesstattliche Versicherung	177

Preface

This cumulative dissertation is based on the following sequence of publications, which throughout the thesis will be referenced with double brackets [[.]].

List of publications this cumulative dissertation is based on:

- [[1]] K. Keiler, S. Krönke and P. Schmelcher, Correlation induced localization of lattice trapped bosons coupled to a Bose–Einstein condensate, *New J. Phys.* **20**, 033030 (2018).
- [[2]] K. Keiler and P. Schmelcher, State engineering of impurities in a lattice by coupling to a Bose gas, *New J. Phys.* **20**, 103042 (2018).
- [[3]] K. Keiler and P. Schmelcher, Interaction-induced single impurity tunneling in a binary mixture of trapped ultracold bosons, *Phys. Rev. A* **100**, 043616 (2019).
- [[4]] K. Keiler, S. I. Mistakidis and P. Schmelcher, Doping a lattice-trapped bosonic species with impurities: From ground state properties to correlated tunneling dynamics, *New J. Phys.* **22**, 083003 (2020).
- [[5]] F. Theel, K. Keiler, S. I. Mistakidis and P. Schmelcher, Entanglement-assisted tunneling dynamics of impurities in a double well immersed in a bath of lattice trapped bosons, *New J. Phys.* **22**, 023027 (2020).
- [[6]] F. Theel, K. Keiler, S. I. Mistakidis and P. Schmelcher, Many-body collisional dynamics of impurities injected into a double-well trapped Bose-Einstein condensate, *Phys. Rev. Research* **3**, 023068 (2021).
- [[7]] K. Keiler, S. I. Mistakidis and P. Schmelcher, Polarons and their induced interactions in highly imbalanced triple mixtures, [arXiv:2012.04034 \[cond-mat.quant-gas\]](https://arxiv.org/abs/2012.04034) (2020).
Status: Submitted to *Phys. Rev. Lett.*, currently under review.

Further publications:

- [[8]] F. Köhler, K. Keiler, S. I. Mistakidis, H.-D. Meyer and P. Schmelcher, Dynamical Pruning of the Non-Equilibrium Quantum Dynamics of Trapped Ultracold Bosons, *J. Chem. Phys.* **151**, 054108 (2019).
- [[9]] F. Hummel, K. Keiler and P. Schmelcher, Electric field-induced wave-packet dynamics and geometrical rearrangement of Trilobite molecules, *Phys. Rev. A* **103**, 022827 (2021).
- [[10]] J. Chen, K. Keiler, G. Xianlong and P. Schmelcher, Impurity induced quantum chaos for an ultracold bosonic ensemble in a double-well, [arXiv:2101.11209 \[cond-mat.quant-gas\]](https://arxiv.org/abs/2101.11209) (2020).
Status: Submitted to *Phys. Rev. A*, currently under review.
- [[11]] M. Pyzh, K. Keiler, S. I. Mistakidis and P. Schmelcher, Entangling lattice-trapped bosons with a free impurity: impact on stationary and dynamical properties, *Entropy* **23**, 290 (2021).

Outline

In Chapter 1 we provide an introduction to the field of ultracold atoms with a special emphasis on highly particle imbalanced mixtures. Since most of the publications on which this cumulative dissertation is based on deal with bosonic atoms confined in lattice geometries we further elaborate on the physics of lattice trapped atoms. Moreover, we introduce the notion of particle correlations and thereby motivate the numerical method that has been employed in all works. Finally, we comment on the key quantities that were utilized in order to extract information from the high-dimensional many-body wave function. An outline of the scientific contributions followed by the publications themselves is given in Chapter 2 and Chapter 3. In Chapter 4 we conclude with a discussion of the presented results and motivate potential future research directions.

Declaration of the personal contributions to the publications [[1-7]]

The research projects [[1-3]] were conducted entirely by myself, while project [[1]] was partially supervised by Dr. Sven Krönke in my previous Master thesis. I have performed all necessary numerical simulations and data analysis, provided appropriate physical interpretations as well as conceptualized and written the corresponding manuscripts. Concerning [[4]], Dr. Simeon I. Mistakidis invoked the project and together we worked out the concept. The corresponding numerical simulations, data analysis as well as interpretation of the results were carried out by myself. The manuscript was mainly written by myself, while Dr. Simeon I. Mistakidis significantly contributed to the presentation of the results.

Publications [[5,6]] have emerged from the Master thesis of M.Sc. Friethjof Theel, who has been supervised by myself to a large extent and also by Dr. Simeon I. Mistakidis. M.Sc. Friethjof Theel and me discussed the physical interpretation of the results and the technical issues almost on a daily basis. In [[5]], together with Dr. Simeon I. Mistakidis I have developed the concept of the work as well as the research strategy. M.Sc. Friethjof Theel carried out all simulations by himself, while most of the tools and ideas for the data analysis were worked out by myself. The manuscript was mainly written by M.Sc. Friethjof Theel and myself, while Dr. Simeon I. Mistakidis was involved in the optimization of the presentation of the results. Also project [[6]] was conceptualized by Dr. Simeon I. Mistakidis and me, while M.Sc. Friethjof Theel performed all the numerical simulations. I contributed greatly to the interpretation of the results and provided additional analysis tools which were not used in [[5]]. The manuscript was mainly written by M.Sc. Friethjof Theel, while Dr. Simeon I. Mistakidis and me were responsible for the optimization of the presentation of the results.

The research idea and strategy in project [[7]] emerged from discussions with Dr. Simeon I. Mistakidis. The extension to triple mixtures in [[7]] involved a change in the input files for the code as well as in the data analysis tools which were already written by myself. All of this was carried out by myself including also the extensive numerical simulations and interpretation of the results. Dr. Simeon I. Mistakidis provided valuable knowledge regarding the polaron problem and helped with the presentation of the results, while the whole manuscript was conceptualized and written by myself. The progress of all projects was discussed with Prof. Dr. Peter Schmelcher on a regular basis.

List of abbreviations and symbols

ML-MCTDHX	Multi-Layer Multi-Configuration Time-Dependent Hartree method for atomic mixtures
$g_{\sigma\sigma}$	intraspecies interaction strength among particles of species σ
$g_{\sigma\sigma'}$	interspecies interaction strength between particles of species σ and σ'
V_0	depth of the lattice potential
N_σ	number of particles of species σ
$\rho_\sigma^{(1)}(x)$	one-body density of species σ
$\rho_\sigma^{(2)}(x_1, x_2)$	two-body density of species σ

Introduction

Inspired by a work of Bose [1], Einstein's realization that at sufficiently low temperatures an ideal gas of massive particles exhibits a matter wave behavior set the stage for the famous Bose-Einstein condensation [2, 3], where all particles occupy the same single-particle state. While having been a theoretically predicted state of matter, the physics of ultracold gases [4–6] has experienced a boost with the first experimental implementation of a Bose-Einstein condensate. Due to the tremendous effort that has been conducted on building new laser systems as well as trapping techniques relying on magnetic fields, experimentalists were able to cool down gases of neutral atoms to very low temperatures. Thus, Bose-Einstein condensation could be observed for the first time in the group of Cornell and Wieman with repulsively interacting rubidium atoms [7], while in the group of Ketterle sodium atoms have been utilized [8]. For that spectacular achievement they have been awarded the Nobel prize in physics in 2001. These experiments can be considered as the dawn of the new era of the third quantum revolution [9]. Nowadays, ultracold systems stand out due to their high degree of controllability and are therefore at the frontier of modern quantum physics. Apart from trapping ultracold atoms in potentials of different dimensionality, ranging from three-dimensional to one-dimensional, it is possible to engineer essentially arbitrary potential landscapes [10], which can be even time-dependent [11]. Moreover, the scattering length of the short-range interaction among the atoms can be manipulated with the aid of magnetic or optical Feshbach resonances [12–16], by applying a bias magnetic field or a laser beam, respectively. As such the strength and the sign of the interaction can be steered in a very precise manner. Therefore, ultracold atoms can be exploited as quantum simulators of microscopic phenomena that treat simplified models, thereby permitting the study of quantum systems which cannot be solved even by supercomputers [17]. In this sense, they are ideal to systematically study many-body quantum systems and the plethora of quantum phenomena they exhibit, finding also application in newly emerging fields such as atomtronics [18–32].

In this context, the possibility to generate setups of atoms trapped in optical lattices has sparked a lot of interest in the recent years [33, 34]. Such systems are considered as simple realizations for emulating complex condensed matter models. From the theoretical side the prototype model to unravel the dynamical and static properties of lattice trapped atoms is given by the Hubbard model [35–37]. In its simplest version it consists of a next-neighbor hopping between discrete lattice sites and an on-site interaction term. Closely related to the Hubbard model is the Bose-Hubbard model [38] which was found to exhibit two distinct phases, the Mott insulating one and the superfluid phase. Consequently, it allowed for a description of

the superfluid-insulator transition in a simplified way. The seminal proposal for a superfluid-Mott insulator transition employing ultracold atoms in an optical lattice by Jaksch *et al.* [39], followed by its experimental observation in the Bloch-Hänsch group [40], finally placed ultracold atoms in the regime of strongly correlated systems. Since then this transition has been observed also in disordered Bose systems [41, 42], Bose-Bose [43] and Bose-Fermi [44, 45] mixtures. Moreover, various other phases were studied, among them being Mott insulators of reduced dimensionality [46, 47], fermionic Mott insulators [48, 49], the Tonks-Girardeau gas [50, 51], Mott insulator states of molecules, unconventional superfluids [52–56] and paired fermions [57–60] as well as repulsively bound pairs of bosons [61]. Even though the Bose-Hubbard model is a widely used platform for studying bosonic atoms in a lattice, one should note that it relies on the restriction that the dominant processes happen in the lowest band, while the interaction is of on-site character. However, in experiments processes which lie beyond these restrictions may play an important role, giving rise to extended Bose-Hubbard models [62, 63]. These incorporate for example next-neighbor and next-nearest-neighbor interaction or hopping and interaction channels via excited bands, leading to the formation of novel complex structures, such as charge-density-waves [64–70], supersolids [71–73] and dimerized insulators [74–78].

While the idea of ultracold atoms in optical lattices was inspired by the notion of preparing quantum simulators, the accompanying rapid progress in the field of ultracold gases in general led to a strong interest in few-body ultracold systems. These systems build a bridge between single-particle problems and many-body physics, since they cannot be described in terms of reduced degrees of freedom nor can they be treated within quantum statistical approaches. In the recent years it has become experimentally possible to prepare interacting few-particle systems with a well-defined number of particles [79–81]. Due to the possible three-body recombination associated with bosons, sophisticated tools relying on the loading of bosons in optical lattice structures are needed in order to prepare few-boson systems [82–85]. For few-fermion systems it has been shown in a series of experiments that the number of particles, the interaction strength as well as the shape of the external potential could be systematically manipulated [86–91].

So far we have focused on single-component ultracold gases which already offer a very rich phenomenology. However, the situation becomes even more involved when introducing an additional species. Experimentally two-component Bose mixtures [92–94] can be prepared by considering two hyperfine states of ^{87}Rb , two isotopes such as ^{87}Rb and ^{85}Rb or two different chemical elements in order to achieve a significant mass imbalance. Such setups offer a lot of diversity in terms of the interaction among the particles as one adds to the already present intraspecies interaction in the respective subsystem an additional interspecies interaction in order to entangle the species. New phenomena have been observed such as composite fermionization [95], full fermionization [96–98], phase separation [99–102] and coarse graining effects [103, 104], while known concepts like the Tonks-Girardeau limit and miscible Bose-Einstein condensates can also be recovered. In this context, in particular correlation properties [105–109] have been the focus of many studies uncovering among others quantum droplets [110–113], spin-charge separation [114], paired and counterflow superfluidity [107, 108] as well as the quench dynamics across the miscible-immiscible phase transition [115–117].

In particular, particle imbalanced mixtures have received substantial attention recently [118–121]. Taking this to the extreme, one considers a few impurities immersed in a many-body medium, giving rise to the formation of quasiparticles due to the dressing of the impurities by the medium excitations as a result of the intercomponent interaction. These have led to fundamentally novel insights into the concept of Fermi and Bose polarons [121–125]. As such highly particle imbalanced mixtures serve as a quantum simulator of the corresponding condensed matter setup, e.g. in semiconducting [126] and superconducting devices [127], while

interactions among quasiparticles in liquid Helium mixtures [128] and cuprates [129, 130] are considered to be promising candidates for conventional and high- T_c superconductivity [131–135]. The experimental realization [118–120, 136–140] of these impurity systems has triggered many theoretical investigations [141–157] with respect to the stationary properties of polaronic systems [158–160], unraveling their effective mass [124, 161, 162], excitation spectra [163, 164] and in the case of many impurities their induced interaction [165–167]. Less focus has been placed on the corresponding nonequilibrium dynamics, such as the collisional dynamics [168–173] of impurities with the medium, transport in optical lattices [174–182] and relaxation processes [183–186], which is partially due to the potential formation of strong correlations during the propagation. The notion of impurities immersed in a bath has recently been extended to coherently coupled two-component Bose-Einstein condensates [187, 188] and Bose-Bose mixtures acting as a medium [189], while in lattice setups holes are introduced in a spinor fermionic background [190, 191]. In [[7]] we provide the first detailed study on how a second species in the bath affects the polaronic properties incorporating all necessary correlations in the system, thereby taking the actively studied polaron problem to the next level.

Often for the multi-component mixture the same underlying trapping geometry is assumed. However, one expects qualitatively different phenomena in the case of unequal trapping potentials. For this purpose, experimentally one would use the so-called tune-out wave length in order to create species-dependent potentials [192, 193]. As a result one of the two species experiences a vanishing light shift, while the other one will be trapped in a specific potential landscape due to the non-vanishing light shift. As such it is possible to trap one species in a lattice geometry which interacts with the other species, forming the environment, which in turn does not experience this potential. It has been shown that such a setup can be exploited in order to cool the lattice trapped atoms to very low temperatures [194–196]. Usually, the coupling to an environment leads to a loss of coherence due to dissipation. However, it can also be exploited for the preparation of many-body states by quantum-reservoir engineering [197–199]. Moreover, immersing lattice-trapped impurities into a Bose gas allows for a systematic introduction of phonons to the lattice subsystem due to the coupling to the Bose gas. As a result of the lattice atoms being dressed by the phonons an attractive induced interaction between the lattice trapped atoms emerges. In this context, utilizing a quantum master equation approach dephasing and clustering processes as well as impurity transport were observed [177, 182, 200, 201]. This notion of an induced interaction has been also identified in the context of finite-size systems in [[1-4]] and used to engineer specific system properties with a focus on the role of inter- and intraspecies correlations. By taking explicitly advantage of the coupling to an environment, in particular, it is possible to steer the distribution of impurities in a lattice geometry. Here, the majority species serves as an environment that introduces an additional control parameter via the interspecies coupling, while also experiencing a feedback from the impurities. It is this property of a mutual imprint of information between the species which can be exploited to systematically design many-body wave functions and additionally introduce correlations into the system.

This feature can also be exploited in the context of the collisional dynamics of impurities immersed in a medium where the nature of the underlying trapping potential plays a significant role. This involves for example homogeneous setups [173, 202, 203], harmonic potentials [184, 204, 205] as well as lattice confinements [179, 181, 206–209]. Most of these studies were directed towards the investigation of systems where both species are trapped in the same optical potential. In this sense, it is to be expected that trapping the species in different potentials has a strong impact on the observed dynamical response. Let us consider the case of a lattice trapped majority species which serves as a medium for impurities trapped in a different geome-

try. Due to the interspecies coupling the impurities experience an effective potential generated by the density distribution of the other species on top of their trapping potential. Such an effective potential is in strong contrast to a static confining potential, as it allows for a variation in the course of the dynamics. In this sense, it adapts to the motion of the impurities and thus allows for specific engineered transport properties. In [[5]] we have shown that a bath of lattice trapped bosons acts as multiple material barriers in the context of the tunneling dynamics of an impurity trapped in a double well. Moreover, we have uncovered the necessity of interspecies entanglement for the dynamics of the impurities. In [[6]] the impact of a lattice-trapped bath on the collisional dynamics of impurities has been studied. The study of the collisional dynamics of impurities with a Bose-Einstein condensate has been the focus of experiments [121, 210, 211] and already theoretically revealed within a mean-field approach, the total reflection of the impurities at the condensate, their trapping within the medium and the appearance of dark and bright solitons [168]. Such a setup may allow for scattering processes which are a result of impurity-medium correlations and therefore go beyond the mean-field collision channels. In [[6]] taking into account intra- and interspecies correlations we were able to uncover a multitude of dynamical response regimes depending on the interspecies coupling strength, namely the steady bound state regime, the tunneling region, the dissipative oscillation motion, the pinning and the total reflection regime.

Objectives of this thesis

In this cumulative dissertation we theoretically study the stationary and dynamical formation of correlations within interacting ultracold bosonic mixtures trapped in one-dimensional geometries. We focus on the case of particle imbalanced setups at zero temperature with short-range interaction and trapped in various potential landscapes. Specifically, we demonstrate

- (i) how the stationary and dynamical density distribution of impurities trapped in a lattice can be engineered by coupling to a bosonic medium which is not subject to the lattice potential [[1-3]].
- (ii) the formation of particle-hole pairs in lattice trapped few-body mixtures and their dynamical stability in the course of a transport process [[4]].
- (iii) how the collisional dynamics of impurities with a lattice trapped medium is influenced by interspecies correlations [[5,6]].
- (iv) how the polaronic properties and the underlying correlations are influenced by introducing a second medium, i.e. considering an impurity in a Bose-Bose mixture [[7]].

We were able to gain these insights by employing the Multi-Layer Multi-Configuration Time-Dependent Hartree method for atomic mixtures which allows us to take into account and thereby uncover all the necessary inter- and intraspecies correlations in multi-component systems. In Sect. 1.1 we give an overview of bosons in optical lattices as they are constituents in most of our studies. Since we are concerned with the impact of correlations in our systems under investigation we review the Gross-Pitaevskii mean-field theory in Sect. 1.2 and introduce our treatment of correlations in Sect. 1.3. In Sect. 1.4 we discuss the ab-initio variational method which has been used to treat the multi-component systems. Finally, in Sect. 1.5 we introduce possible ways to analyze the high-dimensional many-body wave function in terms of reduced quantities.

1.1 Atoms trapped in optical lattices

AC Stark shift - Atoms trapped in optical lattices serve as a promising platform for simulating solid state physics. Employing interfering optical laser beams a standing wave can be generated yielding a periodic potential energy landscape [212, 213]. For a classical electromagnetic field in one spatial dimension let us consider a plane wave of the form $E(x, t) = E_0(x)e^{i\omega t} + E_0^*(x)e^{-i\omega t}$ with an amplitude E_0 and a frequency ω . Exposing a neutral atom to the light field induces a dipole moment \hat{d} in the atom. The polarized atom interacts with the electric field under the dipole approximation $\hat{H}_I = -\hat{d} \cdot E(x, t)$. Let us now assume that the atom comprises only two internal states $|g\rangle$ (ground state) and $|e\rangle$ (excited state) with an energetic separation of $\hbar\omega_0$. Expanding the interaction term \hat{H}_I in terms of $|g\rangle$ and $|e\rangle$ while neglecting the diagonal contributions, due to an absent permanent dipole moment, we arrive at the system's total Hamiltonian

$$\hat{H}_L = \overbrace{\hbar\omega_0 |e\rangle \langle e|}^{\hat{H}_A} - \overbrace{(\mu_{eg} |e\rangle \langle g| + \mu_{eg}^* |g\rangle \langle e|) \cdot E(x, t)}^{\hat{H}_I}, \quad (1.1)$$

where $\mu_{eg} = \langle e | \hat{d} | g \rangle$. In order to transform the Hamiltonian into a time-independent one, as a first step one performs a unitary transformation into the interaction picture with $\hat{U} = e^{-i\omega\hat{\sigma}_z/2}$ with $\hat{\sigma}_z = |e\rangle \langle e| - |g\rangle \langle g|$. Since the Schrödinger picture and the interaction picture coincide for the first term in the Hamiltonian, the transformation is effectively only applied to \hat{H}_I as $\hat{U}^\dagger \hat{H}_I \hat{U}$. Applying now the rotating wave approximation, i.e. $\Delta = \omega - \omega_0 \ll \omega + \omega_0$, and transforming back to the Schrödinger picture the Hamiltonian reads

$$\hat{H}_L \approx -\frac{\hbar\Delta}{2} |e\rangle \langle e| - \frac{\hbar\Omega(x)}{2} |e\rangle \langle g| - \frac{\hbar\Omega^*(x)}{2} |g\rangle \langle e|, \quad (1.2)$$

where $\Omega(x) = \frac{\mu_{eg}E_0(x)}{\hbar}$ denotes the Rabi frequency. The effect of the atom-light interaction results in the following eigenvalues $E_\pm = \frac{-\hbar\Delta \pm \hbar\sqrt{\Omega^2 + \Delta^2}}{2}$, leading to a positive (negative) energy shift $E^{(2)} = \pm \frac{\hbar\Omega^2}{4\Delta}$ for the ground (excited) state in the limit of large detuning as compared to the Rabi frequency. This is known as the quadratic AC-Stark shift. Specifying now the spatial extension of the electric field, we obtain in the case of a standing wave a periodic energy shift $E_g^{(2)} = \frac{\hbar\Omega_0^2}{\Delta} \sin^2(kx)$ for the ground state of the neutral atom, with k being the laser wavevector and $\Omega(x) = 2\Omega_0 \sin(kx)$. This energy shift can be interpreted as a lattice potential for the neutral ground state atom such that a single atom being subject to it comprises the following Hamiltonian

$$\hat{H}_0 = -\frac{\hbar^2}{2m} \frac{d^2}{dx^2} + V_0 \sin^2(kx), \quad (1.3)$$

where the lattice depth V_0 can be tuned by the electric field amplitude E_0 as well as the detuning Δ .

Bose-Hubbard model - Considering many particles which are subject to a lattice potential one needs to introduce interactions among the atoms. For ultracold bosonic atoms the latter can be modeled by an s-wave contact interaction of the type $U_I(x, x') = g\delta(x - x')$, where positive (negative) coupling strengths g correspond to repulsive (attractive) interactions between the respective atoms. In second quantization the Hamiltonian for many interacting atoms in a periodic potential reads

$$\hat{H} = \int dx \hat{\Psi}^\dagger(x) \left(-\frac{\hbar^2}{2m} \frac{d^2}{dx^2} + V_0 \sin^2(kx) \right) \hat{\Psi}(x) + g \int dx \hat{\Psi}^\dagger(x) \hat{\Psi}^\dagger(x) \hat{\Psi}(x) \hat{\Psi}(x), \quad (1.4)$$

where $\hat{\Psi}(x)$ is the bosonic field operator and $g = \frac{4\pi\hbar^2 a_s}{m}$ with the s-wave scattering length a_s [214]. Typically such a Hamiltonian is treated by mapping it to a Bose-Hubbard model. While the original Hubbard model [35] has been introduced in order to describe the behavior of strongly correlated electrons, being then applied to a plethora of solid state physics problems, replacing electrons by ultracold bosons allowed for a direct implementation of a Bose-Hubbard model in experimental setups.

In the following let us briefly discuss the derivation of the Bose-Hubbard model starting from a continuous lattice potential in Eq. 1.4. For this purpose it is necessary to recapitulate the eigenstates of Eq. 1.3, which are given by the Bloch functions $\phi_k^n(x)$. The indices k and n denote the quasi-momentum and the band index, respectively¹. Increasing the lattice depth increases the band gap between the first and second band². This eventually prohibits excitations into higher bands, in particular the second one, for low-energy excitation processes. Hence, we are able to restrict ourselves to an effective Hamiltonian in a subspace spanned by lowest band eigenvectors. Since the Bloch functions are delocalized over the lattice geometry, it is convenient to construct a basis set using the Bloch functions which exhibits maximally-localized states with respect to the lattice sites, i.e. Wannier states [215–218]. In one dimension it has been proven that such a basis can be uniquely constructed by choosing the relative phases between the Bloch states appropriately [219]. The localization width of the Wannier states depends on the lattice depth.

We will now expand the bosonic field operators in the basis of the Wannier states of the lowest band by $\hat{\Psi}(x) = \sum_i \hat{a}_i w_i(x)$, where $w_i(x)$ denotes the respective Wannier state at site i . This expansion transforms the Hamiltonian in Eq. 1.4 to the well-known Bose-Hubbard model

$$\hat{H}_{BH} = -J \sum_{\langle i,j \rangle} \hat{a}_i^\dagger \hat{a}_j + \frac{U}{2} \sum_i \hat{n}_i (\hat{n}_i - 1). \quad (1.5)$$

Here, the assumption that the lattice depth V_0 is large, such that the Wannier states are highly localized within each well, leads to the fact that they do not overlap significantly. This tight-binding approximation restricts the creation (\hat{a}_i^\dagger) and annihilation (\hat{a}_i) of bosons only to neighboring sites, indicated by $\langle i,j \rangle$, with a hopping strength $J = \int dx w_i^*(x) \left(-\frac{\hbar^2}{2m} \frac{d^2}{dx^2} + V_0 \sin^2(kx) \right) w_j(x)$. The on-site interaction which can be either attractive or repulsive is given by $U = g \int dx |w_i(x)|^4$. In the derivation of \hat{H}_{BH} usually the term $\sum_i \int dx |w_i(x)|^2 \left(-\frac{\hbar^2}{2m} \frac{d^2}{dx^2} + V_0 \sin^2(kx) \right) \hat{a}_i^\dagger \hat{a}_i$ is neglected since it solely describes a global energy offset. From Eq. 1.5 we can deduce that bosons are able to lower the system's energy by delocalizing along the lattice. However, two particles occupying the same site raise the system's energy by U for repulsive on-site interaction. As can be seen from their definition, U and J can be manipulated by varying the lattice depth. While the increase of V_0 leads to higher barriers and thus reduces J , it increases U due to a stronger localization of the Wannier states. Moreover, U can be additionally tuned by changing the interaction strength g .

The Bose-Hubbard model has successfully predicted the essence of the insulator-superfluid transition, thereby rising to prominence. Such a quantum phase transition has also been realized in the context of ultracold bosonic atoms. This transition is based on the presence of two distinct phases depending on the ratio of the hopping amplitude and the on-site interaction. Focusing on the case of an ideal gas where $U = 0$, the system is only subject to a hopping of the particles, and thus favors delocalization. Consequently, the energy is minimized for all particles occupying

¹For finite-size lattices k is a discrete quantum number within each band and the corresponding eigenstate is degenerate with respect to $\pm k$.

²For discrete lattices also the energetic gap between eigenstates of different k decreases for fixed n .

the energetically lowest-lying Bloch state with $k = 0$. The ground state is therefore given by a product state

$$|\Psi_{SF}\rangle = \prod_i \phi_{k=0}^{n=1}(x_i), \quad (1.6)$$

with x_i denoting the spatial degree of freedom of the i th atom, leading to the system being superfluid (SF) in this regime. In the opposite regime for $J = 0$ the system is no longer dominated by a delocalization of the atoms. Instead, assuming commensurate filling of the lattice, the energy is minimized for each particle occupying one well separately and as a consequence the system becomes a Mott insulator (MI). Placing two particles in the same lattice site would increase the energy by U for $U > 0$, thereby denoting an excited state. The ground state can be again described by a symmetrized product state

$$|\Psi_{MI}\rangle = \prod_i \hat{a}_i^\dagger |vac\rangle, \quad (1.7)$$

where each particle occupies a different Wannier state.

Naturally, the Bose-Hubbard model applies only to a small range of setups since the single band approximation is often insufficient to describe all the intrinsic processes in a system. For example, for strong interaction strengths g as well as shallow lattices contributions from higher bands are expected to be non-negligible. In these cases the Bose-Hubbard model can be extended such that hopping and on-site interaction between different bands is taken into account. Therefore, also the respective hopping amplitudes and on-site interaction strengths are modified. Moreover, in the case that interactions among the particles are not of contact but long range type, interactions are likely to appear at least between next neighbors of the type $\sum_{\langle i,j \rangle} V_{ij} \hat{n}_i \hat{n}_j$. The solution of Bose-Hubbard models has been tackled utilizing analytical and numerical approaches ranging from mean-field theories, renormalization group techniques [220–223] and Monte Carlo methods [162, 224].

1.2 The Gross-Pitaevskii equation and mean-field approximations

Let us consider an ultracold dilute atomic gas of large particle number confined in an external potential $V_{ext}(x)$. We assume that the dominant interaction processes are of two-body character such that we can neglect three-body processes. The occurrence of a Bose-Einstein condensation can be attributed to the fact that one single-particle eigenstate $|\phi\rangle$ becomes macroscopically occupied, which in the ideal case includes all atoms in the system. This results in the system being approximately described by the wave function

$$\Psi(x_1, \dots, x_N, t) = \prod_{i=1}^N \phi(x_i, t), \quad (1.8)$$

with x_i denoting the spatial degree of freedom of the i th atom. Since we are assuming to be in the ultracold regime the interaction among the particles is well approximated by a contact interaction $V(x - x') = g\delta(x - x')$. Employing the ansatz for the wave function in Eq. 1.8 in order to compute the energy functional we arrive at the following expression

$$E[\Phi] = \int dx \left(-\frac{\hbar^2}{2m} \Phi^*(x, t) \frac{d^2}{dx^2} \Phi(x, t) + V_{ext}(x) |\Phi(x, t)|^2 + \frac{g}{2} |\Phi(x, t)|^4 \right), \quad (1.9)$$

where $\Phi(x, t) = \sqrt{N} \phi(x, t)$ is the renormalized single particle wave function. Employing now the variational principle $i\hbar \frac{\partial \Phi(x, t)}{\partial t} = \frac{\partial E}{\partial \Phi^*}$ for the energy density functional we arrive at the

famous Gross-Pitaevskii equation [4, 5, 225, 226]

$$i\hbar \frac{\partial \Phi(x, t)}{\partial t} = \left(-\frac{\hbar^2}{2m} \frac{d^2}{dx^2} + V_{ext}(x) + g|\Phi(x, t)|^2 \right) \Phi(x, t). \quad (1.10)$$

This reduces the many-body problem to a single-particle one where all processes are governed by the behavior of a single orbital. Eq. 1.10 has the form of the Schrödinger equation except for a nonlinear term that takes into account the interaction between the particles. While the Gross-Pitaevskii equation describes an ideal Bose-Einstein condensate, weak excitations can be introduced by applying the Bogoliubov theory [227–236]. To this end one linearizes the wave function by adding small perturbations $\delta\Phi$ and expands Eq. 1.10 while neglecting quadratic terms. Diagonalizing the resulting Hamiltonian using the Bogoliubov transformation one is able to retrieve the elementary excitations of a Bose-Einstein condensate. The corresponding dispersion relation exhibits a linear behavior for small momenta and a quadratic one for large momenta. We note that the treatment of a many-body system within a mean-field theory works remarkably well for the large particle number limit, whereas in few-body systems strong deviations from this theory are to be expected as one introduces significant potential quantum depletion. Applications of the Gross-Pitaevskii equation can be found in various research areas, including in particular the description of the excitation and interaction of dark [237–239], bright [240, 241] and dark-bright solitons [242–245] as well as vortices [246–251] in higher dimensions.

The idea behind the Gross-Pitaevskii equation can be also employed in the case of a weakly interacting mixture of bosonic species A and B . In such a setup we can approximate the system by

$$\Psi(x_1, \dots, x_N, t) = \prod_{i=1}^{N_A} \phi^A(x_i, t) \prod_{j=1}^{N_B} \phi^B(x_j, t), \quad (1.11)$$

if the interactions among the atoms of each species as well as between the species are weak. Computing now the energy functional for the mixture and applying the variational principle leads to a pair of coupled Gross-Pitaevskii equations

$$\begin{aligned} i\hbar \frac{\partial \Phi^A(x, t)}{\partial t} &= \left(-\frac{\hbar^2}{2m_A} \frac{d^2}{dx^2} + V_{ext}^A(x) + g_{AA}|\Phi^A(x, t)|^2 + g_{AB}|\Phi^B(x, t)|^2 \right) \Phi^A(x, t), \\ i\hbar \frac{\partial \Phi^B(x, t)}{\partial t} &= \left(-\frac{\hbar^2}{2m_B} \frac{d^2}{dx^2} + V_{ext}^B(x) + g_{BB}|\Phi^B(x, t)|^2 + g_{AB}|\Phi^A(x, t)|^2 \right) \Phi^B(x, t), \end{aligned} \quad (1.12)$$

where $\Phi^\sigma(x, t) = \sqrt{N_\sigma} \phi^\sigma(x, t)$ is similarly renormalized. Apart from a nonlinear term that is due to the intraspecies couplings g_{AA} and g_{BB} in each equation an additional nonlinear term appears as a result of the interspecies coupling with a strength of g_{AB} .

It is possible to extend the Gross-Pitaevskii mean-field theory by considering a time-dependent multi-orbital mean-field ansatz [252–254]. As such the many-body state is assumed to be a single bosonic number state

$$|\Psi(t)\rangle = |n_1, n_2, \dots, n_L\rangle_t. \quad (1.13)$$

Here, n_i denote the occupation of the i th variationally optimized time-dependent single-particle orbital. Consequently, one is able to consider situations in which not all particles reside in the same single-particle state, instead allowing for the condensate to be fragmented. Nevertheless, one should note that the correlations which are introduced are solely due to the exchange symmetry of the bosons.

1.3 Including correlations beyond the mean-field approximation

So far in Eq. 1.8 and Eq. 1.11 we have assumed that the intra - and interspecies interactions of the system are weak such that the system can be approximated by a product state ansatz within each species and between them. However, such an assumption is only valid for a small range of possible interactions in the system. Therefore, generally a more complex structure of the system's wave function $|\Psi\rangle$ has to be assumed, which we refer to as a correlated state.

Let us begin by formulating the general wave function of a binary mixture as

$$|\Psi\rangle = \sum_{i=1}^M \sqrt{\lambda_i} |\Psi_i^A\rangle |\Psi_i^B\rangle. \quad (1.14)$$

Here, we have used the Schmidt decomposition [255–257] in order to contract the expansion to a single sum with orthonormal species wave functions $|\Psi_i^\sigma\rangle$. The coefficients λ_i in decreasing order denote the entanglement between the species with $\sum_{i=1}^M \lambda_i = 1$. In the case of $\lambda_1 = 1$ the system is described by a single interspecies product state, implying that the species are not entangled. However, in contrast to Eq. 1.11 each species function may be composed of a superposition of several product states. In order to obtain the degree of interspecies entanglement we usually determine the species density matrices

$$\begin{aligned} \hat{\rho}_A &= \text{Tr}_{0,N_B} [|\Psi\rangle \langle\Psi|] = \sum_{i=1}^M \lambda_i |\Psi_i^A\rangle \langle\Psi_i^A|, \\ \hat{\rho}_B &= \text{Tr}_{N_A,0} [|\Psi\rangle \langle\Psi|] = \sum_{i=1}^M \lambda_i |\Psi_i^B\rangle \langle\Psi_i^B|. \end{aligned} \quad (1.15)$$

Here, we perform a trace $\text{Tr}_{P,Q}$ over the P particles of the A -species and the Q particles of the B -species. Consequently, the species functions appearing in the expansion of the wave function Ψ (Eq. 1.14) coincide with the eigenvectors of the species density matrices (Eq. 1.15), while λ_i describe the interspecies correlations.

Having analyzed the correlations between the species, in the next step one can ask for the correlations among particles of each species and their impact on the single particle level. For this purpose, one additionally traces out all atoms except for one of the respective species starting from the species density matrices. This yields the one-body density matrix of the corresponding species

$$\begin{aligned} \hat{\rho}_A^{(1)} &= \text{Tr}_{N_A-1,N_B} [|\Psi\rangle \langle\Psi|] = \sum_i n_i^A |\Phi_i^A\rangle \langle\Phi_i^A|, \\ \hat{\rho}_B^{(1)} &= \text{Tr}_{N_A,N_B-1} [|\Psi\rangle \langle\Psi|] = \sum_i n_i^B |\Phi_i^B\rangle \langle\Phi_i^B|. \end{aligned} \quad (1.16)$$

In the last step we have written the one-body density matrix as a spectral decomposition with eigenvectors $|\Phi_i^\sigma\rangle$ (natural orbitals) and eigenvalues n_i^σ (natural populations) [258–260]. For $n_1^\sigma = 1$ one recovers the Gross-Pitaevskii solution (Eq. 1.10) and as a result species σ is referred to as condensed. Deviations from the condensate fraction can be captured by the depletion $1 - n_1^\sigma$ which is used to judge the validity of the mean-field Gross-Pitaevskii approximation. As soon as more natural orbitals are significantly occupied one speaks of a fragmented state and intraspecies correlations which cannot be described by the Gross-Pitaevskii ansatz. Therefore, other methodological approaches are needed in order to treat systems with inherent intraspecies and interspecies correlations that go beyond mean-field approximation.

1.4 Methodological approach: ML-MCTDHX

The strong control over the system parameters in the field of ultracold atoms, such as the interaction strength, the various trapping potentials as well as the dimensionality to name a few, allows to enter highly correlated regimes which cannot be treated in a single particle framework. Hence, highly sophisticated computational methods are needed in order to compute the spectrum of such regimes or to track their nonequilibrium dynamics. The most direct approach is given by the exact diagonalization [261] which relies on representing and diagonalizing the Hamiltonian in an adequate many-body basis. Other methods include for example density matrix renormalization group techniques [220–223], Monte Carlo methods [162, 224], variational methods [152] and perturbative approaches.

In our studies we employ the Multi-Layer Multi-Configuration Time-Dependent Hartree method for atomic mixtures (ML-MCTDHX) [262–264] which is a variational approach. This method has its origins in the Multi-Configuration Time-Dependent Hartree method (MCTDH) [265–267] which has been developed for the investigation of the wave packet dynamics in molecular systems. Here, the degrees of freedom are distinguishable such that the wave function can be directly decomposed as a product of these. However, in the case of bosons and fermions there is permutation symmetry that needs to be accounted for. MCTDH has been modified to handle indistinguishable particles, namely MCTDHB and MCTDHF [268–270], respectively, employing a (anti-) symmetrized product state basis (number or Fock states) [271, 272]. MCTDHB has turned out to be very powerful in the case of ultracold bosonic systems [95, 273–292]. Based on the multi-layer variant of MCTDH, i.e. ML-MCTDH [293–296], ML-MCTDHX has been recently developed in order to treat bosonic and fermionic mixtures. Let us note that recent progress has been made for dynamical pruning of the wave function configurations [297, 298]. Apart from allowing for a high flexibility in the investigation of atomic mixtures, the multi-layer architecture effectively reduces the number of states that are needed in order to treat the system correctly. So far this method has been efficiently applied for unraveling the ground state properties as well as the nonequilibrium dynamics of Bose-Bose [169, 170, 185, 299–305], Bose-Fermi [179, 205, 306] and Fermi-Fermi [307–310] mixtures including also specific internal degrees of freedom, such as spin components. Recently, in [[7]] the investigations have been even extended to triple mixtures paving the way for a completely new class of systems.

1.4.1 Wave function ansatz for mixtures

ML-MCTDHX is a variational method which is able to take all the necessary correlations into account and therefore allows for going beyond the lowest-band and tight-binding approximation for lattice systems and beyond the Bogoliubov approximation for Bose-Einstein condensates. Within ML-MCTDHX one has access to the complete many-body wave function which allows us consequently to characterize the underlying system in detail. Besides investigating the quantum dynamics it allows us to calculate the ground (or excited) states by using (improved) relaxation, thereby being able to uncover also possible degeneracies of the involved many-body states. Standard approaches for solving the time-dependent Schrödinger equation rely on constructing the wave function as a superposition of time-independent number states with time-dependent coefficients. Instead, the ML-MCTDHX approach considers a co-moving time-dependent basis, such that in addition to time-dependent coefficients the single particle functions spanning the number states are also time-dependent. This leads often to a significantly smaller number of basis states that are needed to obtain an accurate expansion, eventually reducing the computation time and thereby rendering the treatment of mesoscopic systems feasible. The multi-layer

structure of the wave function allows us to uncover and characterize inter- and intraspecies correlations in the system under investigation.

In general, a mixture of K different species is determined by states of a Hilbert space $\mathcal{H} = \mathcal{H}^{\sigma_1} \otimes \dots \otimes \mathcal{H}^{\sigma_K}$, where σ_i denotes the label of species K . For a binary mixture this leads to an expansion of the system's wave function in a truncated Hilbert space as $|\Psi(t)\rangle = \sum_{i,j}^{M_A, M_B} A_{ij}(t) |\tilde{\Psi}_i^A(t)\rangle |\tilde{\Psi}_j^B(t)\rangle$. We are able to restrict the expansion over a single sum by applying a singular value decomposition, commonly known as the Schmidt decomposition [255–257]. The total many-body wave function $|\Psi(t)\rangle$ is then represented by $M = \min(M_A, M_B)$ species functions $|\Psi_i^\sigma(t)\rangle$ of species σ

$$|\Psi(t)\rangle = \sum_{i=1}^M \sqrt{\lambda_i(t)} |\Psi_i^A(t)\rangle |\Psi_i^B(t)\rangle. \quad (1.17)$$

Here, the Schmidt coefficients $\sqrt{\lambda_i}$, in decreasing order, provide information about the degree of population of the i th species function and thereby determine the degree of entanglement between the species. Furthermore, the species wave functions $|\Psi_i^\sigma(t)\rangle$, describing an ensemble of N_σ bosons, are expanded in a set of permanents

$$|\Psi_i^\sigma(t)\rangle = \sum_{\vec{n}^\sigma | N_\sigma} C_{\sigma \vec{n}}(t) |\vec{n}^\sigma; t\rangle, \quad (1.18)$$

where the vector $\vec{n}^\sigma = (n_1^\sigma, n_2^\sigma, \dots)$ denotes the occupations of the m_σ time-dependent single-particle functions of the species σ . The notation $\vec{n}^\sigma | N_\sigma$ indicates that for each $|\vec{n}^\sigma; t\rangle$ we require the condition $\sum_i n_i^\sigma = N_\sigma$, resulting in $\binom{N_\sigma + m_\sigma - 1}{m_\sigma - 1}$ number state configurations. The underlying single-particle functions are typically represented by a finite number of time-independent states in a discrete-variable representation [311–313]. The time propagation of the many-body wave function is achieved by employing the Dirac-Frenkel [314–317] variation principle $\langle \delta\Psi | (i\partial_t - \mathcal{H}) |\Psi\rangle$ with the variation $\delta\Psi$. A detailed derivation of the resulting equations of motion can be found in [264].

Let us note that in the case of triple mixtures the system's wave function cannot be described within a Schmidt decomposition and is rather given by

$$|\Psi(t)\rangle = \sum_{ijk=1}^{M_A, M_B, M_C} A_{ijk} |\Psi_i^A(t)\rangle |\Psi_j^B(t)\rangle |\Psi_k^C(t)\rangle, \quad (1.19)$$

where the coefficients A_{ijk} account for interspecies correlations. Here, the entanglement can be defined between a single species and the bipartite system composed of two species. As such, the entanglement between the A species and the two species B and C is defined by the eigenvalues of the matrix \underline{A} with the matrix elements $\underline{A}_{ij} = \sum_{kl} A_{ikl} A_{jkl}^*$.

1.4.2 Convergence and approximate limiting cases

In general, in many-body physics one encounters the problem of a Hilbert space growing exponentially with the number of particles and orbitals. In some limiting cases, e.g. when considering weak interactions among the constituents of a system, mean-field approaches such as the Gross-Pitaevskii approximation can be applied. However, one should note that also these theories only approximate the solution of the system under investigation. ML-MCTDHX offers an enormous flexibility for the treatment of many-body systems, while suffering like all particle-correlation based ab-initio methods from the size of the Hilbert space. For this reason one needs to be

careful when performing a truncation of the Hilbert space in order to arrive at an expansion of the wave function which is a good approximation to the exact solution. Since the expansion is done on many layers the configuration space is controlled by the tuple $C = (M, m_A, m_B, n_{DVR})$ for binary mixtures. Let us note that this becomes even more involved in the case of a triple mixture, where the tuple extends to $C = (M_A, M_B, M_C, m_A, m_B, m_C, n_{DVR})$ as the Schmidt decomposition can no longer be employed. For the sake of argumentation we will now discuss the case of a binary mixture.

As already discussed, M denotes the number of species functions appearing in the Schmidt decomposition in Eq. 1.14, whereas m_σ refer to the number of single-particle functions of the species σ . In the last step each single-particle function needs to be expanded in a discrete-variable representation, where n_{DVR} gives the number of employed primitive functions. As a result of this layering ML-MCTHDX is able to cover the Gross-Pitaevskii mean-field limit by setting $M = m_A = m_B = 1$ as well as the limit of the full configuration-interaction. The latter describes the case of $M_\sigma = \binom{N_\sigma + m_\sigma - 1}{m_\sigma - 1}$, while the number of single-particle functions equals the size of the discrete-variable representation, i.e. $m_\sigma = n_{DVR}$.

Another typical limit is given by the species mean-field approximation, where one restricts the wave function to a single product state of the species functions, i.e. $M = 1$. This ansatz prohibits entanglement between the species but allows for intra-particle correlations to appear. The latter can be a result of the interactions among the particles of each species as well as interactions between the species, even when interspecies entanglement is neglected. When studying a many-body problem one uses this approximate ansatz in order to illuminate the role of interspecies correlations when comparing to a converged solution which includes interspecies entanglement.

In order to obtain the exact many-body wave function it would be desirable to employ the full configuration-interaction expansion. However, in most cases this is computationally prohibitive, such that one needs to find an optimal truncation between the configuration-interaction and the Gross-Pitaevskii mean-field approximation. Typically one chooses the number of species functions smaller than the size of the respective number state space, $M \ll \binom{N_\sigma + m_\sigma - 1}{m_\sigma - 1}$, and the number of single-particle functions smaller than the size of the discrete-variable representation $m_\sigma \ll n_{DVR}$. Note that in contrast to an exact diagonalization this does not suffer from the restriction to a specific single-particle basis since here the basis is variationally optimized on all layers. As a result the representation of the many-body state becomes very efficient when considering as few relevant coefficients as possible, but trying to capture all relevant correlations at each time step.

We are able to control the convergence of a simulation by systematically increasing the constituents of the tuple $C = (M, m_A, m_B, n_{DVR})$ and comparing the respective observables of interest such as the energy and the one-body densities of the species for each tuple. The natural populations n_i^σ as well as the Schmidt coefficients $\sqrt{\lambda_i}$ are also valuable quantities when analyzing the convergence of a many-body simulation. In this sense one aims at an exponential decay of n_i^σ and λ_i with index i of the species functions and the natural orbitals with the lowest occupation being below 1%. This ensures that adding more species or single-particle functions does not result in a potential significant contribution of the new ones, such that they can be safely neglected. As such the lowest populated species and single-particle functions play a minor role for the description of the wave function and one can assume to have provided a sufficiently large basis set, which incorporates all relevant physical phenomena, while the quantitative differences are controlled to be below the desired number of decimal points.

1.5 Effective potentials and number state analysis

Employing ML-MCTDHX one has access to the whole many-body wave function which is expanded on several layers. However, this object is usually high-dimensional since it depends on several degrees of freedom for many particles and as such it cannot be directly visualized. In order to overcome this and infer information from the wave function one possible way is given by analyzing reduced quantities such as the expectation values $\langle \hat{O}_1 \rangle$ and $\langle \hat{O}_2 \rangle$ of one-body and two-body observables, respectively. In order to compute these it is sufficient to utilize the respective one- and two-body density matrices and performing a trace over the remaining degrees of freedom. Let us explicate this in the case of a binary mixture for observables which act solely on the subspace of species A where the expectation values read

$$\begin{aligned}\langle \hat{O}_1^A \rangle &= \text{Tr}_{1,0} \left[\hat{O}_1^A \hat{\rho}_A^{(1)} \right] \\ \langle \hat{O}_2^A \rangle &= \text{Tr}_{2,0} \left[\hat{O}_2^A \hat{\rho}_A^{(2)} \right],\end{aligned}\tag{1.20}$$

where $\hat{\rho}_A^{(2)} = \text{Tr}_{N_A-2, N_B} \left[|\Psi\rangle \langle \Psi| \right]$ denotes the two-body density matrix of species A similarly defined as in Eq. 1.16. In addition, it is of immediate value to determine the one- and two-body densities which are the diagonal elements of the respective matrices (or tensors) with respect to the eigenstates of the position operator. In this sense, the one-body density $\rho_A^{(1)}(x)$ yields the probability of finding a particle of species A at position x , while the two-body density $\rho_A^{(2)}(x_1, x_2)$ represents the probability of measuring one particle of species A at position x_1 and another one at position x_2 . Similarly, one can define such a probability for one particle of species A and another one of species B using $\hat{\rho}_{AB}^{(2)} = \text{Tr}_{N_A-1, N_B-1} \left[|\Psi\rangle \langle \Psi| \right]$. All of these quantities can provide insights into the behavior of the system under investigation, but suffer from being restricted to one or two particles.

In order to gain access to a microscopic characterization of the many-body wave function one needs to go one step further and analyze the number state basis in which the latter is expanded. One should note that in ML-MCTDHX the underlying basis of the wave function is time-dependent and variationally optimized which means that the single-particle functions can be of arbitrary structure. As a result when considering the occupation of a single-particle function it is not clear how the latter relates to physically motivated basis functions such as e.g. the eigenfunctions of the harmonic oscillator. Nevertheless, it is possible to probe the probability of finding the system's many-body wave function $|\Psi\rangle$ in a number state $|\vec{n}^A\rangle |\vec{n}^B\rangle$ by building the projection $P(|\vec{n}^A\rangle |\vec{n}^B\rangle) = |\langle \Psi | \vec{n}^A \rangle \langle \vec{n}^B | \Psi \rangle|^2$. Naturally, the underlying single-particle functions of the number states are chosen such that they relate to the system at hand. Hence, it is convenient to choose Bloch or Wannier functions when one of the species is trapped in a lattice geometry, whereas for harmonically confined particles Hermite polynomials would be an adequate choice.

Even though this straightforward approach is usually insightful, it does not always yield an appropriate basis representation, i.e. $\sum_{\vec{n}^A | N_A, \vec{n}^B | N_B} P(|\vec{n}^A\rangle |\vec{n}^B\rangle) < 1$. This happens in particular for dynamical processes in binary mixtures. In these cases, it is useful to employ a more sophisticated single-particle basis for building the number states. For this purpose, we construct an effective potential for species σ which takes into account the density distribution of the other species. The derivation of the effective potential is based on the assumption that the two species are not entangled, i.e. they can be described by a single product state. However, let us note that this can be also applied for systems in which entanglement is non-negligible since we employ the effective potential only as a tool in order to describe the full system in terms of

the eigenstates associated with the effective potential. Assuming now a product state ansatz $|\Psi\rangle = |\Psi^A\rangle |\Psi^B\rangle$ for a system described by the Hamiltonian $\hat{H} = \hat{H}_A + \hat{H}_B + \hat{H}_{AB}$ it is possible to reduce the action of the Hamiltonian on the wave function to an effective description for $|\Psi^A\rangle$ by projecting with $|\Psi^B\rangle$ from the left resulting in

$$\left(\hat{H}_A + \langle \Psi^B | \hat{H}_B | \Psi^B \rangle + \langle \Psi^B | \hat{H}_{AB} | \Psi^B \rangle \right) |\Psi^A\rangle = E |\Psi^A\rangle. \quad (1.21)$$

Here, the term $\langle \Psi^B | \hat{H}_B | \Psi^B \rangle$ can be attributed to the energy of species B while $\langle \Psi^B | \hat{H}_{AB} | \Psi^B \rangle$ can be understood as an effective Hamiltonian acting on species A .

In case the interspecies interaction can be approximated by a contact one with a strength of g_{AB} the latter reduces to a one-body potential of the form $\langle \Psi^B | \hat{H}_{AB} | \Psi^B \rangle = g_{AB} N_B \rho_B^{(1)}(x)$ which takes into account the one-body density distribution of species B . The resulting effective potential reads

$$V_{eff}(x) = V_A(x) + g_{AB} N_B \rho_B^{(1)}(x), \quad (1.22)$$

where $V_A(x)$ denotes the trapping potential of the A species. $\rho_B^{(1)}(x)$ is the one-body density associated with the wave function obtained from a many-body simulation within ML-MCTDHX. Therefore, it generally exhibits a complex structure.

Let us briefly discuss the role of the constituents which modify the trapping potential of the A species. Increasing g_{AB} or N_B naturally leads to a stronger impact of the B species on the effective potential experienced by the other species. However, one should note that under this variation $\rho_B^{(1)}(x)$ does not necessarily remain static, but may also change its distribution. Moreover, the latter also depends on the parameters describing \hat{H}_B and as such there are many possibilities to manipulate the effective potential V_{eff} . As described above, the effective potential serves as a tool for gaining insight into the microscopic processes underlying the actual wave function representation while yielding eigenstates which are well adapted to the problem at hand. Consequently, one may also employ it for describing highly entangled systems, even though it is not guaranteed that it always provides an adequate basis set.

Outline of the scientific contributions

In this chapter, we summarize our scientific contributions published in Refs. [[1-7]]. More detailed explanations may be found in the manuscripts provided in Chapter 3. All contributions are based on the characterization of the ground state properties and non-equilibrium dynamics of atomic mixtures subjected to various trapping potentials. In Refs. [[1-3]] the ground state properties of lattice trapped impurities coupled to a Bose gas are studied, while we additionally investigate the dynamical response of the respective many-body ground states upon quenching the interspecies interaction strength in [[3]]. In Ref. [[4]] also the Bose gas is trapped in a lattice geometry such that the whole system can be considered as a lattice trapped system doped with impurities. A different quench scenario is considered in Ref. [[5]] where upon quenching the tilt of the double well the tunneling dynamics of impurities in a double well immersed in a bath of lattice trapped bosons is unraveled. A similar quench protocol is applied in [[6]], while here the impurities are trapped in a displaced harmonic confinement. In [[7]] we extend the notion of a binary mixture to triple mixtures where impurities are immersed in a harmonically confined Bose-Bose mixture.

2.1 Lattice trapped impurities immersed in a Bose gas

The first four publications deal with one-dimensional binary systems comprised of lattice trapped impurities which are immersed in a Bose gas (see Figure 2.1), while in [[4]] also the Bose gas is subject to a lattice potential (see Figure 2.2). Upon variation of the system parameters, e.g. the interspecies interaction strength and the lattice depth, the ground state properties as well as the dynamical response after a sudden quench of the interspecies interaction strength is investigated. We analyze the impact of inter- and intraspecies correlations on the system properties and aim at establishing links to microscopic mechanisms. In particular, we employ the projection onto fixed number state basis sets in order to characterize the many-body wave function. Furthermore, we construct effective Hamiltonians and associated effective trapping potentials in order to obtain an intuitive understanding of the observed phenomena. As a result, we are able to get insight into the localization properties of the impurities due to the coupling to the Bose gas as well as the dynamical response, which involves transport processes of the impurity species.

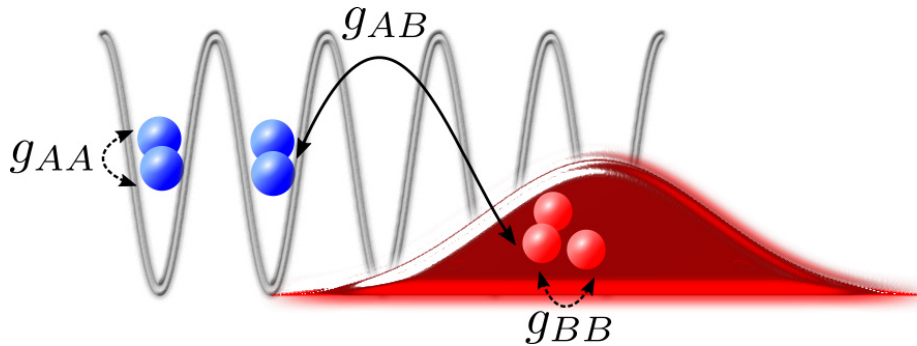


Figure 2.1: (a) Sketch of the two-component mixture in [[1-3]]. The impurities (blue dots) interact repulsively via an intraspecies contact interaction of strength g_{AA} and via an interspecies contact interaction of strength g_{AB} with the atoms of the Bose gas (red dots). The latter atoms in turn weakly interact via an intraspecies contact interaction of strength g_{BB} .

Correlation induced localization of lattice trapped bosons coupled to a Bose–Einstein condensate [[1]]

In [[1]] we examine the ground state properties of a one-dimensional lattice trapped bosonic species immersed in a Lieb-Liniger type gas [318–320], i.e. a Bose gas with periodic boundary conditions. We note that the latter majority species is not subject to the lattice potential. In this work we consider a triple-well in which $N_A = 3$ non-interacting impurity atoms are trapped, while the majority species consists of $N_B = 10$ weakly interacting particles. Our main focus lies on the pure impact of the majority species on the impurity atoms, which is why the impurity atoms are chosen to be non-interacting.

We investigate the system’s ground state under variation of the lattice depth V_0 and the interspecies interaction strength g_{AB} , with a focus on intra- and interspecies correlations. For $g_{AB} = 0$ the subsystems are disentangled and due to the impurities being non-interacting each of them occupies the energetically lowest Bloch state, thereby being delocalized over the whole lattice. An increase of the interspecies coupling strength leads to a disturbance of the uncorrelated state, which we measure in terms of the natural populations, i.e. the eigenvalues of the one-body density operator of the impurity species. For small g_{AB} and V_0 the most populated natural orbital is only weakly depleted, whereas increasing g_{AB} and V_0 leads to a stronger depletion. The depletion saturates towards large interspecies couplings and lattice depths, which manifests itself in the occupation of two additional natural orbitals with an equal population of $1/3$. Additionally, this has an impact on the interspecies entanglement which increases gradually, indicating that the system can no longer be described by a single product state of species functions. By employing the two-body density of the impurity species we observe that for small g_{AB} and V_0 the impurities are delocalized, such that the measurement of one impurity does not impact the detection of the second one. In the correlated regime the impurities localize in a single well due to an effective interaction mediated by the majority species [177, 182, 200]. For small couplings g_{AB} the mechanism of the transition can be understood in terms of energetic arguments. Assuming a product state ansatz we determine the interspecies energy of the system and divide by the number of particles N_A and N_B to obtain the interspecies energy per particle. This energy is assumed to be used in order to excite a single impurity from the energetically lowest Bloch state to one of the excited states in the first band. For small g_{AB}

the parameters which provide the necessary interspecies energy for such a process correspond to the region of transition from an uncorrelated to a correlated state, while for larger g_{AB} this simple model fails to describe the transition.

In order to gain deeper insight into the structure of the system's many-body wave function in the correlated regime, we project the latter onto number states. We construct the number states based on the Wannier states of the lowest band for the impurity species, while the number states of the majority species can be described by any underlying single-particle basis. In order to characterize the transition to the correlated state we compute the probability of finding the impurities in a specific number state configuration irrespective of the number states occupied by the Bose gas. We find that the correlated state can be described by an equal superposition of number states where all impurities occupy the same Wannier state. The corresponding one-body density of the majority species function exhibits a minimum at the well where the impurities cluster.

Finally, we introduce an effective Hamiltonian for the impurity species which contains an induced interaction and an induced hopping term. This Hamiltonian is constructed by utilizing the Bogoliubov approximation for the Bose gas and subsequently applying the Nakajima transformation [321]. We are able to identify an attractive on-site interaction as well as reduced induced hopping terms in the correlated regime, indicating the localization of the lattice atoms. Increasing the number of particles in the majority species to e.g. $N_B = 30$ still results in the transition from an uncorrelated to a correlated state, while the actual transition region is shifted due to the alteration of the induced interactions.

State engineering of impurities in a lattice by coupling to a Bose gas [[2]]

We go a significant step beyond the scenario in [[1]] by including a repulsive intraspecies interaction strength among the impurities in [[2]]. This leads to a competition between the induced long-range interaction which is mediated by the majority species [165, 166] and the repulsive contact interaction among the impurities. By tuning the respective coupling strengths we aim at manipulating the distribution of the impurities in the lattice geometry. In accordance with [[1]] we examine the ground state of lattice trapped bosonic impurities which are interacting repulsively via a contact interaction and are coupled to a majority species which is not trapped in the lattice potential. Here, we consider $N_A = 4$ impurities in a triple-well and $N_B = 10$ weakly interacting majority species atoms. The dependence of the system's ground state on the boundary conditions is analyzed in detail.

As a first step we employ periodic boundary conditions and vary the lattice depth V_0 and the interspecies interaction strength g_{AB} , while setting the intraspecies interaction strength among the impurities g_{AA} to a finite value. We analyze the obtained ground state by projecting onto number states and thereby determine the probability of finding the impurity species in a specific number state irrespective of the number state configuration of the majority species. The number states for the impurities are constructed using a Wannier basis of the lowest band, which is sufficient for a description of the underlying many-body wave function. We classify the ground state by identifying four different regions depending on V_0 and g_{AB} . Similar to [[1]] for small V_0 and g_{AB} all four impurities populate the energetically lowest Bloch state, leading to their delocalization. Setting g_{AB} to a small value and increasing the lattice depth, results in a separate localization of three impurities in different wells with the one extra particle being delocalized over all wells. The increase of g_{AB} leads to two different regimes, being sensitive to the lattice depth. For small V_0 the repulsive interaction among the impurities is not able to counteract the attractive induced interaction, leading to an accumulation of all impurities in a

single lattice site, as in [[1]]. For large lattice depths and large interspecies couplings we observe a pairwise localization of the impurities in adjacent wells, which indicates the long-range type of the induced interaction. For the latter two regimes the ground state is threefold degenerate (triplet) due to the translation symmetry as a result of the periodic boundary conditions. Focusing now on the majority species we investigate its probability distribution with respect to number states spanned by plane waves. In both regimes of large g_{AB} excitations of up to four particles are necessary to correctly describe the many-body state. The two regimes differ with respect to the quantitative distribution of the respective number states, such that in case of a pairwise impurity accumulation the $k = 0$ plane wave is less populated and higher particle excitations are more dominant.

Fixing now the interspecies coupling as well as the lattice depth, we find a transition between the previously observed impurity localization configurations as a function of g_{AA} . Starting from an accumulation of all the impurities in a single well for small intraspecies couplings, an increase of g_{AA} leads to a sharp crossover towards a pairwise accumulation. For large g_{AA} we recover the state where three impurities localize separately in different wells while the one extra particle is delocalized over all three wells. The region of g_{AA} in which the impurities accumulate pairwise can be controlled by varying the interspecies interaction strength. This behavior of the system's ground state allows for a clear and systematic way of implementing ground states with specific impurity distributions.

Finally, we investigate the impact of the boundary conditions on our setup. For periodic boundary conditions we already observed that the pairwise as well as the complete accumulation of the impurities manifest themselves in a ground state triplet. In the case of hard wall boundary conditions [322] the ground state exhibits a twofold degeneracy (doublet) for impurities clustering in a single well, while for the pairwise localization we observe no degeneracy anymore (singlet). In both cases the impurities distribute such that they favor localization in the outer sites of the triple-well. Additionally, including a repulsive Gaussian potential for the majority species in the middle of the box allows for changing the singlet into a doublet, where the impurities tend to localize towards the center, and vice versa. In this sense, we are able to address the states which are missing in the triplet when implementing solely hard wall boundary conditions.

Interaction-induced single-impurity tunneling in a binary mixture of trapped ultracold bosons [[3]]

Exploiting the possibility to engineer the localization properties of impurities as discussed in [[2]], we explore the dynamical response of a system which exhibits a specific impurity distribution upon a quench of the interspecies interaction strength. Specifically, we consider $N_A = 4$ impurity atoms trapped in a five well lattice with hard wall boundary conditions immersed in a majority species of $N_A = 10, 30$ particles which obeys the same boundary conditions but without the lattice potential. Before turning to the dynamics we aim at getting an overview of the ground state in dependence of the interspecies interaction strength g_{AB} and the lattice depth V_0 .

Similar to [[1]] and [[2]] we extract information out of the many-body wave function by projecting it onto number states and determining the probability of finding the system in a specific number state of the impurity species irrespective of the number states occupied by the majority species. The corresponding number states of the impurities are constructed with a generalized Wannier basis of the lowest band [217, 218]. For large lattice depths and small couplings g_{AB} the impurities localize separately in different wells such that the central well is not occupied. Increasing the interspecies interaction strength we observe a transition to a state with

one two-impurity cluster in an outer well next to a single impurity and one impurity residing along the opposite wall. For large g_{AB} the impurities accumulate in pairs in adjacent sites in the outer wells. The latter two regimes exhibit a twofold degeneracy with the corresponding additional states given by the parity-symmetric counterpart.

For the dynamics we prepare our system such that the impurities accumulate in pairs in adjacent sites by choosing large lattice depths and interspecies couplings. Subsequently, we perform a quench of the interspecies interaction strength to a lower value and track the dynamical response of the system. Employing the one-body density of the impurity species we are able to identify four different regimes depending on the post-quench interspecies coupling strength. In case of weak quench amplitudes the impurities remain trapped in the initially occupied wells and do not exhibit a response, while the majority species undergoes high-frequency oscillations. For smaller post-quench g_{AB} a tunneling process to the neighboring lattice site is initiated, which leaves an imprint on the density distribution of the majority species due to the repulsive interspecies coupling on top of the high-frequency oscillations. Quenching to even smaller values of g_{AB} we are able to extend the tunneling of the impurities to the next neighboring site. However, a quench to $g_{AB} = 0$ does not affect the initial impurity configuration, leading to stable two-impurity clusters in the course of time [61]. This is in stark contrast to a single impurity trapped in an outer well interacting with a majority species, where such a quench leads to an impurity transport to the opposite outer well. Additionally, this single impurity will not tunnel under the presence of a finite post-quench interaction strength, emphasizing the role of many-body processes in our many-impurity setup. In order to gain insight into how many impurities actually tunnel to the neighboring sites, we invoke the probability of finding the system in a specific number state of the impurity species irrespective of the states populated by the majority species. Indeed, only a single impurity out of the initial cluster tunnels to the neighboring site, while the remaining cluster remains mostly stable during the dynamics. Quenching to even smaller interspecies couplings leads to a tunneling of that impurity to the next-neighboring unpopulated well, such that an oscillation between this well and the previously populated one occurs.

Focusing now on the role of the majority species, we similarly characterize the underlying microscopic process by projecting onto the number states of the majority species. For this purpose, we introduce single-particle functions which are tailored to the many-body problem and take the effect of the impurities' presence into account. Such an effective single-particle Hamiltonian exhibits a potential which consists of the one-body density of the impurity species (at $t = 0$) weighted by the prequench interspecies interaction strength and the number of impurities, see Chapter 1.5.¹ While the transfer of the impurity to the neighboring site is correlated with single-particle excitations of the majority species into the first and second excited state with respect to the effective Hamiltonian, the impurity transfer to the next-neighboring site induces two-particle excitations. The single-particle excitations are responsible for the high-frequency oscillations observed in the corresponding one-body density of the majority species. Turning now to the impurities again, we need to construct a many-body effective Hamiltonian in order to extract the oscillation frequency of the one-body density, due to the rather strong intraspecies interaction among them. The resulting frequency corresponds to a transition of a single impurity to the first excited state within the effective Hamiltonian. Finally, we are able to extend our results to the case of $N_B = 30$ majority species atoms where it is still possible to transfer the impurity species through the lattice, although the dynamical response in general is changed due to the altered crossover diagram of the ground state exhibiting an additional regime.

¹Note that this single-particle picture is only applicable for weakly interacting majority species particles.

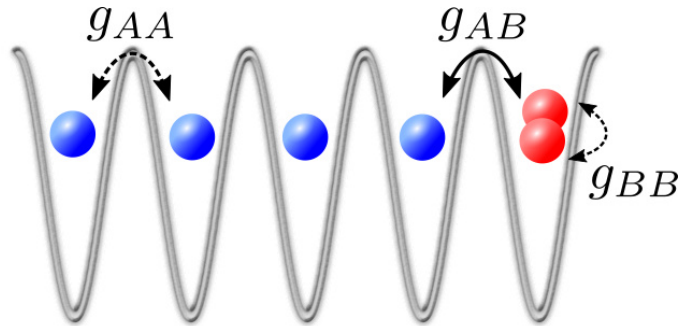


Figure 2.2: Sketch of the two-component lattice trapped bosonic mixture in [[4]]. The majority species atoms (blue dots) interact repulsively via an intraspecies contact interaction of strength g_{AA} and an interspecies repulsion of strength g_{AB} with the bosonic impurities (red dots). The latter atoms repulsively interact via an intraspecies contact interaction of strength g_{BB} .

Doping a lattice-trapped bosonic species with impurities: from ground state properties to correlated tunneling dynamics [[4]]

In [[4]] also the majority species is subject to an external confinement. Consequently our system consists of two bosonic species, i.e. an impurity species and a majority species, trapped in a one-dimensional five-well lattice with hard wall boundary conditions. As a first step, we analyze the ground state properties of the Bose-Bose mixture varying the lattice depth V_0 and the interspecies coupling strength g_{AB} for $N_B = 1, 2$ impurities and $N_A = 4, 5$ majority species atoms.

Fixing V_0 , we find that while increasing g_{AB} the von Neumann entropy exhibits a growth up to a specific value of the interspecies coupling strength, while any further increase leads to a sudden reduction of the entropy close to zero. This manifests itself in the majority and impurity species being localized over the whole lattice geometry for strong interspecies entanglement, i.e. large von Neumann entropy. The sudden reduction of the entropy corresponds to the majority species forming a hole in one of the outer wells, localizing now only over the four remaining wells, while the impurity occupies that specific hole. As a result, the two species undergo a phase-separation [261, 277, 323] which can be understood as the formation of a particle-hole pair [324]. This is accompanied by the formation of a two-fold degeneracy due to the parity symmetry with respect to $x = 0$. Due to the repulsive interaction among the majority species atoms, additionally they form a Mott insulator-like state on the four populated wells, thereby avoiding each other. For two impurities a similar behavior can be recovered above a critical lattice depth, leading to an accumulation of the impurities in a single outer well for large g_{AB} . Below that lattice depth the impurities are delocalized among two neighbouring outer wells and are two-body correlated. Increasing the number of majority species particles to $N_A = 5$, for $N_B = 1$, again the formation of a particle-hole pair can be recovered for large g_{AB} , while the additional particle of the majority species is delocalized over the four remaining lattice sites.

In a second step we prepare our system, for one as well as two impurities, in its ground state for large g_{AB} and V_0 , such that a particle-hole pair is formed. We aim at initiating the tunneling dynamics of the two species by suddenly reducing the interspecies interaction strength. We find a very controlled correlated tunneling dynamics, where the majority species tunnels such that its particles avoid occupying the same lattice site. Moreover, we observe the effective transport

of a particle-hole pair from one of the outer sites to the opposite one, while the stability of the pair, i.e. the probability of measuring the particle-hole pair, strongly depends on the presence of a finite coupling between the species. In this sense, it is necessary not to quench too strongly in order to maintain a stable particle-hole pair. However, a quench that is too weak does not allow for a transport of the initial particle-hole pair through the lattice. During the transport we encounter a strong build-up of interspecies entanglement as well as correlations among the majority species atoms due to the formation of a superposition of particle-hole pair states. The latter are of the same structure as the initial state, but exhibit a localization of the impurity in a different site, while the majority species atoms occupy the remaining four wells separately. In the case of two impurities it is necessary to quench to lower interspecies interaction strengths in order to achieve a transport of the impurities which are initially accumulated in a single outer well. This also has an impact on the stability of the particle-hole pair, being strongly reduced, and leads to a less structured development of correlations. During the transfer of the impurities to the opposite outer well where they cluster again, the initially accumulated impurities delocalize over next-neighbor sites, allowing them to be detected at the same site or in adjacent ones.

2.2 Collisional dynamics of impurities with a lattice trapped bath

The following two works are dedicated to the collisional dynamics of impurities with a larger species, referred to as the medium, which is trapped in a lattice geometry. The system is prepared in its ground state for a finite interspecies coupling strength, while the dynamics is initiated differently in each case. In [[5]] we apply an initial tilt to the double well in which the impurity species is trapped and quench the tilt to zero (see Figure 2.3). In contrast to that, in [[6]] the dynamics is triggered by initially displacing the harmonic confinement of the impurities and quenching the displacement to the center of the trapping potential of the medium (see Figure 2.4). We are able to uncover dynamical response regimes depending on the interspecies coupling strength by inspecting the one-body densities of the two species. In order to understand the underlying microscopic processes we construct a time-averaged effective potential whose shape already allows for an intuitive understanding. The corresponding eigenstates and Wannier states serve as a very helpful tool to characterize the dynamics of the subsystems. Thereby we are able to uncover the transport mechanisms of the impurity species which are a result of the coupling to the majority species.

Entanglement-assisted tunneling dynamics of impurities in a double well immersed in a bath of lattice trapped bosons [[5]]

In [[5]] we explore the tunneling dynamics of an impurity species in a double well which is coupled to a lattice trapped majority species. The latter consists of $N_A = 8$ interacting bosons which experience a six-well lattice with hard wall boundary conditions, while the impurities are subject to a double well with an additional linear tilt. We prepare the system in its ground state for a fixed tilt and varying interspecies coupling strength g_{AB} . This leads to the impurities being localized in one of the wells, whereas the overlap of the two species strongly depends on g_{AB} .

We initiate the tunneling dynamics by quenching the tilt to zero, thus favoring the transport of the impurities to the opposite well. Due to the repulsive coupling to the majority species atoms the impurities collide with the latter species, which acts in general as a material barrier [325, 326]. Thus, the impurities experience an effective potential being formed by the double well

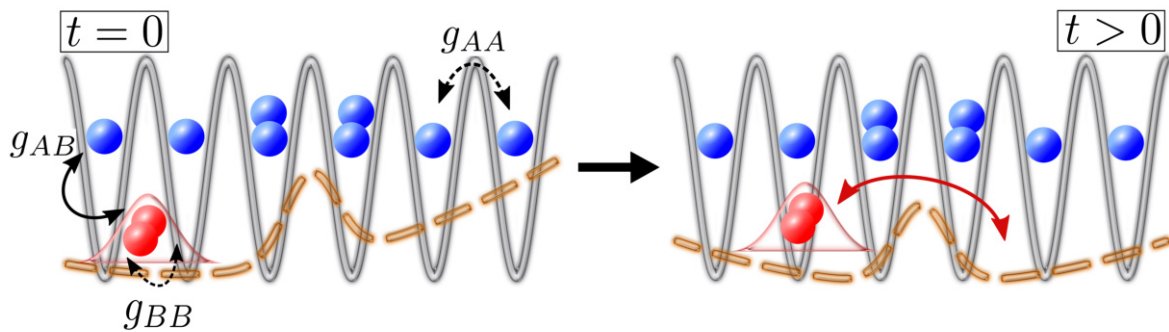


Figure 2.3: Schematic representation of our setup in [[5]] before ($t = 0$, left panel) and after the quench ($t > 0$, right panel). The majority species (blue dots) resides in the lattice potential. The impurities (red dots) are trapped in a double well potential with an initially superimposed tilt. The quench is performed by setting the tilt to zero, thereby quenching to a symmetric double well configuration.

and the material barrier which is expected to strongly alter the resulting transport. Indeed, for a single impurity four different tunneling regimes of the impurity in dependence of the interspecies interaction strength are encountered. For weak couplings the impurity undergoes a rather complex tunneling process to the other site of the double well. It turns out that this is a single-particle effect being caused by the strong initial tilt, such that it is also present for two non-interacting species ($g_{AB} = 0$). For larger g_{AB} the impurity is strongly impacted by the presence of the majority species. As such, the impurity has to overcome the material barriers on top of the double well barrier in order to be transported to the opposite well. Consequently, the impurity oscillates through the density maxima of the majority species and being finally transported to the other site of the double well where it continues the initial material barrier tunneling. In this sense, the tunneling of the impurity to the other site takes place in a very controlled and systematic manner, in particular compared to the case of small g_{AB} . This material barrier tunneling is prolonged for larger interspecies coupling strengths such that the impurity does not tunnel to the other well within the considered time interval. For even larger g_{AB} we observe a trapping of the impurity within the initially occupied site due to the strong repulsion to the majority species, resulting in a self-trapping [292, 327]. In order to emphasize the importance of interspecies entanglement for the observed tunneling dynamics, we additionally perform calculations using a single product state of the two species as an ansatz. We find major deviations with respect to the reported phenomenology employing a many-body ansatz as soon as the entanglement between the species is non-negligible.

In order to characterize the underlying microscopic processes which take place during the dynamics we construct a time-averaged effective potential (TAEP). It is composed of the double well potential and the one-body density of the majority species weighted by the interspecies interaction strength and the number of particles N_A and averaged over the total propagation time. For weak couplings the TAEP resembles a double well structure while increasing g_{AB} leads to an additional substructure in the respective wells which intuitively explains the corresponding material barrier tunneling. Increasing g_{AB} further an asymmetry develops in the potential where a distinct maximum is strongly suppressed which finally leads to the trapping of the impurity in the initially occupied well. Constructing the generalized Wannier functions associated with the TAEP and determining the probability for an impurity occupying one these functions

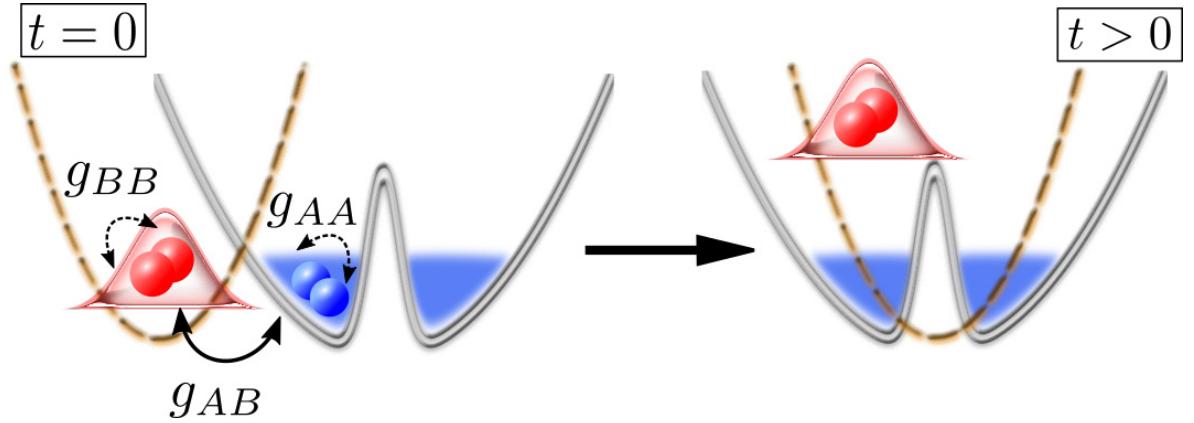


Figure 2.4: Sketch of the setup under consideration in [[6]] at $t = 0$ (left panel) and after quenching the confinement of the impurities (red dots) for $t > 0$ (right panel). The harmonic potential of the impurities is initially displaced with respect to the center of the double-well potential of the bosonic medium (blue dots).

during the dynamics, we are able to describe the transport process in detail. Considering two weakly interacting impurities we are able to identify the previous four tunneling regimes. In this context, it is natural to ask the question how the two impurities are transported, in particular whether they tunnel together or separately. Indeed, we find that the transport process to the opposite well is rather complex consisting of single particle and pair tunneling.

Many-body collisional dynamics of impurities injected into a double-well trapped Bose-Einstein condensate [[6]]

Similar to [[5]], in [[6]] we consider a harmonically trapped impurity species that collides with a medium of $N_B = 20$ particles that is subject to a double well. Here, we initiate the dynamics of the impurities by preparing the latter in a displaced harmonic oscillator and quenching it to the center of the double well. In analogy to [[5]] we vary the interspecies interaction strength g_{AB} from strongly attractive to strongly repulsive and analyze the corresponding dynamical response [168]. We encounter a very rich phenomenology for the different coupling strengths, capturing five dynamical response regimes [170].

For strong attractive couplings the impurity is bound to a density maximum, performing oscillations with a small amplitude, and thus does not completely penetrate the medium [159]. For less attractive couplings the impurity performs an effective tunneling from one density maximum of the majority species to the other one, which is reminiscent of the tunneling in a double well [292, 327]. In the region of small attractive and repulsive couplings the impurity is able to pass through the bosonic gas due to the sufficiently small coupling strength. Hence, it undergoes a dissipative oscillatory motion [169] which can be attributed to a continuous energy transfer to the majority species. In this regime, we are able to describe the mean position of the impurity employing the solution of a damped harmonic oscillator. Fitting the analytical solution to our numerical results we are able to extract an effective damping constant, an effective trapping frequency as well as the effective mass of the impurity. We find an increased damping for increasing attractive and repulsive couplings in the region of small couplings which is due to the enhanced influence of the medium, while the behavior of the trapping frequency can be explained within an effective potential approach. Interestingly, the effective mass decreases with

increasing absolute values of the interspecies coupling. This can be explained in terms of the accumulation of the impurity's density in the trap center such that effectively the impurity mass contributing in the oscillatory motion is reduced. Increasing g_{AB} further a spatial localization of the impurity in the center of the harmonic confinement, and thus between the density maxima of the bath, occurs. For very large interspecies interaction strengths the impurity is reflected at a density maximum of the majority species and is consequently not able to penetrate it due to the strong repulsion. In all regimes the system exhibits non-negligible interspecies entanglement which is maximized in the regime where the impurity is pinned and during the dissipative motion of the impurity. In both regimes the entanglement saturates towards a finite value in the course of time indicating the development of a steady state. In order to explicate the robustness of the dynamical response regimes we vary different system parameters which are of immediate interest. Changing the intraspecies interaction strength between the particles of the medium it is again possible to realize the respective dynamical response regimes, while the corresponding regimes are shifted with respect to the interspecies interaction strength. Additionally, a variation of the initial displacement impacts the amplitude of the oscillation but leaves the regimes intact.

Employing the notion of a time-averaged effective potential, as introduced in [[5]], we are able to classify the excitations of the impurity during the collisional dynamics. In particular, in case the impurity is pinned in the center of the trap we find that it is excited into a superposition of several eigenstates of the effective potential. However, judging from the corresponding one-body density of the impurity these cannot be identified and can consequently be referred to as *hidden*. Moreover, by analyzing the impurity species functions we unravel that the three dominantly occupied ones correspond to the three energetically lowest eigenfunctions of the effective potential. Finally, we extend our setup to the case of two non-interacting impurities, employing the same quench protocol as for a single impurity. Analogously to a single impurity we unravel five dynamical response regimes which are only slightly shifted with respect to the system parameters. However, the regime corresponding to the effective tunneling of the impurity for attractive interspecies couplings does not appear. Instead, the impurities localize at the two density maxima of the majority species, while exhibiting small amplitude oscillations in the course of time. As a showcase for the involved microscopic processes we focus on the case where the impurities are bound to one density maximum of the majority species. For this purpose, we determine the probability for one impurity occupying a specific eigenstate of the respective effective potential, while the other impurity populates a different or the same eigenstate. Both impurities predominantly occupy the energetically lowest eigenstate of the effective potential. However, we observe that also single-particle excitations as well as two-particle excitations contribute to the dynamics. Moreover, the intraspecies coupling strength among the medium atoms is identified as an additional control parameter influencing the compressibility of the latter and thereby its penetrability.

2.3 Highly imbalanced triple mixtures

The final work on which this cumulative thesis is based on focuses on the first detailed study of the polaron problem when considering a bath consisting of two species. It also provides the first application of ML-MCTDHX in the framework of a triple mixture setting.

Polarons and their induced interactions in highly imbalanced triple mixtures [[7]]

In [[7]] we investigate the emergent polaronic properties of impurities immersed in a correlated one-dimensional Bose-Bose mixture (see Figure 2.5). The Bose-Bose mixture consists of two

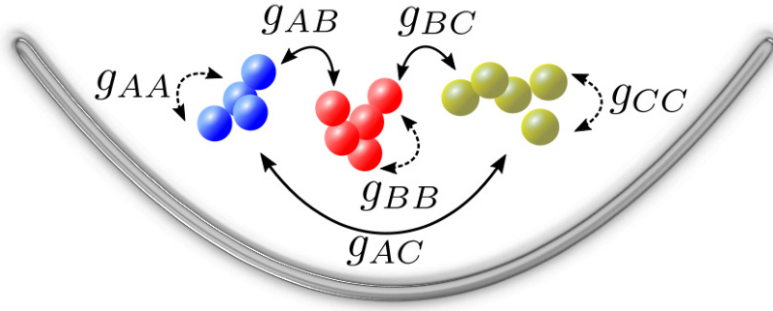


Figure 2.5: (a) Sketch of a general harmonically confined triple mixture setup in [[7]]. The bosonic atoms interact via a contact interaction of strength $g_{\sigma\sigma'}$ with $\sigma(\sigma') \in \{A, B, C\}$. Dashed lines indicate intraspecies interactions while solid lines represent interspecies interactions.

species A and B with equal masses $m_A = m_B$ and $N_A = N_B = 10$ particles, while the results also persist for larger N_A, N_B . $N_C = 1, 2$ bosonic impurities are immersed in this cumulative bath, while all species experience the same harmonic confinement. The generalization to such a triple mixture setting allows for the impurities to couple either attractively or repulsively to the individual hosts, thus offering an efficient platform for steering the polaronic properties.

We study this system by varying the impurity-medium coupling strengths g_{AC} and g_{BC} , which are of contact type, and compute the corresponding ground state. As a first step, we compute the impurity residue [122] for a single impurity immersed in the cumulative bath and find a broad peak of the residue with respect to g_{AC} for all g_{BC} . For strongly attractive or repulsive g_{AC} the residue decreases towards zero which indicates the decay of the polaron. The strong repulsion leads to a phase-separation of the impurity with respect to its host, while forming a shell structure, and thereby renders no dressing possible. On the other hand, for strong attractions g_{AC} the impurity either resides within both hosts for $g_{BC} < 0$ or solely lies within host A while B forms a shell structure for $g_{BC} > 0$. Due to the variation of the coupling strengths the polaronic residue peak can be flexibly controlled. Remarkably, for attractive couplings g_{BC} the quasiparticle character can be maintained for larger interaction strengths as compared to the case of impurities immersed in a single component bath. Such a behavior is also present for heavier impurities, where the baths are formed by the hyperfine states of ^{87}Rb and impurities are either ^{133}Cs or ^{174}Yb . Here, only minor deviations to ^{87}Rb are found, which manifest themselves in slightly larger (smaller) widths of the residue peak for $g_{BC} < 0$ ($g_{BC} > 0$).

The presence of a binary host is also reflected in the polaron binding energy, being defined as the energy difference due to the injection of the impurity. Similar, to the case of a single component host the binding energy decreases towards attractive g_{AC} and saturates for repulsive g_{AC} . However, we find a clear hierarchy of the binding energy in dependence of g_{BC} , such that for any g_{AC} a decrease of the coupling g_{BC} also leads to a reduction of the binding energy. As a consequence, utilizing experimental radiofrequency schemes [184, 185], the respective polaronic resonances are well distinguishable from each other. A similar behavior can be retrieved for a larger cumulative bath of $N_A = N_B = 50$ particles. An intuitive understanding of the impurity's state can be gained when considering the associated effective potential. For weak impurity-medium couplings it is adequately described within the effective potential approach (see Chapter 1.5) which transits from a double well to a deformed harmonic confinement depending on the impurity-medium interaction strength. Accordingly, for stronger attractive or repulsive

impurity-medium couplings an increasing number of excited states of the effective potential start to contribute. Consequently, the effective potential is no longer an adequate description and does not provide a proper description for the impurity immersed in a cumulative bath.

Turning now to the case of two impurities coupling to the Bose-Bose mixture, we also observe a peak structure of the impurity residue. The effect of the additional impurity manifests itself in the strong suppression of the residue for all impurity-bath couplings g_{BC} as compared to the case of $N_C = 1$. For two impurities it is natural to investigate the relative distance in order to infer from it the impact of the cumulative bath on the coalescence of the impurities. The relative distance exhibits a decrease towards zero for attractive g_{AC} and saturates towards a finite value for repulsive g_{AC} . For the latter these finite values lie close together in the case of $g_{BC} \geq 0$, while saturating towards smaller values for $g_{BC} < 0$. In order to gain insight into the underlying microscopic process and in particular unravel whether indeed attractive induced interactions are established, we investigate the two-body density of the two impurities. For sufficiently attractive couplings to one of the hosts bipolaron formation can be observed [301, 328], indicated by a suppression of the off-diagonal contributions in the two-body density. In contrast, for repulsive g_{AC} the impurities form a shell structure, exhibiting a slight elongation towards the diagonal of the two-body density. By varying the coupling g_{BC} to the other bath it is possible to steer the strength of the induced interactions as well as the width of the shell.

Scientific contributions

3.1 Correlation induced localization of lattice trapped bosons coupled to a Bose–Einstein condensate

PAPER • OPEN ACCESS

Correlation induced localization of lattice trapped bosons coupled to a Bose–Einstein condensate

To cite this article: Kevin Keiler *et al* 2018 *New J. Phys.* **20** 033030

View the [article online](#) for updates and enhancements.

Related content

- [The impact of spatial correlation on the tunneling dynamics of few-boson mixtures in a combined triple well and harmonic trap](#)
Lushuai Cao, Ioannis Brouzos, Budhaditya Chatterjee *et al.*
- [Beyond mean-field dynamics of ultra-cold bosonic atoms in higher dimensions: facing the challenges with a multi-configurational approach](#)
V J Bolsinger, S Krönke and P Schmelcher
- [Non-standard Hubbard models in optical lattices: a review](#)
Omjyoti Dutta, Mariusz Gajda, Philipp Hauke *et al.*



PAPER

Correlation induced localization of lattice trapped bosons coupled to a Bose–Einstein condensate

OPEN ACCESS

RECEIVED

15 December 2017

REVISED

15 February 2018

ACCEPTED FOR PUBLICATION

12 March 2018

PUBLISHED

29 March 2018

Kevin Keiler^{1,3}, Sven Krönke^{1,2} and Peter Schmelcher^{1,2}¹ Zentrum für Optische Quantentechnologien, Universität Hamburg, Luruper Chaussee 149, D-22761 Hamburg, Germany² The Hamburg Centre for Ultrafast Imaging, Universität Hamburg, Luruper Chaussee 149, D-22761 Hamburg, Germany³ Author to whom any correspondence should be addressed.E-mail: kkeiler@physnet.uni-hamburg.de and pschmelc@physnet.uni-hamburg.de**Keywords:** correlations, Bose–Einstein condensate, impurities, optical lattice, induced interactionOriginal content from this work may be used under the terms of the [Creative Commons Attribution 3.0 licence](https://creativecommons.org/licenses/by/4.0/).

Any further distribution of this work must maintain attribution to the author(s) and the title of the work, journal citation and DOI.

**Abstract**

We investigate the ground state properties of a lattice trapped bosonic system coupled to a Lieb–Liniger type gas. Our main goal is the description and in depth exploration and analysis of the two-species many-body quantum system including all relevant correlations beyond the standard mean-field approach. To achieve this, we use the multi-configuration time-dependent Hartree method for mixtures (ML-MCTDHX). Increasing the lattice depth and the interspecies interaction strength, the wave function undergoes a transition from an uncorrelated to a highly correlated state, which manifests itself in the localization of the lattice atoms in the latter regime. For small interspecies couplings, we identify the process responsible for this cross-over in a single-particle-like picture. Moreover, we give a full characterization of the wave function's structure in both regimes, using Bloch and Wannier states of the lowest band, and we find an order parameter, which can be exploited as a corresponding experimental signature. To deepen the understanding, we use an effective Hamiltonian approach, which introduces an induced interaction and is valid for small interspecies interaction. We finally compare the ansatz of the effective Hamiltonian with the results of the ML-MCTDHX simulations.

1. Introduction

Nowadays, ultracold gases stand out due to the high degree of controllability, especially of trapping potentials and inter-atomic interactions. Thereby, capturing the atoms of a gas by using light fields allows for the realization of a variety of even rather complex many-body systems. Especially one-dimensional (1D) systems are under intense investigation and show unique properties [1, 2]. Here, the inverse scaling of the effective interaction strength to the density allows for entering the strongly correlated regime in the dilute regime [3, 4]. Moreover, the transversal confinement allows for a tuning of the interaction strength among the atoms via a so-called confinement induced resonance [5]. Alternatively, the same effect could be achieved via an atom-molecule Feshbach resonance [6]. This freedom of adjusting the interaction strength makes it feasible to enhance the deviation from the mean-field behavior of the bosons, in a very controlled and systematic manner. Therefore, 1D ultracold gases are particularly suited to access physical regimes, in which effective free theories cease to be valid. Such strongly interacting Bose gases tend to be very sensitive to additional external trapping potentials such as lattices [7, 8]. Here, a Mott insulating state can be formed for arbitrarily weak lattice amplitudes, in contrast to the conventional superfluid to Mott insulator transition [9, 10].

Correlations can not only appear within one type of species, but in particular between different bosonic species [11, 12], offering a rich phenomenology. Due to the fact that we add to the already present intra-species interactions in the respective subsystems an interspecies interaction, mixtures show a plethora of intriguing phenomena, such as pair-tunneling effects [13, 14] and paired superfluidity [15, 16]. Setups of impurities in a bath can be viewed as such a species mixture, covering the aspects mentioned above, and are a subject of ongoing research. They have been studied in various cases, e.g. the transport and the related collisions of the impurity

through the bath [17] and correlation effects due to the entanglement of the species [18]. In particular, 1D impurity-bath systems exhibit large interaction effects, bringing to light many peculiar phenomena [19–23]. In addition, impurities in Bose–Einstein condensates (BECs) can be exploited as a quantum simulator for polaron physics [25, 24, 26]. One of the first theoretical descriptions of polarons, including phonon clouds, was introduced by Fröhlich [27]. Since then a lot of progress has been made in the limiting cases of weak [28, 29] and strong electron–phonon coupling [30]. While the ongoing theoretical study of 1D polarons [31–35] has predicted a lot of intriguing properties, recent experiments [17, 23, 36, 37] have finally opened the door to the implementation of 1D polaronic systems, providing a deeper understanding of 1D polarons. When immersing more than one impurity in the bath, an induced interaction among the polarons appears, which counteracts the repulsive interaction among the impurities. The description in terms of polarons is in general of major interest for the understanding of the electron–phonon coupling in condensed matter physics. In order to manipulate impurities in a controlled, systematic way in ultracold physics, it would be useful to load the impurities first in a lattice, which is in turn inserted into the bath, since lattices allow for single-site excitation as well as collective excitations. To some extent, such a setup has been investigated in the tight-binding limit recently [38–40], where the authors especially focussed on the behavior of the combined systems under the influence of increasing temperature, e.g. the clustering of polarons in the wells of the lattice due to an attractive induced interaction in dependence of the temperature.

In the present work, we focus on the role of interspecies correlations of lattice trapped atoms immersed in a Lieb–Liniger gas, and in particular how it impacts the structure of the many-body wave function. After a brief description of the specific system under investigation, we present the phenomenology of the ground state as a function of the lattice trap depth and interspecies interaction strength. Via the introduction of a correlation measure, we can identify a cross-over diagram exhibiting a transition from an uncorrelated to a strongly correlated state. We unravel the nature of the cross-over in an effective single-particle picture for small interspecies couplings. Moreover, we give a full characterization of the wave function in the limiting cases of weak and strong correlations. This enables us to derive and understand the properties of the ground state, employing the structural form for the ground state wave function. Finally, we aim at describing the correlated state using an effective Hamiltonian approach [41], thereby introducing an induced attractive interaction between the atoms trapped by the lattice, as well as an induced hopping. We find qualitative agreement with the full multi-configuration time-dependent Hartree method for bosonic (fermionic) mixtures (ML-MCTDHX) calculations and identify the weak interspecies interaction regime, to which this effective approach is applicable.

2. Setup, Hamiltonian and methodology

Our system consists of bosons trapped in a 1D lattice with periodic boundary conditions, which is immersed in a Lieb–Liniger-like gas [42–44] of a second species of bosons. We note that this setup lies within reach of current experimental techniques, since beyond controlling the dimensionality, various trapping potentials for the atoms can be achieved [45], including in particular 1D ring geometries. Moreover, it is possible to create an optical lattice potential, which does not affect the Lieb–Linger gas by choosing the right laser wavelengths and atomic species [46]. This allows for the creation of a two-component system with each species trapped individually on the same ring geometry. In the following, the species trapped by a lattice potential will be denoted as the A species, whereas the Lieb–Liniger-like gas refers to the B species. Furthermore, we introduce a coupling Hamiltonian \hat{H}_{AB} between the two species. Both subsystems are confined to a longitudinal direction, accounting for the 1D character, and excitations in the corresponding transversal direction can be neglected. This finally results in a Hamiltonian of the form $\hat{H} = \hat{H}_A + \hat{H}_B + \hat{H}_{AB}$. The Hamiltonian of the A species reads

$$\hat{H}_A = \int_0^L dx \hat{\chi}^\dagger(x) \left[-\frac{\hbar^2}{2m_A} \frac{d^2}{dx^2} + V_0 \sin^2(\pi kx/L) \right] \hat{\chi}(x), \quad (1)$$

where $\hat{\chi}^\dagger$ is the field operator of the lattice bosons, m_A their mass, k the number of wells in the lattice and L is the circumference of the ring. We focus on the regime, where interactions among the lattice atoms can be neglected, setting $g_{AA} = 0$. The B species is described by the Hamiltonian of the Lieb–Liniger model

$$\hat{H}_B = \int_0^L dx \hat{\phi}^\dagger(x) \left[-\frac{\hbar^2}{2m_B} \frac{d^2}{dx^2} + g_{BB} \hat{\phi}^\dagger(x) \hat{\phi}(x) \right] \hat{\phi}(x), \quad (2)$$

where $\hat{\phi}^\dagger$ describes the field operator of the Lieb–Liniger gas atoms, $g_{BB} > 0$ is the interaction strength of the two-body contact interaction among the B species and m_B the mass of the B species atoms. Moreover, we assume equal masses for the species $m_A = m_B$. The coupling between the species is given by

$$\hat{H}_{AB} = g_{AB} \int_0^L dx \hat{\chi}^\dagger(x) \hat{\chi}(x) \hat{\phi}^\dagger(x) \hat{\phi}(x). \quad (3)$$

Throughout this work we consider a triple-well and we focus on the scenario of small particle numbers with three lattice atoms $N_A = 3$ and ten atoms in the Lieb–Liniger gas $N_B = 10$. The interaction among the latter atoms is set to a value where the depletion is negligible in case of no interspecies coupling, i.e. $g_{BB}/E_R \lambda = 6.8 \times 10^{-3}$, with $E_R = (2\pi\hbar)^2/2m_A \lambda^2$ being the recoil energy and $\lambda = 2L/k$ the optical lattice wavelength. Therefore, we view the Lieb–Liniger gas as a BEC, in which impurities of species A are immersed. In particular, we shall analyze the ground state of the coupled system for different values of the repulsive interspecies interaction strength g_{AB} and the lattice depth V_0 .

Our numerical simulations are performed with the *ab initio* ML-MCTDHX [47–49], which takes all correlations into account and therefore allows for going beyond the lowest-band and tight-binding approximation for the lattice system and beyond the Bogoliubov approximation for the BEC. Within ML-MCTDHX one has access to the complete many-body wave function which allows us consequently to derive all relevant characteristics of the underlying system. Besides investigating the quantum dynamics it allows us to calculate the ground (or excited) states. Compared to the standard approach for solving the time-dependent Schrödinger equation, where one constructs the wave function as a superposition of time-independent basis states with time-dependent coefficients, the ML-MCTDHX approach considers a co-moving time-dependent basis on different layers in addition to time-dependent coefficients. This leads to a significantly smaller amount of basis states that are needed to obtain an accurate description and eventually reduces the computation time. Moreover, the multi-layering of the method allows for a construction of the total wave function $|\Psi\rangle$, as sum of species product states, using the Schmidt decomposition [50]

$$|\Psi\rangle = \sum_i \sqrt{\lambda_i} |\Psi_A^i\rangle \otimes |\Psi_B^i\rangle. \quad (4)$$

With the aid of this wave function decomposition, we are able to characterize and introduce interspecies correlations in a controlled and systematic manner. The case of a single contributing product state in the sum we call the species mean-field case, whereas deviations from it indicate interspecies correlations. The reader should note that the species mean-field is not to be confused with the Gross–Pitaevskii mean-field, which restricts the orbitals in each subsystem to a single one. In contrast to that, subsystems in the species mean-field case are allowed to carry arbitrary correlations and may be described by many contributing (optimized) orbitals.

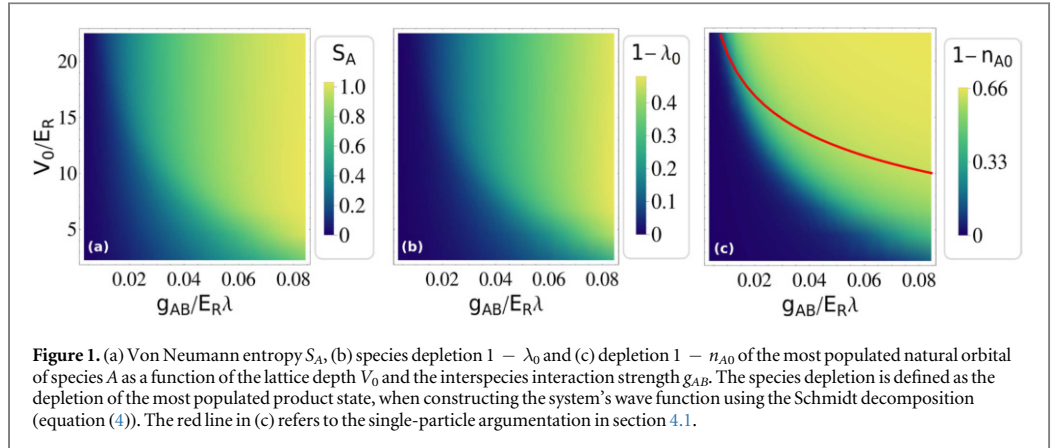
3. Ground state transition

In the following, we investigate ground state properties of our system for different values of the lattice depth and the interspecies interaction strength, strongly focussing on intra- and interspecies correlations, that appear beyond mean-field. Thereby, we view the A species as an impurity species which is immersed into a homogeneous background gas. In the case of $g_{AB} = 0$ both subsystems can be described separately and no interspecies correlations appear in the system's ground state. For the lattice atoms, this means that each atom occupies the energetically lowest Bloch state, and is therefore delocalized, since $g_{AA} = 0$. Increasing the coupling strength $g_{AB} > 0$, disturbs this uncorrelated state. As a measure for correlations, we consider the eigenvalues n_{Ai} and eigenvectors $|n_{Ai}\rangle$ of the one-body density operator $\hat{\rho}_A^{(1)}$ of the A species⁴, i.e. the natural populations and natural orbitals [51–53]. The one-body-density operator is defined as the partial trace of the density operator $\hat{\rho} = |\Psi\rangle\langle\Psi|$, $|\Psi\rangle$ being the ground state wave function, over all particles except for one particle of the A species

$$\hat{\rho}_A^{(1)} = \text{Tr}_{N_B, N_A-1}[\hat{\rho}] = \sum_i n_{Ai} |n_{Ai}\rangle\langle n_{Ai}|, \quad (5)$$

where $\sum_i n_{Ai} = 1$. In the case of a single non-zero eigenvalue equalling unity ($n_{A0} = 1$), the particles in subsystem A can be considered as uncorrelated, while deviations from this value indicate correlations. In figure 1(c), we plot the depletion $1 - n_{A0}$ of the most populated natural orbital. As can be seen for small values of V_0 and g_{AB} , the depletion is approximately zero, describing a state which shows no significant correlations for the atoms of species A . Increasing the lattice depth or interspecies interaction strength leads to a stronger deviation from the mean-field behavior. The greenish area indicates the transition between an uncorrelated and a correlated ground state. In the yellow region, a correlated state with a depletion of $1 - n_{A0} = 2/3$ is reached. Interestingly, we find here that only two other natural orbitals become significant, whose populations saturate for deep lattices and strong interspecies interaction to $n_{A1} = n_{A2} = 1/3 = n_{A0}$, leading to a triple degeneracy. In order to see that this effect is due to physics beyond the species mean-field picture, it is useful to analyze the von Neumann entropy

⁴ We are well aware of the fact that fragmentation might also occur in the case of a ground state wave function, which can be represented by a single product state in the species mean-field. In order to be precise, one has to take additionally the species depletion or von Neumann entropy into account.



$$S_A = -\text{Tr}[\hat{\rho}_A \ln(\hat{\rho}_A)] \quad \text{and} \quad \hat{\rho}_A = \text{Tr}_{N_B}[\hat{\rho}] \quad (6)$$

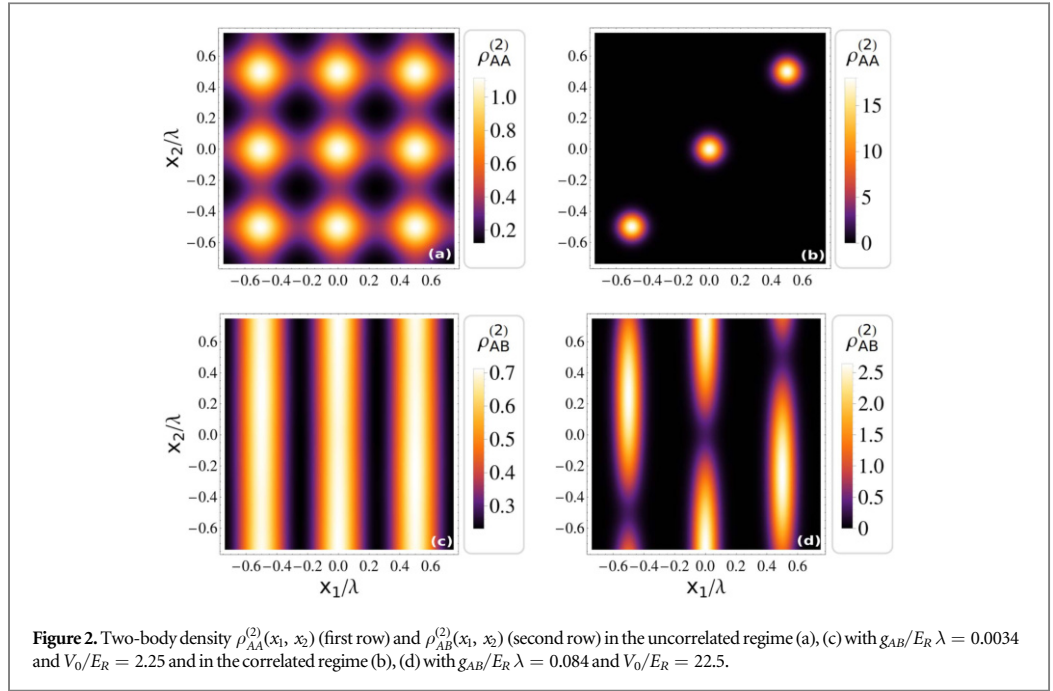
for the subsystem A in the different regimes. Here, $\hat{\rho}_A$ is defined as the trace of the density operator over all particles of the B species. In case the A species is in a pure state, the entropy S_A equals zero, whereas a mixed state will lead to deviations from zero. In figures 1(a) and (b), it becomes clear that for high lattice depth and interspecies interaction strength the wave function of the coupled system can no longer be described by a product ansatz of the subsystems. Hence, a species mean-field description is not valid and one has to go beyond it. In the representation of the wave function by a sum of products of species functions (equation (4)), two additional degenerate product states (w.r.t. λ_i) become important. For large values of V_0 and g_{AB} the interspecies correlations are dominant, such that the contribution of these product states is of the same order as the previously, i.e. for smaller values of V_0 and g_{AB} , dominant one, resulting in a strongly entangled state. In order to understand the physical processes behind the transition from an uncorrelated to a correlated state, one naturally as a first step would investigate the spatial density profile, i.e. the one-body density, of the species A . While expecting a change in the spatial atomic density distribution with varying V_0 , what we indeed find is a comparatively minor change of the density profile crossing the transition region of the cross-over diagram with only slightly enhanced localization in the wells due to a deeper lattice. Instead, the effect of correlations can be observed in the two-body density

$$\rho_{AA}^{(2)}(x_1, x_2) = \text{Tr}_{N_B, N_A-2}[\hat{\rho}], \quad (7)$$

which describes the probability of finding one lattice atom at the position x_1 and another one at x_2 . We note here, that all appearing densities are normalized to unity. In figure 2, a drastic difference of the distribution of the two-body density $\rho_{AA}^{(2)}(x_1, x_2)$ for the two regimes, identified in figure 1(c), is visible. In the uncorrelated state, the existence of a particle at the position x_1 has no effect on the measurement probability of a second lattice atom at x_2 , see figure 2(a). Moreover, here one can see that both lattice atoms are delocalized over the lattice, as it is expected in case of almost decoupled subsystems A and B . For higher values of the lattice depth and the interspecies interaction strength, the effect of correlations becomes evident, see figure 2(b). They manifest themselves in a localization of lattice atoms in the wells. In other words, a detection of an atom in any well is followed by a definite second measurement of another atom in that same well. Please note that this effect is not due to direct (attractive) interaction among the lattice atoms, since the latter is set to zero. Instead, here it is the interspecies interaction with the B species atoms, which induces these correlations to the A atoms. Moreover, as we have already discussed above in the context of figure 1(b), also interspecies correlations are present in the strongly correlated regime suggesting the two-body density

$$\rho_{AB}^{(2)}(x_1, x_2) = \text{Tr}_{N_B-1, N_A-1}[\hat{\rho}], \quad (8)$$

as a valuable observable. The latter describes the probability of finding one lattice atom at the position x_1 and a B atom at position x_2 . In figure 2(c), we find for an almost decoupled system that an initial measurement of a lattice atom has no visible impact on the distribution of a B atom. However, in the correlated regime (figure 2(d)) the probability of measuring a B atom at the same position as the lattice atom drops to zero. In conclusion, the correlated state can be understood as a localization of A atoms while expelling the B atoms from the position of the latter. Since all wells are energetically equivalent, this holds for each well.



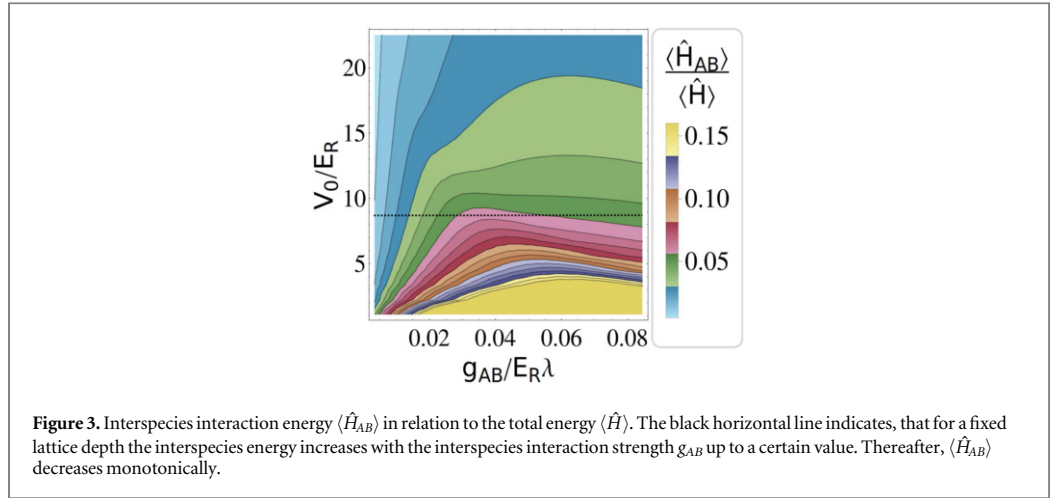
4. Physical mechanisms and state characterization

In this section, we explore the physical mechanisms underlying the ground state transition described in the previous section. Firstly, we focus on the regime of small interspecies interaction strengths, thereby comparing the interspecies interaction energy with the width of the first Bloch band. We provide then a full characterization of the system's wave function in terms Wannier states and derive the relevant observables. Finally, we use the transformation of the Hamiltonian into the so-called Nakajima frame, in order to calculate the ground state in an effective model approach. This will help us to develop an understanding for the complex many-body physics in a simplified picture, based on induced interactions.

4.1. Mechanism of the transition

As stated above, the localization of the lattice atoms of the A species, reminiscent of the phase separation of two Bose gases [55], is solely induced by the interaction with the BEC of B atoms. Therefore, we should observe a change of the interspecies interaction energy, which is defined as the expectation value $\langle \hat{H}_{AB} \rangle$ with respect to the ground state, for increasing lattice depth and interspecies interaction strength. For a fixed lattice depth, it turns out that instead of monotonously increasing with the interaction strength g_{AB} , the interspecies energy reaches a maximum at a certain value of g_{AB} and decreases for even higher values of g_{AB} (figure 3). Interestingly, the points of maximal $\langle H_{AB} \rangle$ in the cross-over diagram appear in the transition region where correlations become important (see figure 1(c)). Hence, the formation of correlations is connected to a reduction of the interspecies energy. The eigenstates of a single atom in a periodic potential are the Bloch states [54], which can be grouped into bands. For the case of three lattice sites with periodic boundary conditions, the lowest band consists of an energetically lowest Bloch state and two degenerate excited states. In the previous section, we have seen that in the uncorrelated regime ($g_{AB} \approx 0$) the atoms of the A species are delocalized over the lattice, which is due the fact that each of them occupies exactly the energetically lowest Bloch state for $g_{AB} = 0$. In the correlated regime, the ground state exhibits a localization of the A atoms. We can now interpret this localization as a superposition of the Bloch states of the first band, resulting, as a matter of fact, in principal in a Wannier state. Therefore, we now aim at an explanation for the responsible mechanism in a single-particle-like picture. Based on the findings above, we assume that the reduction of the interspecies energy is related to a coupling of the Bloch states in the first band. Without any correlations between the species, using a product ansatz $|\Psi_{\Pi}\rangle = |\Psi_A\rangle \otimes |\Psi_B\rangle$, the interspecies energy is determined by the integral over the product of one-body densities of each subsystem

$$\langle \Psi_{\Pi} | \hat{H}_{AB} | \Psi_{\Pi} \rangle = g_{AB} N_A N_B \int_0^L dx \rho_A^{(1)}(x) \rho_B^{(1)}(x). \quad (9)$$



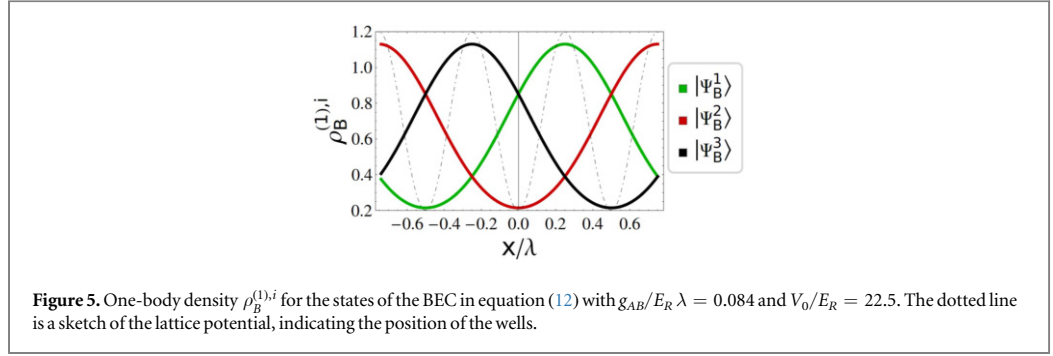
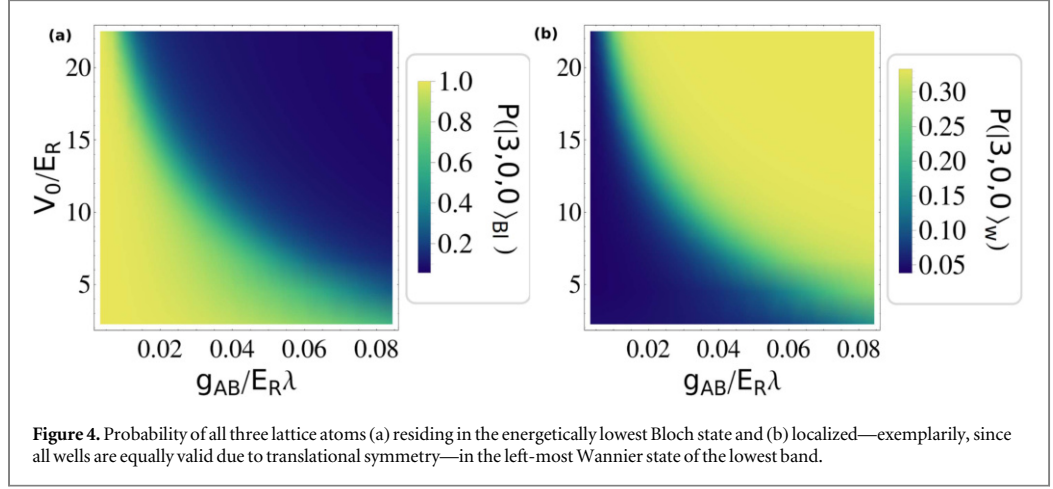
This ansatz works well in the uncorrelated regime, where almost no interspecies correlations are present. We observe that the one-body density of the B species exhibits rather small modulations, compared to the modulations of the one-body density of the A species (not shown here). The latter is due to the fact that $\rho_B^{(1)}(x)$ is approximately homogeneous, which further approximates the interspecies energy to $\langle \Psi_{\Pi} | \hat{H}_{AB} | \Psi_{\Pi} \rangle = g_{AB} N_A N_B / L$. In a single-particle picture, we now argue that this interspecies energy per particle (of the A and B species) g_{AB}/L is used, in order to excite a lattice atom occupying the energetically lowest Bloch state to one of the excited states in the first band. We use this as an estimation for the transition region and therefore search for the interaction strength g_{AB} that leads to an interspecies energy per particle, equalling the band width for a given lattice depth V_0 , i.e. being sufficiently large for this excitation process. In figure 1(c), we find that for small values of g_{AB} the resulting curve (red) describes the phase border appropriately. For larger values this curve fails to describe the transition region indicating a break-down of the above given simple single-particle picture. We have seen that we can explain the onset of the transition from the uncorrelated state towards the strongly correlated state in a correlation-free effective single-particle picture for small g_{AB} , where sufficient interaction energy is supplied to excite the A species atoms within the first Bloch band.

4.2. State characterization

The fact that the two-body density suggests a localization of A atoms, paired with the possibility of excited Bloch states, motivates the following procedure. In this sense, it is intuitive to approximately describe the ground state in the correlated regime in terms of number states, spanned by the Wannier states of the lowest band. The Wannier states we employ are generalized ones, i.e. the eigenstates of the position operator projected onto the respective band [56, 57]. In order to find out, whether the localization in figure 2 can be understood in terms of a number state with all particles residing in the same Wannier state for the entire correlated regime, we calculate the projection of the ground state wave function $|\Psi\rangle$ on that number state of species A and sum over all configurations for the B species. The corresponding number state notation reads $|n_1, n_2, n_3\rangle_W$, where n_i denotes the number of particles in the corresponding Wannier states sorted from the left to the right well. We proceed in the same manner for the case of number states, which are spanned by Bloch states in the lattice potential. The corresponding state reads $|n_1, n_2, n_3\rangle_{Bl}$, where n_1 refers to the energetically lowest Bloch state, while n_2 and n_3 refer to the two degenerate excited ones in the first Bloch band. The probability of finding the ground state in a number state $|\vec{n}^A\rangle$ of the subsystem A is then defined as

$$P(|\vec{n}^A\rangle) = \sum_i |\langle \vec{n}_B^i | \otimes \langle \vec{n}^A | \Psi \rangle|^2, \quad (10)$$

where $\{|\vec{n}_B^i\rangle\}$ describes any number state basis set for the subsystem B with fixed particle number. For an uncorrelated state, we expect all the lattice atoms to reside in the energetically lowest Bloch state of the first band, since $g_{AA} = 0$. In figure 4(a) we find, that in the uncorrelated regime the probability for all lattice atoms to be in the lowest Bloch state is $P(|3, 0, 0\rangle_{Bl}) = 1$. Compared to that, the probability for all particles to be e.g. in the left Wannier state is $P(|3, 0, 0\rangle_W) = \frac{1}{27}$, which can be derived analytically for $g_{AB} = 0$. Increasing the values of the lattice depth and interspecies interaction strength, the energetically lowest Bloch number state gets depopulated. Instead, the lattice atoms strongly populate the Wannier number state, saturating towards a value for the probability of $P(|3, 0, 0\rangle_W) = \frac{1}{3}$. Due to translational symmetry this is true for all number states with all lattice atoms residing in the same well, meaning $P(|3, 0, 0\rangle_W) = P(|0, 3, 0\rangle_W) = P(|0, 0, 3\rangle_W) = \frac{1}{3}$. To summarize, for small values of g_{AB} and V_0 the energetically lowest Bloch state is occupied by all A atoms, whereas for large



values the correlated state is a superposition of number states, where all A atoms occupy the same Wannier state, implying their clustering in the corresponding wells. Now that we know more about the structure of the system's wave function, we are able to specify the wave function in the corresponding regimes. In the uncorrelated regime, the ground state reads

$$|\Psi\rangle_{uc} \approx |3, 0, 0\rangle_{BI} \otimes |\Psi_B\rangle, \quad (11)$$

where $|\Psi_B\rangle$ is the ground state of the Hamiltonian \hat{H}_B . Based on the projection of the ground state for the correlated regime onto the respective number states (figure 4(b)), the wave function is of the form

$$|\Psi\rangle \approx \frac{1}{\sqrt{3}} [|3, 0, 0\rangle_W \otimes |\Psi_B^1\rangle + |0, 3, 0\rangle_W \otimes |\Psi_B^2\rangle + |0, 0, 3\rangle_W \otimes |\Psi_B^3\rangle], \quad (12)$$

where $\{|\Psi_B^i\rangle\}$ are non-orthogonal basis states for the B species. Measuring a lattice atom in a specific well, we then know that all the other lattice atoms will be in that same well. Additionally, measuring the subsystem A to be in well i implies a collapse of the ground state onto a definite wave function $|\Psi_B^i\rangle$ for the B species. Due to the repulsive interspecies interaction the density $\rho_B^{(1),i} = \text{Tr}_{N_B-1} [|\Psi_B^i\rangle \langle \Psi_B^i|]$ exhibits a minimum at the well where the A atom was measured, shown in figure 5. Employing the structural form of the wave function given by equation (12), we can now derive the observed one- and two-body density of the A species atoms discussed above, using the Wannier states $|w_i\rangle$, where the index i corresponds to the localization in the i th well. We obtain

$$\hat{\rho}_A^{(1)} = \frac{1}{3} \left[\sum_{i=1}^3 |w_i\rangle \langle w_i| \right] \quad \text{and} \quad (13)$$

$$\rho_{AA}^{(2)}(x_1, x_2) = \frac{1}{3} \left[\sum_{i=1}^3 |w_i(x_1)|^2 |w_i(x_2)|^2 \right]. \quad (14)$$

Now, it is obvious that the natural populations of $\hat{\rho}_A^{(1)}$ are degenerate, equalling $\frac{1}{3}$, in the correlated regime. The spatial structure of the two-body density $\rho_{AA}^{(2)}$ is governed by the overlap of the density of equal Wannier states in that regime. This corresponds to a two-dimensional representation of the Wannier states, so that one arrives at a localized structure in the two-body density (figure 2(b)).

Table 1. Variance of the particle number operator $\hat{n}_i = \hat{a}_i^\dagger \hat{a}_i$ for a specific site i .

	$(\Delta n_i)^2$
Uncorrelated regime	$\frac{2}{3}$
Correlated regime	2
Mott insulator	0

Above, we have identified the natural populations of the A species as a quantity, which reflects the transition from the correlated to the uncorrelated regime. While for our specific scenario it is sufficient for the characterization of the two regimes, other states, such as the Mott insulator state, cannot be distinguished from the correlated state. The latter shows the same behavior in terms of natural populations as the A species in the correlated regime. Therefore, we cannot distinguish the Mott insulator state from the ansatz in equation (12), using only the natural populations. Instead, it is useful to consider the variance of the particle number operator $\hat{n}_i = \hat{a}_i^\dagger \hat{a}_i$ for a specific site i , where \hat{a}_i^\dagger is the creation operator for creating a lattice atom in the i th Wannier state. Using the respective wave function ansatz, we can derive the variances $(\Delta n_i)^2 = \langle \hat{n}_i^2 \rangle - \langle \hat{n}_i \rangle^2$ for the different states. In table 1, we see that the particle number variances differ strongly for the three states, allowing for a clear assignment and identification. Therefore, $(\Delta n_i)^2$ can be exploited as an experimental signature for the different states and thus also for correlations, since it is accessible via quantum gas microscopy [58, 59].

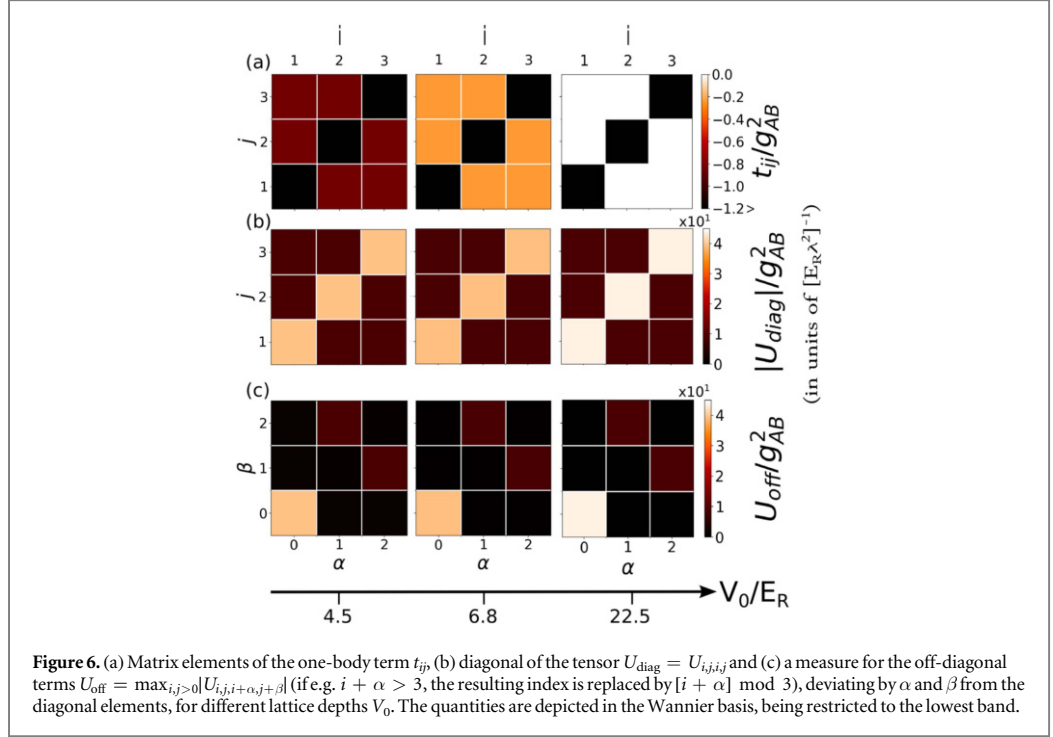
4.3. Induced interaction

In subsection 4.1, we have described the transition region for small interspecies interaction strengths in terms of a coupling of Bloch states induced by the interspecies interaction. However, it is possible to gain a deeper understanding of the localization of A atoms, introducing an effective Hamiltonian for the A species which exhibits an induced interaction and an induced hopping term. With the aid of these, we will discuss the effective attractive interaction among the A species. The effective description in terms of an induced impurity–impurity interaction is a topic of ongoing research, ranging from Casimir-like forces between static impurities [60, 61] to the inclusion of correlation effects for mobile impurities [62, 63]. In order to arrive at an effective Hamiltonian, we need to apply the Nakajima transformation and use the Bogoliubov approximation for the B species, which finally decouples the subsystems [64–66]. We note that due to the non-unitarity of the transformation, in general observables are not invariant under the transformation. Setting $\hbar = L = m_{A/B} = 1$, the effective Hamiltonian \hat{H} in the transformed frame reads

$$\begin{aligned} \hat{H} &= \hat{H}_0 + \hat{V}_{\text{ind}} \quad \text{where,} \\ \hat{V}_{\text{ind}} &= \frac{1}{2} \sum_{k,q,k',q'} U_{k,k',q,q'} \hat{a}_k^\dagger \hat{a}_{k'}^\dagger \hat{a}_q \hat{a}_{q'} \quad \text{and} \\ \hat{H}_0 &= \sum_k \epsilon_k \hat{a}_k^\dagger \hat{a}_k + \sum_i \omega_i \hat{b}_i^\dagger \hat{b}_i + \sum_{kq} t_{kq} \hat{a}_k^\dagger \hat{a}_q, \end{aligned} \quad (15)$$

with $U_{k,k',q,q'} = \sum_i \left[\frac{g_i^{kq'} (g_i^{qk})^*}{\epsilon_k - \epsilon_q - \omega_i} - \frac{g_i^{kq} (g_i^{qk'})^*}{\epsilon_k - \epsilon_q + \omega_i} \right]$ and $t_{kq} = \frac{1}{2} \sum_r U_{rkqr}$. The derivation of \hat{H} can be found in the appendix. \hat{a}_k^\dagger is the creation operator for a particle in the Bloch state $|\chi_k\rangle$ with energy $\epsilon_k^{(1)}$, while $\epsilon_k = \epsilon_k^{(1)} + g_{AB}$, and \hat{b}_i^\dagger the one for the Bogoliubov mode v_i^* . The matrix elements $g_i^{kq} = \sqrt{N_B} g_{AB} \langle \chi_k | u_i(x) + v_i(x) | \chi_q \rangle$ can be interpreted as a coupling of Bloch states, mediated by Bogoliubov modes. This coupling is resonantly enhanced, when the band width $\epsilon_k - \epsilon_q$, assuming $k \neq q$ and restricting to the lowest band, matches the energy of a Bogoliubov mode ω_i . On top of the induced interaction \hat{V}_{ind} , an additional one-body term, having the character of a hopping term with hopping elements t_{kq} , occurs in the Hamiltonian. The ground state of the total wave function is a product state of the ground state of the Bogoliubov Hamiltonian and the ground state of the residual Hamiltonian, consisting of the induced terms and \hat{H}_A . We can now easily calculate the ground state for the B species, which is given by the Bogoliubov vacuum. The calculation for the lattice A species is simplified, since there is no direct coupling to the B species. For all the upcoming considerations we restrict everything to the lowest band and set an upper-bound for the energy of the Bogoliubov modes. Before calculating the ground state for the A species, we analyze the tensor elements $U_{k,k',q,q'}$ and hopping elements t_{kq} , thereby gaining an understanding of the induced attractive interaction.

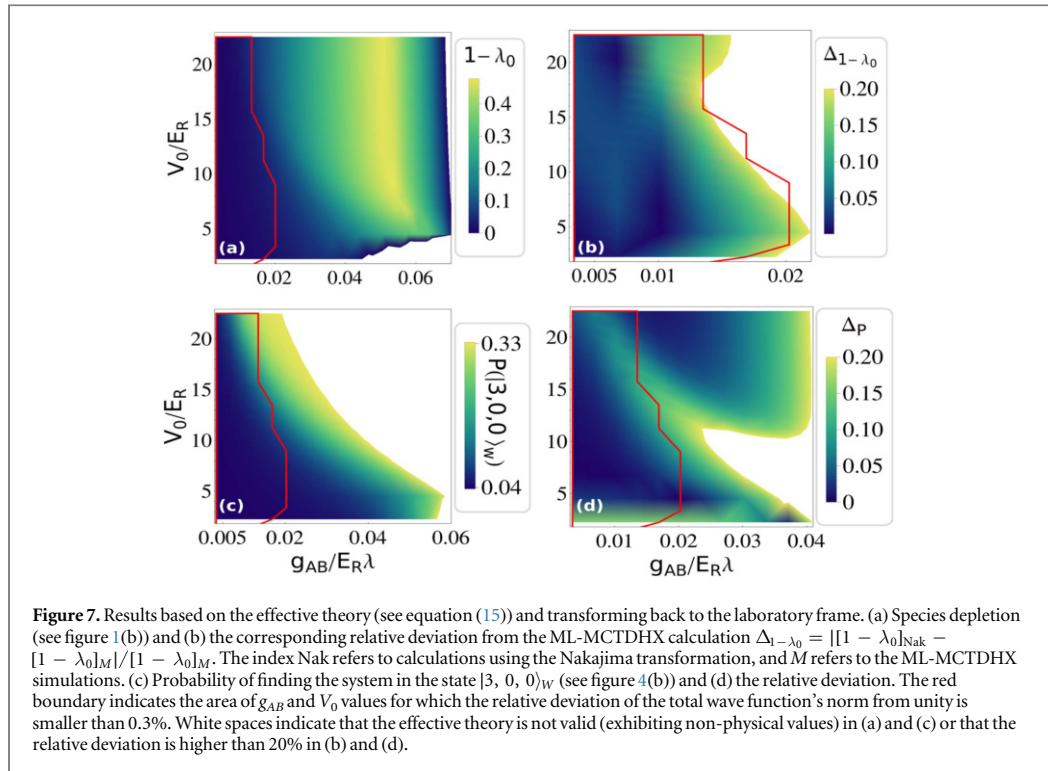
In figure 6 we show the diagonal elements and a measure for the off-diagonal elements of the tensor U , as well as the induced hopping terms t_{ij} for different values of the lattice depth. In figures 6(b)–(c) we can see that the dominant elements are those for equal indices ($U_{i,i,i,i}$), followed by diagonal terms with respect to the particles ($U_{i,j,i,i}$). The particle exchange symmetry and the spatial translation symmetry is also reflected in the figures. All the



other elements, which are off-diagonal, have almost no contribution compared to the diagonal terms. Moreover, for increasing V_0 the elements $U_{i,i,i,i}$ corresponding to the operator $\hat{a}_i^\dagger \hat{a}_i^\dagger \hat{a}_i \hat{a}_i = \hat{n}_i(\hat{n}_i - 1)$, become larger. Since this element is negative and the most dominant one, the total term $U_{i,i,i,i} \hat{n}_i(\hat{n}_i - 1)$ suggests an attractive on-site interaction among the A species. Still, we cannot make any definite statements concerning the structure of the wave function, based solely on the tensor elements $U_{i,j,k,l}$. Instead, it is useful to additionally analyze the behavior of the matrix elements of the one-body term t_{ij} for different lattice depths. Here, the off-diagonal terms are of interest, since they describe an induced hopping, whereas the diagonal elements just form an energetic offset. In figure 6(a) we observe that the hopping tends towards zero for increasing V_0 , which can be viewed as an indicator for the localization of the lattice atoms in this transformed frame.

Now, one might expect that the ground state for the subsystem A will consist of localized lattice atoms for large lattice depths and interspecies interaction strengths. But since the above analysis is performed in the transformed frame, we finally have to transform back to the laboratory frame. In order to obtain the ground state of the coupled two-species system, we do the following: firstly, we determine the ground state of the subsystem A , by performing a diagonalization of the Hamiltonian $\hat{H} - \sum_i \omega_i \hat{b}_i^\dagger \hat{b}_i$ in the number state basis, spanned by the Wannier states of the lowest band. The ground state of the subsystem B is given by the Bogoliubov vacuum. The total ground state, consisting of a tensor product of both subsystem ground states, we transform back to the laboratory frame by applying the operator $\exp(-\hat{S}) \approx 1 - \hat{S} + \hat{S}^2/2$ (see appendix) to the total ground state up to second order. This is motivated by our initial assumption of small interactions, where terms of \hat{S} which are higher than second order in g_{AB} are neglected. Finally, we compute the probability of finding the ground state in the number state $|3, 0, 0\rangle_W$, spanned by lowest band Wannier states, as well as the species depletion. Both quantities are available exactly within the ML-MCTDHX approach, being quantitatively well converged for all interspecies interaction strengths and lattice depths we investigated. For the calculations using the detour via the transformed frame, we expect appropriate results for small interspecies interaction strengths. Figure 7 shows the above-mentioned quantities and compares with the results of the ML-MCTDHX simulations in terms of a relative deviation.

At first glance, the species depletion in figure 7(a) resembles the one in figure 1(b) up to an interspecies interaction strength of $g_{AB}/E_R \lambda \approx 0.05$. However, this resemblance is solely of qualitative nature, which becomes obvious in the relative deviation (figure 7(b)). Here, we see a quantitative difference of the two methods, being of the order of up to 20% for a maximum value of $g_{AB}/E_R \lambda \approx 0.02$. A relative deviation of 20% corresponds to a relative deviation of $|\langle \Psi | \Psi \rangle_{Nak} - 1| \approx 0.3\%$ —due to the non-unitarity of the transformation—for the total wave function's norm from unity, where $|\Psi\rangle_{Nak}$ is the ground state wave function calculated by the effective approach. Also, the behavior of the probability of finding the ground state in the number state $|3, 0, 0\rangle_W$ (figure 7(c)) qualitatively agrees with the results obtained by the ML-MCDTHX method, but again



quantitatively deviates for large enough g_{AB} . But here, the range of validity w.r.t. the domains of g_{AB} and V_0 values is more extended. Nevertheless, both the species depletion as well as the probability show the same qualitative behavior we observe for the corresponding ML-MCTDHX results. In particular, with this effective Hamiltonian approach the cross-over diagram could be qualitatively reproduced for the uncorrelated regime, extending towards the border of the transition region and thereby indicating the latter.

5. Conclusions

In the present paper we have investigated the appearance of correlations of a lattice trapped bosonic species coupled to a BEC. We have found a transition from an uncorrelated to a highly correlated state and characterized the associated quantum states from a many-body perspective. This transition is driven by interspecies correlations, bringing the system from an uncorrelated to a strongly correlated state. For small interspecies couplings we identified the transition region by energetic and mean-field arguments. Furthermore, we deduced expressions for the full system wave function for both regimes, using a Wannier and a Bloch basis analysis. In the uncorrelated state, the A atoms populate the lowest Bloch state and the B atoms are approximately homogeneously spread. In contrast, the correlated state is a superposition of states where all A atoms cluster together in this well, while the B atoms are expelled from it. In order to measure the transition and in particular the correlated state, we propose to use the variance of the number of particles per well as an experimental signature and order parameter for correlations. Alternatively, we calculated the ground state, using the transformation into the Nakajima frame, which is valid for small interspecies couplings. With this ansatz, we could reproduce only a small portion of the cross-over diagram for small lattice depths and interspecies interaction strengths, but gained a deeper insight into the role of induced interactions and induced hoppings for the process of localization. Eventually, this also demonstrated the uniqueness and power of the ML-MCTDHX method, which allowed—compared to the effective Hamiltonian ansatz—for calculations far beyond the mean-field approach. This analysis is also applicable for a larger number of particles in the environment, while still remaining in the few particle regime (we have tested this for $N_b \in [10, 30]$), resulting in the same transition from an uncorrelated to a correlated state. However, such a particle increase will also increase the attractive induced interaction for a given choice of V_0 and g_{AB} , thereby shifting the transition region.

The understanding of the cross-over in terms of a localized states analysis and induced interactions serves as a perfect starting-point for even more complex setups. For example, when introducing more lattice atoms or a repulsive intra-species interaction g_{AA} , it is reasonable to assume that the cross-over diagram will exhibit

additional states with the number of bunched atoms at one site smaller than the total number of particles. Also the increase of the intra-species interaction strength g_{BB} and/or correspondingly N_B of the environment might lead to a more complex state, by coupling to the second Bloch band due to an increase of the interspecies interaction energy as a result of a smaller density modulation in the BEC. Furthermore, it is of particular interest how the correlated state will respond dynamically, for example to an external quench through the cross-over diagram. Especially, the possibility of reducing correlations dynamically by lowering the lattice depth is of immediate interest. Beyond that, also dynamically driven setups might exhibit particularly interesting effects, such as persistent currents [67] induced by the interspecies interaction.

Acknowledgments

The authors acknowledge fruitful discussions with J Schurer, J Chen and M Pyzh. PS gratefully acknowledges funding by the Deutsche Forschungsgemeinschaft in the framework of the SFB 925 ‘Light induced dynamics and control of correlated quantum systems’. SK and PS gratefully acknowledge support for this work by the excellence cluster ‘The Hamburg Centre for Ultrafast Imaging-Structure, Dynamics and Control of Matter at the Atomic Scale’ of the Deutsche Forschungsgemeinschaft.

Appendix. Derivation of the effective Hamiltonian

The intra-species interaction among the BEC atoms triggers an excitation of Bogoliubov modes [68, 69], so that we can write the field operator for the subsystem of the B species as $\hat{\phi}(x) = \phi_0(x) + \delta\hat{\phi}$ with $\delta\hat{\phi} = \sum_p [u_p(x)\hat{b}_p + v_p^*(x)\hat{b}_p^\dagger]$. $\phi_0 = \sqrt{N_B}$ is the condensate mode, being spatially homogeneous and depending only on the number of BEC atoms. $u_p(x)$ and $v_p^*(x)$ are the Bogoliubov modes for a homogeneous BEC and \hat{b}_p^\dagger the respective creation operator. For the Hamiltonian of the B species this leads to the well-known effective Hamiltonian within the Bogoliubov approximation $\hat{H}_B = \sum_i \omega_i \hat{b}_i^\dagger \hat{b}_i$, setting $\hbar = L = m_{A/B} = 1$. Plugging this ansatz for $\hat{\phi}(x)$ into the expression of the interspecies coupling Hamiltonian \hat{H}_{AB} we arrive at the following expression

$$\hat{\Delta}_{AB} = g_{AB} \int_0^L dx \sum_i [f_i(x)\hat{b}_i + f_i^*(x)\hat{b}_i^\dagger] \hat{\chi}^\dagger(x) \hat{\chi}(x), \quad (\text{A.1})$$

with $f_i(x) = \phi_0^*(x)u_i(x) + \phi_0(x)v_i(x)$ and $\hat{\chi}^\dagger(x)$ the creation field operator for the A species. Here, we have neglected terms of the order $g_{AB}(\delta\hat{\phi})^2$, assuming that $(\delta\hat{\phi})^2 \ll |\phi_0|^2$ and $g_{AB}(\delta\hat{\phi})^2 \ll \delta\hat{\phi}$. This can be fulfilled for small interspecies interaction strengths and in the case of a small number of Bogoliubov mode excitations. Representing $\hat{\chi}^\dagger(x)$ in terms of Bloch states $\chi_k^*(x)$ with corresponding creation operators \hat{a}_k^\dagger , the Hamiltonian takes the form

$$\hat{H} \approx \sum_k \epsilon_k \hat{a}_k^\dagger \hat{a}_k + \sum_i \omega_i \hat{b}_i^\dagger \hat{b}_i + \sum_{i,k,q} [g_i^{kq} \hat{b}_i + (g_i^{qk})^* \hat{b}_i^\dagger] \hat{a}_k^\dagger \hat{a}_q, \quad (\text{A.2})$$

with $g_i^{kq} = g_{AB} \langle \chi_k | f_i(x) | \chi_q \rangle$ and $\epsilon_k = \epsilon_k^{(1)} + g_{AB}$ with the single particle energy $\epsilon_k^{(1)}$, corresponding to the k th Bloch state. We omit off-set energy terms in the Hamiltonian stemming solely from the mean-field $\phi_0(x)$. So far, we have rewritten the Hamiltonian using the Bogoliubov approximation. Now, we transform the Hamiltonian in order to decouple the subsystems, using a unitary transformation $\exp(-\hat{S})\hat{H}\exp(\hat{S})$ with \hat{S} being anti-hermitian. If we neglect terms which are higher than second order in g_{AB} , the transformation gives

$$\hat{\tilde{H}} = \hat{H}_0 + \frac{1}{2}[\hat{H}_1, \hat{S}]. \quad (\text{A.3})$$

Here, we assumed $[\hat{H}_0, \hat{S}] = -\hat{H}_1$ in order to cancel the two-body term in the Hamiltonian. This condition allows us to determine the operator \hat{S} . Making an ansatz, resembling the two-body term

$\hat{S} = \sum_{i,k,q} [x_i^{kq} g_i^{kq} \hat{b}_i + y_i^{kq} (g_i^{qk})^* \hat{b}_i^\dagger] \hat{a}_k^\dagger \hat{a}_q$, and determining x_i^{kq} and y_i^{kq} we arrive at the final Hamiltonian

$$\begin{aligned} \hat{\tilde{H}} &= \hat{H}_0 + \hat{V}_{\text{ind}} \quad \text{where,} \\ \hat{V}_{\text{ind}} &= \frac{1}{2} \sum_{k,q,k',q'} U_{k,k',q,q'} \hat{a}_k^\dagger \hat{a}_{k'}^\dagger \hat{a}_q \hat{a}_{q'} \\ \hat{H}_0 &= \sum_k \epsilon_k \hat{a}_k^\dagger \hat{a}_k + \sum_i \omega_i \hat{b}_i^\dagger \hat{b}_i + \sum_{kq} t_{kq} \hat{a}_k^\dagger \hat{a}_q, \end{aligned} \quad (\text{A.4})$$

with $U_{k,k',q,q'} = \sum_i \left[\frac{g_i^{k'q'} (g_i^{qk})^*}{\epsilon_k - \epsilon_{q'} - \omega_i} - \frac{g_i^{kq} (g_i^{q'k'})^*}{\epsilon_k - \epsilon_q + \omega_i} \right]$ and $t_{kq} = \frac{1}{2} \sum_r U_{rkqr}$. The transformation leads to a decoupling of the subsystems, thereby introducing an effective interaction term \hat{V}_{ind} for the A species.

References

- [1] Giamarchi T 2004 *Quantum Physics in One Dimension* (Oxford: Oxford University Press)
- [2] Cazalilla M A, Citro R, Giamarchi T, Orignac E and Rigol M 2011 *Rev. Mod. Phys.* **83** 1405
- [3] Kinoshita T, Wenger T and Weiss D S 2005 *Phys. Rev. Lett.* **95** 190406
- [4] Haller E, Hart R, Mark M J, Danzl J G, Reichsöllner L, Gustavsson M, Dalmonde M, Pupillo G and Nägerl H-C 2010 *Nature* **466** 597
- [5] Olshanii M 1998 *Phys. Rev. Lett.* **81** 938
- [6] Chin C, Grimm R, Julienne P and Tiesinga E 2010 *Rev. Mod. Phys.* **82** 1225
- [7] Büchler H P, Blatter G and Zwirger W 2003 *Phys. Rev. Lett.* **90** 130401
- [8] Lazarides A and Haque M 2012 *Phys. Rev. A* **85** 063621
- [9] Greiner M, Mandel O, Esslinger T, Hänsch T W and Bloch I 2002 *Nature* **415** 39
- [10] Jaksch D, Bruder C, Cirac J I, Gardiner C W and Zoller P 1998 *Phys. Rev. Lett.* **81** 3108
- [11] Modugno G, Ferrari G, Rosati G, Brecha R J, Simoni A and Inguscio M 2001 *Science* **294** 1320
- [12] Myatt C, Burt E, Ghrist R, Cornell E and Wieman C 1997 *Phys. Rev. Lett.* **78** 586
- [13] Pflanzner A C, Zöllner S and Schmelcher P 2009 *J. Phys. B: At. Mol. Opt. Phys.* **42** 231002
- [14] Pflanzner A C, Zöllner S and Schmelcher P 2010 *Phys. Rev. A* **81** 023612
- [15] Hu A, Mathey L, Danshita I, Tiesinga E, Williams C J and Clark C W 2009 *Phys. Rev. A* **80** 023619
- [16] Hu A, Mathey L, Danshita I, Tiesinga E, Williams C J and Clark C W 2011 *Phys. Rev. A* **84** 041609
- [17] Palzer S, Zipkes C, Sias C and Köhl M 2009 *Phys. Rev. Lett.* **103** 150601
- [18] Krönke S, Knörzer J and Schmelcher P 2015 *New J. Phys.* **17** 053001
- [19] Gangardt D M and Kamenev A 2009 *Phys. Rev. Lett.* **102** 070402
- [20] Schecter M, Gangardt D M and Kamenev A 2016 *New J. Phys.* **18** 065002
- [21] Schecter M, Gangardt D M and Kamenev A 2012 *Ann. Phys.* **327** 639
- [22] Zvonarev M B, Cheianov V V and Giamarchi T 2007 *Phys. Rev. Lett.* **99** 240404
- [23] Meinert F, Knap M, Kirilov E, Jag-Lauber K, Zvonarev M B, Demler E and Nägerl H-C 2017 *Science* **356** 948
- [24] Cucchiatti F M and Timmermans E 2006 *Phys. Rev. Lett.* **96** 210401
- [25] Kalas R M and Blume D 2006 *Phys. Rev. A* **73** 043608
- [26] Hu M, Van de Graaff M J, Kedar D, Corson J P, Cornell E A and Jin D S 2016 *Phys. Rev. Lett.* **117** 055301
- [27] Fröhlich H 1954 *Adv. Phys.* **3** 325
- [28] Lee T D, Low F E and Pines D 1953 *Phys. Rev.* **90** 297
- [29] Schultz T D 1959 *Phys. Rev.* **116** 526
- [30] Landau L D and Pekar S I 1948 *Zh. Eksp. Teor. Fiz.* **18** 419
Landau L 2008 *J. Phys.* **53** 25
- [31] Massignan P, Zaccanti M and Bruun G M 2014 *Rep. Prog. Phys.* **77** 034401
- [32] Grusdt F, Astrakharchik G E and Demler E A 2017 *New J. Phys.* **19** 103035
- [33] Volosniev A G and Hammer H-W 2017 *Phys. Rev. A* **96** 031601(R)
- [34] Dehkharghani A S, Volosniev A G and Zinner N T 2015 *Phys. Rev. A* **92** 031601(R)
- [35] García-March M A, Dehkharghani A S and Zinner N T 2016 *J. Phys. B: At. Mol. Opt. Phys.* **49** 075303
- [36] Catani J, Lamporesi G, Naik D, Gring M, Inguscio M, Minardi F, Kantian A and Giamarchi T 2012 *Phys. Rev. A* **85** 023623
- [37] Fukuhara T et al 2013 *Nat. Phys.* **9** 235
- [38] Bruderer M, Klein A, Clark S R and Jaksch D 2007 *Phys. Rev. A* **76** 011605
- [39] Bruderer M, Klein A, Clark S R and Jaksch D 2007 *New J. Phys.* **9** 411
- [40] Bruderer M, Klein A, Clark S R and Jaksch D 2008 *New J. Phys.* **10** 033015
- [41] Nakajima S 1955 *Adv. Phys.* **4** 363
- [42] Lieb E H and Liniger W 1963 *Phys. Rev.* **130** 1605
- [43] Lieb E H 1963 *Phys. Rev.* **130** 1616
- [44] Meinert F, Panfil M, Mark M J, Lauber K, Caux J-S and Nägerl H-C 2015 *Phys. Rev. Lett.* **115** 085301
- [45] Henderson K, Ryu C, MacCormick C and Boshier M G 2009 *New J. Phys.* **11** 043030
- [46] LeBlanc L J and Thywissen J H 2007 *Phys. Rev. A* **75** 053612
- [47] Krönke S, Cao L, Vendrell O and Schmelcher P 2013 *New J. Phys.* **15** 063018
- [48] Cao L, Krönke S, Vendrell O and Schmelcher P 2013 *J. Chem. Phys.* **139** 134103
- [49] Cao L, Bolsinger V, Mistakidis S I, Koutentakis G, Krönke S, Schurer J M and Schmelcher P 2017 *J. Chem. Phys.* **147** 044106
- [50] Horodecki R, Horodecki P, Horodecki M and Horodecki K 2009 *Rev. Mod. Phys.* **81** 865
- [51] Penrose O and Onsager L 1956 *Phys. Rev.* **104** 576
- [52] Mueller E J, Ho T-L, Ueda M and Baym G 2006 *Phys. Rev. A* **74** 033612
- [53] Löwdin P O 1955 *Phys. Rev.* **97** 1474
- [54] Bloch F 1929 *Z. Phys.* **52** 555
- [55] García-March M A, Julià-Díaz B, Astrakharchik G E, Busch Th, Boronat J and Polls A 2014 *New J. Phys.* **16** 103004
- [56] Kivelson S and Schrieffer J R 1982 *Phys. Rev. B* **25** 6447
- [57] Kivelson S 1982 *Phys. Rev. B* **26** 4269
- [58] Ashida Y and Ueda M 2015 *Phys. Rev. Lett.* **115** 095301
- [59] Yamamoto R, Kobayashi J, Kato K, Kuno T, Sakura Y and Takahashi Y 2017 *Phys. Rev. A* **96** 033610
- [60] Recati A, Fuchs J N, Peça C S and Zwirger W 2005 *Phys. Rev. A* **72** 023616
- [61] Klein A and Fleischhauer M 2005 *Phys. Rev. A* **71** 033605
- [62] Dehkharghani A S, Volosniev A G and Zinner N T 2017 arXiv:1712.01538v2
- [63] Chen J, Schurer J M and Schmelcher P 2017 arXiv:1711.05171
- [64] Fröhlich H 1952 *Proc. R. Soc. A* **215** 296
- [65] Bardeen J and Pines D 1955 *Phys. Rev.* **99** 1140
- [66] Bardeen J, Cooper L N and Schrieffer J R 1957 *Phys. Rev.* **108** 1175
- [67] Cominotti M, Rossini D, Rizzi M, Hekking F and Minguzzi A 2014 *Phys. Rev. Lett.* **113** 025301
- [68] Stringari S and Pitaevskii L P 2003 *Bose–Einstein Condensation* (Oxford: Oxford University Press)
- [69] Pethick C J and Smith H 2008 *Bose–Einstein Condensation in Dilute Gases* 2nd edn (Cambridge: Cambridge University Press)

3.2 State engineering of impurities in a lattice by coupling to a Bose gas

PAPER • OPEN ACCESS

State engineering of impurities in a lattice by coupling to a Bose gas

To cite this article: Kevin Keiler and Peter Schmelcher 2018 *New J. Phys.* **20** 103042

View the [article online](#) for updates and enhancements.



IOP | ebooks™

Bringing you innovative digital publishing with leading voices to create your essential collection of books in STEM research.

Start exploring the collection - download the first chapter of every title for free.

This content was downloaded from IP address 134.100.111.101 on 02/11/2018 at 16:01



PAPER

State engineering of impurities in a lattice by coupling to a Bose gas

OPEN ACCESS

RECEIVED

29 August 2018

REVISED

12 October 2018

ACCEPTED FOR PUBLICATION

19 October 2018

PUBLISHED

31 October 2018

Kevin Keiler^{1,3} and Peter Schmelcher^{1,2}¹ Zentrum für Optische Quantentechnologien, Universität Hamburg, Luruper Chaussee 149, D-22761 Hamburg, Germany² The Hamburg Centre for Ultrafast Imaging, Universität Hamburg, Luruper Chaussee 149, D-22761 Hamburg, Germany³ Author to whom any correspondence should be addressed.E-mail: kkeiler@physnet.uni-hamburg.de and pschmelc@physnet.uni-hamburg.de

Keywords: many-body physics, correlations, Bose gas, optical lattice, impurities

Original content from this work may be used under the terms of the [Creative Commons Attribution 3.0 licence](https://creativecommons.org/licenses/by/4.0/).

Any further distribution of this work must maintain attribution to the author(s) and the title of the work, journal citation and DOI.



Abstract

We investigate the localization pattern of interacting impurities, which are trapped in a lattice potential and couple to a Bose gas. For small interspecies interaction strengths, the impurities populate the energetically lowest Bloch state or localize separately in different wells with one extra particle being delocalized over all the wells, depending on the lattice depth. In contrast, for large interspecies interaction strengths we find that due to the fractional filling of the lattice and the competition of the repulsive contact interaction between the impurities and the attractive interaction mediated by the Bose gas, the impurities localize either pairwise or completely in a single well. Tuning the lattice depth, the interspecies and intraspecies interaction strength correspondingly allows for a systematic control and engineering of the two localization patterns. The sharpness of the crossover between the two states as well as the broad region of their existence supports the robustness of the engineering. Moreover, we are able to manipulate the ground state's degeneracy in the form of triplets, doublets and singlets by implementing different boundary conditions, such as periodic and hard wall boundary conditions.

1. Introduction

The interest in the properties and dynamics of ultracold atomic mixtures has been substantially increasing in the last few decades. This is not only due to their high degree of controllability, especially of the underlying trapping potentials and inter-atomic interactions [1, 2], but also because they show a plethora of intriguing phenomena. These range from pair-tunnelling effects in lattices [3, 4] to phase separation processes [5–8] and composite fermionization [9–11], and go as far as the spontaneous generation of solitons [12, 13]. Compared to systems with a single species the multi-component case of different bosons [14, 15] allows for correlations to appear not only within one type of species, but especially between different bosonic species. One-dimensional systems are of particular interest, since they allow for strong correlations in the dilute regime [16, 17] which is related to the inverse scaling of the effective interaction strength to the density [18, 19].

A specific case of bosonic mixtures is given by the immersion of a minority species, consisting of a few particles and typically called impurities, into a majority species of many particles. Such setups have been studied theoretically [20–29] and experimentally [30–34] for a single impurity, as simulator for polaron physics, as well as for many impurities [35–38]. Especially the latter case is of immediate interest since the bath, into which the impurities are immersed, mediates an effective attractive interaction between the impurities, leading to a clustering of these very particles [39–41].

One could think of exploiting this mediated interaction in order to configure the impurities, e.g. in a lattice, in a controlled and systematic manner. Such state preparations are indeed relevant for applications e.g. in quantum information processing and atomtronics [42–44]. One pathway is to use a small number of minority atoms in order to influence a larger number of majority atoms. In a triple-well structure this is achieved by increasing the number of minority atoms in the central well, exploiting the increase of atom–atom interactions, and thereby initiating and enhancing tunnelling from the left to the right well of the majority atoms [45]. Pushing this to the extreme, it is in principle possible to implement a single-atom-transistor, which shall serve as

a switch [46–50]. In other atomtronic switching devices, often a triple-well is considered, where one identifies the wells as source, gate and drain. The middle well which is called the gate serves as a mediator of particle transfer between the outer wells, i.e. the source and the drain [51, 52]. Such electronic analogues have the potential to serve as building blocks for cold atom-based quantum computation [53, 54] as well as atom chip technologies [55]. A problem most of these systems suffer from, is the fact that they are considered to be isolated and would lose their coherence when coupled to an environment due to dissipation. However, dissipation can also be used as a resource for quantum state engineering [56–58].

In the present work, we explicitly take advantage of the coupling to an environment in order to engineer the properties of impurities in a triple-well. Instead of following the path that is mentioned above in the context of atomtronics, we control the behaviour of a minority species by coupling to a majority one. Hence, we concentrate on static configurations of the impurities, which might be used as an input to logical gates or starting-points for the control of particle transfer. In the system under investigation, the competition of the attractive interaction which is mediated by the majority species and the repulsive contact interaction among the minority impurity species allows for the engineering of the impurity distribution in the lattice. The induced interaction hereby depends on the interplay between the lattice depth and the interspecies interaction strength, whereas the impurity repulsion can be directly influenced by the intraspecies interaction strength among the impurities. Setting the latter to zero and increasing the lattice depth and the interspecies interaction strength, the ground state wave function undergoes a transition from an uncorrelated to a highly correlated state, which manifests itself in the localization of the lattice atoms in the latter regime [59]. This means that all impurity atoms cluster in a single well, while the majority Bose gas atoms are expelled from it. In the present work we go a significant step beyond the latter scenario and include a repulsive intraspecies interaction among the impurities. We find that for small interspecies interaction strengths and depending on the lattice depth the system can be divided into the unit filling insulator state and one extra particle delocalized over the wells and the state where all impurities populate the energetically lowest Bloch state. In particular, we show that for large interspecies interaction strengths our binary mixture exhibits two specific impurity distributions for a fractional filling of the lattice. These are either a pairwise clustering of the impurities or a full localization. For periodic boundary conditions the many-body ground states exhibiting these two distributions are threefold degenerate (triplets) in both regimes of pairwise and complete clustering and can be changed to doublets or singlets by implementing different boundary conditions.

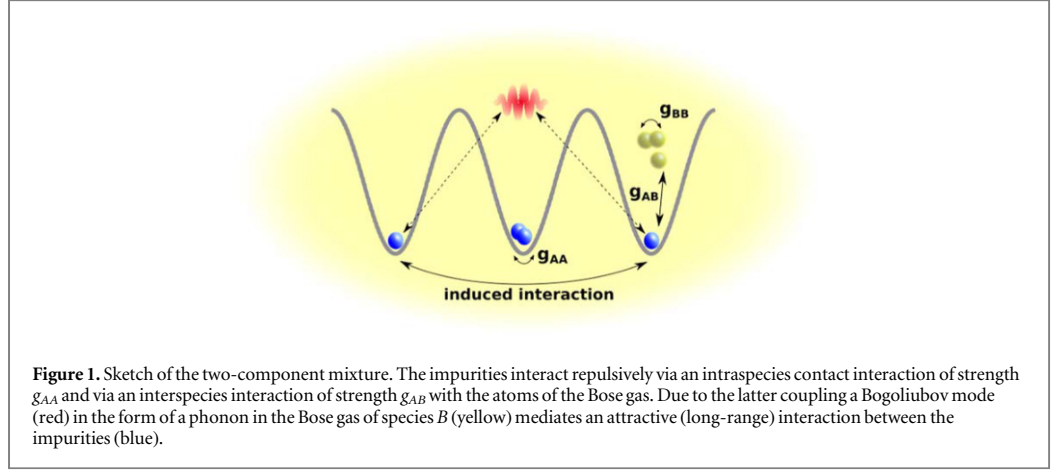
Our work is structured as follows: in section 2 we present the system under investigation consisting of a bosonic impurity species which is trapped in a one-dimensional lattice with periodic or hard wall boundary conditions and couples to a Bose gas of a second majority species of bosons. Afterwards, we briefly discuss the computational method which is used for obtaining our results. Sections 3.1 and 3.2 provide a thorough analysis of the system's possible many-body ground states in dependence of the interspecies interaction strength, the lattice depth and the intraspecies interaction strength among the impurities. We conclude in section 3.3 with a discussion of the ground state's degeneracy in the different regimes in dependence of the boundary conditions. In section 4 we summarize our findings and present possible applications and future studies.

2. Setup and methodology

Our system consists of a mixture of two bosonic species. The bosonic A species is trapped in a one-dimensional lattice with periodic or hard wall boundary conditions. It is immersed in a Bose gas of a second B species of bosons obeying the same boundary conditions but without the lattice potential. This setup lies within reach of current experimental techniques, since beyond controlling the dimensionality, various trapping potentials for the atoms can be achieved, including in particular one-dimensional ring geometries [60] and box potentials [61]. The optical lattice potential for the A atoms (impurities) does not affect the Bose gas, which is achievable by choosing the corresponding laser wavelengths and atomic species [62]. Thereby, we create a two-component system with each species being trapped individually. Furthermore, we introduce a coupling Hamiltonian \hat{H}_{AB} between the two species. Both subsystems are confined to a longitudinal direction, accounting for the one-dimensional character, and excitations in the corresponding transversal direction are energetically suppressed and can therefore be neglected. This finally results in a Hamiltonian of the form $\hat{H} = \hat{H}_A + \hat{H}_B + \hat{H}_{AB}$. The Hamiltonian of the A species reads

$$\hat{H}_A = \int_0^L dx \hat{\chi}^\dagger(x) \left[-\frac{\hbar^2}{2m_A} \frac{d^2}{dx^2} + V_0 \sin^2\left(\frac{\pi kx}{L}\right) + g_{AA} \hat{\chi}^\dagger(x) \hat{\chi}(x) \right] \hat{\chi}(x), \quad (1)$$

where $\hat{\chi}^\dagger$ is the field operator of the lattice A bosons, m_A their mass, V_0 the lattice depth, g_{AA} the intraspecies interaction strength, k the number of wells in the lattice and L is the length of the system. The B species is described by the Hamiltonian of the Lieb–Liniger model [63–65] for periodic boundary conditions



$$\hat{H}_B = \int_0^L dx \hat{\phi}^\dagger(x) \left[-\frac{\hbar^2}{2m_B} \frac{d^2}{dx^2} + g_{BB} \hat{\phi}^\dagger(x) \hat{\phi}(x) \right] \hat{\phi}(x), \quad (2)$$

where $\hat{\phi}^\dagger$ is the field operator of the B species, $g_{BB} > 0$ is the interaction strength of the two-body contact interaction among the B atoms and m_B is the corresponding mass. Moreover, we assume equal masses for the species $m_A = m_B$. The interaction between the species A and B is given by

$$\hat{H}_{AB} = g_{AB} \int_0^L dx \hat{\chi}^\dagger(x) \hat{\chi}(x) \hat{\phi}^\dagger(x) \hat{\phi}(x), \quad (3)$$

where g_{AB} is the interspecies interaction strength. The interaction strengths g_α ($\alpha \in \{A, B, AB\}$) can be expressed in terms of three dimensional s-wave scattering lengths a_α^{3D} , when assuming the above-mentioned strong transversal confinement with the same trapping frequencies $\omega_\perp^\sigma = \omega_\perp$ for both species $\sigma \in \{A, B\}$. In this case it is possible to integrate out frozen degrees of freedom, leading to a quasi one-dimensional model with $g_\alpha = 2\hbar\omega_\perp a_\alpha^{3D}$.

Throughout this work we consider a triple-well and focus on the scenario of small particle numbers with four impurities $N_A = 4$, thereby having fractional filling in the lattice, and $N_B = 10$ atoms in the Bose gas. The interaction among the latter atoms is set to a value where the depletion is negligible in case of no interspecies coupling, i.e. $g_{BB}/E_R \lambda = 6.8 \times 10^{-3}$, with $E_R = (2\pi\hbar)^2/2m_A \lambda^2$ being the recoil energy and $\lambda = 2L/k$ the optical lattice wavelength.

Our numerical simulations are performed using the *ab initio* Multi-Layer Multi-Configuration Time-Dependent Hartree method for bosonic (fermionic) Mixtures (ML-MCTDHX) [66–68], which is able to take all correlations into account. Within ML-MCTDHX one has access to the complete many-body wave function which allows us consequently to derive all relevant characteristics of the underlying system. In particular, this means that we are able to characterize the system in terms of number states by projecting onto an appropriate basis [69, 70]. Besides investigating the quantum dynamics it allows us to calculate the ground (or excited) states by using either imaginary time propagation or improved relaxation [71], thereby being able to uncover also possible degeneracies of the many-body states. In standard approaches for solving the time-dependent Schrödinger equation, one typically constructs the wave function as a superposition of time-independent Fock states with time-dependent coefficients. Instead, the ML-MCTDHX approach considers a co-moving time-dependent basis on different layers, i.e. the Fock states and thus the single particle functions spanning them are time-dependent, in addition to time-dependent coefficients. This leads to a significantly smaller amount of basis states that are needed to obtain an accurate description and eventually reduces the computation time.

3. State control and engineering

Let us analyse the ground state of our mixture in dependence of the lattice depth V_0 , the interspecies coupling strength g_{AB} and the intraspecies interaction strength g_{AA} . As a first step, we calculate the ground state using ML-MCTDHX, thereby obtaining the full wave function. In order to be able to interpret the wave function, we project in a second step the numerically obtained ground state wave function onto number states $|\vec{n}^A\rangle \otimes |\vec{n}^B\rangle$. The number states $|\vec{n}^A\rangle$ for the A species are spanned by generalized Wannier states [72, 73], whereas the number states for the Bose gas of species B are either plane waves or infinite square well eigenstates, i.e. the eigenstates of the kinetic energy operator using either periodic or hard wall boundary conditions. As a result,

we gain a clear insight into the ground state in the different regimes, which will be defined by the distribution of the A species atoms among the Wannier states or Bloch states. In the following, tensor products $|\vec{n}^A\rangle \otimes |\vec{n}^B\rangle$ with different number states $|\vec{n}^A\rangle$ will be called configurations. Additionally, we explore the effect of hard wall boundary conditions compared to periodic ones, thereby revealing how they affect the ground state properties.

3.1. Localization pattern of impurities

In the following, we explore the ground state of the system with periodic boundary conditions for varying V_0 and g_{AB} , fixing the intraspecies interaction strength to $g_{AA}/E_R \lambda = 0.0236$. It turns out, that this interaction strength lies within the range of possible values which lead to the manifestation of regimes in which the ground states differ substantially. An analysis of the dependence on g_{AA} is performed in section 3.2. In order to extract information out of the complete many-body wave function, we project onto the above-mentioned number states $|\vec{n}^A\rangle \otimes |\vec{n}^B\rangle$ and determine the probability of being in the number state $|\vec{n}^A\rangle$ for the impurity A species, irrespective of the number state configurations of the B species, namely

$$P(|\vec{n}^A\rangle) = \sum_i |\langle \vec{n}_i^B | \otimes \langle \vec{n}^A | \Psi \rangle|^2, \quad (4)$$

where $\{|\vec{n}_i^B\rangle\}$ could be any number state basis set of the Bose gas with fixed particle number and $|\Psi\rangle$ is the total many-body ground state wave function. In order to associate the impurity state $|n_1^A, n_2^A, n_3^A\rangle$ with a spatial distribution we construct the number states either with a generalized Wannier basis of the lowest band or the corresponding Bloch basis set, indicated in the following by the subscript W or B , respectively. In principle it is necessary to consider also Wannier states of higher bands, but it turns out that the many-body ground state wave function is approximately well described by a superposition of tensor products of number states $|\vec{n}^A\rangle \otimes |\vec{n}^B\rangle$ with the Fock space of the A species restricted to the lowest band. Number states spanned by Wannier or Bloch states of higher bands do not contribute. The order of the entries in the number state, built of Wannier states, is connected to the localization of the Wannier states in the wells from left to right, e.g. n_1 describes the number of A atoms in the left localized Wannier state of the lowest band. In contrast to that, the ordering for the number states, built of Bloch states, follows the energy of the Bloch states of the lowest band, e.g. n_1 corresponds to the energetically lowest Bloch state. The transformation between Bloch and Wannier states is given by

$$w_R^b(x) = \frac{1}{\sqrt{k}} \sum_p \exp(-ipR) \phi_p^b(x), \quad (5)$$

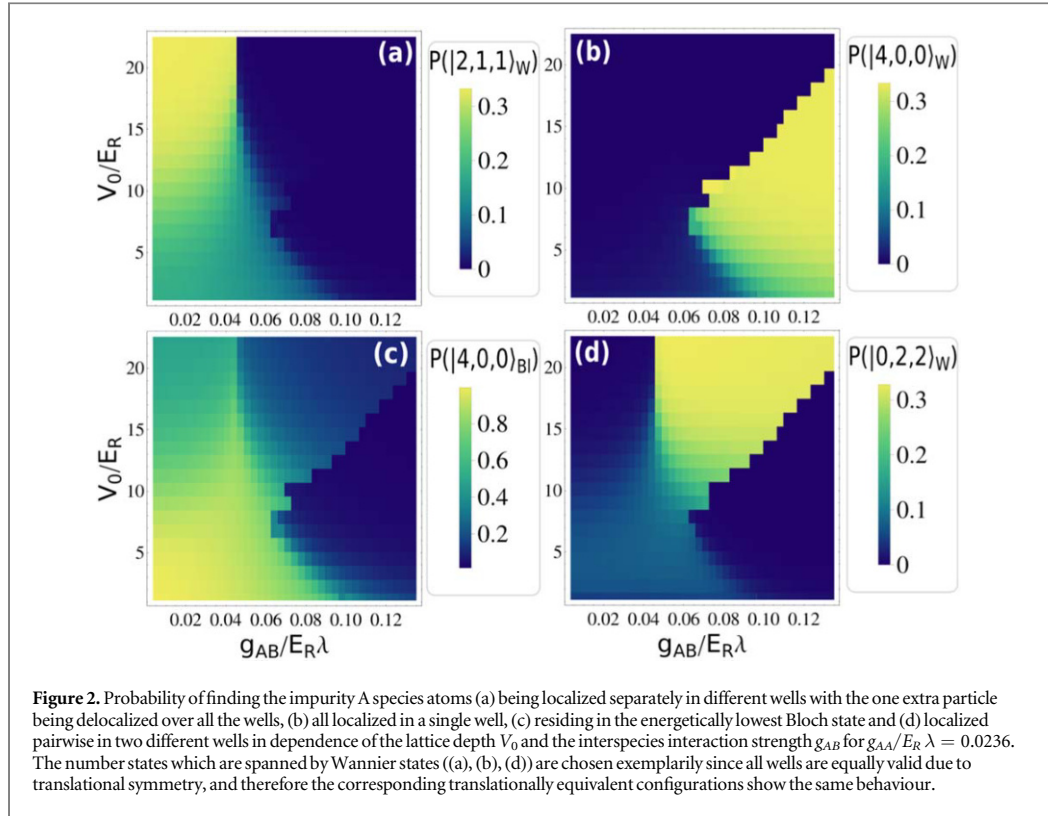
where $w_R(x)$ is the Wannier state associated with the position R of the corresponding well, k the number of lattice sites, p the momentum of the Bloch states $\phi_p(x)$ and b the index of the band.

Figure 2 shows that the many-body ground state can be divided into four different regions. For small lattice depths and interspecies interaction strengths all four particles of the A species populate the energetically lowest Bloch state (figure 2(c)). Increasing the lattice depth for small g_{AB} three lattice atoms will localize separately in different wells with the one extra particle being delocalized over all the wells (figure 2(a)). This can be seen by the fact that the corresponding probability is given by $P(|2, 1, 1\rangle_W) = \frac{1}{3}$, meaning that the remainder of the probability is equally distributed over the states $|1, 2, 1\rangle_W$ and $|1, 1, 2\rangle_W$, resulting in the state

$$|\Psi\rangle_M = \frac{1}{\sqrt{3}} \left[|2, 1, 1\rangle_W \otimes |\psi_B^1\rangle + |1, 2, 1\rangle_W \otimes |\psi_B^2\rangle + |1, 1, 2\rangle_W \otimes |\psi_B^3\rangle \right]. \quad (6)$$

Due to translational symmetry each of the states contributes equally with a probability of $\frac{1}{3}$. The reader should note that the structure of the wave function, given in equation (6), can only be uncovered by the procedure of projection onto number states $|\vec{n}^A\rangle \otimes |\vec{n}^B\rangle$ and is not explicitly given by the numerical simulation. Therefore, $|\Psi\rangle_M$ is not the exact result of ML-MCTDHX but an approximation to it. Our approach is to perform the correlation-including ML-MCTDHX calculations and to subsequently analyse them.

Interestingly, the increase of g_{AB} leads to two different regions in the configuration space, in contrast to the case of $g_{AA} = 0$ [59]. For $g_{AA} = 0$, increasing the lattice depth and the interspecies interaction strength, the ground state wave function undergoes a transition from an uncorrelated to a highly correlated state, which manifests itself in the localization of the lattice atoms in the latter regime of large lattice depths and interspecies interaction strengths. This means that all A atoms cluster in a single well, while the B atoms are expelled from it. This clustering can be understood in terms of an attractive induced impurity–impurity interaction, which is mediated by the B species (see figure 1). In contrast to that, allowing for a repulsive intraspecies interaction of strength g_{AA} among the A atoms counteracts the induced interaction. However, these two types of interactions do not simply add up, since the induced interaction is of long-range type, whereas the intraspecies interaction is of contact type. As a result, depending on the choice of the lattice depth V_0 and the interspecies interaction strength g_{AB} the impurities of species A either accumulate all in one well (figure 2(b)), which is already happening in the case of $g_{AA} = 0$, or pairwise in two different wells (figure 2(d)). Apparently, in the case of pairwise localization of the lattice atoms (figure 2(d)) the repulsive interaction counteracts an accumulation of all lattice



atoms due to the induced interaction. Performing a thorough analysis of the excitation spectrum of the many-body system, we find that the ground state for large g_{AB} is in both regions threefold degenerate (triplet). This essentially means that in the corresponding region the ground states are either given by

$$|2, 2, 0\rangle_W \otimes |\bar{\Psi}_B^1\rangle, |2, 0, 2\rangle_W \otimes |\bar{\Psi}_B^2\rangle \text{ and } |0, 2, 2\rangle_W \otimes |\bar{\Psi}_B^3\rangle \quad \text{or by} \quad (7)$$

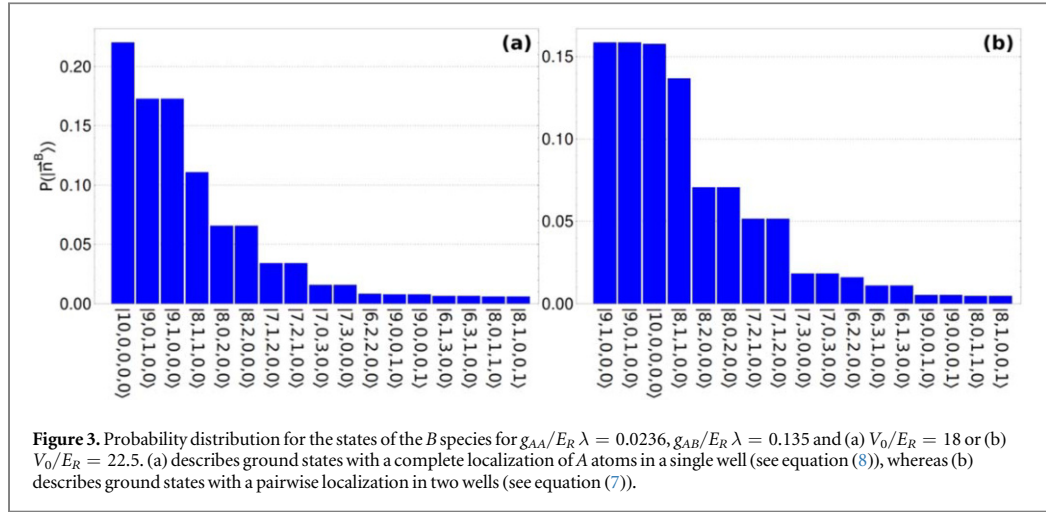
$$|4, 0, 0\rangle_W \otimes |\Psi_B^1\rangle, |0, 4, 0\rangle_W \otimes |\Psi_B^2\rangle \text{ and } |0, 0, 4\rangle_W \otimes |\Psi_B^3\rangle. \quad (8)$$

The states $\{|\Psi_B^i\rangle\}$ and $\{|\bar{\Psi}_B^i\rangle\}$ ⁴ are each normalized to unity and incorporate the localization effect of the A species by e.g. spatially avoiding the impurities correspondingly, which can be seen in the one-body density (see section 3.3, figure 5). Due to the degeneracy of the ground state one can choose such superpositions of the states in equations (7) and (8), which preserve the translational invariance of the total Hamiltonian. For this reason the probabilities in figures 2(a), (b), (d) are bounded by a maximum value of $1/3$ ⁵. Furthermore, it is now possible to use this degeneracy in order to select any of the states in the respective degenerate manifold. Technically, this is simply done by applying a small asymmetry to the lattice potential, thereby energetically favouring one of the above-mentioned states. For example, marginally increasing the depth of the left well of the lattice potential will break the translational symmetry and thereby lift the degeneracy, such that the ground state is solely given by $|4, 0, 0\rangle_W \otimes |\Psi_B^1\rangle$ in one regime. In this sense, with the lattice depth of individual wells we have introduced an additional control parameter for the manipulation of impurity configurations.

So far, we gained insight into the state configurations that are populated by the impurities. While this finding itself allows for a systematic control of the impurities in the lattice, it is nevertheless of interest in which way the correlation with the Bose gas impacts this very species. Therefore, we also analyse the probability distribution $P(|\vec{n}^B\rangle)$ of the number states $|\vec{n}^B\rangle$ that build the corresponding B species states $\{|\Psi_B^i\rangle\}$ and $\{|\bar{\Psi}_B^i\rangle\}$. We find that for each of the strongly coupled degenerate ground states the B species states $\{|\Psi_B^i\rangle\}$ and $\{|\bar{\Psi}_B^i\rangle\}$ each populate the same number states with equal probability, i.e. $|\langle \vec{n}^B | \Psi_B^i \rangle|^2 = |\langle \vec{n}^B | \bar{\Psi}_B^i \rangle|^2$ with $i, j \in \{1, 2, 3\}$, while differing only in a relative phase for each coefficient of the number state. This is why it is sufficient to show only the probability distribution of one B species state for the states in equations (7) and (8). As a basis for the number

⁴ In the following, $\{|\Psi_B^i\rangle\}$ will refer to the B species states corresponding to fully localized impurity states and $\{|\bar{\Psi}_B^i\rangle\}$ corresponding to pairwise localized impurity states.

⁵ However, this effect is solely due to the fact that imaginary time propagation with ML-MCTDHX for obtaining the ground state wave function will conserve translational symmetry, if it is, as we did, initially assumed.



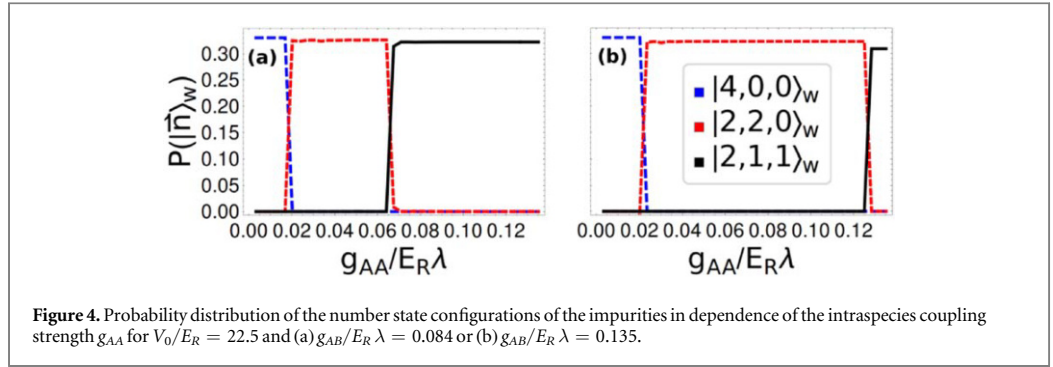
states $|n_1^B, n_2^B, n_3^B, n_4^B, n_5^B\rangle$ we choose plane waves $(1/\sqrt{L})\exp(i\kappa x)$, with wave vectors $\kappa = 2\pi z/L$ ($z = 0, \pm 1, \pm 2, \dots$), where n_1 corresponds to the $\kappa = 0$ mode, n_2, n_3 correspond to $z = \pm 1$ and n_4, n_5 to $z = \pm 2$. It turns out that the population of all higher momentum states is negligible, which we checked explicitly by projecting onto the corresponding number states. In figure 3, we see that due to the correlation with the impurity species the Bose gas can no longer be described by a single number state with all particles occupying the $\kappa = 0$ mode⁶. Interestingly, it is also not sufficient to consider only single particle excitations. It is rather necessary to consider up to four particle excitations for the B species states in both regimes. Comparing the B species states in the two regimes, one finds that they strongly populate the same number states, but differ w.r.t. the quantitative distribution among those number states. For example, in figure 3(a) the number states $|9, 1, 0, 0, 0\rangle$ and $|9, 0, 1, 0, 0\rangle$ are less populated than the number state $|10, 0, 0, 0, 0\rangle$, whereas their probability exceeds that of $|10, 0, 0, 0, 0\rangle$ in figure 3(b). These findings support the choice of our treatment of the many-body problem using a method that is in particular capable of taking all necessary correlations into account. An approximation of the many-body Hamiltonian which relies on few-particle excitations, will not capture the localization pattern presented in figure 2.

3.2. Dependence on the intraspecies coupling

In the previous subsection, we have identified four different number state configurations for the impurity species, while assuming a fixed intraspecies interaction strength of $g_{AA}/E_R \lambda = 0.0236$. However, it is not clear whether this holds for a broad regime of couplings g_{AA} . In order to explore the range of validity of this crossover, we fix the lattice depth as well as the interspecies interaction strength such that for $g_{AA} = 0$ we arrive at a degenerate subspace of ground states given by equation (8), instead of the one given by equation (7) for $g_{AA}/E_R \lambda = 0.0236$. The reader should note that for $g_{AA} = 0$ the correlated region, which is split into two sub-regions for $g_{AA}/E_R \lambda = 0.0236$, is solely described by the degenerate manifold in equation (8) (see [59]). Again, we calculate the probability $P(|\vec{n}^A\rangle)$, while varying the coupling strength g_{AA} for fixed V_0 and g_{AB} . In figure 4, we see that for small g_{AA} the correlated region is well described by a single triplet of ground states, as in the case of $g_{AA} = 0$, where all impurities accumulate in a single well. A further increase of the intraspecies interaction strength leads to a break-up of the cluster into two pairs (equation (7)) and finally results in a ground state with all A atoms localized separately in different wells with the one extra particle being delocalized over all the wells (see equation (6)). Essentially, this means that one needs a certain intraspecies interaction strength g_{AA} between the impurities in order to arrive at a crossover diagram as in figure 2. Below that critical value the crossover is well captured by the $g_{AA} = 0$ case, including, if $g_{AA} \neq 0$, a regime for small g_{AB} and large V_0 where the ground state is given by $|\Psi\rangle_M$ (equation (6)). In other words, for small g_{AA} the crossover diagram in figure 2 will consist of three different regimes, where the two regimes in figures 2(b) and (d) will merge into a single one, describing complete localization of the impurities in a single well (equation (8)). Thus, the ground state comprising pairwise localization of the A atoms will not exist in this case.

Qualitatively, the crossover in figure 4 can be understood again in terms of a competition between the attractive induced interaction and the repulsive intraspecies contact interaction. For small g_{AA} the induced

⁶Of course, the depletion of the Bose gas due to intraspecies interactions of strength g_{BB} will also lead to population of $\kappa \neq 0$ momentum states. But since the depletion is rather small for $g_{AB} = 0$ this effect plays a minor role.



interaction is dominating the behaviour of the A species atoms, leading to their complete localization in a single well. At a certain interaction strength g_{AA} this is no longer the case, resulting in a pairwise accumulation of A atoms. Apparently, the different nature of the competing interactions (long-range and contact) does not lead to a trivial reduction of the four-impurity cluster to a three-impurity cluster, but rather leaves this out as a possibility and directly favours a two-impurity cluster. Astonishingly, the crossover between the different configurations is very sharp, such that the system occupies only one of the triplets without superposing them. Furthermore, it is possible to control the width of the plateau of the pairwise localization by adjusting the interspecies coupling strength g_{AB} correspondingly. The plateau (red) corresponding to a degenerate manifold of ground states with pairwise localization of A atoms is much broader for a larger value of g_{AB} (see figure 4(b)). This also means that a smaller value of the interspecies interaction strength g_{AB} leads to a smaller critical value of g_{AA} (see figure 4(a)) at which the transition to the ground state $|\Psi\rangle_M$ takes place (black plateau, equation (6)). In essence, we find that by tuning the intraspecies interaction strength, we are able to control and engineer the localization of the A atoms in the lattice. The sharpness of the crossovers allows for a clear and systematic way of choosing the ground states, while the broad plateaus make the triplets robust with respect to fluctuations of g_{AA} . In this sense, the coupled system serves as a transistor-like switching device for number state preparation of impurities in a lattice.

3.3. Boundary conditions

Our findings in the previous sections so far relied on the fact that we assumed periodic boundary conditions. It is therefore of immediate interest in which way the localization pattern in figures 2(b) and (d) depends on the choice of the boundary conditions. For this reason, we consider solely values of the lattice depth V_0 and interspecies interaction strength g_{AB} of the crossover diagram such that we arrive at the ground state configurations in equations (7) and (8). The corresponding values are given in table 1. Subsequently, for those two regimes we change the boundary conditions to hard wall boundary conditions. Obviously, this change will break the translational symmetry of the Hamiltonian. Instead, the Hamiltonian now obeys parity symmetry, suggesting that the former ground state degeneracy of a triplet might now be given by a doublet. Indeed, for the states comprising complete localization of the A atoms in a single well (equation (8)) we arrive at the subspace of degenerate ground states, where the atoms of species A localize in the outer wells, i.e. $|4, 0, 0\rangle_W \otimes |\Psi_B^1\rangle$ and $|0, 0, 4\rangle_W \otimes |\Psi_B^2\rangle$ ⁷. However, the degenerate ground state with pairwise localization for periodic boundary conditions does not exhibit any degeneracy for hard wall boundary conditions anymore. In this sense, the ground state in that regime is given by a non-degenerate parity symmetric ground state of the form $|2, 0, 2\rangle_W \otimes |\bar{\Psi}_B\rangle$ (singlet).

Investigating the one-body density of the Bose gas of species B , one gets an intuition for the reason why in one region the ground state triplet becomes a doublet and in the other it becomes a singlet for hard wall boundary conditions. The one-body density shows that the Bose gas accumulates in the centre of the box potential⁸ (not shown here), because it is energetically favourable for the majority of the bosons of the Bose gas to occupy the energetically lowest eigenmode of the box potential and not accumulate to either side of the box. As a consequence, the A atoms localize in the outer wells due to the repulsive coupling to the B species, thereby avoiding occupation of the middle well. For the ground states comprising complete localization of A atoms in a single well, the restriction of the A atoms to the outer wells allows for two possible many-body states out of three

⁷The reader should note that the Wannier states building the number states are calculated using hard wall boundary conditions. Furthermore, the states of the B species will change correspondingly. We omit indication of the boundary conditions in order to avoid confusion.

⁸We introduce the equally valid term ‘box potential’ as a synonym for hard wall boundary conditions.

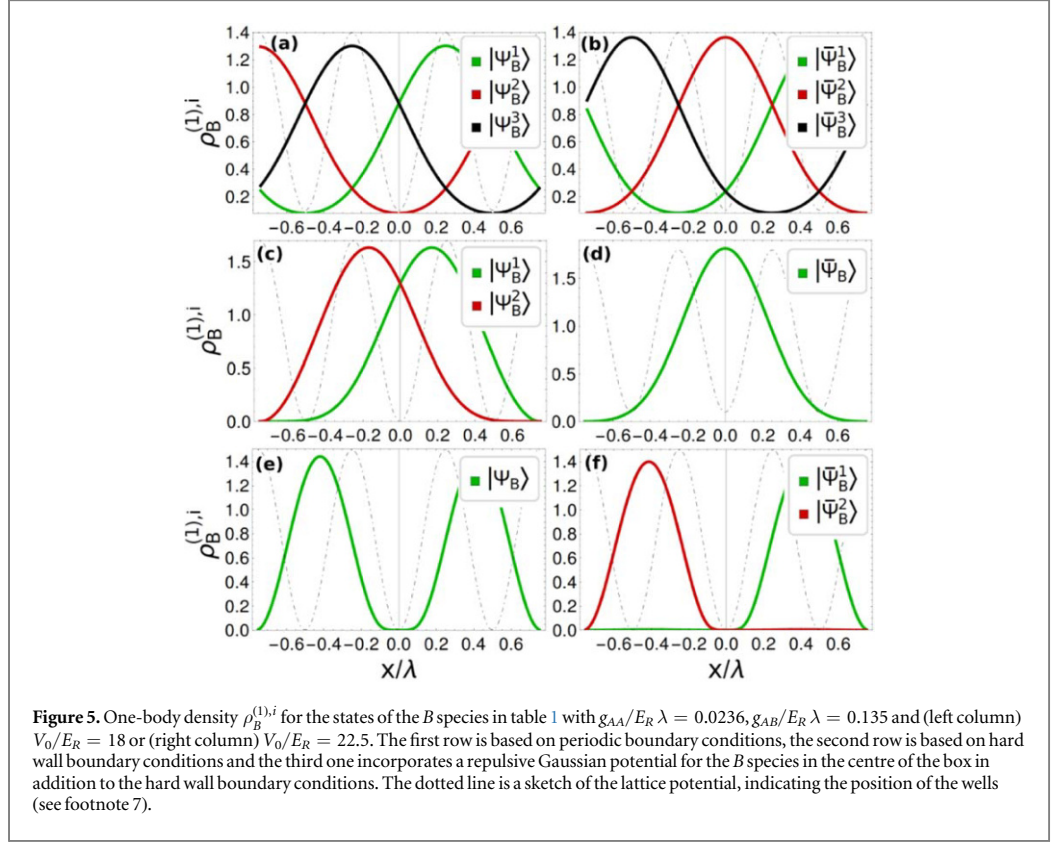


Table 1. Degenerate subspaces of the ground state for different boundary conditions for $g_{AB}/E_R \lambda = 0.135$ and $g_{AA}/E_R \lambda = 0.0236$. The third row incorporates a repulsive Gaussian potential for the B species in the centre of the box in addition to the hard wall boundary conditions. The different values of the lattice depth V_0 lead either to a complete localization of A atoms in a single well or to a pairwise localization (see footnote 7).

Boundary conditions	$V_0/E_R = 18$	$V_0/E_R = 22.5$
Periodic	$ 4, 0, 0\rangle_W \otimes \Psi_B^1\rangle$ $ 0, 4, 0\rangle_W \otimes \Psi_B^2\rangle$ $ 0, 0, 4\rangle_W \otimes \Psi_B^3\rangle$	$ 2, 2, 0\rangle_W \otimes \bar{\Psi}_B^1\rangle$ $ 2, 0, 2\rangle_W \otimes \bar{\Psi}_B^2\rangle$ $ 0, 2, 2\rangle_W \otimes \bar{\Psi}_B^3\rangle$
Hard walls	$ 4, 0, 0\rangle_W \otimes \Psi_B^1\rangle$ $ 0, 0, 4\rangle_W \otimes \Psi_B^2\rangle$	$ 2, 0, 2\rangle_W \otimes \bar{\Psi}_B\rangle$
Hard walls and repulsive Gaussian potential	$ 0, 4, 0\rangle_W \otimes \Psi_B\rangle$	$ 2, 2, 0\rangle_W \otimes \bar{\Psi}_B^1\rangle$ $ 0, 2, 2\rangle_W \otimes \bar{\Psi}_B^2\rangle$

in equation (8), whereas for the ground states with pairwise localization of A atoms only a single state in equation (7) obeys this restriction.

Following the above line of argumentation, one might now ask whether it is possible to change the singlet ground state into a doublet and vice versa by forcing the Bose gas out of the centre and thereby to either side of the box. In order to achieve this we implement a repulsive Gaussian potential for the B species in the middle of the box which is localized in the middle well of the lattice and has an amplitude A_0 that is approximately twice as large as V_0 , i.e. $A_0/E_R = 50$. It turns out that this procedure has the effect we aim for, leaving an imprint on the one-body density of the corresponding B species states (see figures 5(e) and (f)), which is defined as

$$\rho_B^{(1),i}(x) = \int dx_2 \dots dx_{N_B} |\Psi_B^i(x, x_2, \dots, x_{N_B})|^2, \quad (9)$$

integrating over all B atoms except for one.

In figure 5, we show the one-body density $\rho_B^{(1),i}$ ($i \in \{1, 2, 3\}$) of the states of the B species, following the nomenclature in table 1. Figure 5(e) shows that the one-body density of the B species indeed exhibits a minimum in the centre of the box, leading to an accumulation to both sides. Consequently, the A atoms accumulate in the

middle well, such that only one many-body ground state out of equation (8) fulfills this restriction, namely $|0, 4, 0\rangle_W \otimes |\Psi_B\rangle$. In contrast to that, for pairwise impurity localization forcing the B species out of the centre of the box allows for two possible ground states from equation (7) (see figure 5(f)), namely $|2, 2, 0\rangle_W \otimes |\Psi_B^1\rangle$ and $|0, 2, 2\rangle_W \otimes |\Psi_B^2\rangle$. Table 1 summarizes the engineering of the degenerate subspace of the ground state in dependence of the boundary conditions for pairwise and complete localization of the A atoms in a single well. Figure 5(a) resembles the case of $g_{AA} = 0$, where the particles of species B are expelled from the well where all the A atoms fully localize, leaving an imprint on the one-body density. In figure 5(b) the B species atoms need to be expelled from two wells due to the pairwise localization of A atoms. Because of the fact that there are less impurities per well the hereby reduced interspecies interaction allows for a larger one-body density of species B in the region of the pairwise occupied wells. Figures 5(c) and (d) are similar to (a) and (b) except for a shifting of the density closer to the centre of the box potential. This is simply an effect of the change to hard wall boundary conditions. Apart from two specific ground state configurations (figure 5(b) red and 5(d) green) it is possible to identify any of the many-body ground states in table 1 just by analysing the position of the one-body density of the B species states with respect to the lattice potential—irrespective of the boundary conditions.

Thus, we are able to engineer the character of degeneracy of the ground state by choosing the boundary conditions correspondingly (in combination with a Gaussian potential). Combining this with the fact that it is possible to switch between differently localized configurations of the impurities by tuning V_0 , g_{AB} and g_{AA} , one might think of an (adiabatic) particle transfer of the following type. Initially, we prepare the ground state in one of the doublet states (using hard wall boundary conditions), e.g. $|4, 0, 0\rangle_W \otimes |\Psi_B^1\rangle$. Increasing the intraspecies interaction strength g_{AA} adiabatically the ground state will reconfigure to the singlet $|2, 0, 2\rangle_W \otimes |\Psi_B\rangle$. Essentially, this can be interpreted as a transfer of two impurities from the left to the right well.

4. Conclusions

We have shown that it is possible to manipulate the configuration space of lattice trapped impurities with fractional filling immersed in a Bose gas. For small interspecies interaction strengths, the impurities populate the energetically lowest Bloch state or localize separately in different wells with the one extra particle being delocalized over all the wells, depending on the lattice depth. In contrast, for large interspecies interaction strengths and depending on the lattice depth and intraspecies coupling we find that the impurities either localize pairwise or completely in a single well of the lattice. Astonishingly, in dependence of the intraspecies and interspecies coupling as well as the lattice depth the system switches between those two internal state configurations, allowing for an engineering of the impurity distribution in a systematic and controlled manner. Furthermore, the change from periodic to hard wall boundary conditions will reconfigure the ground state from a triplet to either a doublet for ground states where the A atoms fully localize in one well, or to a singlet for ground states where they localize pairwise in one well. We can exploit this degeneracy even further in order to select individual states out of the manifold by applying a small asymmetry to the lattice potential. Eventually, we are not only able to let the impurities cluster in a certain way, but also manipulate in which wells they accumulate. Additionally, we are able to influence the ground state's character of degeneracy. In the spirit of atomtronics, we have developed a switching device for many-body state preparation, thereby controlling the accumulation of impurities in a lattice. This analysis is also applicable for a larger number of particles in the environment, while still remaining in the few particle regime (we have tested this for $N_B \in [10, 30]$), resulting in the same crossover to the two localization patterns for large g_{AB} . However, such a particle increase will also increase the attractive induced interaction for a given choice of V_0 and g_{AB} , thereby shifting the transition region. Increasing the number of impurities, the impurities might form multi-atom clusters of different types depending on the parameter regime due to the long-range character of the induced interaction. We have additionally performed calculations for three impurities in the same setup. In this case the splitting into the two regions of pairwise and complete localization for large g_{AB} does not occur. Instead, for large interspecies interaction strengths we find only one regime in which the impurities cluster completely in a single well. Furthermore, it is of interest for future studies how the number of lattice sites affects the localization pattern. A natural question appearing in the case of four lattice sites is related to how the two-impurity clusters will distribute in the lattice. They might appear next to each other or such that one lattice site is empty between two two-impurity clusters.

The control over the impurity distribution serves as a perfect starting point for dynamical particle transfer scenarios, where one would prepare the impurities in a fully localized state and dynamically transfer it to a pairwise localized state, thereby transferring two particles. In particular, this could also be of interest for the implementation of quantum logical gates, where the position of the impurities shall indicate a logical operation. Especially the dynamical response may pave new pathways to applications in atomtronics. Moreover, one could think of exploiting this engineering of the impurity distribution in order to create multi-atom clusters which are

not of binary type. These clusters could serve as a static-disordered potential for the study of Anderson localization using ultracold atoms as proposed in previous works [74–76].

Acknowledgments

The authors appreciate fruitful and insightful discussions with K Sengstock. KK acknowledges helpful discussions with J Schurer and M Pyzh. PS gratefully acknowledges funding by the Deutsche Forschungsgemeinschaft in the framework of the SFB 925 ‘Light induced dynamics and control of correlated quantum systems’ and support by the excellence cluster ‘The Hamburg Centre for Ultrafast Imaging-Structure, Dynamics and Control of Matter at the Atomic Scale’ of the Deutsche Forschungsgemeinschaft. KK acknowledges a scholarship of the Studienstiftung des deutschen Volkes.

References

- [1] Olshanii M 1998 *Phys. Rev. Lett.* **81** 938
- [2] Chin C, Grimm R, Julienne P and Tiesinga E 2010 *Rev. Mod. Phys.* **82** 1225
- [3] Pflanzner A C, Zöllner S and Schmelcher P 2009 *J. Phys. B* **42** 231002
- [4] Pflanzner A C, Zöllner S and Schmelcher P 2010 *Phys. Rev. A* **81** 023612
- [5] García-March M A, Juliá-Díaz B, Astrakharchik G E, Boronat J and Polls A 2014 *Phys. Rev. A* **90** 063605
- [6] Alon O E, Streltsov A I and Cederbaum L S 2006 *Phys. Rev. Lett.* **97** 230403
- [7] Cazalilla M A and Ho A F 2003 *Phys. Rev. Lett.* **91** 150403
- [8] García-March M A and Busch T 2013 *Phys. Rev. A* **87** 063633
- [9] Hao Y and Chen S 2009 *Phys. Rev. A* **80** 043608
- [10] Pyzh M, Krönke S, Weitenberg C and Schmelcher P 2018 *New J. Phys.* **20** 015006
- [11] Zöllner S, Meyer H-D and Schmelcher P 2008 *Phys. Rev. A* **78** 013629
- [12] Mistakidis S I, Katsimiga G C, Kevrekidis P G and Schmelcher P 2018 *New J. Phys.* **20** 043052
- [13] Katsimiga G C, Koutentakis G M, Mistakidis S I, Kevrekidis P G and Schmelcher P 2017 *New J. Phys.* **19** 073004
- [14] Modugno G, Ferrari G, Rosati G, Brecha R J, Simoni A and Inguscio M 2001 *Science* **294** 1320
- [15] Myatt C, Burt E, Ghrist R, Cornell E and Wieman C 1997 *Phys. Rev. Lett.* **78** 586
- [16] Giamarchi T 2004 *Quantum Physics in One Dimension* (Oxford: Oxford University Press)
- [17] Cazalilla M A, Citro R, Giamarchi T, Orignac E and Rigol M 2011 *Rev. Mod. Phys.* **83** 1405
- [18] Kinoshita T, Wenger T and Weiss D S 2005 *Phys. Rev. Lett.* **95** 190406
- [19] Haller E, Hart R, Mark M J, Danzl J G, Reichsöllner L, Gustavsson M, Dalmonde M, Pupillo G and Nägerl H-C 2010 *Nature* **466** 597
- [20] Krönke S, Knörzer J and Schmelcher P 2015 *New J. Phys.* **17** 053001
- [21] Kalas R M and Blume D 2006 *Phys. Rev. A* **73** 043608
- [22] Massignan P, Zaccanti M and Bruun G M 2014 *Rep. Prog. Phys.* **77** 034401
- [23] Grusdt F, Astrakharchik G E and Demler E A 2017 *New J. Phys.* **19** 103035
- [24] Volosniev A G and Hammer H-W 2017 *Phys. Rev. A* **96** 031601(R)
- [25] Dehkharghani A S, Volosniev A G and Zinner N T 2015 *Phys. Rev. A* **92** 031601(R)
- [26] García-March M A, Dehkharghani A S and Zinner N T 2016 *J. Phys. B: At. Mol. Opt. Phys.* **49** 075303
- [27] Lampo A, Lim S H, García-March M A and Lewenstein M 2017 *Quantum* **1** 30
- [28] Charalambous C, García-March M A, Lampo A, Mehboudi M and Lewenstein M 2018 arXiv:1805.00709
- [29] Cucchiatti F M and Timmermans E 2006 *Phys. Rev. Lett.* **96** 210401
- [30] Palzer S, Zipkes C, Sias C and Köhl M 2009 *Phys. Rev. Lett.* **103** 150601
- [31] Meinert F, Knap M, Kirilov E, Jag-Laubert K, Zvonarev M B, Demler E and Nägerl H-C 2017 *Science* **356** 948
- [32] Catani J, Lamporesi G, Naik D, Gring M, Inguscio M, Minardi F, Kantian A and Giamarchi T 2012 *Phys. Rev. A* **85** 023623
- [33] Fukuhara T *et al* 2013 *Nat. Phys.* **9** 235
- [34] Hu M, Van de Graaff M J, Kedar D, Corson J P, Cornell E A and Jin D S 2016 *Phys. Rev. Lett.* **117** 055310
- [35] Recati A, Fuchs J N, Peça C S and Zwerger W 2005 *Phys. Rev. A* **72** 023616
- [36] Klein A and Fleischhauer M 2005 *Phys. Rev. A* **71** 033605
- [37] Dehkharghani A S, Volosniev A G and Zinner N T 2018 *Phys. Rev. Lett.* **121** 080405
- [38] Chen J, Schurer J M and Schmelcher P 2018 *Phys. Rev. Lett.* **121** 043401
- [39] Bruderer M, Klein A, Clark S R and Jaksch D 2007 *Phys. Rev. A* **76** 011605
- [40] Bruderer M, Klein A, Clark S R and Jaksch D 2007 *New J. Phys.* **9** 411
- [41] Bruderer M, Klein A, Clark S R and Jaksch D 2008 *New J. Phys.* **10** 033015
- [42] Seaman B T, Krämer M, Anderson D Z and Holland M J 2007 *Phys. Rev. A* **75** 023615
- [43] Schlagheck P, Malet F, Cremon J C and Reimann S M 2010 *New J. Phys.* **12** 065020
- [44] Zhang Z, Dunjko V and Olshanii M 2015 *New J. Phys.* **17** 125008
- [45] Stickney J A, Anderson D Z and Zozulya A A 2007 *Phys. Rev. A* **75** 013608
- [46] Micheli A, Daley A J, Jaksch D and Zoller P 2004 *Phys. Rev. Lett.* **93** 140408
- [47] Daley A J, Clark S R, Jaksch D and Zoller P 2005 *Phys. Rev. A* **72** 043618
- [48] Fedichev P O and Fischer U R 2003 *Phys. Rev. Lett.* **91** 240407
- [49] Bausmerth I, Fischer U R and Posazhennikova A 2007 *Phys. Rev. A* **75** 053605
- [50] Fischer U R, Iniotakis C and Posazhennikova A 2008 *Phys. Rev. A* **77** 031602(R)
- [51] Marchukov O V, Volosniev A G, Valiente M, Petrosyan D and Zinner N T 2016 *Nat. Commun.* **7** 13070
- [52] Wittmann Wilsmann K, Ymai L H, Prestes Tonel A, Links J and Foerster A 2017 arXiv:1710.05831
- [53] Brennen G K, Caves C M, Jessen P S and Deutsch I H 1999 *Phys. Rev. Lett.* **82** 1060
- [54] Steane A 1998 *Rep. Prog. Phys.* **61** 117
- [55] Folman R, Krüger P, Schmiedmayer J, Denschlag J and Henkel C 2002 *Adv. At. Mol. Opt. Phys.* **48** 263

- [56] Verstraete F, Wolf M M and Cirac J I 2009 *Nat. Phys.* **5** 633
- [57] Pastawski F, Clemente L and Cirac J I 2011 *Phys. Rev. A* **83** 012304
- [58] Diehl S, Micheli A, Kantian A, Kraus B, Büchler H P and Zoller P 2008 *Nat. Phys.* **4** 878
- [59] Keiler K, Krönke S and Schmelcher P 2018 *New J. Phys.* **20** 033030
- [60] Henderson K, Ryu C, MacCormick C and Boshier M G 2009 *New J. Phys.* **11** 043030
- [61] Gaunt A L, Schmidutz T F, Godlibovych I, Smith R P and Hadzibabic Z 2013 *Phys. Rev. Lett.* **110** 200406
- [62] LeBlanc L J and Thywissen J H 2007 *Phys. Rev. A* **75** 053612
- [63] Lieb E H and Liniger W 1963 *Phys. Rev.* **130** 1605
- [64] Lieb E H 1963 *Phys. Rev.* **130** 1616
- [65] Meinert F, Panfil M, Mark M J, Lauber K, Caux J-S and Nägerl H-C 2015 *Phys. Rev. Lett.* **115** 085301
- [66] Krönke S, Cao L, Vendrell O and Schmelcher P 2013 *New J. Phys.* **15** 063018
- [67] Cao L, Krönke S, Vendrell O and Schmelcher P 2013 *J. Chem. Phys.* **139** 134103
- [68] Cao L, Bolsinger V, Mistakidis S I, Koutentakis G, Krönke S, Schurer J M and Schmelcher P 2017 *J. Chem. Phys.* **147** 044106
- [69] Cao L, Brouzos I, Zöllner S and Schmelcher P 2011 *New J. Phys.* **13** 033032
- [70] Cao L, Brouzos I, Chatterjee B and Schmelcher P 2012 *New J. Phys.* **14** 093011
- [71] Meyer H-D, Gatti F and Worth G A 2009 *Multidimensional Quantum Dynamics: MCTDH Theory and Applications* (New York: Wiley)
- [72] Kivelson S and Schrieffer J R 1982 *Phys. Rev. B* **25** 6447
- [73] Kivelson S 1982 *Phys. Rev. B* **26** 4269
- [74] Gavish U and Castin Y 2005 *Phys. Rev. Lett.* **95** 020401
- [75] Massignan P and Castin Y 2006 *Phys. Rev. A* **74** 013616
- [76] Gadway B, Pertot D, Reeves J, Vogt M and Schneble D 2011 *Phys. Rev. Lett.* **107** 145306

3.3 Interaction-induced single-impurity tunneling in a binary mixture of trapped ultracold bosons

Interaction-induced single-impurity tunneling in a binary mixture of trapped ultracold bosonsKevin Keiler¹ and Peter Schmelcher^{1,2}¹*Center for Optical Quantum Technologies, University of Hamburg, Department of Physics,
Luruper Chaussee 149, 22761 Hamburg, Germany*²*The Hamburg Centre for Ultrafast Imaging, University of Hamburg, Luruper Chaussee 149, 22761 Hamburg, Germany*

(Received 20 July 2019; published 29 October 2019)

We investigate the tunneling dynamics of an ultracold bosonic impurity species which interacts repulsively with a second, larger Bose gas. Both species are held in a finite-sized quasi-one-dimensional box potential. In addition, the impurity bosons experience a periodic potential generated by an optical lattice. We initially prepare our binary mixture in its ground state, such that the impurities and Bose gas are phase separated and the impurities localize pairwise in adjacent sites of the periodic potential, by tuning the interaction strengths and the lattice depth correspondingly. The dynamics is initiated by suddenly lowering the repulsive interspecies interaction strength, thereby entering a different regime in the crossover diagram. For specific postquench interspecies interaction strengths we find that a single impurity tunnels first to the neighboring empty site and depending on the quench strength can further tunnel to the next-neighboring site. Interestingly, this effect is highly sensitive to the presence of the Bose gas and does not occur when the Bose gas does not interact with the impurity species throughout the dynamics. Moreover, we find that the tunneling process is accompanied by strong entanglement between the Bose gas and the impurity species as well as correlations among the impurities.

DOI: [10.1103/PhysRevA.100.043616](https://doi.org/10.1103/PhysRevA.100.043616)**I. INTRODUCTION**

Ultracold atoms have proven to represent a very flexible platform for exploring many-body (MB) quantum effects. They allow for varying the trapping potential in numerous ways, ranging from the manipulation of the dimensionality to “painting” arbitrary external confinements [1]. Additionally, Feshbach and confinement induced resonances [2,3] enable the tuning of the interaction strength between the atoms. In this spirit ultracold atoms allow one to realize even rather complex many-body systems. In particular, one-dimensional (1D) systems are under intense investigation since they exhibit intriguing phenomena. Due to their inverse scaling of the effective interaction strength to the density [4–6] they allow for entering the strong-interaction regime, while remaining dilute [7,8]. Consequently, 1D ultracold systems provide us with the possibility to enter regimes where effective theories are no longer valid.

Apart from controlling single-component fermionic or bosonic ensembles in a systematic manner it is possible to extend this control to mixtures of ultracold atoms [9,10] such as Bose-Bose, Fermi-Fermi, and Bose-Fermi mixtures. The fact that we add to the already present intraspecies interactions an interspecies interaction leads to a significant extension of the already very rich phenomenology of the case of a single species, ranging from pair-tunneling [11,12] to phase separation processes [13–16] and composite fermionization [17–19]. Here, especially particle-imbalanced mixtures are currently of immediate interest. Such a setup can consist of an impurity species of a few particles which are immersed in a majority species of many particles. Extensive theoretical [20–31] as well as experimental [32–36] studies have been performed for this case. A single impurity immersed in a

majority species leads to the notion of a polaron, which plays a central role in our understanding of quantum matter. Considering several impurities interacting with a majority species, one finds that the latter mediates an effective attractive interaction between the impurities [37–43], leading to a clustering of the impurities assuming they are bosons [44–47]. As it turns out, it is even possible to engineer the localization properties of the impurities by including a repulsive intraspecies interaction between them [48].

In the present paper, we investigate a binary Bose-Bose mixture consisting of an ultracold bosonic impurity species which interacts repulsively with a second, larger majority species. Both species are held in a finite-sized quasi-one-dimensional box potential. In addition, the impurity bosons experience a periodic potential generated by an optical lattice. Exploiting the aforementioned possibility to engineer the localization properties of the impurities, we prepare an initial wave function which constitutes a phase separation of the impurity species and the Bose gas, while the impurities accumulate pairwise in adjacent wells of the lattice potential. Upon lowering the interspecies interaction strength we explore the dynamical response of the system. The corresponding quench is performed across crossover boundaries of regimes which constitute different distributions of the impurities in the lattice depending on the interspecies interaction strength. Building upon this, we aim at a dynamical particle transfer, which takes place in a systematic manner due to the presence of the majority species. We find that a sufficiently strong quench leads to the tunneling of a single impurity through the lattice out of the initial four-impurities cluster. Interestingly, this process is only possible for a finite postquench interspecies interaction strength and does not appear when the Bose gas is transparent to the impurity species in the course of

time. We observe that the tunneling process of the impurity species is accompanied by a strong entanglement between the subsystems as well as strong correlations among the impurities. Increasing the number of particles in the majority species, we observe that the tunneling of the impurity species persists, while exhibiting a slightly lower tunneling amplitude.

Our paper is structured as follows. In Sec. II we present the system under investigation along with the numerical method employed for simulating the correlated many-body dynamics. Section III provides a discussion of the quench protocol as well as the initial ground state. Section IV is dedicated to a thorough analysis of the dynamical response as a function of the interspecies interaction strength and the number of majority species particles. We conclude in Sec. V with a summary of our findings, present possible applications, and discuss directions for future studies.

II. SETUP AND COMPUTATIONAL APPROACH

A. Computational approach

Our numerical simulations are performed using the *ab initio* multilayer multiconfiguration time-dependent Hartree method for bosonic (fermionic) mixtures (ML-MCTDHX) [49–51], which is able to take all correlations into account [52–57]. As a first step, the total many-body wave function $|\Psi_{\text{MB}}(t)\rangle$ is expanded in M species functions $|\Psi^\sigma(t)\rangle$ of species σ and written as a Schmidt decomposition [58]:

$$|\Psi_{\text{MB}}(t)\rangle = \sum_{i=1}^M \sqrt{\lambda_i(t)} |\Psi_i^A(t)\rangle \otimes |\Psi_i^B(t)\rangle. \quad (1)$$

Here, the Schmidt coefficients $\sqrt{\lambda_i}$, in decreasing order, provide information about the degree of population of the i th species function and thereby about the degree of entanglement between the impurities and the majority species. In case that $\lambda_1 = 1$ the species A and B are not entangled and the system can be described with a species mean-field ansatz ($M = 1$).

Furthermore, the species wave functions $|\Psi^\sigma(t)\rangle$ describing an ensemble of N_σ bosons are expanded in a set of permanents:

$$|\Psi_i^\sigma(t)\rangle = \sum_{\vec{n}^\sigma | N_\sigma} C_{\sigma \vec{n}}(t) |\vec{n}^\sigma; t\rangle, \quad (2)$$

where the vector $\vec{n}^\sigma = (n_1^\sigma, n_2^\sigma, \dots)$ denotes the occupations of the time-dependent single-particle functions of the species σ . The notation $\vec{n}^\sigma | N_\sigma$ indicates that for each $|\vec{n}^\sigma; t\rangle$ we require the condition $\sum_i n_i^\sigma = N_\sigma$. The time propagation of the many-body wave function is achieved by employing the Dirac-Frenkel variation principle $\langle \delta \Psi_{\text{MB}} | (i\partial_t - \mathcal{H}) | \Psi_{\text{MB}} \rangle$ [59–61] with the variation $\delta \Psi_{\text{MB}}$. Within ML-MCTDHX one has access to the complete many-body wave function which allows us consequently to derive all relevant characteristics of the underlying system. In particular, this means that we are able to characterize the system by projecting onto number states with respect to an appropriate single-particle basis [62,63]. Besides investigating the quantum dynamics it allows us to calculate the ground (or excited) states by using either imaginary-time propagation or improved relaxation [64], thereby being able to uncover also possible de-

generacies of the many-body states. In standard approaches for solving the time-dependent Schrödinger equation, one typically constructs the wave function as a superposition of time-independent Fock states with time-dependent coefficients. Instead, it is important to note that the ML-MCTDHX approach considers a comoving time-dependent basis on different layers, meaning that in addition to time-dependent coefficients the single-particle functions spanning the number states are also time dependent. This leads to a significantly smaller number of basis states and configurations that are needed to obtain an accurate description and thus reduces the computation time [65].

B. Setup

Our system consists of a mixture of two bosonic species. The minority species A (impurities) is trapped in a one-dimensional lattice with hard wall boundary conditions. It is immersed in a majority species B obeying the same boundary conditions but without the lattice potential. This setup lies within reach of current experimental techniques. Various trapping potentials for the atoms can be achieved, including in particular one-dimensional ring geometries [1] and box potentials [66]. The optical lattice potential for the impurities does not affect the Bose gas, which is achievable by choosing the corresponding laser wavelengths and atomic species [67]. Thereby, we create a two-component system with each species being trapped individually. Furthermore, we introduce a coupling Hamiltonian \hat{H}_{AB} between the two species. Both subsystems are confined to a longitudinal direction, accounting for the one-dimensional character, and excitations in the corresponding transversal direction are energetically suppressed and can therefore be neglected. This results in a Hamiltonian of the form $\hat{H} = \hat{H}_A + \hat{H}_B + \hat{H}_{AB}$. The Hamiltonian of the A species reads

$$\hat{H}_A = \int_{-L/2}^{L/2} dx \hat{\Psi}_A^\dagger(x) \left[-\frac{\hbar^2}{2m_A} \frac{d^2}{dx^2} + V_0 \sin^2\left(\frac{\pi kx}{L}\right) + g_{AA} \hat{\Psi}_A^\dagger(x) \hat{\Psi}_A(x) \right] \hat{\Psi}_A(x), \quad (3)$$

where $\hat{\Psi}_A^\dagger$ is the field operator of the lattice A bosons, m_A is their mass, V_0 is the lattice depth, g_{AA} is the intraspecies interaction strength of the two-body contact interaction among the A atoms, k is the number of wells in the lattice, and L is the length of the system, while $x \in [-L/2, L/2]$. The B species is described by the Hamiltonian

$$\hat{H}_B = \int_{-L/2}^{L/2} dx \hat{\Psi}_B^\dagger(x) \left[-\frac{\hbar^2}{2m_B} \frac{d^2}{dx^2} + g_{BB} \hat{\Psi}_B^\dagger(x) \hat{\Psi}_B(x) \right] \hat{\Psi}_B(x), \quad (4)$$

where $\hat{\Psi}_B^\dagger$ is the field operator of the B species, $g_{BB} > 0$ is the interaction strength of the two-body contact interaction among the B atoms, and m_B is the corresponding mass. Moreover, we assume equal masses for the species $m_A = m_B$. Experimentally this can be achieved by preparing, e.g., ^{87}Rb atoms in two different hyperfine states, i.e., $|F = 2, m_F = -2\rangle$ represents the impurity species and $|F = 1, m_F = -1\rangle$ represents the Bose gas, thereby obtaining a two-species bosonic mixture.

Using the so-called tune-out wavelength of the $|F = 1, m_F = -1\rangle$ state it is possible to create species-dependent potentials [67,68], such that the optical lattice potential for the impurities does not affect the Bose gas. Consequently, the Bose gas experiences a vanishing light shift, while the light shift for the impurity species can be used to trap this species in an optical lattice potential. The interaction between the species A and B is given by

$$\hat{H}_{AB} = g_{AB} \int_{-L/2}^{L/2} dx \hat{\Psi}_A^\dagger(x) \hat{\Psi}_A(x) \hat{\Psi}_B^\dagger(x) \hat{\Psi}_B(x), \quad (5)$$

where g_{AB} is the interspecies interaction strength. The interaction strengths g_α ($\alpha \in \{A, B, AB\}$) can be expressed in terms of the three-dimensional s -wave scattering lengths a_α^{3D} . By assuming the above-mentioned strong transversal confinement with the same trapping frequencies $\omega_\perp^\sigma = \omega_\perp$ for both species $\sigma \in \{A, B\}$ it is possible to integrate out frozen degrees of freedom, leading to a quasi-one-dimensional model with $g_\alpha = 2\hbar\omega_\perp a_\alpha^{3D}$.

Throughout this paper we consider a $k = 5$ well lattice and focus on small particle numbers with $N_A = 4$ impurities, leading thus to a fractional filling in the lattice, and $N_B \in \{10, 30\}$ majority atoms. The interaction among the majority atoms is set to a value where the quantum depletion of the Bose gas is negligible in case of an absent interspecies coupling, i.e., $g_{BB}/E_R\lambda = 6.8 \times 10^{-3}$, with $E_R = (2\pi\hbar)^2/2m_A\lambda^2$ being the recoil energy and $\lambda = 2L/k$ the optical lattice wavelength. In the following, we present the quench protocol which induces the tunneling dynamics. We prepare our system in its ground state with $g_{AA}/E_R\lambda = 0.067$, $g_{AB}/E_R\lambda = 0.142$, and $V_0/E_R = 13$. This choice of parameters ensures that we arrive approximately at the following MB wave function $|\Psi_{MB}\rangle \approx |2, 2, 0, 0, 0\rangle_W \otimes |\Psi_B\rangle$, where the impurities accumulate pairwise in adjacent sites (see Fig. 1). The number state $|2, 2, 0, 0, 0\rangle_W$ is spanned by Wannier states of the lowest band for the impurity species, whereas $|\Psi_B\rangle$ denotes the species wave function of the majority species. Hence, initially the subsystems are not entangled, thereby forming a single product state. We further note that the two species strongly avoid overlap in this ground-state configuration (see [48]), reminiscent of the phase separation of two Bose gases [13]. This can be seen in the one-body density of the ground state $|\Psi_{MB}\rangle$ of the species σ [see Fig. 1(b)], which is defined as

$$\rho_\sigma^{(1)}(x) = \langle \Psi_{MB} | \hat{\Psi}_\sigma^\dagger(x) \hat{\Psi}_\sigma(x) | \Psi_{MB} \rangle. \quad (6)$$

The quench is performed by lowering the interspecies interaction strength. Varying the postquench interspecies interaction strength g_{AB} , we explore the dynamical response of the binary mixture, focusing in particular on the tunneling behavior of the impurity species.

III. THE QUENCH PROTOCOL AND ITS UNDERLYING PHYSICS

A. Crossover diagram

Before discussing the dynamical response of the binary mixture upon quenching the interspecies interaction strength g_{AB} , we shall motivate the employed quench protocol. For this purpose, we determine the ground state of the system for

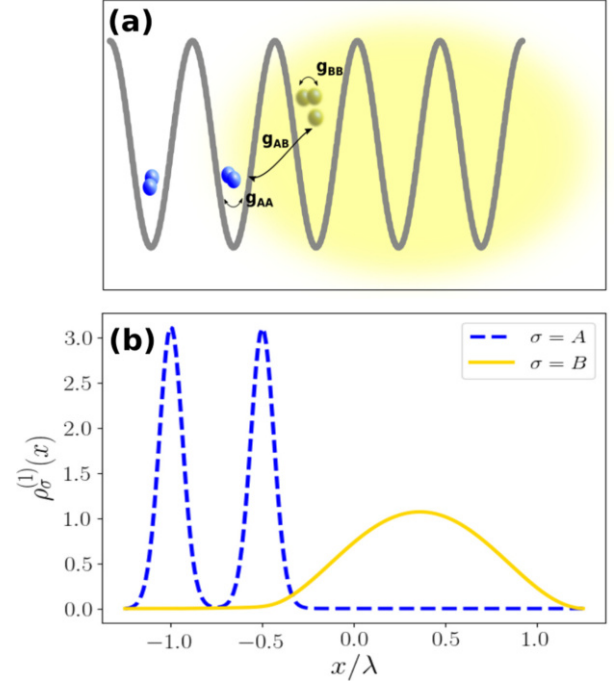


FIG. 1. (a) Sketch of the initial state of the two-component mixture. The impurities [blue (dark shading) dots] interact repulsively via an intraspecies contact interaction of strength g_{AA} and via an interspecies contact interaction of strength g_{AB} with the atoms of the Bose gas. The latter atoms in turn weakly interact via an intraspecies contact interaction of strength g_{BB} . Due to the interplay between the interspecies and the intraspecies interaction among the impurities the latter accumulate pairwise in adjacent sites, minimizing the overlap with the majority species. (b) One-body density of the many-body ground state of the σ species $\rho_\sigma^{(1)}(x, t)$ for $N_A = 4$, $N_B = 10$, a lattice depth of $V_0/E_R = 13$, intraspecies interaction strengths of $g_{AA}/E_R\lambda = 0.067$ and $g_{BB}/E_R\lambda = 6.8 \times 10^{-3}$, and an interspecies interaction strength of $g_{AB}/E_R\lambda = 0.142$. x is given in units of λ .

different lattice depths V_0 and g_{AB} . We note that the underlying single-particle functions of the ground state are optimized with respect to the respective many-body problem and can in general be of arbitrary structure. We extract information from the complete many-body wave function by projecting onto number states $|\vec{n}^A\rangle \otimes |\vec{n}^B\rangle$ and determine the probability of being in the number state $|\vec{n}^A\rangle$ for the impurity species A , irrespective of the number state configurations of the B species, namely,

$$P(|\vec{n}^A\rangle) = \sum_i |\langle \vec{n}_i^B | \otimes \langle \vec{n}^A | \Psi_{MB} \rangle|^2, \quad (7)$$

where $\{|\vec{n}_i^B\rangle\}$ could be any number state basis set of the Bose gas with fixed particle number and $|\Psi_{MB}\rangle$ is the total many-body ground-state wave function. In order to associate the impurity state $|\vec{n}^A\rangle = |n_1^A, n_2^A, n_3^A, n_4^A, n_5^A\rangle$ with a spatial distribution we construct the number states with a generalized Wannier basis (see subscript W) of the lowest band [69–71].

In Fig. 2 we show the probability $P(|\vec{n}^A\rangle)$ of finding the impurity A species atoms in the respective number state

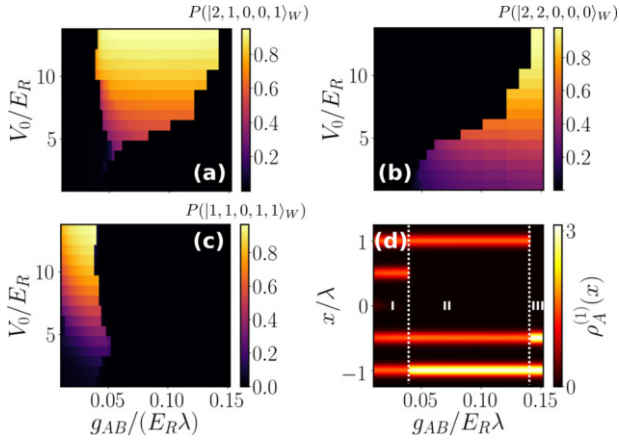


FIG. 2. Probability of finding the impurity species (a) forming one two-impurity cluster next to a single impurity and one impurity residing along the opposite wall, (b) localized pairwise in adjacent wells, and (c) localized separately in the outer wells as a function of the lattice depth V_0 and the interspecies interaction strength g_{AB} for $g_{AA}/E_R\lambda = 0.067$. The number states in panels (a) and (b) are chosen as an example and therefore the corresponding parity-symmetric configurations show the same behavior. In panel (d) we show the one-body density of the species A as a function of the interspecies interaction strength for a fixed lattice depth of $V_0/E_R = 13$. In region I the impurities localize separately in the outer wells. In region II they form one two-impurity cluster next to a single impurity and one impurity residing along the opposite wall and in region III they are localized pairwise in adjacent wells (see Table I). The particle number of the respective species is chosen as $N_A = 4$ and $N_B = 30$. x is given in units of λ , V_0 is given in units of E_R , and g_{AB} is given in units of $E_R\lambda$.

$|\vec{n}^A\rangle$ as a function of V_0 and g_{AB} . Predominantly the states $|1, 1, 0, 1, 1\rangle_W$, $|2, 1, 0, 0, 1\rangle_W$, and $|2, 2, 0, 0, 0\rangle_W$ are occupied. Focusing on large lattice depths the impurity species is well described by a single number state of the aforementioned kind depending on the interspecies interaction strength. For small g_{AB} and large lattice depths we observe that the impurities are localized separately in the outer wells [see Fig. 2(c)]. Increasing g_{AB} we find a transition to a state exhibiting one two-impurity cluster next to a single impurity and one impurity residing along the opposite wall [see Fig. 2(a)]. For even larger g_{AB} , the impurities accumulate pairwise in adjacent sites [see Fig. 2(b)]. This behavior is also reflected in the one-body density $\rho_A^{(1)}(x)$ of the impurity species, shown in Fig. 2(d). We note here that the many-body ground states in Figs. 2(a) and 2(b) for large lattice depths are degenerate with an energetically equivalent counterpart of the type

TABLE I. Degenerate subspaces of the ground state referring to the regimes in Fig. 2(d) for $N_B = 10$ and $V_0/E_R = 13$.

Regime		
I	II	III
$ 1, 1, 0, 1, 1\rangle_W \otimes \Psi_B^1\rangle$	$ 2, 1, 0, 0, 1\rangle_W \otimes \Psi_B^2\rangle$	$ 2, 2, 0, 0, 0\rangle_W \otimes \Psi_B^3\rangle$
	$ 1, 0, 0, 1, 2\rangle_W \otimes \Psi_B^2\rangle$	$ 0, 0, 0, 2, 2\rangle_W \otimes \Psi_B^3\rangle$

$|1, 0, 0, 1, 2\rangle_W \otimes |\bar{\Psi}_B^2\rangle$ or $|0, 0, 0, 2, 2\rangle_W \otimes |\bar{\Psi}_B^3\rangle$, where $|\bar{\Psi}_B^i\rangle$ and $|\Psi_B^i\rangle$ denote the respective species wave function of the majority species B (the bar denotes the species wave function B for the degenerate counterpart). For large lattice depths we can now classify the ground states for varying interspecies interaction strengths into three regimes as depicted in Table I.

Next, we prepare the binary mixture in the ground-state many-body wave function $|\Psi_0\rangle \approx |2, 2, 0, 0, 0\rangle_W \otimes |\Psi_B^3\rangle$ by choosing a lattice depth of $V_0/E_R = 13$ and an interspecies interaction strength of $g_{AB}/E_R\lambda = 0.142$. Lowering now instantaneously the interspecies interaction strength and thereby crossing the different regimes in the crossover diagram in Fig. 2, the corresponding ground states would be given by more delocalized configurations (see Table I). In this spirit, one might expect that the former two-impurity cluster will split up in the course of the dynamics, leading to a tunneling of the impurities in the lattice. Of course, this simple picture will not give insight into the explicit complex dynamical response of our system, but rather serves as a starting point as well as a motivation for the chosen quench protocol. An extensive study of the actual dynamics observed in the two-component system will be the subject of the following sections.

B. Single-impurity dynamics

Instead of diving directly into the results for the case of $N_A = 4$ impurities in the subsystem A , we will first briefly discuss the case of a single impurity, i.e., $N_A = 1$, coupled to a majority species of $N_B = 10$ particles. Assuming the same parameters as discussed above and setting the lattice depth to $V_0/E_R = 13$ and the interspecies interaction strength to $g_{AB}/E_R\lambda = 0.14$, the impurity will accumulate to one of the most outer lattice sites, similar to the case of $N_A = 4$ impurities. Quenching now the interspecies interaction strength to a lower value, we find two distinct regimes for the dynamical response of the impurity, identified by the temporal evolution of the one-body density for both species upon quenching g_{AB} . We observe that initially the impurity is localized in the rightmost well, whereas the majority species distributes such that it avoids the overlap with the impurity. For a postquench interspecies interaction strength of $g_{AB}/E_R\lambda = 0$, we observe a tunneling of the impurity through the lattice potential structure to the leftmost well [see Fig. 3(a)]. This is followed by a rather complex tunneling between the various lattice sites. Throughout the dynamics the majority species exhibits high-frequency oscillations of the one-body density [see Fig. 3(c)]. For any postquench interspecies interaction strength not close to zero the impurity remains localized in the initially populated well in the course of the dynamics [see Fig. 3(b)], whereas the B species exhibits again high-frequency oscillations on top of an overall breathing of the one-body density [see Fig. 3(d)]. Apparently, the finite repulsive coupling of the impurity to the majority species does not allow for a transfer of the impurity to the neighboring lattice sites due to the latter species acting as an effective material barrier. Instead it is necessary to quench the system such that the majority species basically becomes transparent to the impurity in order to achieve a tunneling of the impurity. In this sense, the dynamical response of the system can be defined by two distinct regimes. Either the impurity performs

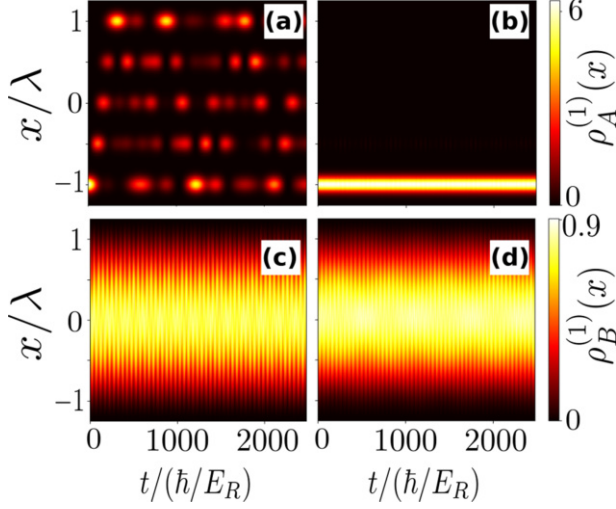


FIG. 3. Temporal evolution of the one-body density of the A species $\rho_A^{(1)}(x, t)$ (upper row) and B species $\rho_B^{(1)}(x, t)$ (lower row) for a single impurity coupled to the majority species B for a lattice depth of $V_0/E_R = 13$ and a postquench interspecies interaction strength of (a, c) $g_{AB}/E_R\lambda = 0$ and (b, d) $g_{AB}/E_R\lambda = 0.032$. x is given in units of λ and t is given in units of \hbar/E_R .

a rather complex tunneling through the lattice potential, while exhibiting traces of an oscillation from one side to the other side of the system, for postquench $g_{AB} = 0$ or close to zero, or it remains localized in the initially populated well for weaker quench amplitudes. In the following discussion we will explicitly show that the case of four impurities initially accumulating pairwise in adjacent sites exhibits impurity tunneling for finite postquench couplings to the majority species and strong enough quench amplitudes, whereas quenching to $g_{AB}/E_R\lambda = 0$ results in a localization of the impurity species in the initially populated wells in the course of time.

IV. CORRELATED TUNNELING DYNAMICS

A. Density evolution and correlation analysis

We explore the dynamics of $N_A = 4$ impurities coupled to a majority species of $N_B = 10$ bosons. Motivated by the crossover diagram in the previous section [see Fig. 2] we choose a lattice depth of $V_0/E_R = 13$ and an interspecies interaction strength of $g_{AB}/E_R\lambda = 0.14$ in order to prepare the binary mixture in the ground state $|\Psi_0\rangle \approx |2, 2, 0, 0, 0\rangle_W \otimes |\Psi_B^3\rangle$. We perform a quench of the interspecies interaction strength to a lower value and determine the dynamical response of the system numerically using ML-MCTDHX, which is capable of taking all correlations into account. In the first step, we identify four different regimes of the dynamical response of our system, depending on the postquench interspecies interaction strength g_{AB} , based on qualitatively different dynamical patterns of the one-body densities. Figure 4 shows the temporal evolution of the one-body density of the A and B species for various postquench interspecies interaction strengths. For weak quench amplitudes [see Figs. 4(d) and 4(h)], the impurities remain trapped in the initially occupied wells and appear not to respond dynamically to the quench, whereas the majority species performs high-frequency oscillations in the one-body density. The origin of these oscillations will be discussed in Sec. IV B. This scenario resembles the case of a single impurity coupled to the majority, which has been discussed in the context of Fig. 3. However, quenching to even lower values of g_{AB} initiates a tunneling process to the neighboring unoccupied lattice site [see Fig. 4(c)]. We observe a rather periodic oscillation of the one-body density $\rho_A^{(1)}(x, t)$ between the second and third lattice site. These oscillations are imprinted on the one-body density profile of the majority species, which tries to minimize the overlap to the minority species [see Fig. 4(g)], on top of the high-frequency oscillations. We can extend this tunneling behavior of the impurities by reducing the postquench interspecies interaction strength even further. This leads to a tunneling of the impurity

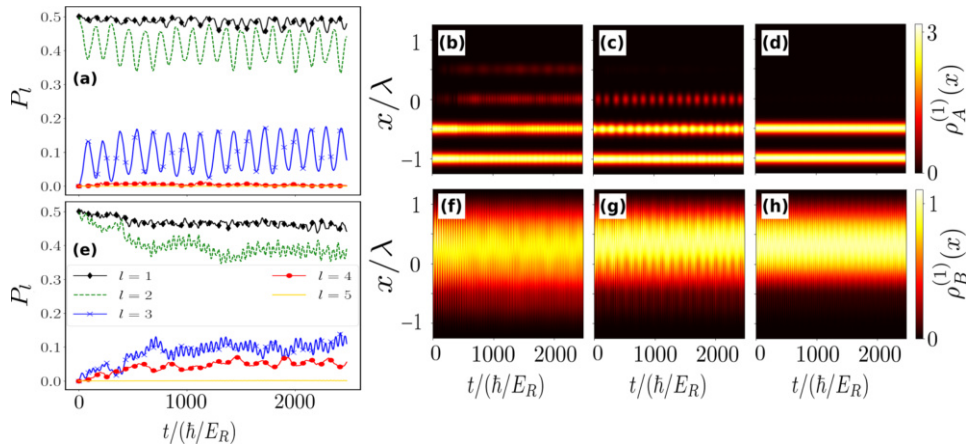


FIG. 4. Temporal evolution of the probability P_l of finding an impurity particle in the l th Wannier state upon quenching to (a) $g_{AB}/E_R\lambda = 0.051$ and (e) $g_{AB}/E_R\lambda = 0.032$. Temporal evolution of the one-body density of the A species $\rho_A^{(1)}(x, t)$ (upper row) and B species $\rho_B^{(1)}(x, t)$ (lower row) for a lattice depth of $V_0/E_R = 13$ and a postquench interspecies interaction strength of (b, f) $g_{AB}/E_R\lambda = 0.032$, (c, g) $g_{AB}/E_R\lambda = 0.051$, and (d, h) $g_{AB}/E_R\lambda = 0.065$. The particle number of the respective species is chosen as $N_A = 4$ and $N_B = 10$. x is given in units of λ and t is given in units of \hbar/E_R .

species into the third, as in the previous case, and in particular into the fourth well. Again, this will leave an imprint on the one-body density of the B species [see Fig. 4(f)]. Remarkably, for a postquench interspecies interaction strength of $g_{AB} = 0$, such that the majority species is transparent to the impurities, the latter will remain localized in the initially populated wells (not shown here). In contrast to the case of a single impurity (see Fig. 3), the two-impurity cluster remains stable and does not deviate from its initial configuration in the course of time. Such stable composite objects exhibit rather large lifetimes and have already been observed experimentally in optical lattices [72]. The majority species, however, does respond strongly to the quench, which manifests itself in an initial dipolelike motion of the species, which stabilizes in time due to interference processes (not shown here).

In order to deepen our insight into the mechanisms underlying the dynamics in the binary mixture, we will now analyze the correlations which accompany the dynamics, in particular the entanglement between the impurity species and the majority species. For this purpose we introduce the von Neumann entropy

$$S_{AB}(t) = - \sum_i \lambda_i(t) \ln[\lambda_i(t)] \quad (8)$$

as a measure for the entanglement between the subsystems A and B , where λ_i are the Schmidt coefficients defined in Eq. (1). In the case of a single contributing product state in Eq. (1), the subsystems are disentangled and the von Neumann entropy is given by $S_{AB} = 0$, whereas any deviation from this value indicates entanglement between the A and the B species. In the same manner we want to define a measure for the correlations which are present in each subsystem itself. Let us first remember the spectral decomposition of the one-body density of species σ , which reads

$$\rho_\sigma^{(1)}(x, t) = \sum_j n_{\sigma j}(t) \Phi_{\sigma j}^*(x, t) \Phi_{\sigma j}(x, t), \quad (9)$$

where $n_{\sigma j}(t)$ in decreasing order, obeying $\sum_j n_{\sigma j} = 1$, are the so-called natural populations and $\Phi_{j\sigma}(x, t)$ are the corresponding natural orbitals. In this sense, the natural orbitals are the eigenstates, while the natural populations are the corresponding eigenvalues, which are determined by diagonalizing the one-body density matrix. Similar to the Schmidt coefficients the natural populations serve as a measure for the correlations in a subsystem. In this spirit, we define the fragmentation in the subsystem σ as

$$S_\sigma(t) = - \sum_j n_{\sigma j}(t) \ln[n_{\sigma j}(t)]. \quad (10)$$

Here, the case of $S_\sigma = 0$ means that the subsystem σ is not depleted, meaning that all particles occupy the same single-particle state, i.e., $n_{\sigma 1} = 1$.

Figure 5 shows the temporal evolution of the von Neumann entropy $S_{AB}(t)$ and the fragmentation of the impurity species $S_A(t)$ as well as of the majority species $S_B(t)$ for the four different regimes of the dynamical response of our system, depending on the postquench interspecies interaction strength g_{AB} . Again, we start by analyzing the results for the weak quench to $g_{AB}/E_R\lambda = 0.065$. Analogously to the one-body

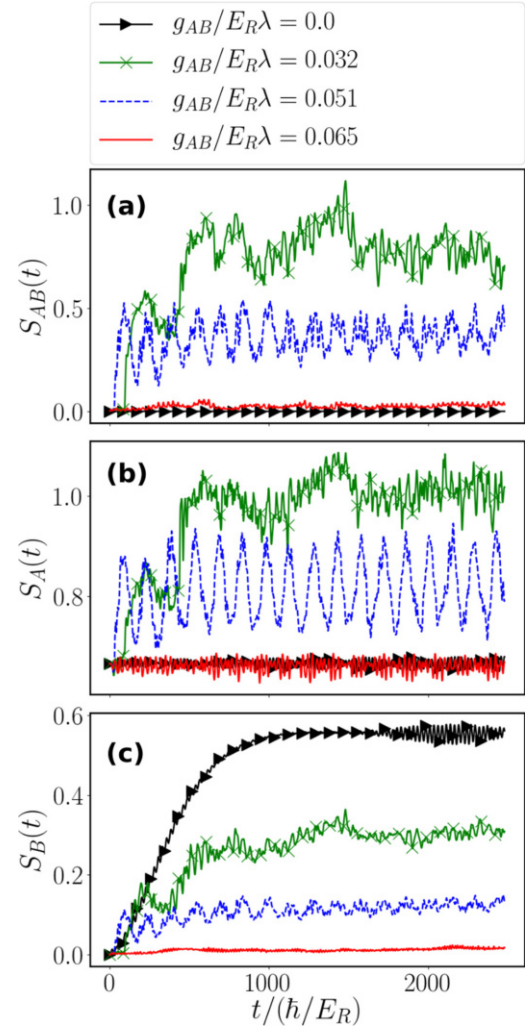


FIG. 5. Temporal evolution of (a) the von Neumann entropy $S_{AB}(t)$, (b) the fragmentation of the impurity species $S_A(t)$, and (c) the fragmentation of the majority species $S_B(t)$ for the postquench interspecies interaction strengths in Fig. 4 corresponding to the four emerging regimes. t is given in units of \hbar/E_R .

density of the impurity species the fragmentation $S_A(t)$ is in general dynamically stable, while showing only marginal fluctuations. The same is true for the von Neumann entropy $S_{AB}(t)$ as well as the fragmentation of the majority species $S_B(t)$. Quenching to $g_{AB}/E_R\lambda = 0.051$ leads to a strong response of the aforementioned quantities. The initial tunneling of the impurity species into the third well is accompanied by an increase of the fragmentation $S_A(t)$ and $S_B(t)$ as well as the von Neumann entropy $S_{AB}(t)$, whereas the reduction of the impurity species' density in the third well will reduce said quantities. We note that this effect is the strongest for the von Neumann entropy and the fragmentation of species A . The impact on the fragmentation of the majority species is minor and appears to stabilize in the course of time. Initially, the subsystems are disentangled, i.e., $S_{AB}(t=0) = 0$, which manifests itself in the system being described by a single

product state $|\Psi_0\rangle \approx |2, 2, 0, 0, 0\rangle_W \otimes |\Psi_B^3\rangle$. The moment the impurity species tunnels into the third well it will become entangled with the majority species, while in the case when the impurity species tunnels back the entanglement is reduced. However, in this case the von Neumann entropy does not drop to $S_{AB} = 0$, but rather the subsystems remain entangled to some extent. This is due to the fact that a fraction of the impurity species density remains in the third well, thereby increasing the overlap with the majority species, even though it is not clearly visible in the one-body density in Fig. 4(c). This will become evident in the following discussion of Fig. 4(e).

For stronger quenches, i.e., $g_{AB}/E_R\lambda = 0.032$, the subsystems will get even more entangled, while at the same time the impurity species exhibits stronger correlations. However, these correlations as well as the von Neumann entropy evolve less regularly compared to the previously discussed postquench interspecies interaction strength. As expected, when quenching to $g_{AB} = 0$ and thereby making the majority species transparent to the impurity species the subsystems remain disentangled in the course of time. Since the impurity species remains localized in the first and second well, also the fragmentation S_A only weakly deviates from the initial value with time. In contrast to that, the impact of this quench on the fragmentation of the subsystem B is rather strong, but shall not be the focus of the current paper's analysis. In summary, we have found four different regimes for the dynamical response of the binary mixture upon quenching the interspecies interaction strength. In the regimes in which the impurity species undergoes a tunneling to the neighboring wells, we observe strong entanglement between the majority and the impurity species as well as correlations among the impurity atoms.

B. Microscopic characterization of the tunneling process

This section is dedicated to an in-depth analysis of the many-body wave function, in particular focusing on the regimes where the impurity species undergoes a tunneling to the neighboring wells. In a first step, we want to analyze the probability of finding an impurity particle in a specific single-particle state. Naturally, for the impurity species we consider generalized Wannier functions, which are obtained by diagonalizing the position operator in the eigenbasis of the single-particle Hamiltonian $H_A^{(1)} = -\frac{\hbar^2}{2m_A} \frac{d^2}{dx^2} + V_0 \sin^2(\frac{\pi kx}{L})$, while being restricted to the lowest band. In a second step, we build number states using the Wannier functions and project the time-dependent full many-body wave function onto these number states, as described in Eq. (7). Again, the reader should note that the complete many-body wave function is obtained via ML-MCTDHX and subsequently we analyze this high-dimensional object by projecting onto the corresponding number states. In order to obtain the probability of finding an impurity particle in a specific Wannier state, we construct the operator

$$\hat{O}_l^{(1)} = \frac{1}{N_A} \sum_i^{N_A} |w_l^i\rangle\langle w_l^i|, \quad (11)$$

where $|w_l^i\rangle\langle w_l^i|$ projects the i th particle of the A species onto the l th Wannier state. Evaluating this operator with respect to

the complete many-body wave function yields the probability $P_l = \langle \Psi_{\text{MB}} | \hat{O}_l^{(1)} | \Psi_{\text{MB}} \rangle$ of finding an impurity particle in the l th Wannier state. In the following the Wannier states are ordered from left to right, i.e., $|w_1\rangle$ and $|w_2\rangle$ describe the Wannier states which are associated with the initially ($t = 0$) populated wells. The Wannier states prove to be a suitable basis set, since in all cases analyzed in the following we find that $\sum_l P_l \approx 99.97\%$. Figures 4(a) and 4(e) show the probability P_l of finding an impurity particle in the l th Wannier state upon quenching g_{AB} . For a weak quench, i.e., $g_{AB}/E_R\lambda = 0.065$, a single impurity is to be found either in the first or second Wannier state (not shown here), and therefore in the first or second well. For larger quenches, $g_{AB}/E_R\lambda = 0.051$ [see Fig. 4(a)], we mainly find oscillations between a single impurity populating the second and third well, which confirm our assumptions regarding the tunneling discussed in Sec. IV. We additionally find small fluctuations for populating the first Wannier state, which were not directly visible in the respective one-body density of the impurity species. Finally, quenching to $g_{AB}/E_R\lambda = 0.032$ a single impurity will in the course of time populate the fourth Wannier state, i.e., the fourth well, apart from populating Wannier states 1–3. Apparently, the tunneling is of such nature that mainly the second well is depleted, whereas the probability of finding an impurity in the first well only slightly reduces [see Fig. 4(e)]. Using these quantities we gain a first quantitative description of the tunneling behavior of the impurity species in terms of Wannier states.

There remains the question of how many particles actually tunnel to the neighboring wells. Such an insight can be gained by analyzing $P(|\vec{n}^A\rangle)(t)$ [see Eq. (7)]. We will in particular focus on the two postquench interspecies interaction strengths, $g_{AB}/E_R\lambda = 0.032$ and 0.051 , featuring a tunneling of the impurity species. In Fig. 6 we show the probability $P(|\vec{n}^A\rangle)(t)$ of finding the impurity species in the number state $|\vec{n}^A\rangle$ upon quenching to $g_{AB}/E_R\lambda = 0.032$ and 0.051 . We find that the number states with the largest contribution to the complete many-body wave function $|\Psi_{\text{MB}}\rangle$ are given by $|2, 2, 0, 0, 0\rangle_W$, $|2, 1, 1, 0, 0\rangle_W$, and $|2, 1, 0, 1, 0\rangle_W$, whereas for the quench to $g_{AB}/E_R\lambda = 0.051$ predominantly the first two states contribute. For $t = 0$ the impurities accumulate pairwise in adjacent sites and the corresponding many-body wave function is well described by $|\Psi_0\rangle \approx |2, 2, 0, 0, 0\rangle_W \otimes |\Psi_B^3\rangle$. Directly after the quench the probability of finding the impurities in the configuration $|2, 2, 0, 0, 0\rangle_W$ reduces, while the probability of finding the impurities in the configuration $|2, 1, 1, 0, 0\rangle_W$ increases. In essence, this means that a single impurity out of the cluster of impurities tunnels to the third well. In that way we have identified the tunneling process, discussed in Sec. IV, as a single-particle process. Focusing now on the stronger quench to $g_{AB}/E_R\lambda = 0.032$, the increased density in the fourth well [see Fig. 4(b)] can be again associated with a single-particle tunneling into that well. Considering solely the time evolution in Fig. 6(b) one might assume that the tunneling to the fourth well (blue line), i.e., the probability of finding the impurity species in the number state $|2, 1, 0, 1, 0\rangle_W$, shows a rather irregular behavior. However, analyzing the long-time evolution of the respective probabilities [Fig. 6(c)] one finds a more regular behavior of the aforementioned probabilities. It appears that the single impurity tunnels between the third

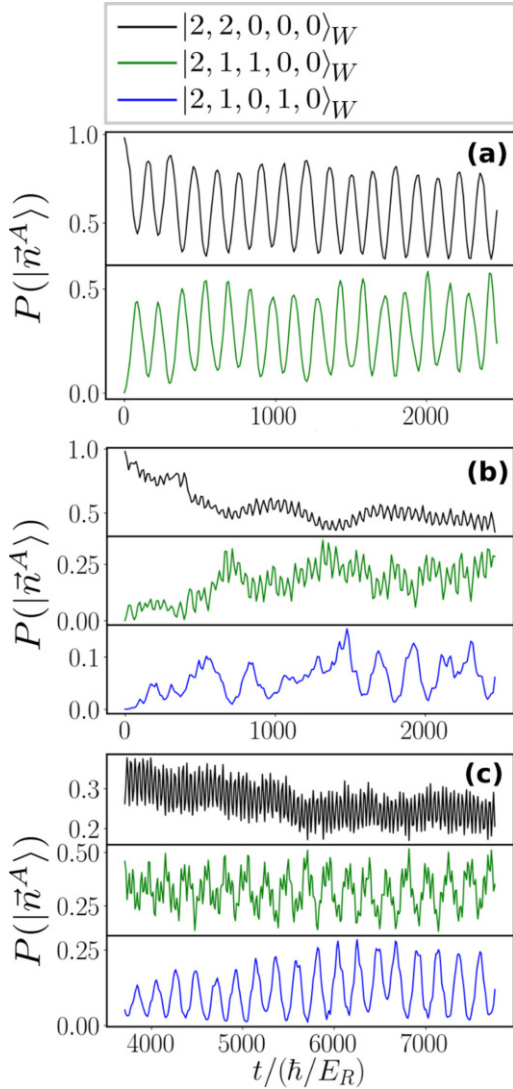


FIG. 6. Temporal evolution of the probability $P(|\vec{n}^A\rangle)(t)$ of finding the impurity species in the number state $|2, 2, 0, 0, 0\rangle_W$ [(a)–(c), first row], $|2, 1, 1, 0, 0\rangle_W$ [(a)–(c), second row], and $|2, 1, 0, 1, 0\rangle_W$ [(b, c), third row], irrespective of the number state configurations of the B species upon quenching to (a) $g_{AB}/E_R\lambda = 0.051$ and (b, c) $g_{AB}/E_R\lambda = 0.032$. Panel (c) shows the long-time evolution for a quench to $g_{AB}/E_R\lambda = 0.032$. The particle number of the respective species is chosen as $N_A = 4$ and $N_B = 10$. t is given in units of \hbar/E_R .

and fourth well, while the probability of finding the impurities in the configuration $|2, 2, 0, 0, 0\rangle_W$ is strongly reduced and exhibits high-frequency fluctuations.

Employing the projection onto number states, we obtained a detailed description of the actual character of the tunneling process in the impurity species. The initial pairwise accumulated impurity cluster breaks up in such a way that a single impurity is transferred to the neighboring well. Increasing the strength of the quench it is even possible to transfer this single impurity to the fourth well. We note that this effect is due to a finite coupling to the majority species during the

dynamics and cannot be achieved when the impurity species is not coupled to the majority species in the course of the dynamics, i.e., $g_{AB} = 0$.

Since the majority species plays an important role for the tunneling process it is of imminent interest to understand in which way this species is excited due to the quench. For this purpose, we aim at projecting the complete many-body wave function onto number states $|\vec{n}^A\rangle \otimes |\vec{n}^B\rangle$, but rather determine the probability of being in the number state $|\vec{n}^B\rangle$ irrespective of the number state configurations of the impurity species. Before this can be done we need to find an appropriate single-particle basis set upon which to build the number states $|\vec{n}^B\rangle$, which is defined as

$$P(|\vec{n}^B\rangle) = \sum_i |\langle \vec{n}^B | \otimes \langle \vec{n}^A | \Psi_{\text{MB}} \rangle|^2. \quad (12)$$

Instead of using the single-particle functions associated with the geometry, i.e., the eigenstates of a single particle in a box (hard wall boundary conditions), we rather want to employ a basis which is more tailored to the many-body problem and exhibits an impact of the interspecies interaction. For this reason we determine the effective single-particle Hamiltonian for the B species, assuming the product ansatz $|\Psi_0\rangle \approx |2, 2, 0, 0, 0\rangle_W \otimes |\Psi_B^3\rangle$ of our ground state for $t = 0$. Integrating out the impurity species we arrive at the following effective noninteracting single-particle Hamiltonian for the B species:

$$\hat{H}_B^{(1)} = -\frac{\hbar^2}{2m_B} \frac{d^2}{dx^2} + g_{AB} N_A \rho_A^{(1)}(x, t = 0). \quad (13)$$

Through diagonalization of $\hat{H}_B^{(1)}$ in a discrete variable representation basis [73] we obtain an eigenbasis for the majority species which takes the density modulation due to the presence of the impurity species into account. In Fig. 7(a) we show the corresponding eigenstates $f_{B_i}^{(1)}(x)$ together with their eigenenergies $E_{B_i}^{(1)}$. The single-particle ground-state wave function $f_{B_1}^{(1)}(x)$ is localized such that it strongly avoids the effective potential imposed by the impurity species. Apart from a slightly larger overlap with the potential $g_{AB} N_A \rho_A^{(1)}(x)$, the first excited state $f_{B_2}^{(1)}(x)$ also avoids the latter, but additionally it exhibits a single node. The next energetically higher state $f_{B_3}^{(1)}(x)$ is distributed between the peaks of the effective potential, as well as in the region where the potential is zero, having two nodes in total.

Using these single-particle functions we build the corresponding number states $|\vec{n}^B\rangle$ and determine analogously to the previous analysis $P(|\vec{n}^B\rangle)(t)$. Again we only focus on the most populated number states in the following. We note that excitations into higher excited states are negligible and it is sufficient to consider only three single-particle states for the construction of the number states. In Fig. 8 we observe that the temporal evolution of the probability $P(|\vec{n}^B\rangle)(t)$ of finding the majority species in a specific number state is dominated by single-particle excitations, i.e., $|9, 1, 0\rangle_B$ and $|9, 0, 1\rangle_B$. In this sense, the tunneling of the impurity into the neighboring sites is correlated with single-particle excitations in the majority species. Compared to the rather regular behavior of excitations in the impurity species, the excitations in the majority species fluctuate strongly, which is related to the

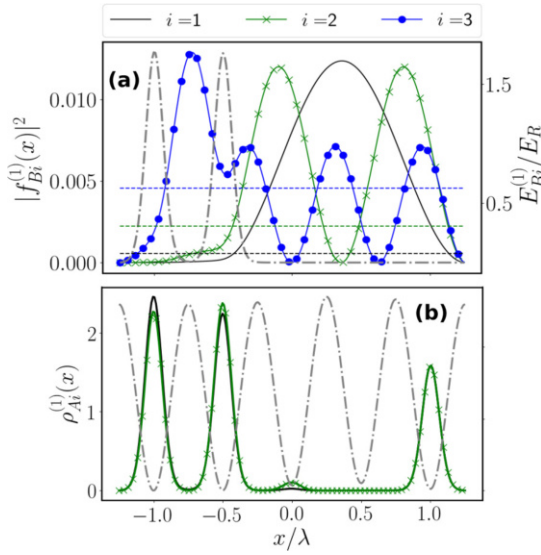


FIG. 7. (a) Spatial resolution of the eigenvectors $f_{Bi}^{(1)}(x)$ of the effective single-particle Hamiltonian $\hat{H}_B^{(1)}$ [Eq. (13)] and their respective eigenenergies $E_{Bi}^{(1)}$ (dashed lines). (b) One-body density of the many-body ground state ($i=1$) and first excited state ($i=2$) with respect to the Hamiltonian $\hat{H}_{A,\text{eff}}$. The dash-dotted gray line in panel (a) refers to the potential $g_{AB}N_A\rho_A^{(1)}(x)$ (with prequench $g_{AB}/E_R\lambda = 0.142$) and that in panel (b) refers to $g_{AB}N_B\rho_B^{(1)}(x) + V_0 \sin^2(\frac{\pi kx}{L})$ (with postquench $g_{AB}/E_R\lambda = 0.051$) in the respective effective Hamiltonian with $V_0/E_R = 13$. The particle number of the respective species is chosen as $N_A = 4$ and $N_B = 10$. x is given in units of λ and $E_{Bi}^{(1)}$ is given in units of E_R .

high-frequency oscillations of the corresponding one-body density. The initial species wave function of the B species is given by $|\Psi_B^3\rangle \approx |10, 0, 0\rangle_B$. Following the quench, the population of the number state $|10, 0, 0\rangle_B$ is reduced dramatically in the course of time. Additionally, we observe two-particle excitations which contribute strongly shortly after the quench, but reduce in the course of time to a few percent [see Fig. 8(c)]. A similar observation is made for a quench to $g_{AB}/E_R\lambda = 0.051$, but with a lowered contribution of two-particle excitations. Concluding, we have found that the tunneling of a single impurity to the neighboring wells of the lattice is accompanied by single-particle excitations in the majority species with respect to the eigenstates of an effective Hamiltonian.

Finally, using the obtained knowledge about the microscopic processes we give an explanation of the origin of the frequency content of the one-body densities $\rho_\sigma^{(1)}(x, t)$ in Fig. 4, and in particular unravel the nature of the different time scales of the corresponding oscillations. In the following we focus on the quench to $g_{AB}/E_R\lambda = 0.051$, where we observe tunneling of a single impurity solely to the third well [Fig. 4(c)]. The employed effective Hamiltonians are constructed with respect to the postquench interspecies interaction strength (i.e., $g_{AB}/E_R\lambda = 0.051$) which appears in $g_{AB}N_\sigma\rho_\sigma^{(1)}(x)$, $\sigma \in \{A, B\}$. In $\rho_B^{(1)}(x, t)$ [Fig. 4(g)] we observed high-frequency oscillations upon quenching to $g_{AB}/E_R\lambda = 0.051$. We can identify two dominant fundamental frequen-

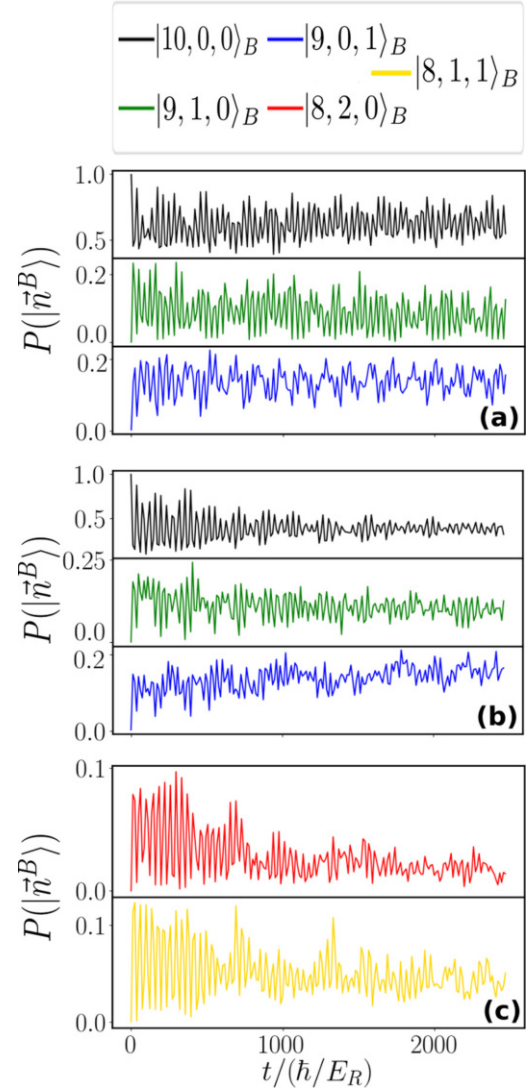


FIG. 8. Temporal evolution of the probability $P(|\vec{n}^B\rangle)(t)$ of finding the majority species in the number state $|10, 0, 0\rangle_B$ [(a, b), first row], $|9, 1, 0\rangle_B$ [(a, b), second row], $|9, 0, 1\rangle_B$ [(a, b), third row], $|8, 2, 0\rangle_B$ [(c), first row], and $|8, 1, 1\rangle_B$ [(c), second row], irrespective of the number state configurations of the A species upon quenching to (a) $g_{AB}/E_R\lambda = 0.051$ and (b, c) $g_{AB}/E_R\lambda = 0.032$. Panel (c) shows the probability for two-particle excitations for the latter quench. The particle number of the respective species is chosen as $N_A = 4$ and $N_B = 10$. t is given in units of \hbar/E_R .

cies with single-particle excitations from the state $f_{B1}^{(1)}(x)$ to $f_{B2}^{(1)}(x)$ with $(E_{B2}^{(1)} - E_{B1}^{(1)})/E_R \approx 0.18$ and from $f_{B1}^{(1)}(x)$ to $f_{B3}^{(1)}(x)$ with $(E_{B3}^{(1)} - E_{B1}^{(1)})/E_R \approx 0.37$. This single-particle picture is justified by the fact that the particles of the majority species are interacting weakly with each other. However, the fundamental frequency of $\rho_A^{(1)}(x, t)$ with respect to the tunneling into the third well cannot be identified in a single-particle picture since the impurities interact rather strongly via an intraspecies interaction of strength $g_{AA}/E_R\lambda = 0.067$. For this reason, we construct a many-body Hamiltonian for

TABLE II. Degenerate subspaces of the ground state referring to the regions in Fig. 9(c) for $V_0/E_R = 13$ and $N_B = 30$ particles in the majority species.

Regime			
I	II	III	IV
$ 1, 1, 0, 1, 1\rangle_W \otimes \Psi_B^1\rangle$	$ 2, 1, 0, 0, 1\rangle_W \otimes \Psi_B^2\rangle$ $ 1, 0, 0, 1, 2\rangle_W \otimes \tilde{\Psi}_B^2\rangle$	$ 2, 0, 0, 0, 2\rangle_W \otimes \Psi_B^3\rangle$	$ 2, 2, 0, 0, 0\rangle_W \otimes \Psi_B^4\rangle$ $ 0, 0, 0, 2, 2\rangle_W \otimes \tilde{\Psi}_B^4\rangle$

the impurity species by integrating out the majority species analogously to Eq. (13), yielding

$$\hat{H}_{A,\text{eff}} = \sum_{i=1}^{N_A} \left[-\frac{\hbar^2}{2m_A} \frac{d^2}{dx_i^2} + g_{AB} N_B \rho_B^{(1)}(x_i, t=0) + V_0 \sin^2\left(\frac{\pi k x_i}{L}\right) \right] + g_{AA} \sum_{i<j} \delta(x_i - x_j). \quad (14)$$

In Fig. 7(b) we present the one-body density of the ground state ($i = 1$) and first excited state ($i = 2$) of the many-body Hamiltonian $\hat{H}_{A,\text{eff}}$. We find that the fundamental frequency of $\rho_A^{(i)}(x, t)$ corresponds to a transition from the ground state to the first excited state with $(E_{A2} - E_{A1})/E_R \approx 0.043$. In the one-body density of the excited state this manifests itself in a higher density in the third and fifth well of the effective potential, thereby indicating the observed tunneling of the impurity species.

C. Increasing the number of majority species particles

Let us now find out whether the observed tunneling processes for $N_B = 10$ particles in the majority species persist if the number of particles in the majority species is increased. For this purpose, we set the latter to $N_B = 30$ and perform a similar analysis as compared to the previous sections. Before we turn to the dynamical response of the binary mixture let us first investigate the ground-state wave function for varying interspecies interaction strength. Instead of analyzing the explicit form of the wave function by projecting onto the corresponding number states as done in Sec. III we investigate the one-body density of the impurity species. In Fig. 9(c) we show the one-body density of the impurity species for varying interspecies interaction strengths g_{AB} . We find four different regimes for the distribution of the impurities in the lattice, whereas for $N_B = 10$ the ground-state wave function was classified by three regimes. The additional regime is characterized by impurities accumulated pairwise in the outermost wells, while the majority species occupies the central region (see [48]). The corresponding regimes, taking into account the degenerate subspaces of the wave function, are summarized in Table II. We now prepare our system with the same parameters as in the previous sections, i.e., we choose a lattice depth of $V_0/E_R = 13$ and an interspecies interaction strength of $g_{AB}/E_R\lambda = 0.14$. This leads to an initial wave function $|\Psi_0\rangle \approx |2, 2, 0, 0, 0\rangle_W \otimes |\Psi_B^4\rangle$ of the same form as in Sec. IV. Again by quenching the interspecies interaction strength to lower values we initiate the tunneling dynamics of the impurity species. In order to quantify the tunneling of the impurity species we analyze the probability $P_l = \langle \Psi_{\text{MB}} | \hat{O}_l^{(1)} | \Psi_{\text{MB}} \rangle$ of

finding an impurity particle in the l th Wannier state. In Fig. 9 we show the temporal evolution of P_l upon quenching to (a) $g_{AB}/E_R\lambda = 0.03$ and (b) $g_{AB}/E_R\lambda = 0.051$. For a quench to $g_{AB}/E_R\lambda = 0.03$ we observe a tunneling of the impurity species to the third and fourth site, while being slightly reduced in the intensity [Fig. 9(a)] compared to the case of $N_B = 10$ particles [see Fig. 4(b)]. However, for a quench to $g_{AB}/E_R\lambda = 0.051$ we solely observe a tunneling of the impurity species between the initially populated wells [Fig. 9(b)]. A reduction of the probability of finding a single impurity in the first well is accompanied by an increase of that probability in the second well and vice versa. Compared to the previous study with $N_B = 10$ particles in the majority species we do not find scenarios with a tunneling of the impurities which is restricted to the the third well [see Fig. 4(c)]. Apparently, the increased repulsive interspecies interaction with the majority species due to the increased particle number leads to the fact that the impurity species will be forced to populate the outermost well more strongly compared to the case of $N_B = 10$ particles. Nevertheless, quenching to $g_{AB}/E_R\lambda = 0$ still results in a localization of the impurities in the initially populated wells in the course of time (not shown here).

In conclusion, we have found that increasing the number of particles in the majority species leads to an altered crossover diagram where an additional regime appears. The dynamical response of the binary mixture changes due to the increased number of majority species particles. However, it is still possible to transfer the impurity species through the lattice by quenching the interspecies interaction strength. Again, this effect is due to the presence of the majority species, i.e., a finite coupling to the latter, and does not occur when the majority species is transparent to the impurities, i.e., $g_{AB} = 0$. Quenching to $g_{AB} = 0$ barely alters the initial distribution of the impurities, such that they remain localized throughout the dynamics.

V. CONCLUSIONS AND OUTLOOK

We have demonstrated that it is possible to transfer a single impurity out of initially clustered impurities through a lattice by coupling this species to a majority species. Starting from four impurities which accumulate pairwise in adjacent lattice sites we have quenched the interspecies interaction strength to a lower value. Utilizing this quench protocol we cross the boundaries of the crossover diagram of the ground state. The different regimes show different impurity distributions as a function of the interspecies interaction strength. For sufficiently small postquench interspecies interaction strengths we observe the tunneling of a single impurity out of the cluster, whereas a quench to $g_{AB} = 0$ leads to a localization of

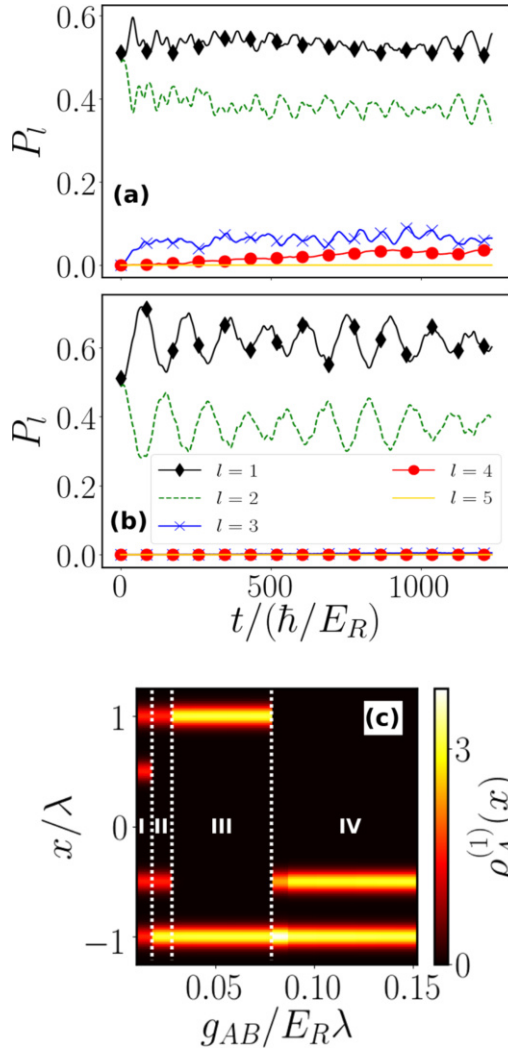


FIG. 9. Temporal evolution of the probability P_l of finding an impurity particle in the l th Wannier state upon quenching to (a) $g_{AB}/E_R\lambda = 0.03$ and (b) $g_{AB}/E_R\lambda = 0.051$. (c) One-body density $\rho_A^{(1)}(x)$ of the species A as a function of the interspecies interaction strength for a fixed lattice depth of $V_0/E_R = 13$ (see Table II). The particle number of the respective species is chosen as $N_A = 4$ and $N_B = 30$. x is given in units of λ , t is given in units of \hbar/E_R , and g_{AB} is given in units of $E_R\lambda$.

the impurities in the initially populated wells. The tunneling process of the impurity species is accompanied by strong entanglement of the subsystems as well as strong correlations among the impurities. The effect on the majority species manifests itself predominantly in single-particle excitations with respect to the eigenstates of an effective Hamiltonian which accounts for the initial one-body density distribution of the impurity species. In contrast to this we find that a single impurity does not lead to a controlled tunneling in the presence of a majority species. Furthermore, we have investigated the robustness of the tunneling process by increasing the number of particles in the majority species and revealed that it is still possible to transfer the impurity species through

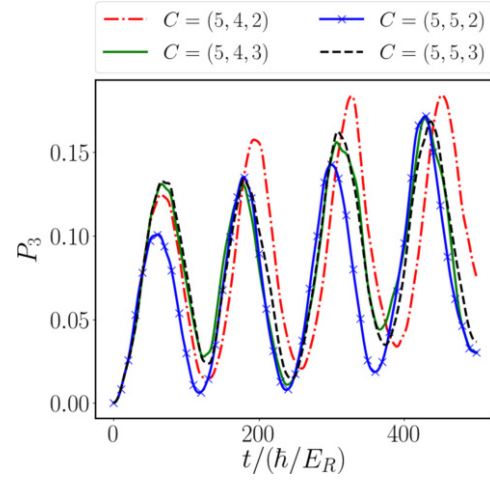


FIG. 10. Temporal evolution of the probability P_3 of finding an impurity particle in the third Wannier state upon quenching to $g_{AB}/E_R\lambda = 0.051$ for $N_B = 10$ particles in the majority species. t is given in units of \hbar/E_R

the lattice by quenching the interspecies interaction strength in case of a larger majority species. This controlled ejection of a single impurity may indeed be of interest for future applications in atomtronics [74]. In this context, it might pave new pathways, since we explicitly take advantage of the coupling to an environment, whereas usually such systems would lose their coherence when coupled to an environment due to dissipation.

There are several possible directions of future investigations. For example, it would be of immediate interest to allow for a spin degree of freedom in the impurity species, such that the initial distribution is characterized not only by a spatial distribution of the impurities but also by a spin distribution. In this spirit, a quench of the interspecies interaction strength might lead to a spatial transport of the impurities as well as a spin transport.

ACKNOWLEDGMENTS

K.K. thanks M. Pyzh for many insightful discussions. P.S. gratefully acknowledges funding by the Deutsche Forschungsgemeinschaft in the framework of SFB 925, “Light induced dynamics and control of correlated quantum systems” Project No. 170620586 and support by the excellence cluster “The Hamburg Centre for Ultrafast Imaging: Structure, Dynamics and Control of Matter at the Atomic Scale” of the Deutsche Forschungsgemeinschaft Project No. 194651731. K.K. gratefully acknowledges a scholarship of the Studienstiftung des deutschen Volkes.

APPENDIX: CONVERGENCE ANALYSIS WITHIN ML-MCTDHX

In the following, we briefly discuss the convergence of our results using a specific example case and the necessity of a computational approach which is able to take beyond mean-field effects into account for the description of the dynamical response of our binary mixture. The degree of truncation of

the underlying Hilbert space is given by the orbital configuration $C = (M, d_A, d_B)$. Here, M refers to the number of species functions in the Schmidt decomposition [see Eq. (1)], while d_σ with $\sigma \in \{A, B\}$ denote the number of single-particle functions spanning the time-dependent number states $|\vec{n}^\sigma; t\rangle$ [see Eq. (2)]. For $M = d_A = d_B = 1$ we obtain the solution of the Gross-Pitaevskii mean-field approximation. Increasing the number of species functions as well as single-particle functions we are able to recover the solution of the many-body quantum system with an increasing degree of accuracy. However, choosing too many species and single-particle functions is computationally prohibitive. Nevertheless, numerical solutions which incorporate the relevant correlations and go

beyond mean-field approximations can be obtained using ML-MCTDHF. In order to determine the effect of the truncation, we investigate as a representative example the probability P_3 of finding the impurity species in the third well [see Eq. (11)] upon varying the orbital configuration C . In Fig. 10 we show this, for example, for a quench to $g_{AB}/E_R\lambda = 0.051$ and $N_B = 10$ particles in the majority species. We observe that it is possible to achieve convergence by systematically increasing the number of species functions M and single-particle functions d_σ . Therefore, the orbital configuration $C = (5, 5, 3)$ has been employed for all many-body calculations in the main text, yielding sufficiently converged results of our observables.

-
- [1] K. Henderson, C. Ryu, C. MacCormick, and M. G. Boshier, *New J. Phys.* **11**, 043030 (2009).
- [2] C. Chin, R. Grimm, P. Julienne, and E. Tiesinga, *Rev. Mod. Phys.* **82**, 1225 (2010).
- [3] M. Olshani, *Phys. Rev. Lett.* **81**, 938 (1998).
- [4] T. Kinoshita, T. Wenger, and D. S. Weiss, *Phys. Rev. Lett.* **95**, 190406 (2005).
- [5] E. Haller, R. Hart, M. J. Mark, J. G. Danzl, L. Reichsöllner, M. Gustavsson, M. Dalmonte, G. Pupillo, and H.-C. Nägerl, *Nature (London)* **466**, 597 (2010).
- [6] G. Boeris, L. Gori, M. D. Hoogerland, A. Kumar, E. Lucioni, L. Tanzi, M. Inguscio, T. Giamarchi, C. D'Errico, G. Carleo, G. Modugno, and L. Sanchez-Palencia, *Phys. Rev. A* **93**, 011601(R) (2016).
- [7] T. Giamarchi, *Quantum Physics in One Dimension* (Oxford University, New York, 2004).
- [8] M. A. Cazalilla, R. Citro, T. Giamarchi, E. Orignac, and M. Rigol, *Rev. Mod. Phys.* **83**, 1405 (2011).
- [9] G. Modugno, G. Ferrari, G. Rosati, R. J. Brecha, A. Simoni, and M. Inguscio, *Science* **294**, 1320 (2001).
- [10] C. J. Myatt, E. A. Burt, R. W. Ghrist, E. A. Cornell, and C. E. Wieman, *Phys. Rev. Lett.* **78**, 586 (1997).
- [11] A. C. Pflanzner, S. Zöllner, and P. Schmelcher, *J. Phys. B* **42**, 231002 (2009).
- [12] A. C. Pflanzner, S. Zöllner, and P. Schmelcher, *Phys. Rev. A* **81**, 023612 (2010).
- [13] M. A. García-March, B. Juliá-Díaz, G. E. Astrakharchik, J. Boronat, and A. Polls, *Phys. Rev. A* **90**, 063605 (2014).
- [14] O. E. Alon, A. I. Streltsov, and L. S. Cederbaum, *Phys. Rev. Lett.* **97**, 230403 (2006).
- [15] M. A. Cazalilla and A. F. Ho, *Phys. Rev. Lett.* **91**, 150403 (2003).
- [16] M. A. García-March, and T. Busch, *Phys. Rev. A* **87**, 063633 (2013).
- [17] Y. Hao and S. Chen, *Phys. Rev. A* **80**, 043608 (2009).
- [18] M. Pyzh, S. Krönke, C. Weitenberg, and P. Schmelcher, *New J. Phys.* **20**, 015006 (2018).
- [19] S. Zöllner, H.-D. Meyer, and P. Schmelcher, *Phys. Rev. A* **78**, 013629 (2008).
- [20] S. Krönke, J. Knörzer, and P. Schmelcher, *New J. Phys.* **17**, 053001 (2015).
- [21] R. M. Kalas and D. Blume, *Phys. Rev. A* **73**, 043608 (2006).
- [22] P. Massignan, M. Zaccanti, and G. M. Bruun, *Rep. Prog. Phys.* **77**, 034401 (2014).
- [23] F. Grusdt, G. E. Astrakharchik, and E. A. Demler, *New J. Phys.* **19**, 103035 (2017).
- [24] A. G. Volosniev and H.-W. Hammer, *Phys. Rev. A* **96**, 031601(R) (2017).
- [25] A. S. Dehkharghani, A. G. Volosniev, and N. T. Zinner, *Phys. Rev. A* **92**, 031601(R) (2015).
- [26] M. A. García-March, A. S. Dehkharghani, and N. T. Zinner, *J. Phys. B* **49**, 075303 (2016).
- [27] A. Lampo, S. H. Lim, M. A. García-March, and M. Lewenstein, *Quantum* **1**, 30 (2017).
- [28] C. Charalambous, M. A. García-March, A. Lampo, M. Mehboudi, and M. Lewenstein, *SciPost Phys.* **6**, 010 (2019).
- [29] G. C. Katsimiga, S. I. Mistakidis, G. M. Koutentakis, P. G. Kevrekidis, and P. Schmelcher, *Phys. Rev. A* **98**, 013632 (2018).
- [30] S. I. Mistakidis, G. C. Katsimiga, G. M. Koutentakis, T. Busch, and P. Schmelcher, *Phys. Rev. Lett.* **122**, 183001 (2019).
- [31] F. M. Cucchiatti and E. Timmermans, *Phys. Rev. Lett.* **96**, 210401 (2006).
- [32] S. Palzer, C. Zipkes, C. Sias, and M. Köhl, *Phys. Rev. Lett.* **103**, 150601 (2009).
- [33] F. Meinert, M. Knap, E. Kirilov, K. Jag-Lauber, M. B. Zvonarev, E. Demler, and H.-C. Nägerl, *Science* **356**, 945 (2017).
- [34] J. Catani, G. Lamporesi, D. Naik, M. Gring, M. Inguscio, F. Minardi, A. Kantian, and T. Giamarchi, *Phys. Rev. A* **85**, 023623 (2012).
- [35] T. Fukuhara, A. Kantian, M. Endres, M. Cheneau, P. Schaul, S. Hild, D. Bellem, U. Schollwöck, T. Giamarchi, C. Gross, I. Bloch, and S. Kuhr, *Nat. Phys.* **9**, 235 (2013).
- [36] M.-G. Hu, M. J. Van de Graaff, D. Kedar, J. P. Corson, E. A. Cornell, and D. S. Jin, *Phys. Rev. Lett.* **117**, 055301 (2016).
- [37] A. Recati, J. N. Fuchs, C. S. Peça, and W. Zwerger, *Phys. Rev. A* **72**, 023616 (2005).
- [38] A. Klein and M. Fleischhauer, *Phys. Rev. A* **71**, 033605 (2005).
- [39] A. S. Dehkharghani, A. G. Volosniev, and N. T. Zinner, *Phys. Rev. Lett.* **121**, 080405 (2018).
- [40] J. Chen, J. M. Schurer, and P. Schmelcher, *Phys. Rev. Lett.* **121**, 043401 (2018).
- [41] J. Chen, J. M. Schurer, and P. Schmelcher, *Phys. Rev. A* **98**, 023602 (2018).

- [42] S. I. Mistakidis, G. C. Katsimiga, G. M. Koutentakis and P. Schmelcher, *New J. Phys.* **21**, 043032 (2019).
- [43] A. Camacho-Guardian, L. A. P. Ardila, T. Pohl, and G. M. Bruun, *Phys. Rev. Lett.* **121**, 013401 (2018).
- [44] M. Bruderer, A. Klein, S. R. Clark, and D. Jaksch, *Phys. Rev. A* **76**, 011605(R) (2007).
- [45] M. Bruderer, A. Klein, S. R. Clark, and D. Jaksch, *New J. Phys.* **9**, 411 (2007).
- [46] M. Bruderer, A. Klein, S. R. Clark, and D. Jaksch, *New J. Phys.* **10**, 033015 (2008).
- [47] K. Keiler, S. Krönke, and P. Schmelcher, *New J. Phys.* **20**, 033030 (2018).
- [48] K. Keiler and P. Schmelcher, *New J. Phys.* **20**, 103042 (2018).
- [49] S. Krönke, L. Cao, O. Vendrell, and P. Schmelcher, *New J. Phys.* **15**, 063018 (2013).
- [50] L. Cao, S. Krönke, O. Vendrell, and P. Schmelcher, *J. Chem. Phys.* **139**, 134103 (2013).
- [51] L. Cao, V. Bolsinger, S. I. Mistakidis, G. Koutentakis, S. Krönke, J. M. Schurer, and P. Schmelcher, *J. Chem. Phys.* **147**, 044106 (2017).
- [52] S. I. Mistakidis, G. C. Katsimiga, G. M. Koutentakis, P. G. Kevrekidis, and P. Schmelcher, *New J. Phys.* **20**, 043052 (2018).
- [53] J. Erdmann, S. I. Mistakidis, and P. Schmelcher, *Phys. Rev. A* **98**, 053614 (2018).
- [54] J. Erdmann, S. I. Mistakidis, and P. Schmelcher, *Phys. Rev. A* **99**, 013605 (2019).
- [55] P. Siegl, S. I. Mistakidis, and P. Schmelcher, *Phys. Rev. A* **97**, 053626 (2018).
- [56] R. Roy, A. Gammal, M. C. Tsatsos, B. Chatterjee, B. Chakrabarti, and A. U. J. Lode, *Phys. Rev. A* **97**, 043625 (2018).
- [57] B. Chatterjee, M. C. Tsatsos, and A. U. J. Lode, *New J. Phys.* **21**, 033030 (2019).
- [58] R. Horodecki, P. Horodecki, M. Horodecki, and K. Horodecki, *Rev. Mod. Phys.* **81**, 865 (2009).
- [59] P. A. M. Dirac, *Proc. Cambridge Philos. Soc.* **26**, 376 (1930).
- [60] J. Frenkel, *Wave Mechanics: Advanced General Theory* (Clarendon, Oxford, 1934).
- [61] A. Raab, *Chem. Phys. Lett.* **319**, 674 (2000).
- [62] L. Cao, I. Brouzos, S. Zöllner, and P. Schmelcher, *New J. Phys.* **13**, 033032 (2011).
- [63] L. Cao, I. Brouzos, B. Chatterjee, and P. Schmelcher, *New J. Phys.* **14**, 093011 (2012).
- [64] H.-D. Meyer, F. Gatti, and G. A. Worth, *Multidimensional Quantum Dynamics: MCTDH Theory and Applications* (Wiley, New York, 2009).
- [65] F. Köhler, K. Keiler, S. I. Mistakidis, H.-D. Meyer, and P. Schmelcher, *J. Chem. Phys.* **151**, 054108 (2019).
- [66] A. L. Gaunt, T. F. Schmidutz, I. Gotlibovych, R. P. Smith, and Z. Hadzibabic, *Phys. Rev. Lett.* **110**, 200406 (2013).
- [67] L. J. LeBlanc and J. H. Thywissen, *Phys. Rev. A* **75**, 053612 (2007).
- [68] A. Rubio-Abadal, J.-y. Choi, J. Zeiher, S. Hollerith, J. Rui, I. Bloch, and C. Gross, *Phys. Rev. X* **9**, 041014 (2019).
- [69] S. Kivelson and J. R. Schrieffer, *Phys. Rev. B* **25**, 6447 (1982).
- [70] S. Kivelson, *Phys. Rev. B* **26**, 4269 (1982).
- [71] In principle it is necessary to consider also Wannier states of higher bands, but it turns out that the many-body ground-state wave function is approximately well described by a superposition of tensor products of number states $|\vec{n}^A\rangle \otimes |\vec{n}^B\rangle$ with the Fock space of the A species restricted to the lowest band. Number states spanned by Wannier states of higher bands do not contribute.
- [72] K. Winkler, G. Thalhammer, F. Lang, R. Grimm, J. Hecker Denschlag, A. J. Daley, A. Kantian, H. P. Büchler, and P. Zoller, *Nature (London)* **441**, 853 (2006).
- [73] J. C. Light, I. P. Hamilton, and J. V. Lill, *J. Chem. Phys.* **82**, 1400 (1985).
- [74] B. T. Seaman, M. Krämer, D. Z. Anderson, and M. J. Holland, *Phys. Rev. A* **75**, 023615 (2007).

3.4 Doping a lattice-trapped bosonic species with impurities: from ground state properties to correlated tunneling dynamics

PAPER • OPEN ACCESS

Doping a lattice-trapped bosonic species with impurities: from ground state properties to correlated tunneling dynamics

To cite this article: Kevin Keiler *et al* 2020 *New J. Phys.* **22** 083003

View the [article online](#) for updates and enhancements.



PAPER

Doping a lattice-trapped bosonic species with impurities: from ground state properties to correlated tunneling dynamics

OPEN ACCESS

RECEIVED
27 April 2020REVISED
11 June 2020ACCEPTED FOR PUBLICATION
18 June 2020PUBLISHED
4 August 2020Kevin Keiler¹, Simeon I Mistakidis¹  and Peter Schmelcher^{1,2} ¹ Center for Optical Quantum Technologies, Department of Physics, University of Hamburg, Luruper Chaussee 149, 22761 Hamburg, Germany² The Hamburg Centre for Ultrafast Imaging, University of Hamburg, Luruper Chaussee 149, 22761 Hamburg, GermanyE-mail: kkeiler@physnet.uni-hamburg.de

Keywords: correlations, optical lattice, impurities

Original content from
this work may be used
under the terms of the
[Creative Commons
Attribution 4.0 licence](https://creativecommons.org/licenses/by/4.0/).Any further distribution
of this work must
maintain attribution to
the author(s) and the
title of the work, journal
citation and DOI.

Abstract

We investigate the ground state properties and the nonequilibrium dynamics of a lattice trapped bosonic mixture consisting of an impurity species and a finite-sized medium. For the case of one as well as two impurities we observe that, depending on the lattice depth and the interspecies interaction strength, a transition from a strongly delocalized to a localized impurity distribution occurs. In the latter regime the two species phase separate, thereby forming a particle–hole pair. For two impurities we find that below a critical lattice depth they are delocalized among two neighboring outer lattice wells and are two-body correlated. This transition is characterized by a crossover from strong to a suppressed interspecies entanglement for increasing impurity–medium repulsion. Turning to the dynamical response of the mixture, upon quenching the interspecies repulsion to smaller values, we reveal that the predominant tunneling process for a single impurity corresponds to that of a particle–hole pair, whose dynamical stability depends strongly on the quench amplitude. During the time-evolution a significant increase of the interspecies entanglement is observed, caused by the build-up of a superposition of states and thus possesses a many-body nature. In the case of two bosonic impurities the particle–hole pair process becomes unstable in the course of the dynamics with the impurities aggregating in adjacent lattice sites while being strongly correlated.

1. Introduction

Ultracold atomic physics offers an excellent testbed for probing the static properties and in particular the nonequilibrium quantum dynamics of multicomponent systems for both fermions and bosons [1, 2]. It provides an exquisite level of control of several system parameters including, for instance, the intra- and intercomponent scattering lengths via Feshbach resonances [1, 3], the shape of the external trapping potential [4, 5] as well as the particle number with remarkable experimental achievements especially in one spatial dimension [6, 7].

Recently, a major focus has been placed on the study of highly particle imbalanced setups [8–11] namely impurities in a many-body environment. In this context, the presence of intercomponent interactions results in the dressing of the impurities by the excitations of their medium giving rise, among others, to the concept of quasiparticles [12] e.g. polarons [8, 13, 14]. The latter exhibit extraordinary features such as an effective mass [15–17] and induced interactions [18, 19]. Owing to the very recent experimental realization of these impurity systems [9–11, 21, 22], an intense theoretical activity has been triggered for the investigation of their stationary properties [23] e.g. unveiling their excitation spectra [10, 14, 24, 25], induced-interactions [26, 27] and self-localization [28]. However, their corresponding nonequilibrium dynamics still remains largely unexplored. This partly stems from the fact that the impurities consist few-body subsystems and thus correlation-induced phenomena are expected to be pronounced especially during the dynamics, which has also been experimentally confirmed [29]. Notable examples here involve,

for instance, nonlinear pattern formation [15, 30], induced-correlations [31–33], relaxation processes [34–37], collisional aspects of an impurity with its host [38–41] as well as tunneling dynamics of impurities in optical lattices [42–50]. In this latter context transport properties of impurities [42–46], self-trapping phenomena [47, 51] and Bloch oscillations [52] have been evinced.

However, the majority of these lattice trapped impurity investigations have been mainly focusing on the case that only the impurities experience the lattice potential and the host resides in a homogeneous environment. Moreover, they have been predominantly restricted to the single impurity case [53] and operated within the lowest-band approximation [54, 55]. Thus, the situation where both the impurities and their medium are trapped in the same lattice potential remains an open question. In such a setting the impurities act as defects possessing a particle character and it would be intriguing to study the different phases that arise in the ground state of this composite system for variable impurity-medium interactions and unveil their underlying correlation properties. Recall that lattice trapped particle-balanced bosonic mixtures exhibit quantum phases [56–59, 61] being absent in their single-component counterpart. This is, partly, caused by the non-negligible presence of interspecies correlations [62]. For instance, modifications of the Mott-insulator (MI) to the superfluid (SF) phase transition [56–60] have been reported due to the existence of a second component leading to the so-called paired and counterflow superfluid states [63, 64], quantum emulsion states [57, 65] as well as losses of the intracomponent coherence [66]. In this sense, it is natural to investigate the existence and interplay of the different phases in the particle imbalanced scenario with respect to the interspecies interaction strength. As a prototypical example, henceforth we consider one or two bosonic impurities immersed in a majority species of bosons with both components being lattice trapped in one-dimension.

Having established the ground state properties of this setup another fruitful prospect is to inspect its corresponding nonequilibrium dynamics by quenching the system between the different emergent phases. Here the analysis and consequent control of the tunneling dynamics of the impurities is of particular importance since it might give rise to a variety of complex transport phenomena, self-trapping events and formation of (repulsively) bound pairs [48–51, 67, 68]. Furthermore, the identification of the correlated many-body nature of the different tunneling processes will allow us to infer their microscopic origin which is certainly of interest. To track the static properties and the quench dynamics of the particle imbalanced Bose–Bose mixture we utilize the variational multi-layer multi-configuration time-dependent Hartree method for atomic mixtures (ML-MCTDHX) [69–71] which enables us to capture all the relevant interparticle correlations of this multicomponent setup.

Regarding the ground state of a single and two bosonic impurities immersed in a majority bosonic species we find a transition from a SF to a MI phase of the composite system (doped insulator) for a specific lattice depth and increasing interspecies repulsion. This is in sharp contrast to the case of a homogeneous bath where a MI state cannot be naturally achieved. This transition takes place for weaker impurity-medium interactions for deeper lattices, a result which is more pronounced in the two impurity case. Within the SF phase the impurity and the majority species show a delocalized behavior with the interspecies entanglement being enhanced and the medium being characterized by strong two-body correlations. However entering the MI state of the mixture, the species phase separate forming a particle hole-pair and their entanglement is suppressed [48, 72]. The formation of the particle hole-pair is exclusively caused by the impurity acting as a defect for the bath, an effect being absent in particle-balanced mixtures due to their similar intrinsic composition. In this latter case the many-body state of the system exhibits a two-fold degeneracy [74]. Moreover, for two impurities we observe that below a critical lattice depth the impurities are delocalized among two neighboring outer wells of the lattice and are two-body correlated.

Turning to the dynamical response of the mixture, upon quenching the interspecies repulsion from a MI to a SF phase, we reveal that the predominant tunneling process for a single impurity corresponds to that of a particle–hole pair [73], whose dynamical stability depends strongly on the quench amplitude. More specifically, the initially localized impurity becomes spatially delocalized in the course of the evolution while it gradually tunnels from one side of the lattice to the other. On the other hand, the majority species particles tend to avoid the impurity in the course of the tunneling. During the time-evolution a significant increase of the interspecies entanglement is observed, which is due to the build-up of superposition of states and thus possesses a many-body nature. Additionally, strong correlations occur between the particles of the majority species. In the case of two bosonic impurities the particle–hole pair process becomes unstable during the evolution with the impurities aggregating in adjacent lattice sites while being strongly correlated.

This work is structured as follows. In section 2 we introduce our setup and discuss the variational many-body approach. Section 3 presents the ground state properties in a finite lattice for a single and two impurities immersed in a strongly interacting majority bosonic species with filling smaller than unity. The nonequilibrium dynamics of the impurities by quenching the interspecies interaction strength from the

doped insulator to the SF phase is analyzed in section 4. We summarize our results and provide an outlook in section 5. Appendix A elaborates on the lattice trapped ground state phase diagram of an impurity in a unit filling majority species.

2. Setup and variational many-body approach

2.1. Treatment of many-body correlations and dynamics

Our computation approach is the *ab-initio* multi-layer multi-configuration time-dependent Hartree method for bosonic (fermionic) mixtures (ML-MCTDHX) [69–71], which accounts for all the relevant correlations of the atomic mixture [50, 72, 75–78]. As a first step, the total many-body wave function $|\Psi_{\text{MB}}(t)\rangle$ is expanded in M species functions $|\Psi^\sigma(t)\rangle$ of species σ and written as a Schmidt decomposition [79]

$$|\Psi_{\text{MB}}(t)\rangle = \sum_{i=1}^M \sqrt{\lambda_i(t)} |\Psi_i^A(t)\rangle \otimes |\Psi_i^B(t)\rangle. \quad (1)$$

Here, the Schmidt coefficients $\sqrt{\lambda_i}$, in decreasing order, provide information about the degree of population of the i th species function and thereby determine the degree of entanglement between the impurities and the majority species. In case that $\lambda_1 = 1$ the species A and B are not entangled and the system can be described with a species mean-field ansatz corresponding to a single product state ($M = 1$).

Furthermore, the species wave functions $|\Psi^\sigma(t)\rangle$ describing an ensemble of N_σ bosons are expanded in a set of permanents

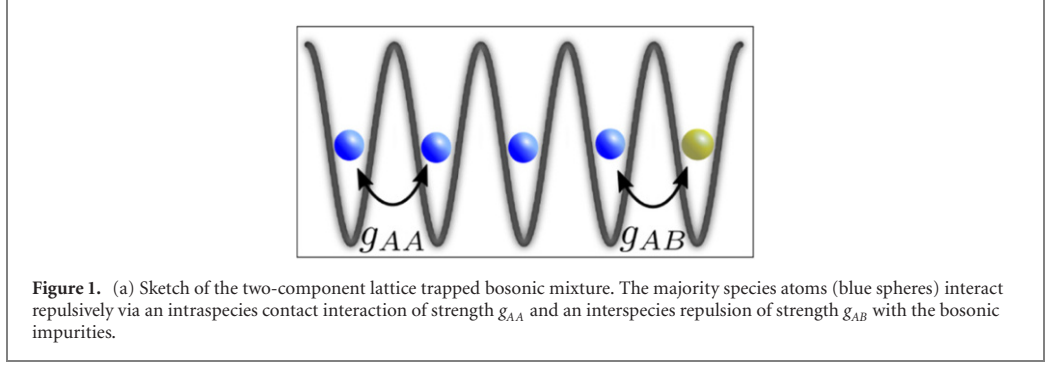
$$|\Psi_i^\sigma(t)\rangle = \sum_{\vec{n}^\sigma | N_\sigma} C_{\sigma\vec{n}}(t) |\vec{n}^\sigma; t\rangle, \quad (2)$$

where the vector $\vec{n}^\sigma = (n_1^\sigma, n_2^\sigma, \dots)$ denotes the occupations of the time-dependent single-particle functions of the species σ . The notation $\vec{n}^\sigma | N_\sigma$ indicates that for each $|\vec{n}^\sigma; t\rangle$ we require the condition $\sum_i n_i^\sigma = N_\sigma$. The time propagation of the many-body wave function is achieved by employing the Dirac–Frenkel variation principle $\langle \delta\Psi_{\text{MB}} | (i\partial_t - \mathcal{H}) | \Psi_{\text{MB}} \rangle$ [80–82] with the variation $\delta\Psi_{\text{MB}}$. ML-MCTDHX provides access to the complete many-body wave function which allows us consequently to derive all relevant characteristics of the underlying system. In particular, this means that we are able to characterize the system by projecting onto number states with respect to an appropriate single-particle basis [83, 84]. Besides investigating the quantum dynamics it allows us to determine the ground (or excited) states by using either imaginary time propagation or improved relaxation [85], thereby being able to uncover also possible degeneracies of the many-body states. We remark that in commonly used approaches for solving the time-dependent Schrödinger equation, one typically constructs the wave function as a superposition of time-independent Fock states with time-dependent coefficients. Instead, it is important to note that the ML-MCTDHX approach considers a co-moving time-dependent basis on different layers, meaning that in addition to time-dependent coefficients the single particle functions spanning the number states are also time-dependent. This leads to a significantly smaller number of basis states and configurations that are needed to obtain an accurate description of the system under consideration and thus reduces the computation time [86].

The degree of truncation of the underlying Hilbert space is given by the orbital configuration $C = (M, d_A, d_B)$. Here, M refers to the number of species functions in the Schmidt decomposition (cf equation (1)), while d_σ with $\sigma \in \{A, B\}$ denote the number of single-particle functions spanning the time-dependent number states $|\vec{n}^\sigma; t\rangle$ (cf equation (2)). The orbital configuration $C = (7, 7, 7)$ has been employed for all many-body calculations presented in the main text, yielding a converged behavior of our observables.

2.2. Lattice trapped bosonic mixture

Our system consists of a mixture of two bosonic species which are trapped in a one-dimensional lattice with hard wall boundary conditions at its endpoints (figure 1). The impurity species with $N_B = 1, 2$ particles is denoted as species B and the majority species containing $N_A = 4$ (main text) or $N_A = 5$ (appendix A) particles is referred to as species A . This setup lies within reach of current experimental techniques [87, 88]. Furthermore, we introduce a coupling Hamiltonian \hat{H}_{AB} between the two species. Both subsystems are confined along the longitudinal spatial direction, accounting for the one-dimensional character of our setup. Excitations in the corresponding transversal direction are energetically suppressed in the scenario under investigation and can therefore be neglected in our setup. This results in a Hamiltonian of the form



$\hat{H} = \hat{H}_A + \hat{H}_B + \hat{H}_{AB}$. The Hamiltonian of the species σ , with $\sigma \in \{A, B\}$, reads

$$\hat{H}_\sigma = \int_{-L/2}^{L/2} dx \hat{\Psi}_\sigma^\dagger(x) \left[-\frac{\hbar^2}{2m_\sigma} \frac{d^2}{dx^2} + V_0 \sin^2\left(\frac{\pi kx}{L}\right) + g_{\sigma\sigma} \hat{\Psi}_\sigma^\dagger(x) \hat{\Psi}_\sigma(x) \right] \hat{\Psi}_\sigma(x), \quad (3)$$

where $\hat{\Psi}_\sigma^\dagger$ is the field operator of species σ , m_σ their mass and V_0 the lattice depth. Also, $g_{\sigma\sigma}$ refers to the intraspecies interaction strength of the two-body contact interaction among the σ atoms, k is the number of lattice wells and L is the length of the system, while $x \in [-L/2, L/2]$. Moreover, we assume equal masses for the species $m_A = m_B$. Experimentally this can be achieved by preparing e.g. ^{87}Rb atoms in two different hyperfine states [89]. The interaction between the species A and B is given by

$$\hat{H}_{AB} = g_{AB} \int_{-L/2}^{L/2} dx \hat{\Psi}_A^\dagger(x) \hat{\Psi}_A(x) \hat{\Psi}_B^\dagger(x) \hat{\Psi}_B(x), \quad (4)$$

where g_{AB} is the effective one-dimensional interspecies interaction strength. The interaction strengths g_α ($\alpha \in \{A, B, AB\}$) can be expressed in terms of the three dimensional s-wave scattering lengths a_α^{3D} . By assuming the above-mentioned strong transversal confinement with the same trapping frequencies $\omega_\perp^\sigma = \omega_\perp$ for both species $\sigma \in \{A, B\}$ it is possible to integrate out frozen degrees of freedom, leading to a quasi one-dimensional model with $g_\alpha = 2\hbar\omega_\perp a_\alpha^{3D}$.

Throughout this work we consider a $k = 5$ well lattice, while the interaction among the majority atoms is set to a value where the particles distribute in a Mott-like state for large lattice depths, namely $g_{AA}/E_R\lambda = 0.04$. Here, $E_R = (2\pi\hbar)^2/2m_A\lambda^2$ is the recoil energy and $\lambda = 2L/k$ the optical lattice wavelength.

3. Ground state properties

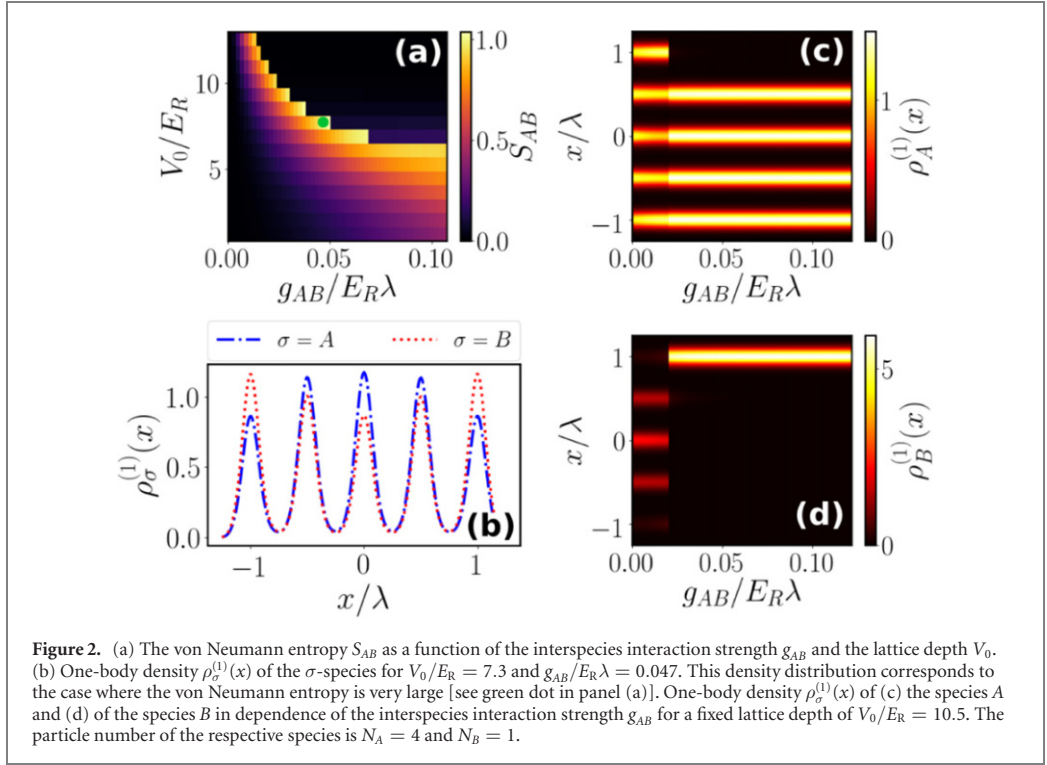
Let us analyze the ground state properties of the Bose–Bose mixture with respect to the lattice depth V_0 and the interspecies coupling strength g_{AB} for $N_B = 1$ and $N_B = 2$ impurities. We calculate the many-body ground state of the Bose–Bose mixture using ML-MCTDHX, which enables us to obtain the resulting full many-body wave function. In order to be able to interpret the wave function, we shall analyze reduced quantities such as the von Neumann entropy and the one- and two-body densities of each species on the basis of the numerically obtained many-body wave function. As a result, we are able to gain an in-depth insight into the spatial distribution of the two species in the lattice potential and the accompanying intra- and inter-species correlations.

3.1. Single impurity

In the following, we explore the ground state of the system containing a single impurity, i.e. $N_B = 1$, for varying V_0 and g_{AB} , while keeping fixed the intraspecies interaction strength to $g_{AA}/E_R\lambda = 0.04$. As a first step, we analyze the spatial distribution of the two species in terms of the one-body density of the ground state $|\Psi_{\text{MB}}\rangle$ of the species σ , which is defined as

$$\rho_\sigma^{(1)}(x) = \langle \Psi_{\text{MB}} | \hat{\Psi}_\sigma^\dagger(x) \hat{\Psi}_\sigma(x) | \Psi_{\text{MB}} \rangle. \quad (5)$$

Additionally, in order to deepen our understanding of the ground state of the binary mixture, we investigate the degree of correlations and, in particular the entanglement between the impurity species and the



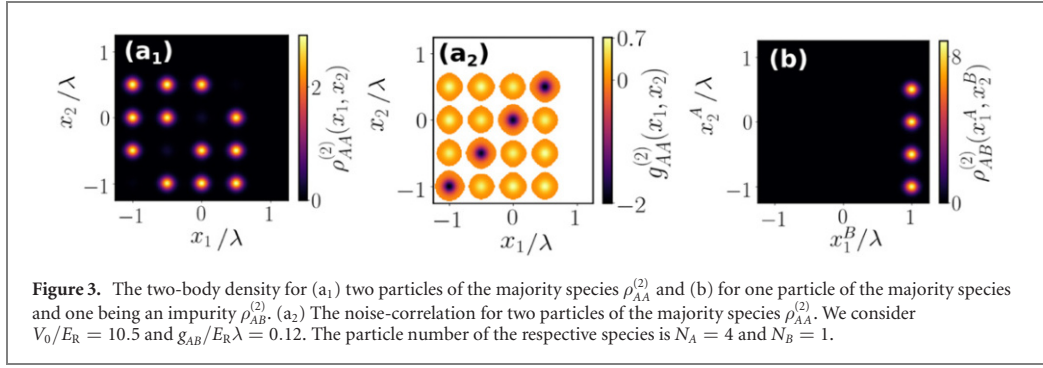
majority species. For this purpose, we introduce the von Neumann entropy

$$S_{AB} = -\sum_i \lambda_i \ln(\lambda_i) \quad (6)$$

as a measure for the entanglement between the subsystems A and B, where λ_i are the Schmidt coefficients defined in equation (1). Recall that in the case of a single contributing product state in equation (1), the subsystems are disentangled and the von Neumann entropy is $S_{AB} = 0$, whereas any deviation from this value indicates entanglement between the A and the B species.

Figure 2(a) shows the von Neumann entropy of the ground state as a function of the interspecies interaction strength g_{AB} and the lattice depth V_0 . For small g_{AB} we observe that $S_{AB} \approx 0$, which indicates that our system is well described by a single product state. Increasing g_{AB} leads to a growth of the von Neumann entropy. For sufficiently large lattice depths S_{AB} is maximized for a specific value of g_{AB} (cf $V_0/E_R = 7.3$ and $g_{AB}/E_R\lambda = 0.047$), while any further increase of the latter leads to a sudden reduction of the entropy becoming subsequently close to zero which again corresponds to a single product state representation of the many-body wave function.

In order to understand the relationship between the particle distribution of each species and the von Neumann entropy it is useful to investigate the one-body density of the σ -species as a function of the interspecies interaction strength (see figures 2(c) and (d)). As it can be seen, up to a specific value g_{AB} the majority species A is distributed over the whole lattice geometry, with a slight decrease (increase) of the density in the central (outer) well(s) for a larger g_{AB} . From this critical value onward the majority species forms a hole in one of the outer wells and it is now only distributed over the four remaining wells. Similarly, we observe for the impurity that up to this critical value of g_{AB} it is distributed over the central three sites, showing an increasing density in the outer wells for larger g_{AB} . However, as soon as a hole is formed in the majority species the impurity localizes in a single outer well which is unoccupied by the majority species. The latter is accompanied by the formation of a two-fold degeneracy in the ground state. In this sense, the ground state is given by the density distribution for large g_{AB} as depicted in figures 2(c) and (d) and its parity-symmetric (with respect to $x = 0$) counterpart. Consequently, the densities shown for large g_{AB} correspond to only one of the two energetically degenerate ground states. Focusing on the above-described critical value of g_{AB} , e.g. for $V_0/E_R = 10.5$ we observe a minor population of the impurity in the outer wells. However, this spatial species distribution in $\rho_B^{(1)}(x)$ is more pronounced for smaller values of V_0 . This means that the corresponding one-body density is increased in the outer wells. Indeed, for $V_0/E_R = 7.3$ and $g_{AB}/E_R\lambda = 0.047$ (as compared to $V_0/E_R = 10.5$ and $g_{AB}/E_R\lambda = 0.02$ in figure 2(d)) the impurity is largely



distributed over the lattice geometry and exhibits an increased density in the outer wells (see figure 2(b)). Correspondingly, the density of the majority species is smaller in the outer wells compared to the central ones. This large overlap between the two species on the level of the one-body densities is responsible for the maximized von Neumann entropy at the critical value of g_{AB} . In turn, this explains the sudden decrease of S_{AB} which is associated with a phase-separation of the two species [90–93] and the formation of a doped insulator for the composite system. Concluding, an increase of the von Neumann entropy is associated with a strong delocalization of the impurity, thereby leading to a large overlap of the two species. From a critical value of g_{AB} onward we observe a phase-separation of the two species which is accompanied by a decrease of the von Neumann entropy to $S_{AB} \approx 0$. This can also be viewed as the formation of a particle–hole pair [73], where the majority species forms the hole in one of the outer wells.

To obtain a deeper understanding of the particle distribution, as a next step, we inspect the two-body reduced density which reads

$$\rho_{\sigma\sigma'}^{(2)}(x_1^\sigma, x_2^{\sigma'}) = \langle \Psi_{MB} | \hat{\Psi}_\sigma^\dagger(x_1^\sigma) \hat{\Psi}_{\sigma'}^\dagger(x_2^{\sigma'}) \hat{\Psi}_\sigma(x_1^\sigma) \hat{\Psi}_{\sigma'}(x_2^{\sigma'}) | \Psi_{MB} \rangle, \quad (7)$$

where $\sigma, \sigma' \in \{A, B\}$. This measure corresponds to the probability of finding a particle of species σ at the position x_1^σ and another particle of species σ' at the position $x_2^{\sigma'}$.³ Figure 3(a₁) illustrates this quantity for two particles of the majority species and figure 3(b) for one particle of the majority species and one impurity for $V_0/E_R = 10.5$ and $g_{AB}/E_R\lambda = 0.12$. This parameter set corresponds to the case where the two species form a particle hole-pair and thereby phase-separate. This fact can also be observed in the behavior of the interspecies two-body density $\rho_{AB}^{(2)}$ (see figure 3(b)). Indeed, the probability of finding a particle of species A and a particle of species B at the same position is approximately zero, i.e. $\rho_{AB}^{(2)}(x, x) \approx 0$. Instead, measuring the impurity in one of the outermost wells, we may find the majority species localized in any other well with approximately the same probability. This indicates that the majority species is equally distributed over four out of the five wells. In this context, the question arises how the majority species particles distribute among each other. As shown, in figure 3(a₁) we find that the probability of detecting two particles of species A at the same position is approximately zero, i.e. $\rho_{AA}^{(2)}(x, x) \approx 0$. This means that two particles of the majority species tend to avoid each other and do not occupy the same well. From this we can conclude, that they form a Mott insulator-like state on the four populated wells. In this sense, the complete wave function of the system in this regime can be well described as follows

$$|\Psi_{MB}\rangle \approx |1, 1, 1, 1, 0\rangle_A \otimes |0, 0, 0, 0, 1\rangle_B. \quad (8)$$

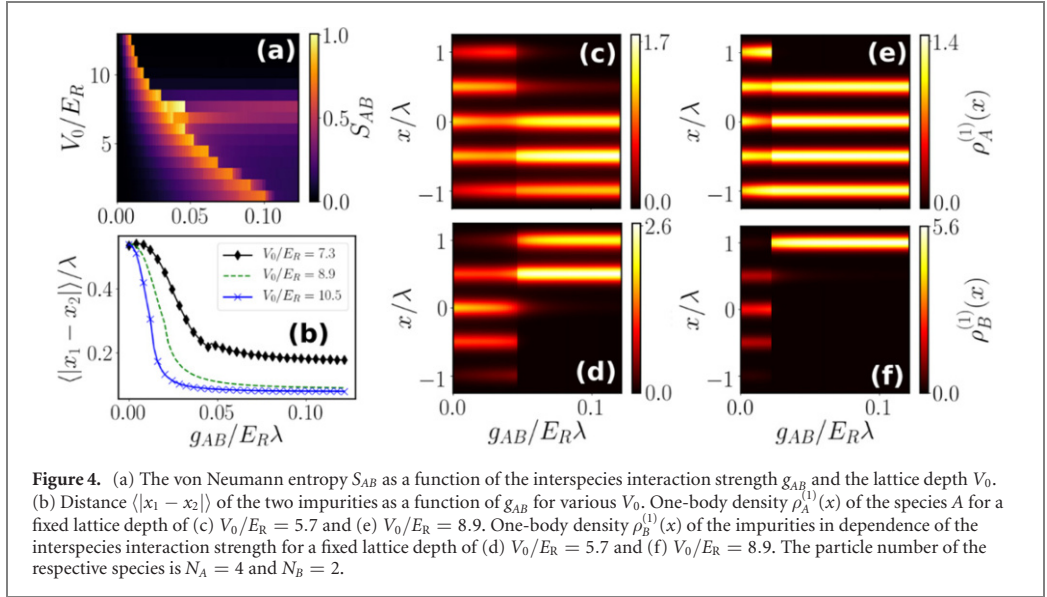
Here, the number state $|\vec{n}^\sigma\rangle = |n_1^\sigma, n_2^\sigma, n_3^\sigma, n_4^\sigma, n_5^\sigma\rangle_\sigma$ is constructed with a generalized Wannier basis of the lowest band [94, 95]. This means that e.g. n_1^σ describes the number of σ atoms in the left localized Wannier state of the lowest band. This state essentially describes the doped insulator configuration of the composite system.

In order to unravel the role of correlations for the ground state distribution in the strong interaction regime, we calculate the noise correlation [64] between particles of species σ and σ' which is defined as

$$g_{\sigma\sigma'}^{(2)}(x_1^\sigma, x_2^{\sigma'}) = \rho_{\sigma\sigma'}^{(2)}(x_1^\sigma, x_2^{\sigma'}) - \rho_\sigma^{(1)}(x_1^\sigma) \rho_{\sigma'}^{(1)}(x_2^{\sigma'}). \quad (9)$$

The noise correlation is a measure for the deviation of the conditional probability of finding two particles at specific positions from the unconditional one given by the product of two single-particle events. In this sense, it gives insight into whether two particles can be viewed as independent from each other or not and

³ Please note, that in the case two particles are of the same species, we omit the superscript of the species label at the position symbol.

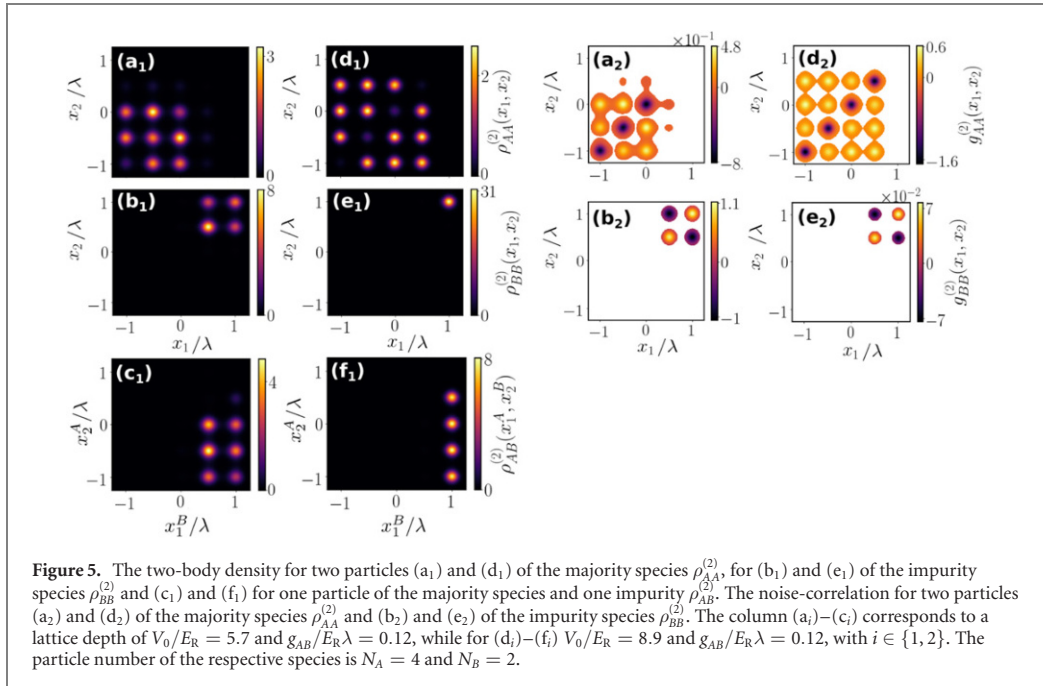


therefore suggest the occurrence of beyond single-particle processes in the system. In the former case $g_{\sigma\sigma'}^{(2)} = 0$ and in the latter case $g_{\sigma\sigma'}^{(2)} \neq 0$. In figure 3(a₂) we show $g_{AA}^{(2)} = 0$ corresponding to the previously discussed two-body density for two particles of the A species for $V_0/E_R = 10.5$ and $g_{AB}/E_R\lambda = 0.12$. Let us remark that in case of $g_{\sigma\sigma'}^{(2)} < 10^{-2}$, two-body processes are negligible and therefore we set the color of the colormap to white. Moreover, we do not show the interspecies noise correlation, since it does not exhibit any significant structures due to the ground state being well described by the wave function of equation (8). The measurement of one particle of species A does not depend on the previous measurement of the particle in species B and vice versa. However, as one might expect the noise correlation between two particles of species A shows a more involved structure. In particular the conditional probability of finding two particles of the majority species at the same position deviates strongly from the unconditional one. This is a clear signature of the Mott insulator-like state formed by the A species. Furthermore, we find a difference between the two probabilities in the off-diagonal elements of $g_{AA}^{(2)}$, which again emphasizes the correlated nature of this state.

In summary, we have found that our system containing a single impurity interacting repulsively with a majority species undergoes a transition regarding the ground state of the system in dependence of the interspecies interaction strength and the lattice depth. This transition manifests itself in an increase of interspecies entanglement with increasing g_{AB} , which is accompanied by a delocalization of the impurity followed by a sudden decrease of the entanglement. The latter is due to the phase-separation (or particle-hole formation) between the species constituting a doped insulator, which takes place for sufficiently large g_{AB} and exhibits an energetic degeneracy of the ground state.

3.2. Two bosonic impurities

In the following, we investigate the ground state of the above-discussed system, but with an additional impurity, i.e. $N_B = 2$. In order to focus on the effect of the interspecies interaction we set the intraspecies interaction strength among the impurity particles to zero, i.e. $g_{BB} = 0$. Analogously to the analysis above we first examine the interspecies entanglement and the corresponding one-body densities of each species. Evidently, in figure 4(a) we observe an alteration of the crossover diagram, given by the von Neumann entropy as a function of g_{AB} and V_0 , compared to the case of a single impurity (see also figure 2(a)). More specifically, for large lattice depths an increase of entanglement between the species takes place up to a critical value of the interspecies interaction strength followed by a sudden reduction of S_{AB} to zero for a further increase of g_{AB} . This increase of entanglement is again related to the delocalization of the impurities in the lattice, thereby enhancing the overlap between the species on the one-body density level (see figure 4(f)). The sudden reduction of S_{AB} in turn is a result of the phase-separation of the two species (see figures 4(e) and (f)), similar to the case of a single impurity. However, for smaller values of the lattice depth (e.g. $V_0/E_R = 5.7$) we observe a slightly different behavior of the entanglement and the related one-body densities, as compared to the case of a single impurity. We still find a critical g_{AB} which is associated with the delocalization of the impurity species, while for larger values of g_{AB} the entanglement does not drop to zero. Instead, S_{AB} saturates towards a finite value, which means that the two species remain entangled and



the ground state cannot be described by a single product state. The reason for this can be traced back to the distribution of the one-body densities of the two species. For large g_{AB} the impurity species distributes over two of the outer wells with an increased density in the well which is closer to the center (see figure 4(d)). The majority species in turn exhibits a residual density in this very well (see figure 4(c)), which leads to a finite overlap of the two species and thereby to a finite entanglement. Let us again remark here that the above-discussed two ground states for $V_0/E_R = 5.7$ and $V_0/E_R = 8.9$ and large g_{AB} (cf figures 4(c)–(f)) are two-fold degenerate with a parity-symmetric counterpart (with respect to $x = 0$).

In the next step, we want to understand how the two impurities are distributed. As a first measure, we investigate the relative distance [30, 32] of the two impurities

$$\langle |x_1 - x_2| \rangle = \int_{-L/2}^{L/2} \int_{-L/2}^{L/2} dx_1 dx_2 |x_1 - x_2| \rho_{BB}^{(2)}(x_1, x_2), \quad (10)$$

with $\rho_{BB}^{(2)}(x_1, x_2)$ being the previously introduced two-body density of two impurities. Figure 4(b) shows the impurity distance as a function of the interspecies interaction strength for various lattice depths. We observe that for increasing g_{AB} and fixed V_0 the distance of the impurities decreases and saturates to a specific value for even larger g_{AB} . Also, for smaller V_0 we identify a larger impurity distance. Apparently, in spite of the delocalization of the impurity species in the one-body density up to a critical value, the distance $\langle |x_1 - x_2| \rangle$ decreases, which suggests that the nature of the delocalization is not completely intuitive and needs to be inspected in detail (see below). The saturation of the impurity distance towards a finite value for large g_{AB} can be associated with the localization of the impurities in a single outer well for very deep lattices or in two adjacent sites for smaller V_0 . The fact that the distance for the latter case should be larger as compared to the former one, becomes evident in the clear separation of the corresponding lines for large g_{AB} (cf black diamonds and green dashed line in figure 4(b)). In general, note that the decay of the relative impurity distance is indicative of an induced attractive interaction between the impurities [18–20, 74]. However, this quantity does not allow for a detailed insight into the actual spatial distribution of the individual impurities. This can be gained by investigating the spatially resolved two-body density of the impurities (see equation (7)).

Let us in the following focus on the two cases of large g_{AB} , where the impurity species either localizes on a single site (cf figure 4(f)) or on two adjacent sites (cf figure 4(d)), a result that depends on the lattice depth. For the case where the impurities localize on a single site we find that the majority species exhibits mostly a Mott insulator like structure (cf figure 5(d_1)) as in the single impurity scenario. This implies that the particles of the majority species mostly tend to avoid each other and each one occupies a single distinct lattice site. Moreover, in this context the probability $\rho_{BB}^{(2)}$ of finding two impurities at specific positions x_1 and x_2 accumulates at a single outer site of the lattice geometry (see figure 5(e_1)). This means that the two

impurities tend to occupy the same site. The previously observed phase-separation of the two species is then also reflected in the corresponding two-body density $\rho_{AB}^{(2)}$ (cf figure 5(f₁)). In general, we can conclude that two impurities behave similarly to a single impurity for large lattice depths and large interspecies interaction strengths. However, the situation is not that intuitive when the impurity species occupies two adjacent sites for smaller lattice depths. Here, the majority species does not exhibit a Mott insulator-like structure, where the particles avoid each other. Instead, two particles of the majority species can be mostly found either at the same site or on two different ones, while the occupied sites are dominantly those which are not populated by the impurity species (see figure 5(a₁)). The latter fact can also be observed in the two-body density $\rho_{AB}^{(2)}$ for two particles of different species (see figures 5(c₁) and (f₁)). Indeed, to a large extent the two species avoid each other, which indicates a phase separation where the impurity species occupies two adjacent outer wells and the majority species populates the other unoccupied wells. Nevertheless, this phase-separation is not complete and there is a finite, but small, overlap of the two species which we already discussed in the framework of the von Neumann entropy (see figure 4(a)).

Coming back to the question of how the individual impurities distribute, in figure 5(b₁) it becomes clear that the impurity species occupying two adjacent sites may either have two particles at the same site or on two different sites. In this sense, the impurities are delocalized over these two sites. We also note that we have a slightly increased probability of finding the impurities at the same site which is adjacent to the sites occupied by the majority species.

In order to understand whether the findings in the two-body densities are dominated by two-body processes we subsequently investigate the noise-correlation for two particles of the same species (see equation (9)) for $V_0/E_R = 5.7$, $V_0/E_R = 8.9$ and $g_{AB}/E_R\lambda = 0.12$. For $V_0/E_R = 8.9$ the structure of the noise-correlation for two particles of the *A* species (figure 5(d₂)) is similar to the one for a single impurity in figure 3(a₂) which is to be expected since the particles of the majority species are in a Mott insulator-like state. Interestingly, in this scenario the noise-correlation for two impurities only shows a very weak structure of the order of 10^{-2-4} (see figure 5(e₂)). This means that the accumulation of the two impurities in a single site is well described by the one-body densities such that the measurement of one impurity is independent of the previous one of the other impurity. However, this is not the case for $V_0/E_R = 5.7$ and $g_{AB}/E_R\lambda = 0.12$, where the impurities accumulate in adjacent sites. Here, the conditional probability of finding two particles of the impurity species at the same position deviates strongly from the unconditional one (see figure 5(b₂)). This is also the case for finding the impurities at different sites. Also, for two particles of the majority species we observe that $g_{AA}^{(2)} \neq 0$ in the relevant occupied sites (see figure 5(a₂)), with a structure similar to figure 5(d₂). Therefore, we can conclude that for $V_0/E_R = 5.7$ not only the particles of the *A* species exhibit two-body correlation effects but also the two impurities as compared to the case of $V_0/E_R = 8.9$.

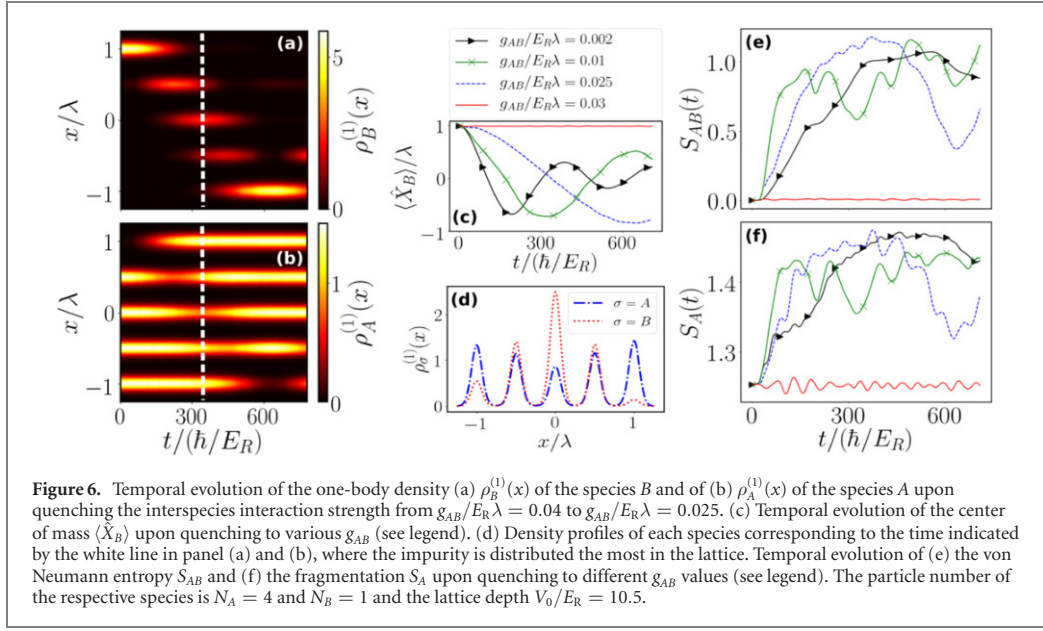
In summary, we have found that for large lattice depths and strong interspecies interaction strengths two impurities accumulate in a single outer lattice well, a behavior that is similar to the case of a single impurity. As a result the majority species occupies the other four lattice sites in a Mott insulator-like state and the composite system forms a doped insulator configuration. However, for smaller lattice depths the impurity species distributes over two adjacent lattice sites which in turn leads to a larger overlap of the two species. Also, the majority species now dominantly populates the three remaining unoccupied wells. This change in the distribution is accompanied by the presence of non-negligible correlations not only among the majority species atoms, as in the previous case, but also between the impurity atoms.

4. Correlated tunneling dynamics

Having analyzed in detail the ground state properties of a lattice trapped bosonic mixture, we subsequently study its dynamical response upon quenching the interspecies interaction strength. To this end, we prepare our system, for one as well as two impurities, in its ground state for large lattice depths and strong interspecies interaction strengths such that the impurity species occupies one of the outer wells. In this regime the two species phase separate and form a particle–hole pair, as discussed in the previous sections⁵. By suddenly lowering the interspecies interaction strength we aim at initiating a tunneling process of the impurity species through the lattice geometry. We start by examining the tunneling properties in the case of a single impurity and then extend it to two impurities.

⁴ These are due to a very small population of the impurity species in the site adjacent to the opposite outer well.

⁵ This selection of one of the two degenerate ground states can be performed by applying for example a small asymmetry to the lattice potential.



4.1. Transporting a single impurity

In the following we prepare our system in its ground state with a lattice depth $V_0/E_R = 10.5$ and an interspecies interaction strength $g_{AB}/E_R\lambda = 0.04$. This choice leads to a doped insulator density distribution of the two species as depicted in figures 2(c) and (d). In this sense the two species phase-separate and thereby form a particle-hole pair where the impurity plays the role of the particle. Moreover, the majority species atoms occupy each well separately. To trigger the dynamics, we quench the interspecies interaction strength to a smaller value such that we cross the transition from $S_{AB} \approx 0$ to large values of S_{AB} regarding the ground state entanglement crossover diagram shown in figure 2(a).

As a representative example of the emergent tunneling dynamics of each species in figures 6(a) and (b) we present the temporal evolution of the corresponding one-body densities following a quench to $g_{AB}/E_R\lambda = 0.025$, while keeping fixed $V_0/E_R = 10.5$. In this case the impurity tunnels through the lattice geometry and ends up well localized in the opposite outer well (see figure 6(a)). On the other hand the hole of the majority species in the initial well vanishes, which means that particles of the majority species travel towards this well which was initially solely populated by the impurity. Finally, for $t/(\hbar/E_R) \approx 600$ a hole can again be found at the opposite outer well where now the impurity resides (see figure 6(b)).

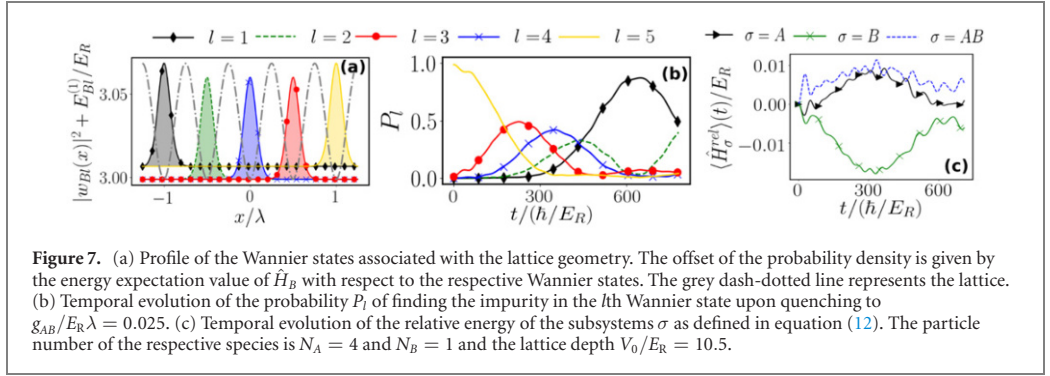
In order to appreciate the involved tunneling processes we next examine the probability of finding an impurity particle in a specific Wannier state. To this end, we construct the operator

$$\hat{O}_l^{(1)} = |w_l^B\rangle\langle w_l^B|, \quad (11)$$

where $|w_l^B\rangle\langle w_l^B|$ projects the particle of the B species onto the l th Wannier state of the lowest band. Evaluating this operator with respect to the complete many-body wave function yields the probability $P_l = \langle \Psi_{\text{MB}} | \hat{O}_l^{(1)} | \Psi_{\text{MB}} \rangle$ of detecting an impurity particle in the l th Wannier state. Note that the complete many-body wave function is obtained via ML-MCTDHF and subsequently we analyze this high-dimensional object by evaluating $\hat{O}_l^{(1)}$ with respect to the wave function. In the following the Wannier states are ordered from left to right, i.e. $|w_5\rangle$ describes the Wannier state which is associated with the initially ($t = 0$) populated well. The Wannier states prove to be a suitable basis set, since in all cases analyzed in the following, we find that $\sum_l P_l \approx 99.9\%$. Figure 7(b), shows the probability P_l of finding the impurity in the l th Wannier state upon quenching to $g_{AB}/E_R\lambda = 0.025$. The energetically ordered associated Wannier states are depicted in figure 7(a). The probability of finding the impurity in the initially occupied well decreases in the course of time to zero, while the other wells are populated such that at the end of the process a maximum probability in the left Wannier state occurs. This behavior clearly leaves an imprint on the relative energy of the subsystems σ

$$\langle \hat{H}_\sigma^{\text{rel}} \rangle(t) = \langle \hat{H}_\sigma \rangle(t) - \langle \hat{H}_\sigma \rangle(t=0), \quad (12)$$

which we define as the deviation of the expectation values of the individual Hamiltonians \hat{H}_σ (with $\sigma \in \{A, B, AB\}$) deviating from their initial value at $t = 0$. The energy of the impurity first decreases during



the transport to the opposite outer well and then increases again (see figure 7(c)). This can be easily understood in terms of the population of the corresponding Wannier states. The energy of the three central Wannier states is smaller as compared to the two outer ones (see figure 7(a)). Since the former are strongly populated in a superposition in the course of time, we observe a decrease of the impurity energy. The revival of the energy is in turn associated with the population of the other outer well which has again an increased energy (due to the hard-wall boundary conditions). The reduction of the impurity energy is accompanied by an increase of the energy of the majority species and the interspecies energy. The reason for the latter will be discussed below.

First, let us turn back to the superposition of the three central Wannier states in the course of time. Interestingly, the propagation of the impurity species cannot be understood as a subsequent tunneling from one well to the adjacent one. The impurity rather delocalizes over the lattice geometry with a maximum delocalization indicated by the white dashed line in figures 6(a) and (b). The one-body density for this scenario is depicted in figure 6(d). Here, the impurity strongly localizes in the central well, with around half of that population in the two directly adjacent sites and a minor density in the outer wells. Apparently, in order to avoid overlap, the majority species exhibits a density minimum in the central well with increasing density towards the outer wells. This can also be observed in the population of the corresponding Wannier states (see figure 7(b)). It is also worth noticing, that the one-body densities of both species clearly deviate from the ones discussed in the context of the ground states in figure 2(b) where the roles of the two species are reversed with respect to the distribution of the one-body densities. However, this increased overlap not only increases the interspecies energy (see figure 7(c)) but additionally leads to a drastic increase of the von Neumann entropy as in the static case for the ground states (see figure 6(e) dashed blue line). Initially, we start with a von Neumann entropy of $S_{AB} \approx 0$ which then increases to a maximum and decreases again when the impurity species resides in the outermost well. This decrease is due to the fact that the two species again phase-separate at later evolution times. Let us remark here that S_{AB} does not drop back to zero since a minor residual density of the impurity remains in the second well.

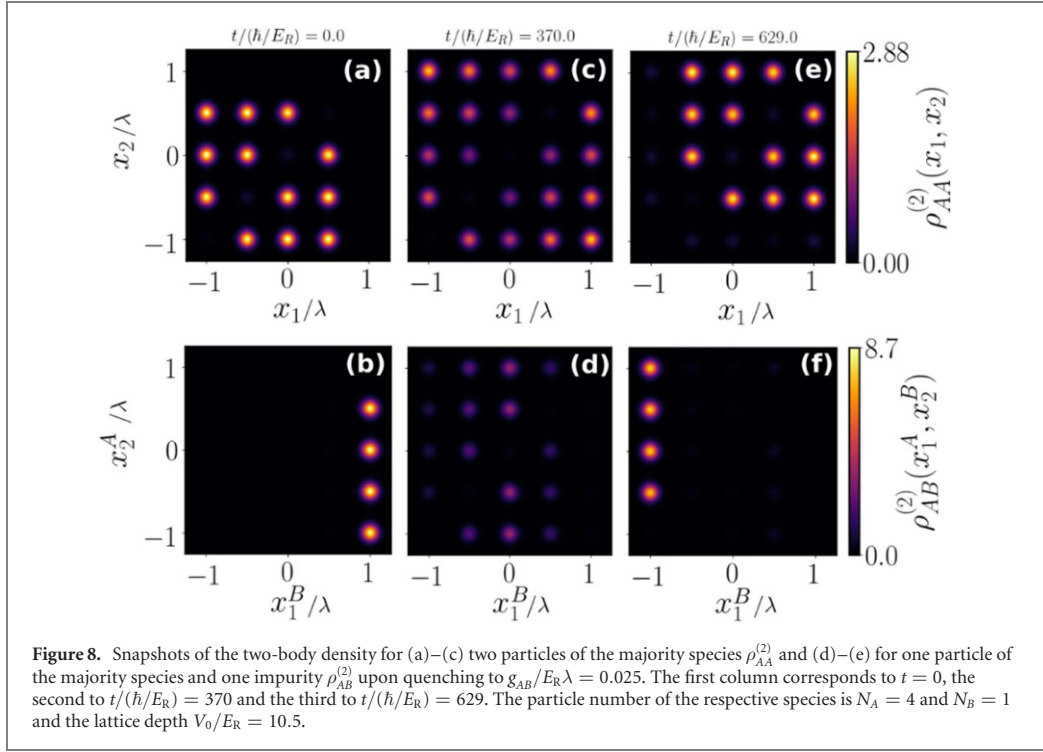
This tunneling process also has an impact on the correlations among the particles of the majority species. To unravel the role of these correlations, we define a measure for the correlations which are present in each subsystem itself. The spectral decomposition of the one-body density of species σ reads

$$\rho_\sigma^{(1)}(x, t) = \sum_j n_{\sigma j}(t) \Phi_{\sigma j}^*(x, t) \Phi_{\sigma j}(x, t), \quad (13)$$

where $n_{\sigma j}(t)$ in decreasing order, obeying $\sum_j n_{\sigma j} = 1$, are the so-called natural populations and $\Phi_{\sigma j}(x, t)$ the corresponding natural orbitals. In this sense, the natural orbitals are the eigenstates, while the natural populations are the corresponding eigenvalues [69, 70, 85], which are determined by diagonalizing the one-body density matrix. Similar to the Schmidt coefficients the natural populations serve as a measure for the correlations in a subsystem. In this spirit, we define the fragmentation [49, 77, 78] in the subsystem σ as

$$S_\sigma(t) = - \sum_j n_{\sigma j}(t) \ln(n_{\sigma j}(t)). \quad (14)$$

Here, the case of $S_\sigma = 0$ means that the subsystem σ is not depleted, implying that all particles occupy the same single particle state, i.e. $n_{\sigma 1} = 1$. As just discussed, the delocalization of the impurity species is accompanied by a delocalization of the majority species. We observe that this is also reflected in the fragmentation S_A of the majority species (see figure 6(f)). At $t = 0$ the majority species already exhibits a non-negligible fragmentation which is due to the fact that this species resides in a Mott insulator-like state. During the transport process, the majority species delocalizes which leads to an increase of S_A , thereby



maximizing the latter. The subsequent decrease of the fragmentation can be associated with the transition back to a Mott insulator-like state. Since this transition is not complete due to residual densities in the wells, the fragmentation does not drop back to its initial value.

In order to clarify that this tunneling process is not unique to a specific post-quench interspecies interaction strength, we show in figure 6(c) the temporal evolution of the center of mass of the impurity which is defined as

$$\langle \hat{X}_B \rangle = \int_{-L/2}^{L/2} dx \rho_B^{(1)}(x)x. \quad (15)$$

The initial value of the impurity's center of mass is given by $\langle \hat{X}_B \rangle / \lambda \approx 1$, while the final position when the impurity is completely transported to the opposite outer well is $\langle \hat{X}_B \rangle / \lambda \approx -1$. For various post-quench g_{AB} we find that the impurity can be transported to the opposite outer well, while the time it takes for the impurity to reach that well decreases with smaller g_{AB} . We also note that the impurity tunnels back to the initially occupied site afterwards, which shall not be the focus of further discussions. Nevertheless, it becomes additionally clear that it needs a certain minimal post-quench interspecies interaction strength in order to observe the impurity tunneling within the depicted time interval. E.g. for post-quench $g_{AB}/E_R\lambda = 0.03$ the impurity rather resides in the initially occupied well, instead of tunneling through the lattice geometry, whereas for smaller g_{AB} the tunneling process takes place. As in the case of $g_{AB}/E_R\lambda = 0.025$, which we discussed in detail, also for smaller g_{AB} the von Neumann entropy as well as the fragmentation of the majority species are affected by the tunneling of the two species. However, the well separated initial increase and the subsequent decrease in both measures become less clear or not even evident anymore, which indicates that also the correlated tunneling takes place in a less structured manner with decreasing post-quench g_{AB} .

In order to understand the above-described difference with varying post-quench g_{AB} , we first analyze the temporal evolution of the two-body densities for an interspecies interaction strength to $g_{AB}/E_R\lambda = 0.025$. These observables provide a more comprehensive insight into the involved correlated processes indicated by the von Neumann entropy and the fragmentation of the majority species. In figure 8 we present temporal snapshots of $\rho_{AB}^{(2)}$ and $\rho_{AA}^{(2)}$. The first column corresponds to $t = 0$, while the second one refers to the case where the impurity species strongly delocalizes over the lattice geometry, thereby maximizing S_{AB} . The third column represents the time instance when the impurity resides in the opposite outer well with $\langle \hat{X}_B \rangle / \lambda \approx -1$. Focusing now on the majority species we clearly identify that throughout the tunneling process two particles of this species avoid to occupy the same site. Even in the case of maximum delocalization of the majority species two particles do not reside in the same site. We can understand this

process as a superposition of all number states where four particles are distributed separately among the five Wannier states, e.g. $|1, 1, 1, 1, 0\rangle_A$, $|1, 1, 1, 0, 1\rangle_A$ etc. In this sense, the hole in the majority species is delocalized over the lattice geometry. Moreover, we can infer that measuring the impurity at a specific site we will most probably not find a majority species atom at the same site. Even in the case of maximum delocalization these two particles will avoid each other. In this manner, the increase of S_{AB} in the context of the delocalization is not a trivial single-particle effect. It is rather due to the strong avoidance of the two species and thereby the involved superposition of many contributing states, e.g. $|1, 1, 1, 1, 0\rangle_A \otimes |0, 0, 0, 0, 1\rangle_B$, $|1, 1, 1, 0, 1\rangle_A \otimes |0, 0, 0, 1, 0\rangle_B$ etc, which leads to the increase of the von Neumann entropy. This in turn leads to the delocalization of the two species on the level of the one-body densities when integrating out the respective degrees of freedom (see equation (5)). Based on these findings we have strong indications that the tunneling of the two species manifests itself in the effective transport of a particle hole-pair from one of the outer wells to the opposite one.

To further quantify this tunneling process we determine the probability of finding a particle hole pair in any lattice site in the course of time. We define this as the expectation value of the operator

$$\hat{O}_{\text{ph}}^{(2)} = \mathbb{1}_A \otimes \mathbb{1}_B - \frac{1}{N_A N_B} \sum_{l=1}^5 |w_l^B\rangle\langle w_l^B| \otimes \sum_i^{N_A} |w_l^{iA}\rangle\langle w_l^{iA}|, \quad (16)$$

with respect to the system's wave function, i.e. $\langle \hat{O}_{\text{ph}}^{(2)} \rangle$. Here, $|w_l^B\rangle\langle w_l^B|$ projects the particle of the B species onto the l th Wannier state and $|w_l^{iA}\rangle\langle w_l^{iA}|$ projects the i th particle of the A species onto the l th Wannier state. $\mathbb{1}_\sigma$ are the unity operators of the respective subsystems σ . Figure 9(a) presents the temporal evolution of the probability of finding a particle hole pair in any lattice site for various post-quench interspecies interaction strengths. Since our system is prepared in its ground state for all post-quench g_{AB} , initial particle-hole pair probability of $\langle \hat{O}_{\text{ph}}^{(2)} \rangle(t=0) \approx 98.8\%$ holds. This means that we can safely assume that our system exhibits a particle-hole pair.

Focusing on the case of $g_{AB}/E_R\lambda = 0.025$, which corresponds to the two-body densities depicted in figure 8, the quench leads to a slight reduction of $\langle \hat{O}_{\text{ph}}^{(2)} \rangle$ which recovers again for larger times. Closely inspecting the particle hole-pair probability (see figure 9(b)), we can deduce that the strongest decrease happens at the time interval in which the two species strongly delocalize over the lattice geometry. For this reason, we can assume that our system is not solely described by the superposition of number states exhibiting a particle-hole pair, e.g. $|1, 1, 1, 1, 0\rangle_A \otimes |0, 0, 0, 0, 1\rangle_B$, $|1, 1, 1, 0, 1\rangle_A \otimes |0, 0, 0, 1, 0\rangle_B$ etc. Nevertheless, the admixture of other states is rather small since in the case with the largest deviations we still find a particle hole-pair with a probability of $\langle \hat{O}_{\text{ph}}^{(2)} \rangle \approx 93.2\%$. Moreover, we observe that $\langle \hat{O}_{\text{ph}}^{(2)} \rangle$ increases again in the course of time, if not completely to its initial value, which is associated with the impurity then occupying dominantly the opposite outer well. In contrast, when quenching to smaller values of g_{AB} , the stability of the particle-hole pair cannot be guaranteed anymore. For a quench to $g_{AB}/E_R\lambda = 0.01$ we lose up to 20% of the particle-hole pair which becomes even more for a quench close to zero, i.e. $g_{AB}/E_R\lambda = 0.002$. In the latter case $\langle \hat{O}_{\text{ph}}^{(2)} \rangle$ drastically decreases to 65% in the first few time steps. In this sense, in order to maintain a stable particle-hole pair during the transport of the impurity to the opposite outer well it is necessary not to quench too strongly. On the other hand a quench which is too weak allows for a stable particle-hole pair, which resides in the well initially occupied by the impurity, e.g. $g_{AB}/E_R\lambda = 0.03$ (see figure 9(a) red line).

In conclusion, we have found that quenching the binary mixture starting in a phase separated state leads to a very controlled correlated tunneling dynamics. On the one hand the majority species tunnels such that its particles do not occupy the same lattice site. On the other hand we observe the effective transport of a particle-hole pair from one of the outer wells to the opposite one whose stability strongly depends on the presence of a finite interspecies interaction strength. Moreover, the tunneling dynamics is accompanied by a strong entanglement between the species as well as correlations among the majority species atoms.

4.2. Transport properties of two bosonic impurities

Having understood the correlated tunneling dynamics of a single impurity interacting repulsively with a majority species we now turn to the case of two non-interacting bosonic impurities. We prepare our system in its ground state characterized by a lattice depth $V_0/E_R = 8.9$ and interspecies interaction strength $g_{AB}/E_R\lambda = 0.05$, while $g_{AA}/E_R\lambda = 0.04$. This leads to a density distribution of the two species as depicted in figures 4(e) and (f), such that the two species phase-separate. Moreover, the two impurities accumulate at the same single lattice site, while the majority species atoms strongly avoid each other, occupying the lattice sites each one separately. In this sense, our initial state is similar to the one with a single impurity, apart from the additionally added impurity.

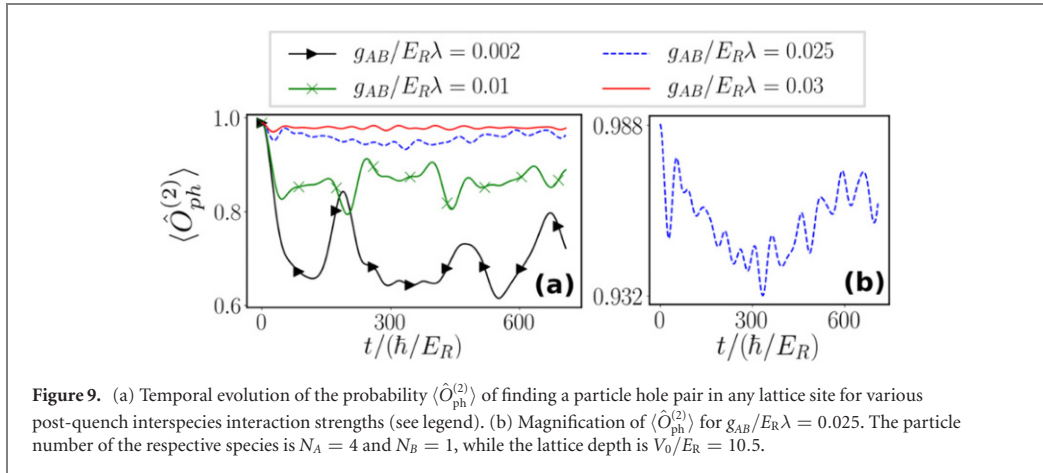
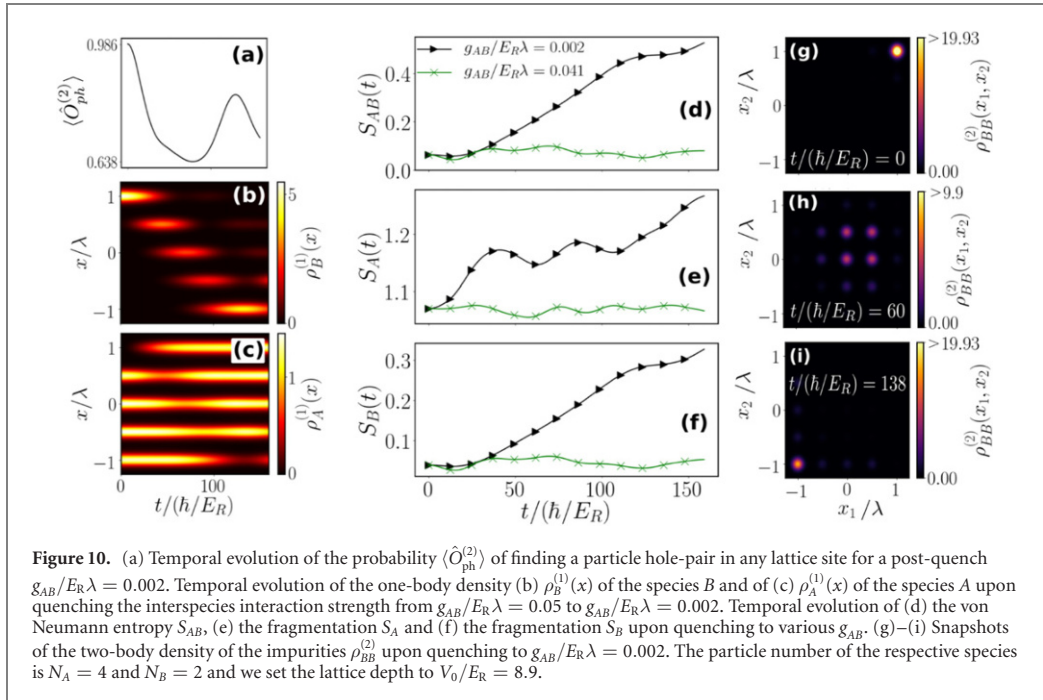


Figure 9. (a) Temporal evolution of the probability $\langle \hat{O}_{ph}^{(2)} \rangle$ of finding a particle hole pair in any lattice site for various post-quench interspecies interaction strengths (see legend). (b) Magnification of $\langle \hat{O}_{ph}^{(2)} \rangle$ for $g_{AB}/E_R\lambda = 0.025$. The particle number of the respective species is $N_A = 4$ and $N_B = 1$, while the lattice depth is $V_0/E_R = 10.5$.

Quenching the interspecies interaction strength to $g_{AB}/E_R\lambda = 0.002$ we observe a tunneling of the impurity species to the opposite outer well (see figure 10(b)). However, compared to the case of a single impurity a larger portion of density remains in the wells which are traversed during the dynamics. This means that compared to the single impurity case the transport portion of two impurities is less complete due to some density remaining in the traversed lattice sites. In turn the majority species tunnels in a counterflow into the opposite direction as compared to the direction of the impurities. In this context, one might again ask whether this process can be described by an effective transport of a particle hole-pair. Figure 10(a) shows the corresponding particle hole-pair probability $\langle \hat{O}_{ph}^{(2)} \rangle$ during the evolution. Initially, the particle hole-pair process is the dominant tunneling channel with a probability of $\langle \hat{O}_{ph}^{(2)} \rangle \approx 98.6\%$ which later on drastically decreases to $\langle \hat{O}_{ph}^{(2)} \rangle \approx 63.8\%$. The subsequent increase of this probability, which is associated with the impurities residing in the opposite outer well, does not revive to its initial value, indicating the loss of the particle hole-pair. This effect is similar to the one discussed for a single impurity when quenching to very small values of g_{AB} , where the stability of the particle hole-pair cannot be guaranteed either. Apart from that, the system still exhibits a rather pronounced increase of correlations in the course of time. This involves for example the increase of the von Neumann entropy which can be traced back to the residual impurity density in the remaining wells during their transport to the other side of the lattice geometry. As a result the spatial overlap between the species is increased and thereby also S_{AB} (see figure 10(d)). Furthermore the initially uncorrelated impurity pair, $S_B(t=0) \approx 0$, develops correlations during the propagation to the opposite outer well which can be attributed to the incomplete transfer of the impurities to this very site (see figure 10(e)). Similarly, the increase of S_A is attributed to the incomplete transfer of the effective hole into the opposite direction (as compared to the propagation direction of the impurities) (see figure 10(f)).

Furthermore, it is of interest to analyze in which manner the two bosonic impurities propagate in relation to each, i.e. whether they move as a pair or they delocalize in the course of time. In order to answer this question we inspect the two-body density of the impurities $\rho_{BB}^{(2)}$ upon quenching to $g_{AB}/E_R\lambda = 0.002$ (see figures 10(g)–(i)). The initially accumulated (in an outer well) impurities delocalize over next-neighbour sites, which means that it is possible for the two impurities to either reside at the same site or in adjacent ones (see figure 10(h)). However, during the propagation there are time instances at which the probability of finding the impurities at the same site is more pronounced as compared to detecting them in adjacent ones (not shown here). From this we can conclude that in general the impurities delocalize during the propagation until they reach the opposite outer well where they eventually strongly localize (see figure 10(i)).

Let us finally remark that in comparison to the single impurity case, for two impurities it is necessary to quench to lower interspecies interaction strengths in order to achieve a significant transport of the impurity species to the opposite outer well. For smaller quench amplitudes we either find no tunneling of the two species (cf figures 10(d)–(f) green crosses) or the impurities delocalize over the lattice geometry without accumulating in the opposite outer well. Therefore, a transport of the impurity species to the opposite outer well as in the case of a single impurity is only possible for large quench amplitudes. However, this leads to a loss of the initial particle–hole pair and a less structured development of correlations.

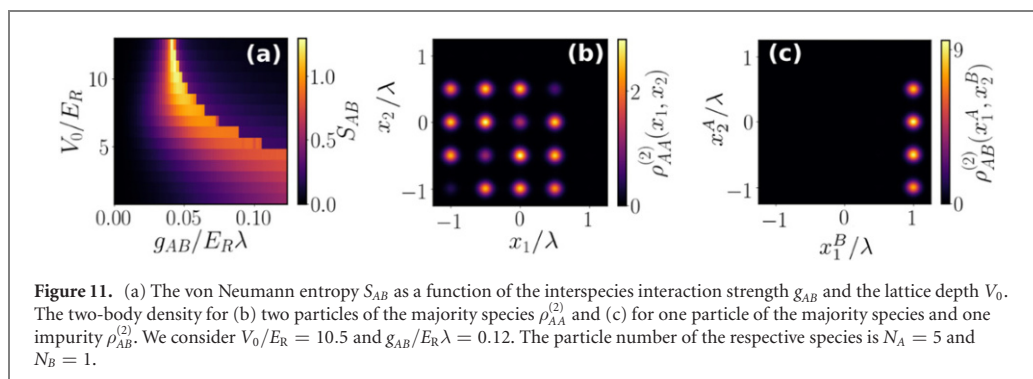


5. Conclusions and outlook

We have investigated the ground state properties of a binary bosonic mixture trapped in a one-dimensional lattice geometry consisting of a majority species which is doped by one or two bosonic impurities. We demonstrate the existence of a crossover diagram of the interspecies entanglement as a function of the lattice depth and the interspecies interaction strength. The transition from strong interspecies entanglement to $S_{AB} = 0$ is accompanied by a crossover from a spatially delocalized impurity species to its strong localization in one of the outer lattice wells. For large lattice depths we find this transition for the case of a single as well as two bosonic impurities. Moreover, analyzing the corresponding two-body densities we can conclude that the majority species occupies a Mott insulator-like state, while the two species phase-separate, thereby forming a particle hole-pair. For two impurities we additionally observe in the case of smaller lattice depths a localization of the impurity species in two adjacent sites. This phenomenon also manifests itself in the impurity–impurity correlations, which we do not find when the impurities localize in a single site.

Having understood the ground state distributions, in the next step we aimed at transporting the impurity species through the lattice by performing an interspecies interaction quench from a Mott to the superfluid phase of the composite system. For a single impurity the initial particle hole-pair tunnels to the opposite outer lattice well, while we are able to control the stability of the particle hole-pair by varying the post-quench interspecies interaction strength. Here, it is important to perform weak amplitude quenches in order to maintain the initial particle hole-pair. However, for two impurities we cannot guarantee a stable transport of this pair. This is due to the fact that only large quench amplitudes can initiate a significant transport of the impurities to the opposite outer well at all. As in the case of a single impurity such large quench amplitudes lead to a strong loss of the particle hole-pair probability.

The understanding of the crossover between a spatially delocalized to a localized bosonic impurity species serves as a perfect starting point for even more complex setups, e.g. by introducing more lattice atoms and sites. Indeed, there are several possible directions of future investigations. For example, it would be of interest to allow for a spin degree of freedom in both species, such that the particle hole-pair may carry an additional effective spin. In this spirit, a quench of the interspecies interaction strength might lead to a redistribution of the spins in the system or an effective spin transport. Another fruitful perspective is to investigate the ground state phase diagram of the setting considered herein but including dipolar interactions within and between the species. In this way, it would be possible to generate more phases due to the long-range character of the interactions.



Acknowledgments

P S gratefully acknowledges funding by the Deutsche Forschungsgemeinschaft in the framework of the SFB 925 ‘Light induced dynamics and control of correlated quantum systems’. K K gratefully acknowledges a scholarship of the Studienstiftung des deutschen Volkes. S I M gratefully acknowledges financial support in the framework of the Lenz–Ising Award of the University of Hamburg.

Appendix A. Doping a unit-filling bosonic majority species

To explicitly showcase the generalization of our findings regarding the ground state properties of the considered lattice trapped bosonic mixture, we consider a unit filling of the majority species, doping it with a single impurity, i.e. $N_A = 5$ and $N_B = 1$. We explore the ground state of the system for varying V_0 and g_{AB} , while fixing the intraspecies interaction strength to $g_{AA}/E_R\lambda = 0.04$. Figure 11(a) shows the von Neumann entropy of the ground state as a function of the interspecies interaction strength g_{AB} and the lattice depth V_0 . As in the case of $N_A = 4$ and $N_B = 1$ (figure 2(a)), we find a region of increased interspecies entanglement, which decreases to zero for a further increase of g_{AB} . This is again associated with a strong delocalization of both species for large S_{AB} and a phase separation in case of $S_{AB} \approx 0$ occurring for large g_{AB} . However, there is a slight change compared to $N_B = 4$ in the corresponding two-body densities for $V_0/E_R = 10.5$ and $g_{AB}/E_R\lambda = 0.12$, where an interspecies phase-separation takes place. Since the majority species exhibits an additional particle, the latter distributes over the four lattice sites which are occupied by the majority species in case of an interspecies phase-separation. For this reason a non-negligible, but small, probability of finding two particles of the A species at the same site occurs. In $\rho_{AB}^{(2)}$ the phase separation is still reflected with an increased probability of finding the majority species in the two central occupied sites, which is due to the additional majority species particle. In this sense, also for $N_A = 5$ we find the formation of a particle hole-pair for large g_{AB} , while the additional particle in the majority species delocalizes over the sites occupied by the latter.

ORCID iDs

Simeon I Mistakidis  <https://orcid.org/0000-0002-5118-5792>

Peter Schmelcher  <https://orcid.org/0000-0002-2637-0937>

References

- [1] Inouye S, Goldwin J, Olsen M L, Ticknor C, Bohn J L and Jin D S 2004 *Phys. Rev. Lett.* **93** 183201
- [2] Fukuhara T, Sugawa S, Takasu Y and Takahashi Y 2009 *Phys. Rev. A* **79** 021601
- [3] Chin C, Grimm R, Julienne P and Tiesinga E 2010 *Rev. Mod. Phys.* **82** 1225
- [4] Henderson K, Ryu C, McCormick C and Boshier M G 2009 *New J. Phys.* **11** 043030
- [5] Grimm R, Weidemüller M and Ovchinnikov Y B 2000 *Adv. At. Mol. Opt. Phys.* **42** 95
- [6] Serwane F, Zürn G, Lompe T, Ottenstein T B, Wenz A N and Jochim S 2011 *Science* **332** 336
- [7] Wenz A N, Zürn G, Murmann S, Brouzos I, Lompe T and Jochim S 2013 *Science* **342** 457
- [8] Massignan P, Zaccanti M and Bruun G M 2014 *Rep. Prog. Phys.* **77** 034401
- [9] Kohstall C, Zaccanti M, Jag M, Trenkwalder A, Massignan P, Bruun G M, Schreck F and Grimm R 2012 *Nature* **485** 615
- [10] Koschorreck M, Pertot D, Vogt E, Fröhlich B, Feld M and Köhl M 2012 *Nature* **485** 619
- [11] Scazza F et al 2017 *Phys. Rev. Lett.* **118** 083602
- [12] Landau L D 1933 *Phys. Z. Sowjetunion* **3** 644

- [13] Grusdt F and Demler E 2015 New theoretical approaches to Bose polarons *Quantum Matter at Ultralow Temperatures* **191** 325
- [14] Schmidt R, Knap M, Ivanov D A, You J S, Cetina M and Demler E 2018 *Rep. Prog. Phys.* **81** 024401
- [15] Grusdt F, Astrakharchik G E and Demler E A 2017 *New J. Phys.* **19** 103035
- [16] Khandekar D C, Bhagwat K V and Lawande S V 1988 *Phys. Rev. B* **37** 3085
- [17] Ardila L P and Giorgini S 2015 *Phys. Rev. A* **92** 033612
- [18] Keiler K, Krönke S and Schmelcher P 2018 *New J. Phys.* **20** 033030
- [19] Chen J, Schurer J M and Schmelcher P 2018 *Phys. Rev. Lett.* **121** 043401
- [20] Dehkharghani A S, Volosniev A G and Zinner N T 2018 *Phys. Rev. Lett.* **121** 080405
- [21] Catani J, Lamporesi G, Naik D, Gring M, Inguscio M, Minardi F, Kantian A and Giamarchi T 2012 *Phys. Rev. A* **85** 023623
- [22] Fukuhara T et al 2013 *Nat. Phys.* **9** 235
- [23] Volosniev A G and Hammer H-W 2017 *Phys. Rev. A* **96** 031601(R)
- [24] Cetina M et al 2016 *Science* **354** 96
- [25] Tajima H and Uchino S 2019 *Phys. Rev. A* **99** 063606
- [26] Dehkharghani A S, Volosniev A G and Zinner N T 2015 *Phys. Rev. A* **92** 031601(R)
- [27] Mistakidis S I, Katsimiga G C, Koutentakis G M and Schmelcher P 2019 *New J. Phys.* **21** 043032
- [28] Sacha K and Timmermans E 2006 *Phys. Rev. A* **73** 063604
- [29] Koepsell J, Vijayan J, Sompet P, Grusdt F, Hilker T A, Demler E, Salomon G, Bloch I and Gross C 2019 *Nature* **572** 358
- [30] Mistakidis S I, Hilbig L and Schmelcher P 2019 *Phys. Rev. A* **100** 023620
- [31] Mistakidis S I, Volosniev A G and Schmelcher P 2020 *Phys. Rev. Research* **2** 023154
- [32] Mistakidis S I, Koutentakis G M, Katsimiga G C, Busch T and Schmelcher P 2020 *New J. Phys.* **22** 043007
- [33] Tajima H, Takahashi J, Nakano E and Iida K 2019 arXiv:1912.12832
- [34] Mistakidis S I, Katsimiga G C, Koutentakis G M, Busch T and Schmelcher P 2020 arXiv:2001.00260
- [35] Boyanovsky D, Jasnow D, Wu X L and Coalson R C 2019 *Phys. Rev. A* **100** 043617
- [36] Lausch T, Widera A and Fleischhauer M 2018 *Phys. Rev. A* **97** 023621
- [37] Mistakidis S I, Katsimiga G C, Koutentakis G M, Busch T and Schmelcher P 2019 *Phys. Rev. Lett.* **122** 183001
- [38] Mistakidis S I, Grusdt F, Koutentakis G M and Schmelcher P 2019 *New J. Phys.* **21** 103026
- [39] Mukherjee K, Mistakidis S I, Majumder S and Schmelcher P 2020 *Phys. Rev. A* **101** 023615
- [40] Gamayun O, Lychkovskiy O, Burovski E, Malcomson M, Cheianov V V and Zvonarev M B 2018 *Phys. Rev. Lett.* **120** 220605
- [41] Mathy C J, Zvonarev M B and Demler E 2012 *Nat. Phys.* **8** 881
- [42] Johnson T H, Clark S R, Bruderer M and Jaksch D 2011 *Phys. Rev. A* **84** 023617
- [43] Cai Z, Wang L, Xie X C and Wang Y 2010 *Phys. Rev. A* **81** 043602
- [44] Palzer S, Zipkes C, Sias C and Köhl M 2009 *Phys. Rev. Lett.* **103** 150601
- [45] Bruderer M, Klein A, Clark S R and Jaksch D 2007 *Phys. Rev. A* **76** 011605
- [46] Bruderer M, Klein A, Clark S R and Jaksch D 2008 *New J. Phys.* **10** 033015
- [47] Bruderer M, Bao W and Jaksch D 2008 *Europhys. Lett.* **82** 30004
- [48] Theel F, Keiler K, Mistakidis S I and Schmelcher P 2020 *New J. Phys.* **22** 023027
- [49] Keiler K and Schmelcher P 2019 *Phys. Rev. A* **100** 043616
- [50] Siegl P, Mistakidis S I and Schmelcher P 2018 *Phys. Rev. A* **97** 053626
- [51] Yin T, Cocks D and Hofstetter W 2015 *Phys. Rev. A* **92** 063635
- [52] Grusdt F, Shashi A, Abanin D and Demler E 2014 *Phys. Rev. A* **90** 063610
- [53] Duncan C W, Bellotti F F, Öhberg I P, Zinner N T and Valiente M 2017 *New J. Phys.* **19** 075001
- [54] Massel F, Kantian A, Daley A J, Giamarchi T and Törmä P 2013 *New J. Phys.* **15** 045018
- [55] Visuri A-M, Giamarchi T and Törmä P 2016 *Phys. Rev. B* **93** 125110
- [56] Guglielmino M, Penna V and Capogrosso-Sansone B 2010 *Phys. Rev. A* **82** 021601
- [57] Buonsante P, Giampaolo S M, Illuminati F, Penna V and Vezzani A 2008 *Phys. Rev. Lett.* **100** 240402
- [58] Gadway B, Pertot D, Reimann R and Schneble D 2010 *Phys. Rev. Lett.* **105** 045303
- [59] Thalhammer G, Barontini G, De Sarlo L, Catani J, Minardi F and Inguscio M 2008 *Phys. Rev. Lett.* **100** 210402
- [60] Suthar K and Angom D 2017 *Phys. Rev. A* **95** 043602
- [61] Kato Y, Yamamoto D and Danshita I 2014 *Phys. Rev. Lett.* **112** 055301
- [62] Wang W, Penna V and Capogrosso-Sansone B 2016 *New J. Phys.* **18** 063002
- [63] Hu A, Mathey L, Danshita I, Tiesinga E, Williams C J and Clark C W 2009 *Phys. Rev. A* **80** 023619
- [64] Hu A, Mathey L, Williams C J and Clark C W 2010 *Phys. Rev. A* **81** 063602
- [65] Roscilde T and Cirac J I 2007 *Phys. Rev. Lett.* **98** 190402
- [66] Catani J, De Sarlo L, Barontini G, Minardi F and Inguscio M 2008 *Phys. Rev. A* **77** 011603
- [67] Zöllner S, Meyer H-D and Schmelcher P 2008 *Phys. Rev. A* **78** 013629
- [68] Zöllner S, Meyer H-D and Schmelcher P 2008 *Phys. Rev. Lett.* **100** 040401
- [69] Krönke S, Cao L, Vendrell O and Schmelcher P 2013 *New J. Phys.* **15** 063018
- [70] Cao L, Krönke S, Vendrell O and Schmelcher P 2013 *J. Chem. Phys.* **139** 134103
- [71] Cao L, Bolsinger V, Mistakidis S I, Koutentakis G, Krönke S, Schurer J M and Schmelcher P 2017 *J. Chem. Phys.* **147** 044106
- [72] Mistakidis S I, Katsimiga G C, Kevrekidis P G and Schmelcher P 2018 *New J. Phys.* **20** 043052
- [73] Endres M et al 2011 *Science* **334** 200
- [74] Keiler K and Schmelcher P 2018 *New J. Phys.* **20** 103042
- [75] Erdmann J, Mistakidis S I and Schmelcher P 2018 *Phys. Rev. A* **98** 053614
- [76] Erdmann J, Mistakidis S I and Schmelcher P 2019 *Phys. Rev. A* **9** 013605
- [77] Roy R, Gammal A, Tsatsos M C, Chatterjee B, Chakrabarti B and Lode A U J 2018 *Phys. Rev. A* **97** 043625
- [78] Chatterjee B, Tsatsos M C and Lode A U J 2019 *New J. Phys.* **21** 033030
- [79] Horodecki R, Horodecki P, Horodecki M and Horodecki K 2009 *Rev. Mod. Phys.* **81** 865
- [80] Dirac P A M 1930 *Math. Proc. Camb. Phil. Soc.* **26** 376
- [81] Frenkel J 1934 *Wave Mechanics Advanced General Theory* (Oxford: Clarendon)
- [82] Raab A 2000 *Chem. Phys. Lett.* **319** 674
- [83] Cao L, Brouzos I, Zöllner S and Schmelcher P 2011 *New J. Phys.* **13** 033032
- [84] Cao L, Brouzos I, Chatterjee B and Schmelcher P 2012 *New J. Phys.* **14** 093011

- [85] Meyer H-D, Gatti F and Worth G A 2009 *Multidimensional Quantum Dynamics: MCTDH Theory and Applications* (New York: Wiley)
- [86] Köhler F, Keiler K, Mistakidis S I, Meyer H-D and Schmelcher P 2019 *J. Chem. Phys.* **151** 054108
- [87] LeBlanc L J and Thywissen J H 2007 *Phys. Rev. A* **75** 053612
- [88] Gaunt A L, Schmidutz T F, Gotlibovych I, Smith R P and Hadzibabic Z 2013 *Phys. Rev. Lett.* **110** 200406
- [89] Rubio-Abadal A, Choi J, Zeiher J, Hollerith S, Rui J, Bloch I and Gross C 2019 *Phys. Rev. X* **9** 041014
- [90] García-March M A, Juliá-Díaz B, Astrakharchik G E, Boronat J and Polls A 2014 *Phys. Rev. A* **90** 063605
- [91] Alon O E, Streltsov A I and Cederbaum L S 2006 *Phys. Rev. Lett.* **97** 230403
- [92] Cazalilla M A and Ho A F 2003 *Phys. Rev. Lett.* **91** 150403
- [93] García-March M A and Busch T 2013 *Phys. Rev. A* **87** 063633
- [94] Kivelson S and Schrieffer J R 1982 *Phys. Rev. B* **25** 6447
- [95] Kivelson S 1982 *Phys. Rev. B* **26** 4269

3.5 Entanglement-assisted tunneling dynamics of impurities in a double well immersed in a bath of lattice trapped bosons

PAPER • OPEN ACCESS

Entanglement-assisted tunneling dynamics of impurities in a double well immersed in a bath of lattice trapped bosons

To cite this article: Friethjof Theel *et al* 2020 *New J. Phys.* **22** 023027

View the [article online](#) for updates and enhancements.

Recent citations

- [Correlated dynamics of fermionic impurities induced by the counterflow of an ensemble of fermions](#)
J. Kwasniok *et al*
- [Pulse- and continuously driven many-body quantum dynamics of bosonic impurities in a Bose-Einstein condensate](#)
K. Mukherjee *et al*
- [Doping a lattice-trapped bosonic species with impurities: from ground state properties to correlated tunneling dynamics](#)
Kevin Keiler *et al*



PAPER

Entanglement-assisted tunneling dynamics of impurities in a double well immersed in a bath of lattice trapped bosons

OPEN ACCESS

RECEIVED

2 September 2019

REVISED

18 December 2019

ACCEPTED FOR PUBLICATION

22 January 2020

PUBLISHED

14 February 2020

Friethjof Theel¹, Kevin Keiler¹, Simeon I Mistakidis¹  and Peter Schmelcher^{1,2} ¹ Center for Optical Quantum Technologies, University of Hamburg, Department of Physics, Luruper Chaussee 149, D-22761, Hamburg, Germany² The Hamburg Centre for Ultrafast Imaging, University of Hamburg, Luruper Chaussee 149, D-22761, Hamburg, Germany**Keywords:** many-body physics, impurities, optical lattice, correlations

Original content from this work may be used under the terms of the [Creative Commons Attribution 3.0 licence](https://creativecommons.org/licenses/by/4.0/).

Any further distribution of this work must maintain attribution to the author(s) and the title of the work, journal citation and DOI.

**Abstract**

We unravel the correlated tunneling dynamics of an impurity trapped in a double well and interacting repulsively with a majority species of lattice trapped bosons. Upon quenching the tilt of the double well it is found that the quench-induced tunneling dynamics depends crucially on the interspecies interaction strength and the presence of entanglement inherent in the system. In particular, for weak couplings the impurity performs a rather irregular tunneling process in the double well. Increasing the interspecies coupling it is possible to control the response of the impurity which undergoes a delayed tunneling while the majority species effectively acts as a material barrier. For very strong interspecies interaction strengths the impurity exhibits a self-trapping behavior. We showcase that a similar tunneling dynamics takes place for two weakly interacting impurities and identify its underlying transport mechanisms in terms of pair and single-particle tunneling processes.

1. Introduction

Ultracold atoms offer a versatile platform for studying many-body effects in an extraordinarily controlled manner. Apart from varying the external confining potential and its dimensionality [1–3], it is also possible to tune the interaction strength between the atoms via Feshbach or confinement induced resonances [4, 5]. This exquisite level of control over single component fermionic or bosonic ensembles can be extended to mixtures of ultracold atoms such as Bose–Bose [6–16], Fermi–Fermi [17, 18] and Bose–Fermi [19, 20] mixtures. In particular, one-dimensional systems exhibit intriguing phenomena since they allow for correlations to appear in the dilute regime [21–24].

In this context, especially strongly particle imbalanced mixtures have attracted a lot of interest recently. In the extreme case such systems consist of a single impurity immersed in a majority species. These setups have been studied theoretically [25–32] and experimentally [33–36], for a single impurity, serving as a simulator of polaron physics, as well as for many impurities [37–42] and are indeed a subject of ongoing research. While the ground state properties of a single impurity in a bath are to a certain extent well understood, less focus has been placed on the transport properties and the emergent collisions of the impurity through the bath [43–46]. Indeed, in these systems correlation effects, such as entanglement, are expected to be a crucial ingredient since the impurities form a few-body subsystem [47]. Moreover, the underlying trapping potential plays an important role for the behavior of the impurity species, which has been analyzed for homogeneous systems [48–50], harmonic confinements [51–55] as well as lattice potentials [33, 56, 57]. The majority of the above-mentioned investigations have been focusing on the case where both species are trapped in the same geometry. However, introducing different trapping potentials for each species is expected to alter significantly the observed dynamics. A setting of particular interest involves a bath of lattice trapped bosons which act as multiple material barriers for the tunneling dynamics of the impurity.

In the present work we explicitly focus on an impurity which is confined in a one-dimensional double well and interacts repulsively via contact interaction with a majority species of bosons trapped in a lattice. For single component bosons in a double well the analog of the well-known superconducting Josephson junction can be

established. The bosonic Josephson junction provides the testbed for many, also experimentally observed, intriguing phenomena, such as Josephson oscillations, macroscopic quantum self-trapping [58–63] and correlated pair tunneling [64–66]. Extensions of these phenomena to multicomponent setups have also been extensively studied, see for instance [67–70]. Herein, we extend these investigations by exploring the dynamics of impurities in a double well immersed in a few-body bath of lattice trapped bosons. This gives rise to an effective potential for the impurities whose shape strongly depends on the interspecies interaction strength. Depending on the latter, one can realize tunneling scenarios which are beyond the well-known regimes of Josephson oscillation and quantum self-trapping and rely on the interspecies entanglement. This can be of particular interest for future applications in atomtronics [71].

In our setup of a single impurity in a double well the dynamics is steered by the repulsive coupling to the majority species. Varying the interspecies interaction strength we unravel different dynamical response regimes of the impurity upon quenching the tilt of the double well. These regimes range from rather irregular tunneling in the double well for small interspecies interaction strengths to dynamical self-trapping in a single site for very strong couplings [6, 7, 55]. For intermediate coupling strengths we observe a strong impact of the density distribution of the majority species on the impurity's tunneling dynamics. The impurity initially collides with the material barrier imposed by the density of the majority species and then tunnels to the corresponding other site of the double well. This offers a controlled way of transporting the impurity within the double well. The entire tunneling process in the case of intermediate interspecies interaction strengths is accompanied by a strong entanglement between the subsystems revealing the complexity of this phenomenon. We remark that in the absence of entanglement this process does not take place. Additionally, in this case the self-trapping behavior is altered. Surprisingly, we find that the dynamics of the impurity can be described in terms of Wannier states [41, 42] which are associated with the superposition of the effective time-averaged potential induced by the density of the majority species and the double well potential. This proves to be a valuable tool that captures the dynamics of the impurity adequately, even though a strong entanglement persists throughout the dynamics [12, 46]. Due to the strong correlations appearing in our system it is necessary to utilize an approach which operates beyond lowest band and mean-field approximations, such as the Bose–Hubbard model or Gross–Pitaevskii approximation. Therefore we track the emergent non-equilibrium dynamics by employing the Multi-Layer Multi-Configurational Time-Dependent Hartree Method for atomic Mixtures (ML-MCTDHX) [72–74] that enables us to capture all the important particle correlations.

Our work is structured as follows: in section 2 we present the system under investigation and the employed computational methodology. In section 3 we unravel the quench-induced tunneling dynamics of the impurity, revealing also the crucial role of the inter- and intraspecies correlations. Section 4 is dedicated to an in-depth characterization of the microscopic effects involved in the dynamical response of the impurity. We extend our results to the case of two weakly interacting impurities in section 5 and conclude with a summary of our findings and a discussion of future directions in section 6.

2. Setup and multi-configurational approach

2.1. Setup and Hamiltonian

Our setup consists of two different species of bosons A and B , also referred to as the majority species and the impurity, respectively, which interact repulsively via a contact potential of strength g_{AB} . Each species is confined in a different one-dimensional optical potential at zero temperature. Experimentally this can be realized by preparing e.g. ^{87}Rb atoms in two different hyperfine states, i.e. $|F = 2, m_F = -2\rangle$ and $|F = 1, m_F = -1\rangle$, thereby obtaining a two-species bosonic mixture. Utilizing the so-called ‘tune-out’ wavelength [75, 76] it is possible to create species-dependent potentials, such that the two species experience different optical potentials [3]. The majority A species, composed of bosons of mass m_A and interacting repulsively via a contact interaction of strength g_{AA} , is trapped in a six-well lattice potential. The minority B species on the other hand, consisting of N_B impurities of mass m_B interacting repulsively via a contact interaction of strength g_{BB} , resides in an initially tilted double well potential. The resulting many-body Hamiltonian of the system reads

$$\begin{aligned} \hat{\mathcal{H}} = & \sum_{i=1}^{N_A} \left(-\frac{\hbar^2}{2m_A} \frac{d^2}{(dx_i^A)^2} + V_0 \cos^2(k_0 x_i^A) \right) + g_{AA} \sum_{i<j} \delta(x_i^A - x_j^A) \\ & + \sum_{i=1}^{N_B} \left(-\frac{\hbar^2}{2m_B} \frac{d^2}{(dx_i^B)^2} + \frac{1}{2} m_B \omega_B^2 (x_i^B)^2 + \frac{\hbar}{\sqrt{2\pi w}} \exp\left(-\frac{(x_i^B)^2}{2w^2}\right) + \alpha x_i^B \right) + g_{BB} \sum_{i<j} \delta(x_i^B - x_j^B) \\ & + g_{AB} \sum_{i=1}^{N_A} \sum_{j=1}^{N_B} \delta(x_i^A - x_j^B). \end{aligned} \quad (1)$$

Here, the lattice potential $V_A = V_0 \cos^2(k_0 x_i^A)$ of the majority species is characterized by its depth V_0 and wave vector $k_0 = \pi/l$ where l denotes the distance between two successive minima of the potential. The double well of

the impurities $V_B = \frac{1}{2}m_B\omega_B^2(x_i^B)^2 + \frac{h}{\sqrt{2\pi}w} \exp\left(-\frac{(x_i^B)^2}{2w^2}\right)$ is constructed by the combination of a harmonic oscillator potential with frequency ω_B and a Gaussian potential characterized by a width w and a height h . Additionally, we superimpose a linear tilting potential $V_{\text{tilt}} = \alpha x_i^B$ to the double well leading to an asymmetry between the two wells, whose degree can be controlled by the parameter α . Assuming zero temperature we can model the inter- and intraspecies interaction potential between the atoms via a bare delta potential with effective coupling strength $g_{\sigma\sigma'} = \frac{2\hbar^2 a_0^{\sigma\sigma'}}{M_{AB} a_{\perp}^2} \left(1 - \frac{|\zeta(1/2)| a_0^{\sigma\sigma'}}{\sqrt{2} a_{\perp}}\right)^{-1}$ where σ and σ' refer to the corresponding species A and B [4]. Here, $M_{AB} = \frac{m_A m_B}{m_A + m_B}$ represents the reduced mass and $a_{\perp} = \sqrt{\frac{\hbar}{M_{AB}\omega_{\perp}}}$ the transversal length scale which is steered by the frequency of the transversal confinement ω_{\perp} perpendicular to the one-dimensional Bose gas. Apart from varying ω_{\perp} , it is possible to control the coupling strength $g_{\sigma\sigma'}$ through the free space, three-dimensional scattering length $a_0^{\sigma\sigma'}$ which can be tuned via Feshbach resonances in magnetic or optical fields [5, 77–80].

Throughout this work we consider a fixed number of bosons for the majority species $N_A = 8$ and set $m = m_A = m_B$. As mentioned above, our setup can be experimentally realized by considering two hyperfine states of ^{87}Rb . Note that we have also simulated the corresponding dynamics of a mass imbalanced system consisting e.g. of a ^{87}Rb bosonic ensemble and a ^{133}Cs impurity. For this latter case we confirmed that an overall similar phenomenology compared to the mass balanced case occurs but the emerging tunneling regimes to be presented below take place at smaller interspecies interaction strengths. The energy scales for the Hamiltonian in equation (1) are given in units of the recoil energy $E_r = \hbar^2 k_0^2 / (2m)$, whereas the length and time scales are expressed in units of k_0^{-1} and $\omega_r^{-1} = \hbar E_r^{-1}$. For the lattice potential of the majority species we use a depth of $V_0/E_r = 8$. The harmonic part of the double well potential of the impurities has a harmonic oscillator frequency of $\omega/\omega_r = 0.1 \cdot \sqrt{2}$ and the barrier height and width are $h/E_r k_0^{-1} = 2$ and $w/k_0^{-1} = 1$, respectively. Furthermore, the intraspecies interaction strength among the bosons of the majority species is kept fixed to the value $g_{AA}/E_r k_0^{-1} = 1$. Hard-wall boundary conditions are imposed at $x/k_0^{-1} = \pm 3\pi$.

In the following, we present the quench protocol which induces the tunneling dynamics. A sketch of the employed procedure is depicted in figure 1. First, we obtain the many-body ground state of our system, assuming the above mentioned parameters. Here, the tilting strength of the double well is set to $\alpha/E_r k_0^{-1} = 0.1$ (the effect of a smaller tilting strength is analyzed in the Appendix), such that the impurities localize in the left well of the asymmetric double well potential. To trigger the tunneling dynamics of the impurities the system is quenched to a geometry, constituting a symmetric double well, i.e. the tilting strength is set to $\alpha = 0$. Varying the interspecies interaction strength g_{AB} , we explore the dependence of the system dynamics on g_{AB} .

2.2. Approach to the correlated many-body dynamics

To unravel the dynamics of the system we employ ML-MCTDHX [72–74]. As explicated below, this *ab initio* method gains its efficiency from the time-dependent and with the system co-moving basis set. In the first step, the total many-body wave function $|\Psi_{\text{MB}}(t)\rangle$ is expanded with respect to M different species functions $|\Psi^{\sigma}(t)\rangle$ for each of the species σ and expressed according to the following Schmidt decomposition [81]

$$|\Psi_{\text{MB}}(t)\rangle = \sum_{i=1}^M \sqrt{\lambda_i(t)} |\Psi_i^A(t)\rangle \otimes |\Psi_i^B(t)\rangle. \quad (2)$$

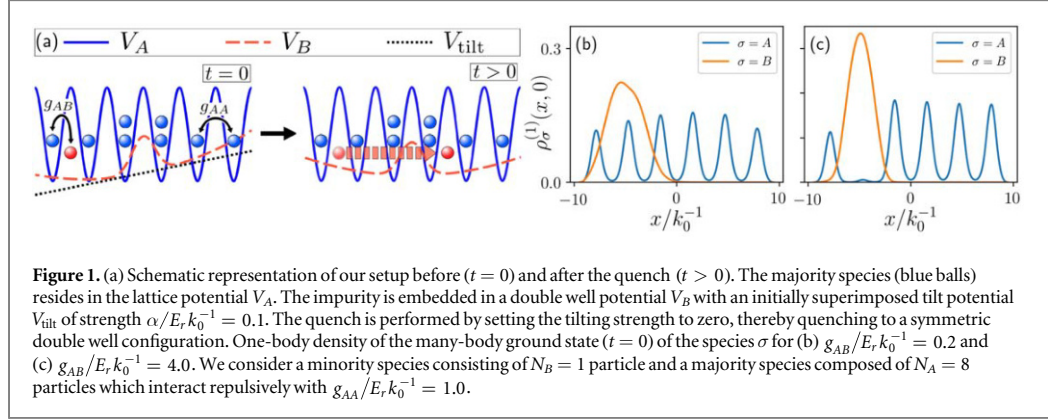
Here, the Schmidt coefficients $\sqrt{\lambda_i(t)}$, in decreasing order, provide information about the degree of population of the i th species function and thereby signify the degree of entanglement between the two species. In the case that only one Schmidt coefficient is non-zero, the species A and B are not entangled with each other and the system can be described by a species mean-field ansatz ($M = 1$). However, in general it is necessary to provide several species functions for the expansion of the total many-body wave function, since entanglement might prove crucial for the adequate description of the systems dynamics.

Furthermore, the species wave functions $|\Psi^{\sigma}(t)\rangle$ describing an ensemble of N_{σ} bosons are expanded in a set of permanents, namely

$$|\Psi_i^{\sigma}(t)\rangle = \sum_{\vec{n}^{\sigma}|N_{\sigma}} C_{\sigma\vec{n}}(t) |\vec{n}^{\sigma}(t)\rangle. \quad (3)$$

Such an expansion allows us to take intraspecies correlations of the σ -species into account. Moreover, in this expression the vector $\vec{n}^{\sigma} = (n_1^{\sigma}, n_2^{\sigma}, \dots)$ describes the occupations of the time-dependent single-particle functions (SPF) of the species σ , which are further expanded in terms of a time-independent discrete variable representation [82]. The notation $\vec{n}^{\sigma}|N_{\sigma}$ indicates that for each n_i^{σ} the particle number conservation condition $\sum_i n_i^{\sigma} = N_{\sigma}$ has to be fulfilled. For the time propagation of the many-body wave function we employ the Dirac-Frenkel variational principle $\langle \delta\Psi_{\text{MB}} | (i\partial_t - \mathcal{H}) | \Psi_{\text{MB}} \rangle$ [83–85] with the variation $\delta\Psi_{\text{MB}}$ and obtain the corresponding equations of motion [74, 86].

In conclusion, the ML-MCTDHX method takes all inter- and intraspecies correlations into account and gives us access to the complete many-body wave function. In contrast to standard approaches, where the wave function for solving the time-dependent Schrödinger equation is built upon time-independent Fock states with



time-dependent coefficients, the ML-MCTDHX method takes a co-moving time-dependent basis into account, where the Fock states, spanned by the SPFs, as well as the coefficients are time-dependent. This concept of a time-dependent basis reduces not only the required number of basis states and, hence, improves the computational effort, but it also provides at the same time an accurate description of the system's many-body state. We note here that in order to ensure the convergence of our many-body simulations, to be presented below, we have employed $M = 6$ ($M = 10$) species and $d_A = 6$, $d_B = 6$ ($d_A = 6$, $d_B = 6$) SPFs respectively for the case of a single (two) impurity atom(s). In this context we define the orbital configuration $C = (M, d_A, d_B)$ which determines the size of the truncated Hilbert space.

3. Correlated tunneling dynamics of a single impurity

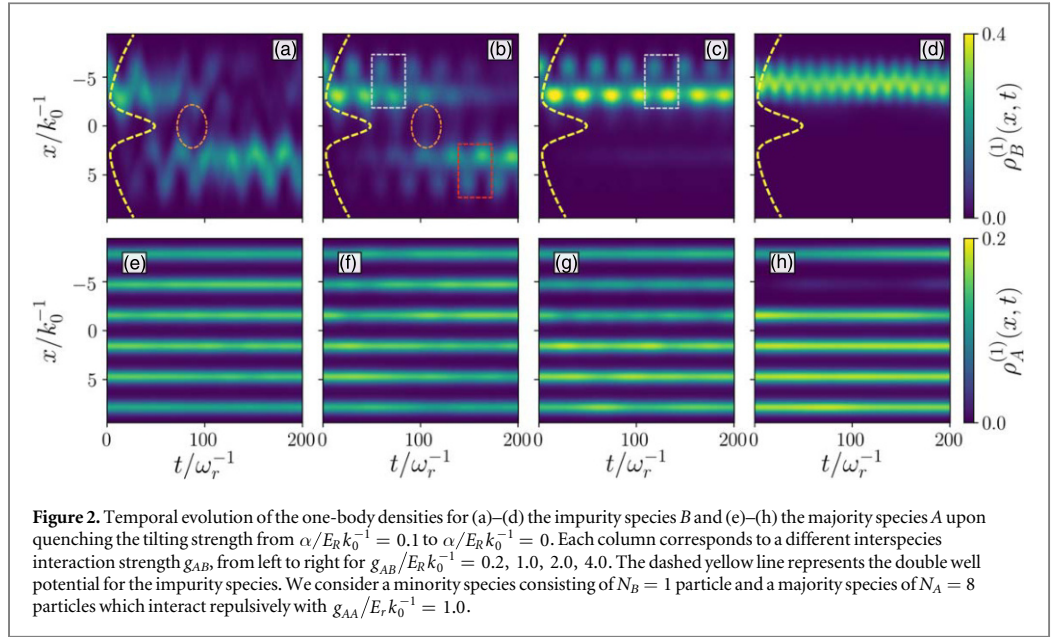
In the following we consider a mass-balanced bosonic mixture described by the Hamiltonian of equation (1) where the majority species consists of $N_A = 8$ and the impurity species of $N_B = 1$ particles. We initially prepare our system in its ground state with a tilting strength of $\alpha/E_r k_0^{-1} = 0.1$ for different interspecies interaction strengths g_{AB} . Due to the initial tilt the impurity is found to be well localized in a single site of the double well potential. Moreover, we find that the impurity species exhibits a rather large spatial overlap with the majority species for small g_{AB} (see figure 1(b)) which of course reduces with increasing repulsive g_{AB} (see figure 1(c)). In particular, for small g_{AB} the majority species occupies all sites of the lattice potential, such that the impurity strongly overlaps with it (see figure 1(b)). However, for strong repulsive interactions the majority species depopulates the well of the lattice potential in which the impurity tends to localize, resulting in a weak spatial overlap of the two species (see figure 1(c)). Upon quenching the tilting strength to $\alpha/E_r k_0^{-1} = 0$ towards a symmetric double well we initiate the tunneling dynamics, thus favoring the tunneling of the impurity to the right well as the corresponding energy offset between the two wells vanishes, see also figure 1(a). As a consequence the impurity becomes mobile, thereby colliding with the lattice trapped majority species which in general acts as a material barrier for the impurity dynamics. Varying the interspecies interaction strength we find four different regimes for the dynamical response of the impurity (see below).

As a first step, we quantify these regimes by monitoring the time evolution of the one-body density $\rho_\sigma^{(1)}(x, t) = \langle \Psi_{\text{MB}}(t) | \hat{\Psi}_\sigma^\dagger(x) \hat{\Psi}_\sigma(x) | \Psi_{\text{MB}}(t) \rangle$ of the corresponding subsystems σ . The spectral decomposition of the σ -species one-body density is given by

$$\rho_\sigma^{(1)}(x, t) = \sum_j n_{\sigma j}(t) \Phi_{\sigma j}^*(x, t) \Phi_{\sigma j}(x, t), \quad (4)$$

where $n_{\sigma j}(t)$ are the so-called natural populations and $\Phi_{\sigma j}(x, t)$ the corresponding natural orbitals. The dynamics of $\rho_\sigma^{(1)}(x, t)$ is presented in figure 2, for different interspecies interaction strengths g_{AB} . As it can be seen $\rho_\sigma^{(1)}(x, t)$ exhibits four distinct dynamical response regimes. For small interspecies interaction strengths, in our case $g_{AB}/E_r k_0^{-1} = 0.2$, the impurity undergoes a rather complex tunneling dynamics to the other site of the double well (figure 2(a)). This is a single-particle effect caused by the strong initial tilt and is therefore also present for $g_{AB} = 0$. For short evolution times, i.e. $0 < t/\omega_r^{-1} < 50$, the impurity performs oscillations in the initial well and then tunnels (see ellipse in figure 2(a)) to the other well. Here, the oscillations within each of the two wells, which still persist even for $g_{AB} = 0$ (not shown here), are caused by the rather strong initial tilt of the double well and are not present for smaller tilts³ (see figure 11(a)). In this sense, the majority species barely affects the

³ We note that this tunneling behavior differs from that of a single particle in a double well potential in the case of smaller tilts, yielding a single frequency Rabi tunneling.

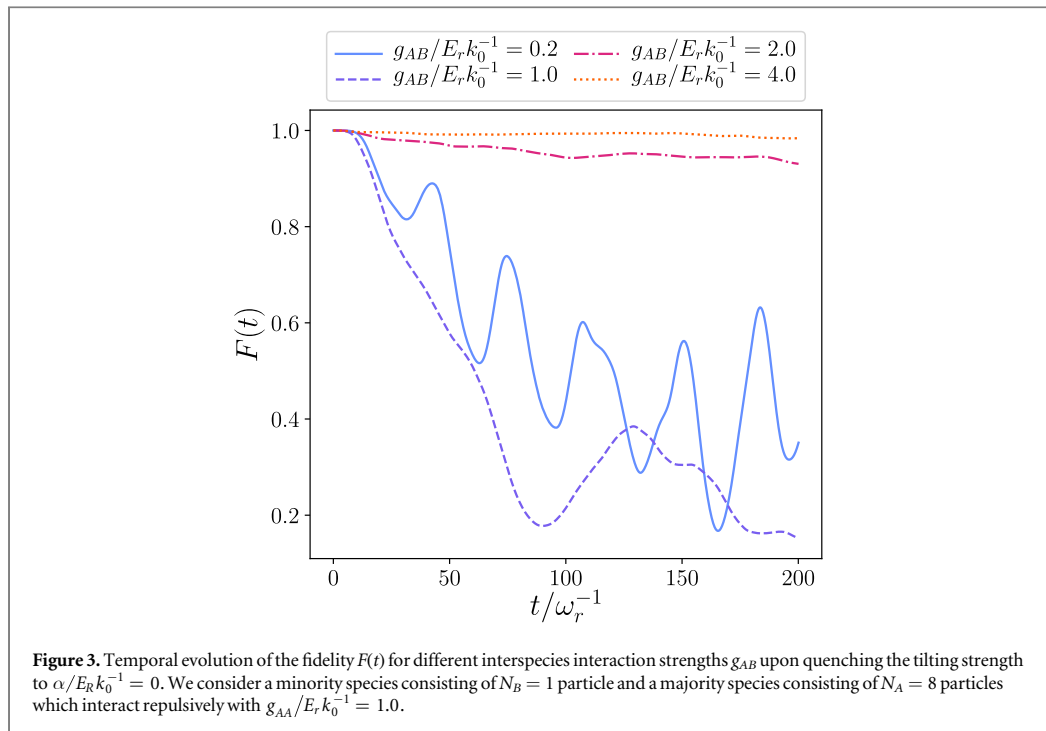


tunneling dynamics of the impurity and exhibits weak amplitude modulations from its initial profile due to the finite g_{AB} (figure 2(e)).

However, for larger coupling strengths the impurity is strongly influenced by the density distribution of the majority species, e.g. see figures 2(b) and (f). The majority species distributes over the lattice such that $\rho_A^{(1)}(x, t)$ is accumulated close to the minima of the lattice potential. Due to the repulsive interspecies interaction the impurity has to overcome on top of the double well barrier these additional material barriers imposed by the accumulation of the density of the majority species. This leads to an oscillation of the impurity through the neighboring density maximum of the A species (see white rectangle in figure 2(b)). This tunneling through the material barrier imposed by the majority species we will refer to as material barrier tunneling in the following. Throughout this enduring oscillation process the impurity performs a transport [87, 88] to the other site of the double well (see ellipse in figure 2(b)) where it again encounters a material barrier of species A and pursues the initial material barrier tunneling behavior (see red rectangle in figure 2(b)). Compared to the weakly interacting regime (figure 2(a)), in the intermediate regime the transport of the impurity to the other site of the double well takes place in a very controlled and systematic manner. Moreover, it is even possible to prolong the initial material barrier tunneling process by further increasing the interspecies interaction strength (figure 2(c)). In this case, the impurity undergoes a weak amplitude tunneling to the other site of the double well (see figure 8(c)), at least within the considered evolution time. In the limit of very large g_{AB} the impurity is trapped in the initial site of the double well due to the strong interspecies repulsion (see figures 1(c) and 2(d)) and as a result we enter the self-trapping regime. We remark that this self-trapping behavior is caused by the presence of the majority species, in sharp contrast to the well-known case of interacting bosons in a double well. Note also that the impurity undergoes dipole-like oscillations within the left site of the double well. Also, we have checked that this self-trapping behavior (see figure 2(d)) of the impurity persists up to $t/\omega_r^{-1} = 400$ evolution times (not shown here).

Considering the behavior of the majority species A , we observe the development of excitations of $\rho_A^{(1)}(x, t)$ as a back-action of the tunneling process of the impurity [12]. In particular, $\rho_A^{(1)}(x, t)$ is transferred through the lattice (figures 2(f) and (g)). Predominantly, this is the case for the inner four wells. This behavior of the majority species is caused by the repulsive interspecies interaction which leads in the course of the impurity tunneling to a shift of the density of species A , thereby reducing the overlap between the species. In the extreme case (see $g_{AB}/E_R k_0^{-1} = 4.0$) where the impurity remains localized in one site of the double well, the majority species redistributes such that a density hole is formed in one lattice site (see figure 2(h)), in order to avoid the impurity. Here, the overall density of the majority species barely changes in time due to the absence of the impurity's tunneling.

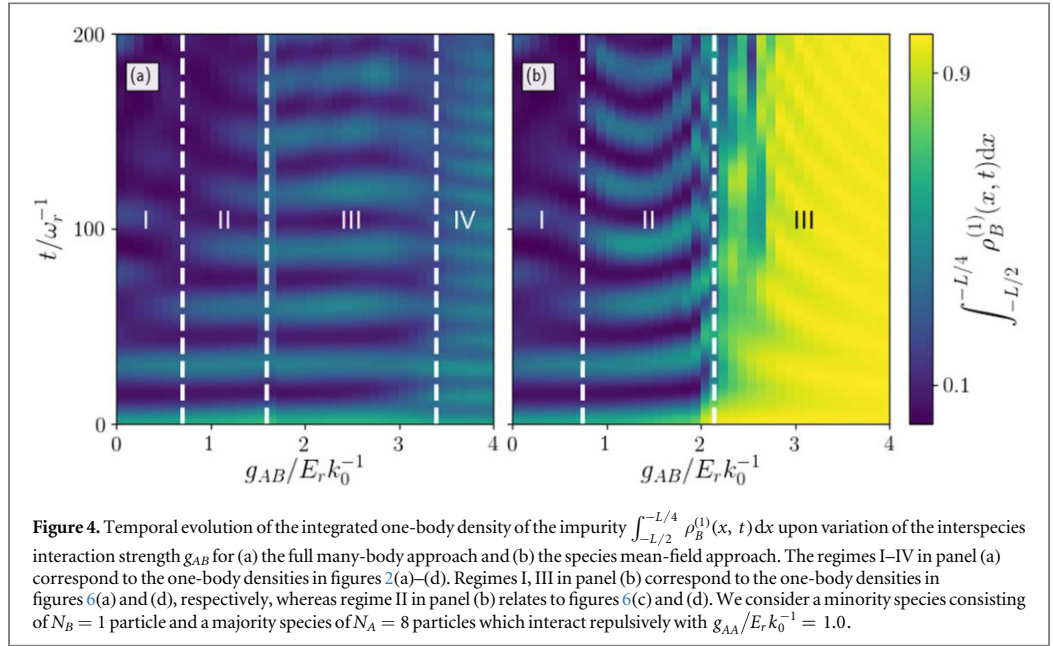
In order to quantify the dynamical response of the system even further it is convenient to analyze how strongly the time-dependent many-body wave function deviates from the initial state $|\Psi_0\rangle$ at $t = 0$ in the course of time. This is well captured by the fidelity $F(t) = |\langle \Psi_{MB}(t) | \Psi_0 \rangle|^2$ which is defined as the overlap between the time-dependent and the initial wave function. Figure 3 shows the fidelity $F(t)$ for various interspecies interaction



strengths corresponding to the four different tunneling regimes identified in the time evolution of the one-body densities in figure 2. We clearly observe that the behavior of the fidelity is qualitatively driven by the one-body density distribution of the impurity over time. For the cases in which the impurity tunnels to the other site of the double well (figures 2(a) and (b)), the fidelity deviates significantly from unity, i.e. $|\Psi_{MB}(t)\rangle$ deviates from the ground state $|\Psi_0\rangle$. However, in the regimes where the tunneling of the impurity is suppressed the fidelity remains close to unity, e.g. see $F(t)$ for $g_{AB} = 2.0, 4.0$. In this sense, the fidelity evolution provides an indicator of the tunneling process of the impurity and serves as a first characterization for the tunneling (figures 2(a) and (b)) and self-trapping regimes (figures 2(c) and (d)). Nevertheless, using solely the fidelity it is not possible to distinguish between the different tunneling mechanisms. In order to discern between the above-mentioned four possible regimes of the impurity's dynamical response it is useful to consider the integrated one-body density of the impurity $\int_{-L/2}^{-L/4} \rho_B^{(1)}(x, t) dx$, where L is the size of the system. This quantity provides the probability of finding the impurity in one half of the initially populated well of the double well. Indeed, the integrated density allows to distinguish between the emergent tunneling dynamics since it incorporates the effect of the material barrier. In figure 4(a) we show the temporal evolution of this quantity for the correlated many-body approach⁴ for different g_{AB} . We clearly observe four distinct regimes for the response of the impurity which correspond to the one-body densities in figures 2(a)–(d). Indeed, in regime I an irregular oscillatory pattern of the integrated density is found. Regime II exhibits regular oscillations whose intensity decays in time. This corresponds to the material barrier tunneling with a final transfer of the impurity to the other site of the double well (see figure 2(b)). In regime III the oscillations of the integrated density remain stable in time which is due to the material barrier tunneling of the impurity in the initially populated well without a transfer to the other site. Finally, in regime IV we find a higher-frequency oscillatory behavior with a finite amplitude throughout the evolution. This behavior corresponds to the self-trapping regime (see figure 2(d)). Regarding the dependence of the tunneling behavior on the different system parameters see appendix B.

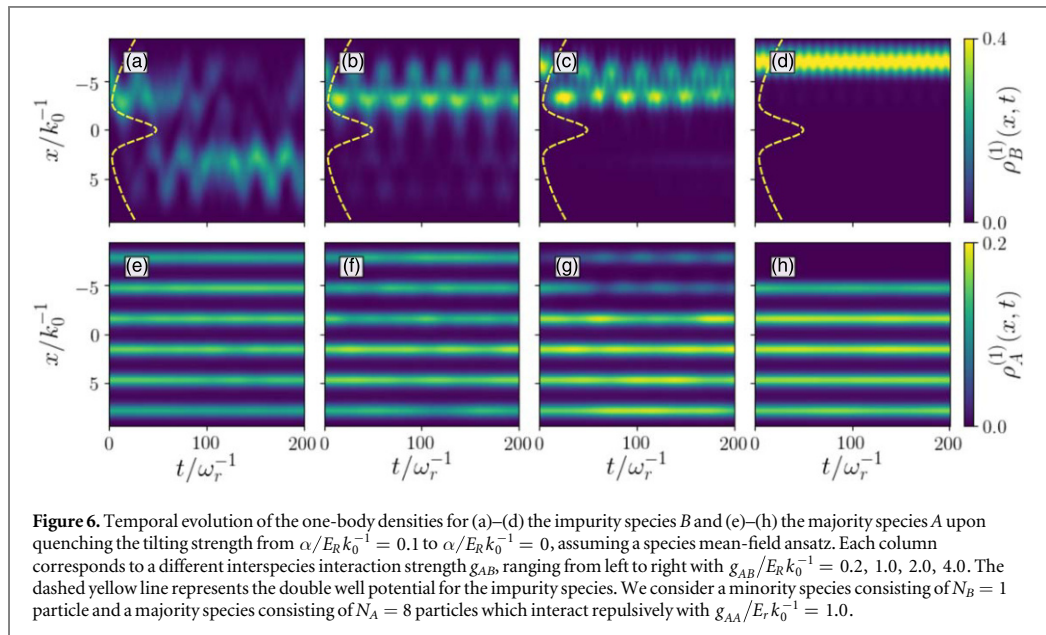
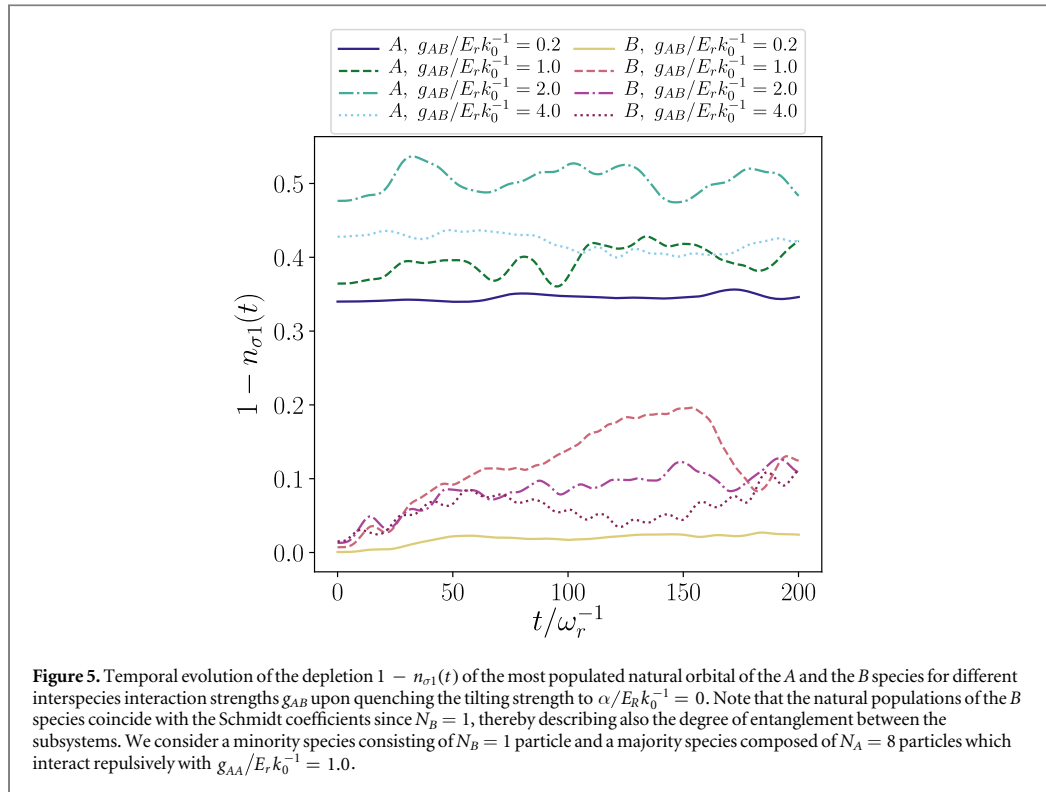
However, so far we did not get insight into the degree of the system's correlation throughout the dynamics. To unravel the degree of correlations which accompanies the tunneling dynamics of the impurity we distinguish between inter- and intraspecies correlations. The former are described by the Schmidt coefficients (equation (2)), which provide a measure for the degree of entanglement between the subsystems, whereas the latter can be inferred from the natural populations (see equation (4)). Since the B species consists of a single particle, the natural populations of the B species coincide with the Schmidt coefficients. Therefore, in the following we invoke the deviation $1 - n_{B_1}(t)$ as a measure of entanglement between the subsystems.

⁴The many-body approach refers to our treatment within ML-MCTDHX in contrast to mean-field approaches.



Accordingly, $1 - n_{A1}(t)$ indicates the degree of intraspecies correlations of the majority species. The temporal evolution of the depletion $1 - n_{\sigma 1}(t)$ of the most populated natural orbital of the A and the B species is illustrated in figure 5 for different g_{AB} upon quenching the tilting strength. We observe that for small interspecies interaction strengths, i.e. $g_{AB} = 0.2$, the subsystems are mainly disentangled throughout the dynamics, since $1 - n_{B1}(t) \approx 0$. Increasing the interspecies interaction strength to $g_{AB}/E_R k_0^{-1} = 1.0$ the subsystems become strongly entangled in the course of time, i.e. $1 - n_{B1}(t) > 0$. This can be associated with tunneling of the impurity to the other site of the double well and the involved increasing interspecies interaction between the subsystems. Naturally, the motion of the impurity through the majority species has an impact on the natural populations of the A species which is connected to the intrinsic tunneling processes of the A species in the lattice potential (see figures 2(e)–(f)). Indeed, $1 - n_{A1} > 0$ independently of g_{AB} and it is maximized in the above-described third tunneling region. Interestingly, the rather strong degree of entanglement remains in the self-trapping regime for $g_{AB}/E_R k_0^{-1} = 4.0$, even though the impurity barely overlaps with the majority species.

In order to emphasize the importance of the entanglement between the subsystems for the tunneling behavior of the impurity, we additionally perform calculations assuming only a single product state $|\Psi_{MB}\rangle = |\Psi_A\rangle \otimes |\Psi_B\rangle$ in equation (2), thereby neglecting all interspecies correlations. The dynamics of the σ -species one-body densities employing a species mean-field ansatz, i.e. assuming a single product state between the species but still including intraspecies correlations, are shown in figure 6. For $g_{AB}/E_R k_0^{-1} = 0.2$ we find no visible differences between the full many-body approach and the species mean-field calculations. This is an expected result, as the degree of entanglement is rather small for these interactions (see figure 5). However, as soon as entanglement becomes important, we find strong deviations in the corresponding one-body densities. In particular, for $g_{AB}/E_R k_0^{-1} = 1.0$ in the species mean-field case (see figure 6(b)) we do not observe the previously predicted tunneling to the other site of the double well (see figure 2(b)). Furthermore, the one-body density of the impurity for $g_{AB}/E_R k_0^{-1} = 2.0$ exhibits additional oscillation frequencies in the species-mean field scenario (see figure 6(c)) compared to the full many-body case (figure 2(c)). In the self-trapping regime, $g_{AB}/E_R k_0^{-1} = 4.0$, the species mean-field calculations seem to capture the dynamics quite well at first glance. However, on a closer inspection of the one-body density it turns out that the spatial position of the impurity differs compared to the complete many-body approach, while the temporal oscillations of the density are also of different amplitude and frequency, see figures 2(d) and 6(d). This general difference in the tunneling dynamics is well captured by the integrated density shown in figure 4. Indeed, the species mean-field ansatz is not able to recover regime II in figure 4(a), while the self-trapping regime III in figure 4(b) is strongly altered compared to that one in figure 4(a) corresponding to regime IV in the many-body treatment. Even regime III in figure 4(a) is quantitatively changed when using the species mean-field ansatz (see figure 4(b) regime II). In this sense, entanglement between the impurity and the majority species plays a crucial role, in order to describe the dynamics correctly.



4. Characterization of the impurity dynamics

To analyze the tunneling behavior of the impurity and the accompanying correlations due to the presence of the majority species (see figure 2) we next develop an effective potential model for the impurity. This effective potential is obtained by superimposing the time-averaged density of the majority species to the external double well potential. To adequately describe the dynamical response of the majority species we employ the associated

Wannier functions. In particular, we project the complete many-body wave function obtained via ML-MCTDHF onto these Wannier functions in order to analyze the behavior of the impurity in a fixed basis set.

4.1. Construction of the effective potential

Initially, we prepare our system such that it is given by the ground state of the Hamiltonian (equation (1)) with an underlying asymmetric double well. With respect to the quenched Hamiltonian ($t > 0$) our system and in particular the impurity is energetically excited due to the tilting. This enables the impurity to tunnel through the potential barrier of the double well into the right well. However, as mentioned in section 3, for specific interspecies interaction strengths this residual energy appears to be not large enough to overcome the potential barrier. Therefore, the impurity B rather performs a tunneling in the initial site of the double well through the material barrier imposed by the one-body density of the majority species (see figure 2(c)).

In the following, we aim at understanding this tunneling behavior using an effective potential for the impurity. We remark that this effective potential serves only as a tool for an analysis of the underlying tunneling processes. Integrating out the majority species we arrive at the following effective potential for the impurity

$$V_{\text{eff}}^B(x^B, t) = N_A g_{AB} \rho_A^{(1)}(x^B, t) + V_B(x^B). \quad (5)$$

This effective potential is composed by the double well potential V_B and the one-body density of the majority species $\rho_A^{(1)}$ being weighted by the number of particles N_A and the interspecies interaction strength g_{AB} . Note that $\rho_A^{(1)}(x^B, t)$ is calculated within the correlated many-body approach and thereby includes all necessary correlations. $\rho_A^{(1)}(x^B, t)$ cannot be recovered within a mean-field approach. To proceed, we average this effective potential over time and obtain a Time-Averaged Effective Potential (TAEP)

$$\bar{V}_{\text{eff}}^B(x^B) = \frac{1}{T} \int_0^T V_{\text{eff}}^B(x^B, t) dt, \quad (6)$$

where T denotes the total propagation time. We can justify this time-average by the small one-body density deformations of the majority species over time. Furthermore, we remark that equation (5) is a species mean-field effective potential and, therefore, only assumes a single product state. Even though we have seen in figure 5 that the entanglement between the subsystems plays a crucial role this ansatz turns out to be a powerful tool to analyze the basic aspects of the tunneling behavior of the impurity and gives an intuitive understanding [12, 46, 91]. The time-averaged effective potentials are depicted in figure 7(a) for the four interspecies interaction strengths $g_{AB}/E_r k_0^{-1} = 0.2, 1.0, 2.0, 4.0$ corresponding to the four tunneling regimes already discussed in section 3. For weak interspecies interaction strengths, e.g. $g_{AB}/E_r k_0^{-1} = 0.2$, the TAEP resembles the shape of the double well potential V_B , and only small deviations are visible raised from the superimposed one-body density of the majority species. Moreover, the height of the central potential barrier of the TAEP ($\approx 0.89E_r$) is approximately the same as for the double well V_B with a value of $h/(\sqrt{2\pi} w) \approx 0.80$ at $x^B = 0$. Therefore, one can assume that the tunneling dynamics of the impurity in the TAEP would differ only marginally compared to the behavior of a single particle confined in the double well V_B , i.e. for $g_{AB} = 0$. Since in the TAEP the one-body density $\rho_A^{(1)}$ of the majority species is weighted by the interspecies interaction strength g_{AB} , the spatial distribution of $\rho_A^{(1)}$ becomes more pronounced for increasing g_{AB} . Consequently, for a larger g_{AB} we observe the appearance of six maxima on top of the double well structure, which stem from the majority species trapped in the minima of the lattice potential V_A . We find that for an interspecies interaction strength of $g_{AB}/E_r k_0^{-1} = 1.0$ the density of the majority species distributes such that we obtain a nearly parity symmetric TAEP with respect to $x = 0$ (see figure 7(d)).

In the following, we refer to the first, second, etc maximum of the TAEP ordered from left to right excluding the case of $g_{AB}/E_r k_0^{-1} = 0.2$ due to the small deviations of the TAEP from the double well structure. Increasing the interspecies interaction strength eventually breaks the spatial symmetry of the TAEP w.r.t. $x = 0$, which can be readily seen e.g. at $g_{AB}/E_r k_0^{-1} = 2.0$ and $g_{AB}/E_r k_0^{-1} = 4.0$ (see figures 7(e) and (f)). In particular, the TAEP for $g_{AB}/E_r k_0^{-1} = 4.0$ exhibits a distinct asymmetry. Here, the second maximum of the TAEP is strongly suppressed compared to the other maxima. This can be attributed to the fact that the one-body density of the majority species $\rho_A^{(1)}$ in the second well of V_A , counted from the left, coincides with the position of the second maximum of the TAEP. Here, $\rho_A^{(1)}$ is strongly depopulated compared to the other wells of V_A (see figure 2(h)) which leads to the suppression of the second maximum of the TAEP. Focusing on the maxima of the TAEP especially, on the third and fourth maximum, we can interpret these maxima as the potential barriers that the impurity has to overcome in order to tunnel from the left to the right side of the TAEP. We observe that the corresponding maxima heights increase with increasing g_{AB} , which indicates that the effective potential barrier for the impurity also increases with g_{AB} .

In the following, we investigate this effective potential barrier that separates the left from the right side of the TAEP. For this purpose, we calculate the relative difference $\Delta_{\text{max},i} = (\Lambda_i^{\text{eff}} - \Lambda_2^{\text{eff}})/\Lambda_2^{\text{eff}}$ between the second maximum height Λ_2^{eff} and third and fourth maximum height, Λ_3^{eff} and Λ_4^{eff} , of the TAEP, where $i=3,4$. Figure 7(b) shows the relative difference $\Delta_{\text{max},i}$, which serves in the following as a measure for the effective potential barrier, in dependence on the interspecies interaction strength g_{AB} . For values below $g_{AB}/E_r k_0^{-1} = 1.0$

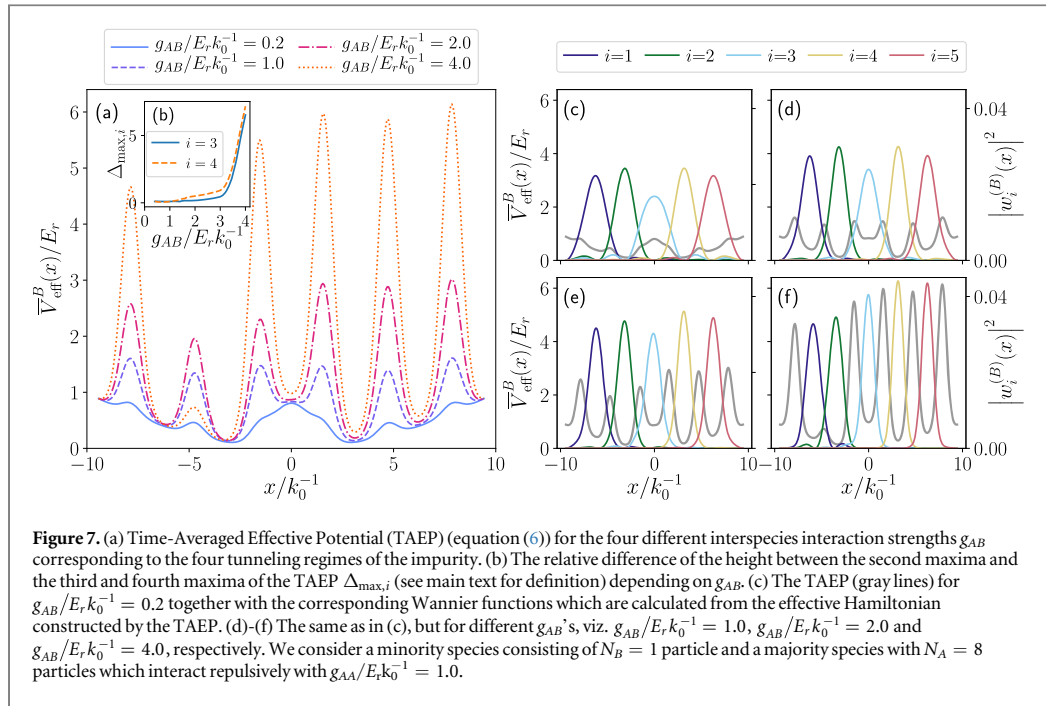


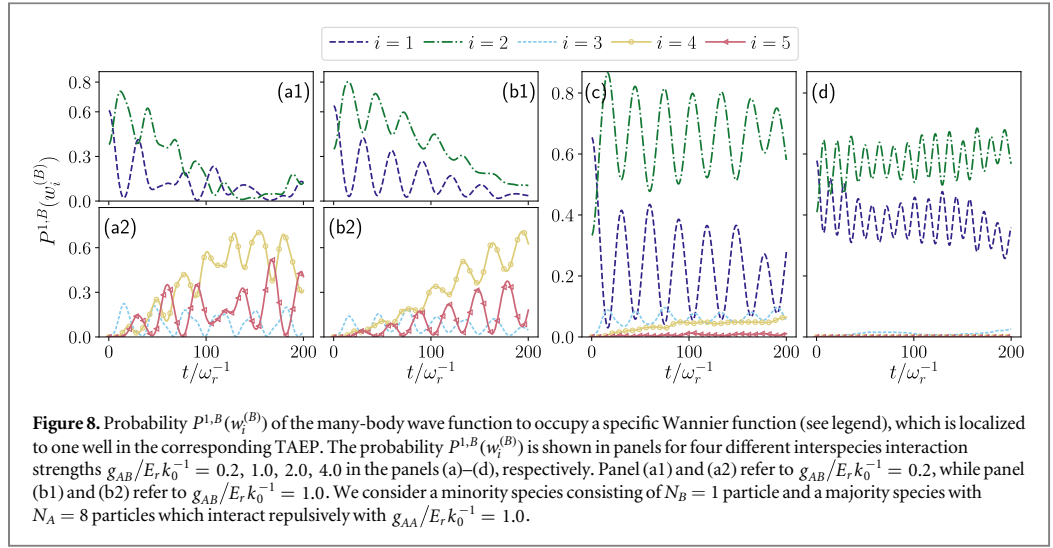
Figure 7. (a) Time-Averaged Effective Potential (TAEP) (equation (6)) for the four different interspecies interaction strengths g_{AB} corresponding to the four tunneling regimes of the impurity. (b) The relative difference of the height between the second maxima and the third and fourth maxima of the TAEP $\Delta_{\text{max},i}$ (see main text for definition) depending on g_{AB} . (c) The TAEP (gray lines) for $g_{AB}/E_r k_0^{-1} = 0.2$ together with the corresponding Wannier functions which are calculated from the effective Hamiltonian constructed by the TAEP. (d)–(f) The same as in (c), but for different g_{AB} 's, viz. $g_{AB}/E_r k_0^{-1} = 1.0$, $g_{AB}/E_r k_0^{-1} = 2.0$ and $g_{AB}/E_r k_0^{-1} = 4.0$, respectively. We consider a minority species consisting of $N_B = 1$ particle and a majority species with $N_A = 8$ particles which interact repulsively with $g_{AA}/E_r k_0^{-1} = 1.0$.

the effective potential barrier $\Delta_{\text{max},i} \approx 0$ for $i = 3, 4$ meaning that the maxima barely deviate. For values above $g_{AB}/E_r k_0^{-1} = 1.0$ the third and fourth maximum height of the TAEP become larger than the second one, breaking in this manner the symmetry of the TAEP. For large interspecies interaction strengths, e.g. $g_{AB}/E_r k_0^{-1} = 4.0$, the effective potential barrier $\Delta_{\text{max},i}$ abruptly increases which is also due to the absence of $\rho_A^{(1)}$ in the second well of the lattice potential and, subsequently, the lowering of the second maximum height of the TAEP. The abrupt increase of the effective potential barrier $\Delta_{\text{max},i}$ intuitively leads to the assumption that for large interspecies interaction strengths, e.g. $g_{AB}/E_r k_0^{-1} = 4.0$, a tunneling of the impurity from the left to the right TAEP should be strongly suppressed, as already seen in the one-body density (see figure 2(d)) obtained within the complete many-body approach.

Let us also describe the tunneling behavior of the impurity in terms of states that are highly localized in the minima of the TAEP. Since, for sufficiently strong interspecies interaction strengths g_{AB} the TAEP resembles a lattice with five sites (see figure 7(a)) we calculate five of those functions. For this purpose, we construct an effective Hamiltonian $\hat{\mathcal{H}}_{\text{eff}}^{(B)} = -\frac{\hbar^2}{2m} \frac{d^2}{(dx^B)^2} + \bar{V}_{\text{eff}}^B(x^B)$ using the TAEP. For the localized functions we use the notion of generalized Wannier functions [89, 90] which have the advantage that they can be also obtained in the presence of a non-periodic potential. To obtain five generalized Wannier functions $w_i^{(B)}$ we first calculate the five energetically lowest eigenfunctions of $\hat{\mathcal{H}}_{\text{eff}}^{(B)}$. Using these eigenfunctions as a basis we diagonalize the position operator \hat{X} yielding eigenstates which are highly localized in the minima of the TAEP. For simplicity, we shall call the generalized Wannier functions in the following Wannier functions and, further, we will refer to the first, second, etc. Wannier function as the Wannier function localized in the first, second, etc. well of the TAEP.

Figures 7(c)–(f) presents the absolute squares of the Wannier functions together with the TAEPs for the four different tunneling regimes corresponding to the interspecies interactions strengths $g_{AB}/E_r k_0^{-1} = 0.2, 1.0, 2.0, 4.0$. For $g_{AB}/E_r k_0^{-1} = 0.2$ (figure 7(c)) we find, compared to the results for larger g_{AB} , the largest overlap between the Wannier functions. This indicates that those Wannier functions are rather ill-defined. The reason can be found in the TAEP which resembles for small interspecies interaction strengths, e.g. $g_{AB}/E_r k_0^{-1} = 0.2$, more a double well than a lattice potential. Increasing g_{AB} (see figures 7(d)–(f)), the Wannier functions become more localized in the minima of the TAEP and, therefore, are suited for the further analysis of the many-body wave function.

In summary, we have developed an effective one-body Hamiltonian using a TAEP for the purpose of constructing generalized Wannier functions from the eigenfunctions of this effective one-body Hamiltonian. This procedure resulted in functions which are highly localized in the wells of the TAEP for sufficiently large interspecies interaction strengths g_{AB} . Projecting these Wannier functions onto the full many-body wave



function, obtained in the course of our numerical simulations, we are in the following able to get a deeper insight into the tunneling dynamics of the impurity.

4.2. Dynamical response in terms of Wannier states

In the following discussion, we analyze the results of the correlated many-body calculations utilizing the Wannier functions derived in the previous section more specifically. Therefore, we project the i th Wannier function $w_i^{(B)}$ onto the many-body wave function and thereby receive the time-dependent probability $P^{1,B}(w_i^{(B)})$ that the impurity occupies the i th well of the TAEP. This probability is defined as

$$P^{1,B}(w_i^{(B)}) = |\langle w_i^{(B)} | \Psi_{\text{MB}} \rangle|^2. \quad (7)$$

Before discussing the results, let us comment on the Wannier functions as a basis set for the species wave function of the impurity. By summing up the five occupation probabilities of the Wannier functions, we obtain for each time instant of the evolution a measure for the accuracy of this basis representation. For our results we find that $\sum_i P^{1,B}(w_i^{(B)}) > 0.95$ so that we can consider the Wannier functions as an adequate basis set for describing the tunneling dynamics of the impurity. The time evolution of the probability $P^{1,B}(w_i^{(B)})$ for the four distinct tunneling regimes corresponding to $g_{AB}/E_r k_0^{-1} = 0.2, 1.0, 2.0, 4.0$ is shown in figure 8. In the following, we aim at understanding the respective one-body densities $\rho_B^{(1)}$ obtained from the many-body calculation (see figures 2(a)–(d)) with the aid of the occupation probabilities $P^{1,B}(w_i^{(B)})$. Starting from $g_{AB}/E_r k_0^{-1} = 0.2$ (figures 8(a1) and (a2)), we observe a rather irregular time evolution of the occupation probabilities. Here, many Wannier functions are occupied simultaneously indicating that the state of the impurity consists of a superposition of the corresponding Wannier functions. At first glance the behavior of the time evolution of $P^{1,B}(w_i^{(B)})$ at $g_{AB}/E_r k_0^{-1} = 1.0$ depicted in figures 8(b1) and (b2) is similar compared to the one in panel (a1) and (a2). In both cases we observe a reduction of the occupation probabilities of the first and second Wannier function, representing the left side of the TAEP, and an increase of $P^{1,B}(w_i^{(B)})$ of the fourth and fifth Wannier function, representing the right side of TAEP. This gradual depopulation of the left and subsequent population of the right side of the TAEP reflects precisely the observed tunneling process observed in the one-body density $\rho_B^{(1)}$ of the impurity. However, we find that at $g_{AB}/E_r k_0^{-1} = 1.0$ the transfer of the occupation probabilities from the left to the right side of the TAEP is more uniform than at $g_{AB}/E_r k_0^{-1} = 0.2$.

Initially, we observe an exchange of probability between the first and second Wannier states (see figure 8(b1)), which represents the material barrier tunneling process in the initial site of the double well. Eventually, probability is transferred from the first and second to the fourth and fifth Wannier state (see figure 8(b2)), reflecting the controlled tunneling behavior observed in figure 2(b). Partially, this can be understood in terms of the TAEP which exhibits a lattice structure on top of the double well, while being still spatially symmetric with respect to $x = 0$. For stronger interspecies interaction strengths, e.g. $g_{AB}/E_r k_0^{-1} = 2.0$ and $g_{AB}/E_r k_0^{-1} = 4.0$, the first two Wannier functions are predominantly occupied. As shown in figure 8(c), for times directly after the quench the first Wannier function is the most occupied one, whereas for larger times the occupation probability for the second Wannier function becomes the dominant one. We can understand this intuitively by inspecting the corresponding TAEP depicted in figure 7(e). Here, the TAEP exhibits a global minimum in the second well which makes it energetically favorable for the impurity to reside there.

Furthermore, the first and second occupation probability exhibit a strong counterwise oscillation behavior. Comparing this with the oscillation of the one-body density of the impurity around a potential barrier imposed by the majority species (see figure 2(c)), we find very good agreement. Moreover, we find that the occupation probability for the other Wannier functions, i.e. the third fourth and fifth, are strongly suppressed, but seem to continuously increase over time. Therefore one might assume that for sufficiently long evolution times the impurity eventually tunnels to the right side of the TAEP.

Turning to the occupation probabilities at $g_{AB}/E_r k_0^{-1} = 4.0$ (figure 8(d)), we observe that the occupation probabilities of the third, fourth and fifth Wannier function are close to zero during the entire time propagation. We can understand this in terms of an effective potential barrier that separates the left side of the TAEP from the right side w.r.t. $x = 0$. Here, the value for the relative difference $\Delta_{\max,i}$ for $g_{AB}/E_r k_0^{-1} = 4.0$ is much larger than for the other considered interspecies interaction strength g_{AB} (see figure 6(b)) and, therefore, it is very unlikely that the impurity will tunnel to the right side of the TAEP even for later times. Additionally, the occupation probabilities of the first and second Wannier function perform a counterwise oscillation, likewise to the probabilities at $g_{AB}/E_r k_0^{-1} = 2.0$ (figure 8(c)). In contrast to the aforementioned oscillation of the occupation probabilities, we observe for $g_{AB}/E_r k_0^{-1} = 4.0$ almost twice the number of oscillation periods during the dynamics as well as a reduction of the amplitudes. A hint for understanding this gives again the corresponding TAEP (see figure 6(f)). Here, the second maximum height is strongly suppressed and the first and second Wannier functions have a large overlap. From this we can infer that the species wave function of the impurity consists mainly of a superposition of the first and second Wannier function whose contributions oscillate over time.

In conclusion, we generated localized Wannier functions associated with the TAEP and projected them onto the time-dependent many-body wave function. Having this at hand we were able to describe the many-body impurity dynamics in terms of the evolution of the occupation probabilities of the respective Wannier functions. As a natural next step, we shall investigate the two-body correlations between the impurity and the majority species. More precisely, we determine the discrete correlation function associated with the impurity occupying a specific well of the TAEP and a single particle of the majority species occupying a certain well of the lattice potential V_A .

First we generate Wannier functions associated with the single-particle Hamiltonian for the majority species $\hat{\mathcal{H}}^{(A)} = -\frac{\hbar^2}{2m} \frac{d^2}{(dx^A)^2} + V_A(x^A)$, following the procedure explained above⁵. Furthermore, we determine the one-body probability for a particle of the majority species to occupy the j th well of the lattice potential V_A by projecting the many-body wave function onto the Wannier function $w_j^{(A)}$, thereby constructing the probability $P^{1,A}(w_i^{(A)}) = |\langle w_i^{(A)} | \Psi_{\text{MB}} \rangle|^2$. The conditional probability $P^{2,AB}(w_i^{(A)}, w_j^{(B)}) = \langle \Psi_{\text{MB}} | \hat{O}_{ij}^{(2)} | \Psi_{\text{MB}} \rangle$ of finding a single particle of the majority species in the i th well of V_A and at the same time the impurity in the j th well of the TAEP is defined as the expectation value of the following operator

$$\hat{O}_{ij}^{(2)} = \frac{1}{N_A} \sum_{l=1}^{N_A} |w_i^{(A),l}\rangle \langle w_i^{(A),l}| \otimes |w_j^{(B)}\rangle \langle w_j^{(B)}|, \quad (8)$$

with respect to the many-body wave function $|\Psi_{\text{MB}}\rangle$. The summation runs over the number of particles of the subsystem A . The discrete two-body correlation function is then given by

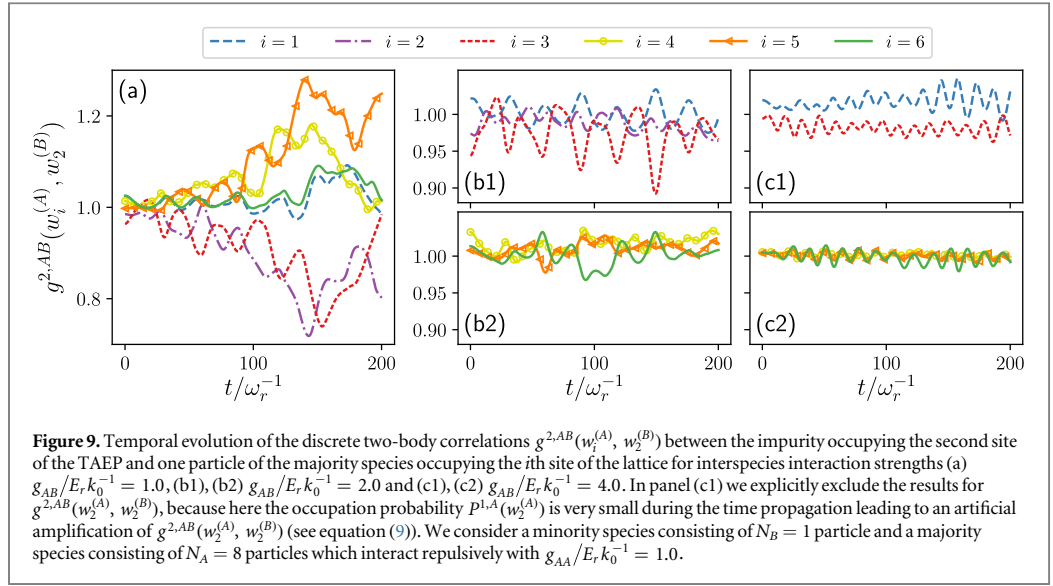
$$g^{2,AB}(w_i^{(A)}, w_j^{(B)}) = \frac{P^{2,AB}(w_i^{(A)}, w_j^{(B)})}{P^{1,A}(w_i^{(A)})P^{1,B}(w_j^{(B)})}. \quad (9)$$

This function provides information about the correlation between a single particle of the majority species localized at the i th well of V_A and the impurity species localized at the j th well of the TAEP. In case the discrete correlation function $g^{2,AB}(w_i^{(A)}, w_j^{(B)})$ equals unity the particle of the majority species and the impurity are termed uncorrelated since the conditional probability equals the unconditional one. However, if $g^{2,AB}(w_i^{(A)}, w_j^{(B)})$ is larger (smaller) than unity the impurity and the particle of the majority species are said to be correlated (anti-correlated) [15, 73].

The time evolution of the discrete correlation function for the impurity occupying the second Wannier function $w_2^{(B)}$ of the TAEP and the particle of the majority species occupying one of the six Wannier functions of the lattice potential V_A is shown in figure 9. We choose to present only results for $g^{2,AB}$ where the impurity is occupying the second Wannier state $w_2^{(B)}$ since for this case we are already able to observe and analyze all relevant properties of the discrete correlation function. Figures 9(a)–(c2) depict $g^{2,AB}$ for the interspecies interaction strengths $g_{AB}/E_r k_0^{-1} = 1.0, 2.0, 4.0$, respectively⁶. At $g_{AB}/E_r k_0^{-1} = 1.0$ (figure 9(a)), we observe that initially the system is rather uncorrelated and develops stronger correlations for larger time. Here, the particle of the

⁵ Note that the Wannier functions are sorted from the left to right regarding the sites of the lattice potential.

⁶ Here, we do not show the results for $g_{AB}/E_r k_0^{-1} = 0.2$, because as already mentioned before the Wannier basis is ill-defined in this case.



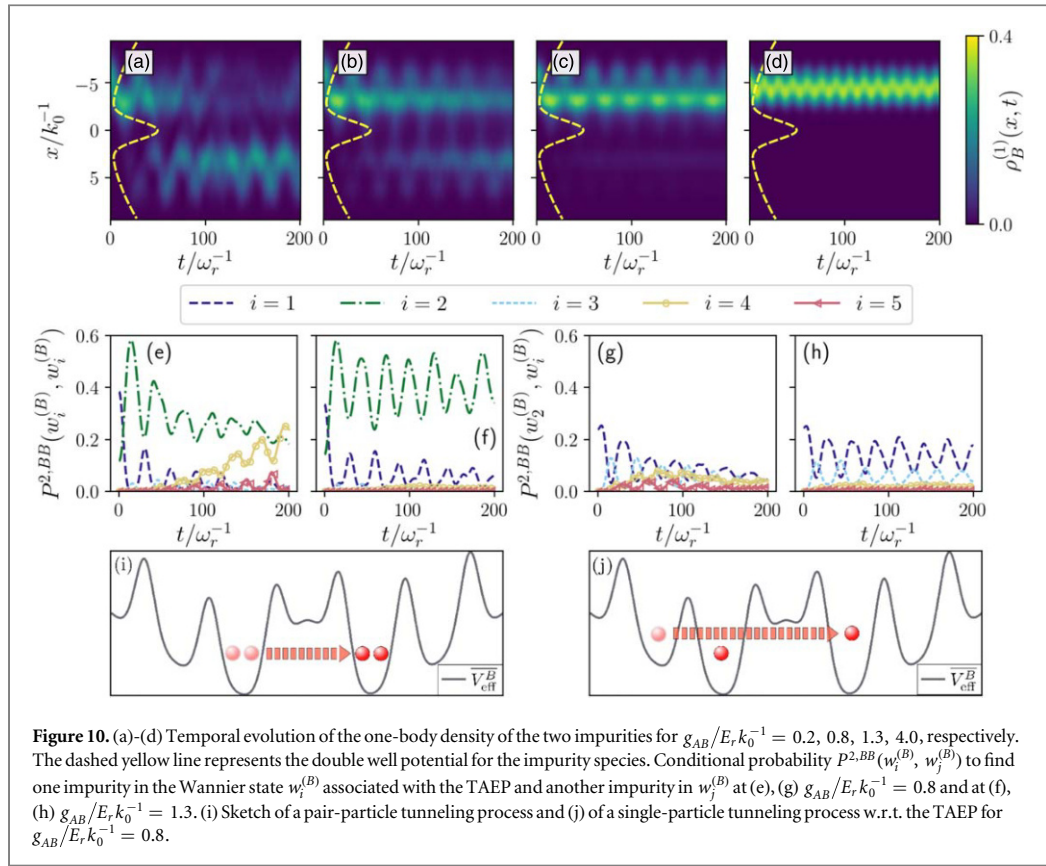
majority species in the fourth/fifth well of V_A and the impurity species in the second well of \bar{V}_{eff}^B show an increasing correlation amplitude over time, whereas an anti-correlation between the particle of the majority species in the second/third well of V_A and the impurity species in the second well of \bar{V}_{eff}^B occurs. The particle of the majority species being in the first and sixth well exhibits a similar correlation behavior with the impurity in the second well. We note that the strongest correlation (anti-correlation) occurs within the time intervals where the impurity tunnels to the right side of the TAEP (see figure 2(b)).

Turning to the discrete correlation functions at $g_{AB}/E_r k_0^{-1} = 2.0, 4.0$, depicted in figures 9(b1), (b2) and (c1), (c2) we find that the system is in both cases slightly two-body correlated. Predominantly, this is the case for $g_{AB}/E_r k_0^{-1} = 4.0$ where the impurity exhibits a self-trapping behavior, showing only a weak distinct correlated or anti-correlated behavior between the impurity in the second well of the TAEP and one particle of the majority species in a specific well of the lattice potential (see figures 9(c1) and (c2)). However, in figure 9(b1) we observe an oscillating correlation behavior between the majority species in the third well of V_A and the impurity species in the second well of \bar{V}_{eff}^B . Here, $g^{2,AB}(w_3^{(A)}, w_2^{(B)})$ oscillates between the anti-correlated and uncorrelated case which might be associated with the material barrier tunneling of the impurity in the initial site of the double well (see figure 2(c)). Concluding, we observe an overall decrease of the discrete correlation with increasing interspecies interaction strength, which appears to be related to the manifestation of the self-trapping of the impurity.

5. Correlated tunneling dynamics of two impurities

So far we have investigated the tunneling dynamics of a single impurity coupled to a majority species and found that the tunneling behavior can be steered by varying the interspecies interaction strength g_{AB} . In the following we unravel whether a similar controlled tunneling process can be realized employing two impurities. For this purpose, we consider two weakly interacting impurities, i.e. they interact repulsively via a contact potential of strength $g_{BB}/E_r k_0^{-1} = 0.2$, embedded in the same potential setup as shown in figure 1. The parameters for the majority species remain unchanged compared to the single impurity case, i.e. $N_A = 8$ and $g_{AA}/E_r k_0^{-1} = 1.0$. The tunneling process is induced by performing the same quench protocol as in the case of a single impurity. Due to tilting potential V_{tilt} the minority species is initially prepared in the left side of the double well V_B . Setting V_{tilt} suddenly to zero we monitor the respective tunneling dynamics.

Figures 10(a)–(d) present the one-body densities $\rho_B^{(1)}(x, t)$ of the two impurities for varying interspecies interaction strengths. As it can be seen, the dynamics of $\rho_B^{(1)}(x, t)$ for $N_B = 2$ resemble the one-body densities in the case of a single impurity (see figures 2(a)–(d)). For weak interspecies interaction strengths, i.e. $g_{AB}/E_r k_0^{-1} = 0.2$, we again observe a rather irregular tunneling dynamics of the impurity species (see figure 10(a)). Increasing g_{AB} , also for $N_B = 2$ the impurity species performs a material barrier tunneling within the initially populated well and finally tunnels to the other well (see figure 10(b)). A further increase of g_{AB} finally yields a self-trapping behavior of the impurity species due to the strong repulsion (see figure 10(d)). As a result also a system with two impurities exhibits the aforementioned four tunneling regimes. However, introducing an



additional impurity to the system leads to a shift of the tunneling regimes (see figures 10(b) and (c)) with respect to the interspecies interaction strength ($g_{AB}/E_r k_0^{-1} = 0.2, 0.8, 1.3, 4.0$). Therefore, we can conclude that also for two impurities we are able to control the quench induced tunneling process via the coupling to the majority species.

Having identified the existence of the four tunneling regimes of the impurity species the question that arises is whether the impurities tunnel pairwise through the potential landscape, which we would refer to as pair tunneling, or whether they tunnel individually, which we would call single particle tunneling. To expose the underlying mechanisms we present in figures 10(e)–(h) the conditional probability $P^{2,BB}(w_i^{(B)}, w_j^{(B)})$ of detecting one impurity in the Wannier state $w_i^{(B)}$ and the other impurity in the Wannier state $w_j^{(B)}$. Here, we will refer to $w_i^{(B)}$ as the generalized Wannier states associated with the TAEP which we introduced in section 4.1 (see also equation (6)). Figures 10(e) and (f) show the conditional probability $P^{2,BB}(w_i^{(B)}, w_i^{(B)})$ that the two impurities occupy the same Wannier state for interspecies interaction strengths $g_{AB}/E_r k_0^{-1} = 0.8$ (figure 10(e)) and $g_{AB}/E_r k_0^{-1} = 1.3$ (figure 10(f)). Thus, we focus on the two cases where a material barrier tunneling of the impurity species takes place or where the latter process is accompanied by a subsequent tunneling to the other site of the double well. In figure 10(e) we observe a decreasing probability $P^{2,BB}(w_i^{(B)}, w_i^{(B)})$ to find both impurities in the second Wannier state, whereas the probability to detect both impurities in the fourth Wannier state increases. This probability transfer indicates a pair tunneling from the left to the right side of the TAEP w.r.t. $x = 0$. Additionally, the impurities perform the material barrier tunneling as a pair, which can be inferred from the alternating increase and decrease of $P^{2,BB}(w_1^{(B)}, w_1^{(B)})$ and $P^{2,BB}(w_2^{(B)}, w_2^{(B)})$. A schematic representation of this process is illustrated in figure 10(i) assuming the TAEP at $g_{AB}/E_r k_0^{-1} = 0.8$. For the investigation of the single particle tunneling we show in figures 10(g) and (h) the conditional probability to find one impurity in the second Wannier state and the other impurity in another Wannier state for the above-mentioned g_{AB} . A decrease of the probability to find one impurity in the second and one impurity in the first Wannier state $P^{2,BB}(w_2^{(B)}, w_1^{(B)})$ is observed for times up to $t/\omega_r^{-1} = 100$ (figure 10(g)), while the conditional probability $P^{2,BB}(w_2^{(B)}, w_4^{(B)})$ increases. This suggests a tunneling of one impurity from the first well of the TAEP to the fourth well, whereas the other impurity remains in the second well. This process is depicted in figure 10(j).

We note that this is one of many single particle tunneling processes that can take place. In this sense, the tunneling process of the impurity species is rather complex, consisting of single particle and pair tunneling processes.

Concluding we have realized the four tunneling regimes which we previously identified in figures 2(a)–(d) also for two weakly interacting impurities coupled to a majority species. This implies that it is also possible to control the tunneling process of two impurities via the interspecies interaction strength. Eventually, we have characterized the tunneling processes underlying the dynamical response of the impurity species in terms of single particle and pair tunneling processes [55].

6. Conclusions and outlook

We have investigated the correlated tunneling dynamics of impurities trapped in a double well potential and immersed in a lattice trapped majority species. The tunneling dynamics was initiated by implementing an initial tilt of the double well, thereby localizing the impurity species in one of the wells, and quenching this to a symmetric potential configuration. In case of a single impurity we have identified four different tunneling regimes w.r.t. the interspecies interaction strength. For very weak interspecies interaction strengths the tunneling of the impurity can be characterized as rather complex, exhibiting no regular or repetitive structure. However, increasing the coupling to the majority species leads to a regular tunneling behavior of the impurity, which consists of an initial material barrier tunneling due to the presence of the majority species and is followed by a transfer of the impurity to the other site of the double well. Additionally, this effect is accompanied by a strong entanglement between the subsystems. A further increase of the interspecies interaction strength leads to a sole material barrier tunneling in the initial site of the double well for long time intervals and finally for very large couplings forces the impurity to localize in the initially populated well and being self-trapped.

In order to gain insight into the underlying microscopic processes of the emergent correlated tunneling dynamics, we have constructed a time-averaged effective potential (TAEP) based on the one-body density of the majority species. Depending on the interspecies interaction strength, this effective potential exhibits an additional structure in each site of the double well, thus explaining the material barrier tunneling. Increasing the coupling to the majority species, the TAEP is predominantly formed by the one-body density of the majority species and the presence of the double well is of minor consequence, resulting in the observed self-trapping of the impurity. Moreover, the generalized Wannier states associated with this potential allowed for a characterization of the impurity's dynamical response as well as the involved correlations. We concluded our study with an investigation of two weakly repulsively interacting impurities which we prepared analogously to the case of a single impurity. We were able to identify the previous four tunneling regimes for smaller interspecies interaction strengths, being shifted to $g_{AB}/E, k_0^{-1} = 0.2, 0.8, 1.3, 4.0$ respectively, compared to the scenario of a single impurity. Employing again the TAEP we have developed an understanding of the tunneling dynamics, which consists of a superposition of pair tunneling as well as single particle tunneling processes.

There are various interesting research directions that prove to be promising for future investigations relying on the findings of the current work. A direct extension involves the inclusion of spin degrees of freedom between the impurities. Here, the possible formation of an analog of a Cooper-pair in the course of the tunneling dynamics would be of immediate interest. Another straightforward direction would be to consider quench protocols which also include a variation of the interspecies interaction strengths. For example, one might think of a subsequent interaction quench after a transfer of the impurity in order to prevent tunneling to the initially populated site. Also, dynamically driving the corresponding parameters of the system might be useful for transferring the impurity species in a more controlled and systematic manner.

Acknowledgments

PS gratefully acknowledges funding by the Deutsche Forschungsgemeinschaft in the framework of the SFB 925 'Light induced dynamics and control of correlated quantum systems'. KK gratefully acknowledges a scholarship of the Studienstiftung des deutschen Volkes. SIM gratefully acknowledges financial support in the framework of the Lenz-Ising Award of the University of Hamburg.

FT and KK contributed equally to this work.

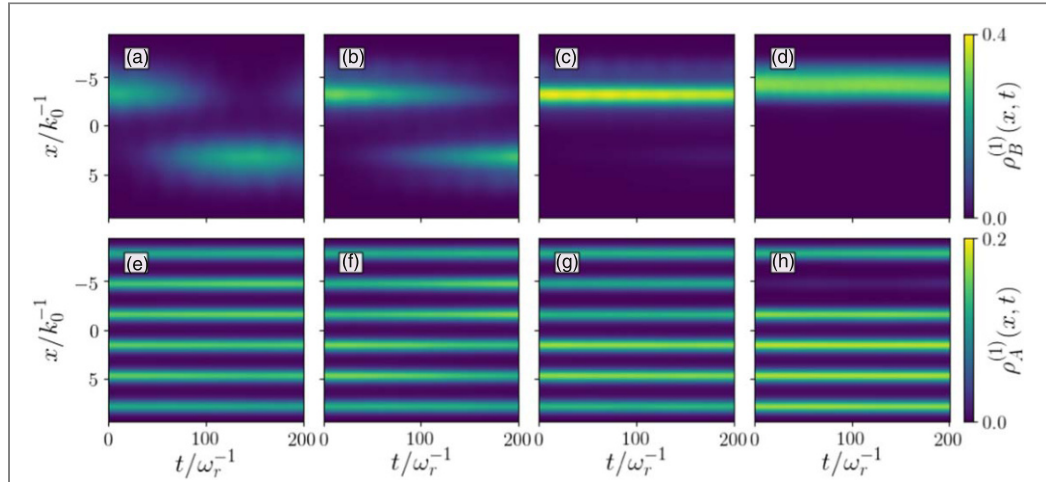


Figure 11. One-body density of (a)–(d) the impurity and (e)–(h) the majority species using a tilting strength $\alpha/E_R k_0^{-1} = 0.01$ within the full many-body approach. The results in each column correspond to the same interspecies interaction strength g_{AB} , ordered from left to right with $g_{AB}/E_r k_0^{-1} = 0.2, 1.0, 2.0, 4.0$. We consider a minority species consisting of $N_B = 1$ particle and a majority species with $N_A = 8$ particles which interact repulsively with $g_{AA}/E_r k_0^{-1} = 1.0$.

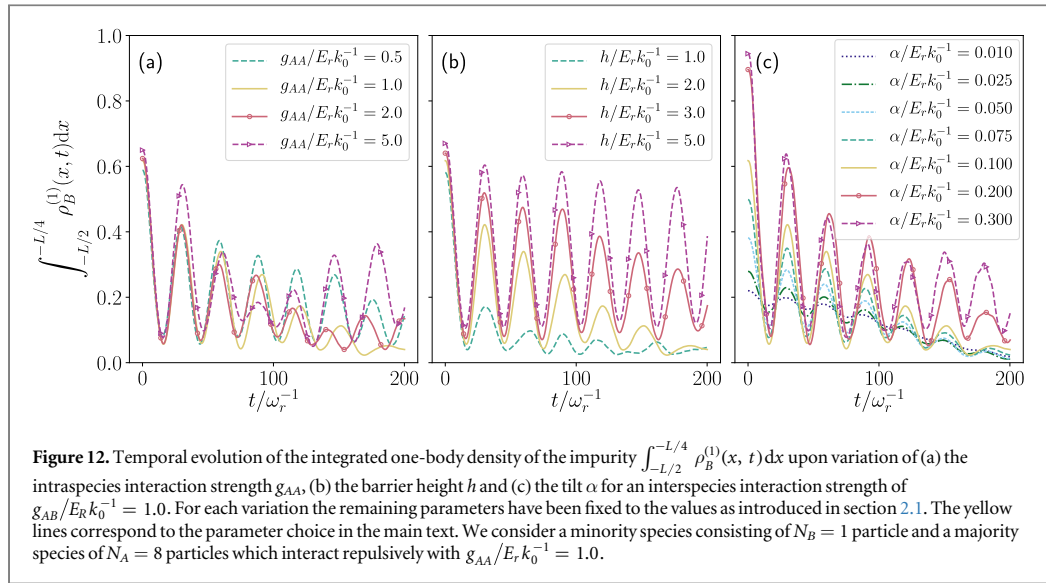
Appendix A. Tunneling dynamics for smaller tilting strength

In the following we demonstrate that a certain minimal tilting strength α is necessary for observing the tunneling dynamics as in figure 2 where we considered a single impurity and $\alpha/E_R k_0^{-1} = 0.1$. Figure 11 shows the temporal evolution of the one-body densities of the impurity (figures 11(a)–(d)) and the majority species (figures 11(e)–(h)) using a tilting strength $\alpha/E_R k_0^{-1} = 0.01$, within the full many-body approach. Analogously to the previous discussion in section 3, we induce the dynamics by initially tilting the double well V_B of the impurity with a tilting strength α and let the system evolve in time for $\alpha = 0$. However, in the present case lowering the initial tilting strength to $\alpha/E_R k_0^{-1} = 0.01$ leads to a smaller initial energy offset between the sites of V_B .

For weak g_{AB} , i.e. $g_{AB}/E_r k_0^{-1} = 0.2, 1.0$, we find a rather regular tunneling of the impurity from the left to the right side of the double V_B (see figures 11(a) and (b)). Comparing this with the dynamical response of an impurity for an initial tilting strength of $\alpha/E_R k_0^{-1} = 0.1$ (see figure 2(b)) we find no material barrier tunneling triggered by the density of the majority species. The difference between the two initial tilting strengths is also evident for larger interspecies interaction strengths, e.g. $g_{AB}/E_r k_0^{-1} = 2.0, 4.0$. Here, the impurity essentially remains localized throughout the dynamics and does not perform any oscillations (see figures 11(c) and (d)). Furthermore, the one-body density of the majority species behaves accordingly and does not exhibit a distinctive dynamics compared to the $\alpha/E_R k_0^{-1} = 0.1$. Namely, $\rho_A^{(1)}$ remains well localized at the sites of the lattice potential during the propagation (see figures 11(e)–(h)). These observations lead to the conclusion that indeed a sufficiently high initial tilting strength α is needed in order to observe a material barrier tunneling with a subsequent controlled transfer of the impurity to the other side of the double well.

Appendix B. Dependence of the tunneling process on the system parameters

We have analyzed the tunneling behavior of the impurity species for a specific choice of the intraspecies interaction strength g_{AA} of the majority species and the barrier height h . In figure 12 we show that the qualitative behavior of the tunneling dynamics discussed in the main text can be recovered for significantly varying g_{AA} and h . As a measure for the characteristic dynamical response of the impurity we again investigate the temporal evolution of the integrated one-body density of the impurity $\int_{-L/2}^{-L/4} \rho_B^{(1)}(x, t) dx$. The latter enables us to distinguish between the different tunneling regimes, for a fixed interspecies interaction strength of $g_{AB}/E_r k_0^{-1} = 1.0$. This value lies in regime II in figure 4(a), where we observe a material barrier tunneling within the initially populated well with a final transport of the impurity to the other site of the double well. In figure 12(a) we observe that an increase of g_{AA} leads to a faster revival of the material barrier tunneling in the initially populated well. Decreasing



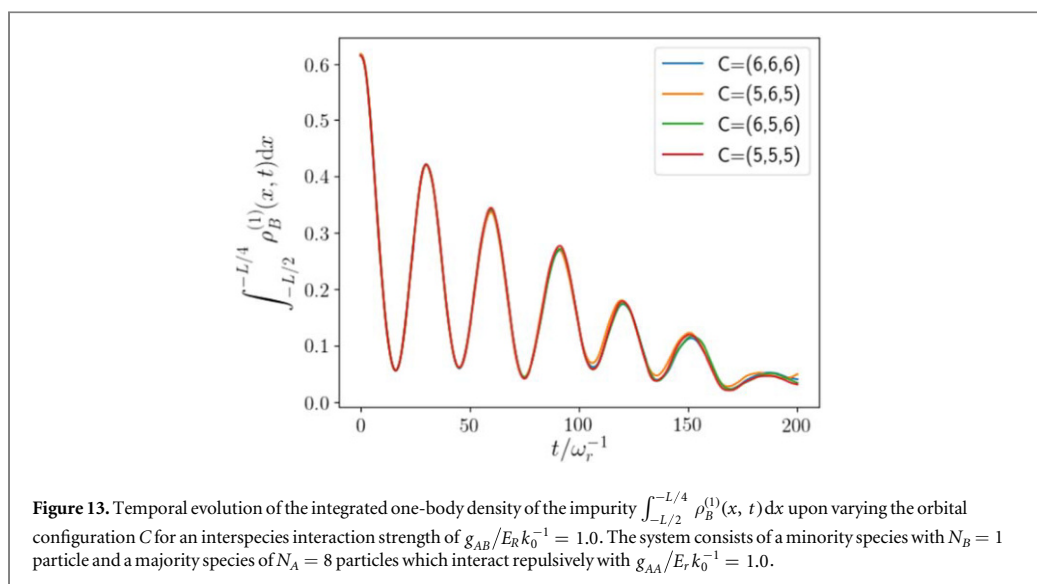
g_{AA} leads to a temporal prolongation of the material barrier tunneling and thereby a delayed transfer of the impurity to the other site of the double well.

A similar process can be observed when increasing the height of the double well barrier (see figure 12(b)). However, at a certain height of the barrier, e.g. $h/E_r k_0^{-1} = 5.0$, the impurity is barely able to tunnel to the other site of the double well within the considered time interval and solely performs the material barrier tunneling in the initial well. In contrast, a sufficiently small barrier height, e.g. $h/E_r k_0^{-1} = 1.0$, leads to a less dominant material barrier tunneling within the initial well since the impurity can be easily transferred to the other well.

Finally, we have investigated the dependence of the impurity's dynamical response on the initial tilt α (see figure 12(c)). For small tilts we find almost no oscillations in the initially populated well and the impurity is directly transferred to the other site of the double well (see also figure 11(b)). For increasing tilts α the oscillations due to the material barrier tunneling become more prominent and thereby the tunneling to the other well is delayed. In this sense, we find that the material barrier tunneling can be recovered for various parameters of the system.

Appendix C. Convergence of the many-body simulations

In the following we briefly discuss the convergence behavior of our results. As discussed in section 2 the size of the Hilbert space is given in terms of the orbital configuration $C = (M, d_A, d_B)$. Here, M describes the number of species functions in the Schmidt representation (see equation (2)), while d_σ with $\sigma \in \{A, B\}$ refer to the number of SPFs building the time dependent number states $|\vec{n}^\sigma(t)\rangle$ (see equation (3)). In the process of increasing the number of species functions and SPFs it is possible to recover the solution of the many-body wave function with an increasing accuracy. Due to the exponentially increasing size of the Hilbert space it is computationally prohibitive to use too many species and SPFs. However, we are able to obtain numerical solutions which incorporate all the necessary correlations and go beyond mean-field approximations utilizing ML-MCTDHX. We determine the effect of the truncation of the Hilbert space by investigating as a representative example the integrated one-body density of the impurity $\int_{-L/2}^{-L/4} \rho_B^{(1)}(x, t) dx$ upon varying the orbital configuration C . In figure 13 we show the latter for an interspecies interaction strength of $g_{AB}/E_r k_0^{-1} = 1.0$ (see figure 2(b)). Note that $g_{AB}/E_r k_0^{-1} = 1.0$ lies in the interval where the degree of correlations is maximized (see figure 5). As it can be seen, increasing the size of the Hilbert space systematically it is possible to achieve convergence. Based on these findings the orbital configuration $C = (6, 6, 6)$ has been employed in all many-body calculations presented in the main text.



ORCID iDs

Simeon I Mistakidis  <https://orcid.org/0000-0002-5118-5792>

Peter Schmelcher  <https://orcid.org/0000-0002-2637-0937>




References

- [1] Henderson K, Ryu C, MacCormick C and Boshier M G 2009 *New J. Phys.* **11** 043030
- [2] Gaunt A L, Schmidutz T F, Godlibovych I, Smith R P and Hadzibabic Z 2013 *Phys. Rev. Lett.* **110** 200406
- [3] Grimm R, Weidemüller M and Ovchinnikov Y B 2000 *Adv. At. Mol. Opt. Phys.* **42** 95
- [4] Olshani M 1998 *Phys. Rev. Lett.* **81** 938
- [5] Chin C, Grimm R, Julienne P and Tiesinga E 2010 *Rev. Mod. Phys.* **82** 1225
- [6] Pflanzner A C, Zöllner S and Schmelcher P 2009 *J. Phys. B: At. Mol. Opt. Phys.* **42** 231002
- [7] Pflanzner A C, Zöllner S and Schmelcher P 2010 *Phys. Rev. A* **81** 023612
- [8] García-March M A, Juliá-Díaz B, Astrakharchik G E, Boronat J and Polls A 2014 *Phys. Rev. A* **90** 063605
- [9] Alon O E, Streltsov A I and Cederbaum L S 2006 *Phys. Rev. Lett.* **97** 230403
- [10] Cazalilla M A and Ho A F 2003 *Phys. Rev. Lett.* **91** 150403
- [11] García-March M A and Busch Th 2013 *Phys. Rev. A* **87** 063633
- [12] Keiler K and Schmelcher P 2019 *Phys. Rev. A* **100** 043616
- [13] Pyzh M, Krönke S, Weitenberg C and Schmelcher P 2018 *New J. Phys.* **20** 015006
- [14] Zöllner S, Meyer H-D and Schmelcher P 2008 *Phys. Rev. A* **78** 013629
- [15] Mistakidis S I, Katsimiga G C, Kevrekidis P G and Schmelcher P 2018 *New J. Phys.* **20** 043052
- [16] Katsimiga G C, Koutentakis G M, Mistakidis S I, Kevrekidis P G and Schmelcher P 2017 *New J. Phys.* **19** 073004
- [17] Wille E et al 2008 *Phys. Rev. Lett.* **100** 053201
- [18] Köhl M, Moritz H, Stöferle T, Günter K and Esslinger T 2005 *Phys. Rev. Lett.* **94** 080403
- [19] Stan C, Zwierlein M, Schunck C, Raupach S and Ketterle W 2004 *Phys. Rev. Lett.* **93** 143001
- [20] Ospelkaus S, Ospelkaus C, Humbert L, Sengstock K and Bongs K 2006 *Phys. Rev. Lett.* **97** 120403
- [21] Giamarchi T 2004 *Quantum Physics in One Dimension* (Oxford: Oxford University Press)
- [22] Cazalilla M A, Citro R, Giamarchi T, Orignac E and Rigol M 2011 *Rev. Mod. Phys.* **83** 1405
- [23] Kinoshita T, Wenger T and Weiss D S 2005 *Phys. Rev. Lett.* **95** 190406
- [24] Haller E, Hart R, Mark M J, Danzl J G, Reichsöllner L, Gustavsson M, Dalmonde M, Pupillo G and Nägerl H-C 2010 *Nature* **466** 597
- [25] Kalas R M and Blume D 2006 *Phys. Rev. A* **73** 043608
- [26] Massignan P, Zaccanti M and Bruun G M 2014 *Rep. Prog. Phys.* **77** 034401
- [27] Grusdt F, Astrakharchik G E and Demler E A 2017 *New J. Phys.* **19** 103035
- [28] Volosniev A G and Hammer H-W 2017 *Phys. Rev. A* **96** 031601
- [29] Dehkharghani A S, Volosniev A G and Zinner N T 2015 *Phys. Rev. A* **92** 031601
- [30] García-March M A, Dehkharghani A S and Zinner N T 2016 *J. Phys. B: At. Mol. Opt. Phys.* **49** 075303
- [31] Cucchiatti F M and Timmermans E 2006 *Phys. Rev. Lett.* **96** 210401
- [32] Bruderer M, Klein A, Clark S R and Jaksch D 2007 *Phys. Rev. A* **76** 011605
- [33] Meinert F, Knap M, Kirilov E, Jag-Lauber K, Zvonarev M B, Demler E and Nägerl H-C 2017 *Science* **356** 948
- [34] Catani J, Lamporesi G, Naik D, Gring M, Inguscio M, Minardi F, Kantian A and Giamarchi T 2012 *Phys. Rev. A* **85** 023623
- [35] Fukuhara T et al 2013 *Nat. Phys.* **9** 235
- [36] Hu M, Van de Graaff M J, Kedar D, Corson J P, Cornell E A and Jin D S 2016 *Phys. Rev. Lett.* **117** 055301
- [37] Recati A, Fuchs J N, Peça C S and Zwerger W 2005 *Phys. Rev. A* **72** 023616
- [38] Klein A and Fleischhauer M 2005 *Phys. Rev. A* **71** 033605

- [39] Dehkharghani A S, Volosniev A G and Zinner N T 2018 *Phys. Rev. Lett.* **121** 080405
- [40] Chen J, Schurer J M and Schmelcher P 2018 *Phys. Rev. Lett.* **121** 043401
- [41] Keiler K, Krönke S and Schmelcher P 2018 *New J. Phys.* **20** 033030
- [42] Keiler K and Schmelcher P 2018 *New J. Phys.* **20** 103042
- [43] Bruderer M, Klein A, Clark S R and Jaksch D 2007 *New J. Phys.* **9** 411
- [44] Bruderer M, Klein A, Clark S R and Jaksch D 2008 *New J. Phys.* **10** 033015
- [45] Palzer S, Zipkes C, Sias C and Köhl M 2009 *Phys. Rev. Lett.* **103** 150601
- [46] Mistakidis S I, Grusdt F, Koutentakis G M and Schmelcher P 2019 *New J. Phys.* **21** 103026
- [47] Krönke S, Knörzer J and Schmelcher P 2015 *New J. Phys.* **17** 053001
- [48] Lampo A, Lim S H, Garcia-March M A and Lewenstein M 2017 *Quantum* **1** 30
- [49] Gamayun O, Lychkovskiy O, Burovski E, Malcomson M, Cheianov V V and Zvonarev M B 2018 *Phys. Rev. Lett.* **120** 220605
- [50] Lychkovskiy O 2014 *Phys. Rev. A* **89** 033619
- [51] Akram J and Pelster A 2016 *Phys. Rev. A* **93** 033610
- [52] Mistakidis S I, Hilbig L and Schmelcher P 2019 *Phys. Rev. A* **100** 023620
- [53] Mistakidis S I, Katsimiga G C, Koutentakis G M, Busch Th and Schmelcher P 2019 *Phys. Rev. Lett.* **122** 183001
- [54] Mistakidis S I, Volosniev A G, Zinner N T and Schmelcher P 2019 *Phys. Rev. A* **100** 013619
- [55] Erdmann J, Mistakidis S I and Schmelcher P 2019 *Phys. Rev. A* **99** 013605
- [56] Kamar N A, Kantian A and Giamarchi T 2019 *Phys. Rev. A* **100** 023614
- [57] Siegl P, Mistakidis S I and Schmelcher P 2018 *Phys. Rev. A* **97** 053626
- [58] Bloch I 2005 *Nature* **1** 23
- [59] Smerzi A, Fantoni S, Giovanazzi S and Shenoy S 1997 *Phys. Rev. Lett.* **79** 4950
- [60] Milburn G, Corney J, Wright E M and Walls D 1997 *Phys. Rev. A* **55** 4318
- [61] Raghavan S, Smerzi A, Fantoni S and Shenoy S 1999 *Phys. Rev. A* **59** 620
- [62] Sakmann K, Streltsov A I, Alon O E and Cederbaum L S 2010 *Phys. Rev. A* **82** 013620
- [63] Sakmann K, Streltsov A I, Alon O E and Cederbaum L S 2014 *Phys. Rev. A* **89** 023602
- [64] Chatterjee B, Brouzos I, Zöllner S and Schmelcher P 2010 *Phys. Rev. A* **82** 043619
- [65] Zöllner S, Meyer H-D and Schmelcher P 2008 *Phys. Rev. A* **78** 013621
- [66] Zöllner S, Meyer H-D and Schmelcher P 2008 *Phys. Rev. Lett.* **100** 040401
- [67] Kuang L-M and Ouyang Z-W 2000 *Phys. Rev. A* **61** 023604
- [68] Sun B and Pindzola M 2009 *Phys. Rev. A* **80** 033616
- [69] Naddeo A and Citro R 2010 *J. Phys. B: At. Mol. Opt. Phys.* **43** 135302
- [70] Satija I I, Balakrishnan R, Naudus P, Heward J, Edwards M and Clark C W 2009 *Phys. Rev. A* **79** 033616
- [71] Seaman B T, Krämer M, Anderson D Z and Holland M J 2007 *Phys. Rev. A* **75** 023615
- [72] Krönke S, Cao L, Vendrell O and Schmelcher P 2013 *New J. Phys.* **15** 063018
- [73] Cao L, Krönke S, Vendrell O and Schmelcher P 2013 *J. Chem. Phys.* **139** 134103
- [74] Cao L, Bolsinger V, Mistakidis S I, Koutentakis G, Krönke S, Schurer J M and Schmelcher P 2017 *J. Chem. Phys.* **147** 044106
- [75] LeBlanc L J and Thywissen J H 2007 *Phys. Rev. A* **75** 053612
- [76] Rubio-Abadal A, Choi J, Zeiher J, Hollerith S, Rui J, Bloch I and Gross C 2019 *Phys. Rev. X* **9** 041014
- [77] Inouye S, Andrews M R, Stenger J, Miesner H-J, Stamper-Kurn D M and Ketterle W 1998 *Nature* **392** 151
- [78] Timmermans E, Tommasini P, Hussein M and Kerman A 1999 *Phys. Rep.* **315** 315
- [79] Fedichev P O, Kagan Yu, Shlyapnikov G V and Walraven J T M 1996 *Phys. Rev. Lett.* **77** 2913
- [80] Theis M, Thalhammer G, Winkler K, Hellwig M, Ruff G, Grimm R and Hecker-Denschlag J 2004 *Phys. Rev. Lett.* **93** 123001
- [81] Horodecki R, Horodecki P, Horodecki M and Horodecki K 2009 *Rev. Mod. Phys.* **81** 865
- [82] Light J C, Hamilton I P and Lill J V 1985 *J. Chem. Phys.* **82** 1400
- [83] Dirac P A M 1930 *Proc. Camb. Phil. Soc.* **26** 376
- [84] Frenkel J 1934 *Wave Mechanics; Advanced General Theory* (Oxford: Clarendon)
- [85] Raab A 2000 *Chem. Phys. Lett.* **319** 674
- [86] Köhler F, Keiler K, Mistakidis S I, Meyer H-D and Schmelcher P 2019 *J. Chem. Phys.* **151** 054108
- [87] Mistakidis S I, Cao L and Schmelcher P 2014 *J. Phys. B: At. Mol. Opt. Phys.* **47** 225303
- [88] Mistakidis S I, Cao L and Schmelcher P 2015 *Phys. Rev. A* **91** 033611
- [89] Kivelson S and Schrieffer J R 1982 *Phys. Rev. B* **25** 6447
- [90] Kivelson S 1982 *Phys. Rev. B* **26** 4269
- [91] Kiehn H, Mistakidis S I, Katsimiga G C and Schmelcher P 2019 *Phys. Rev. A* **100** 023613

3.6 Many-body collisional dynamics of impurities injected into a double-well trapped Bose-Einstein condensate

Many-body collisional dynamics of impurities injected into a double-well trapped Bose-Einstein condensate

Friethjof Theel ¹, Kevin Keiler,¹ Simeon I. Mistakidis ¹, and Peter Schmelcher ^{1,2}

¹Center for Optical Quantum Technologies, University of Hamburg, Department of Physics,
Luruper Chaussee 149, D-22761, Hamburg, Germany

²The Hamburg Centre for Ultrafast Imaging, University of Hamburg, Luruper Chaussee 149, D-22761, Hamburg, Germany



(Received 28 September 2020; accepted 23 March 2021; published 23 April 2021)

We unravel the many-body dynamics of a harmonically trapped impurity colliding with a bosonic medium confined in a double well upon quenching the initially displaced harmonic trap to the center of the double well. We reveal that the emerging correlation dynamics crucially depends on the impurity-medium interaction strength allowing for a classification into different dynamical response regimes. For strong attractive impurity-medium couplings the impurity is bound to the bosonic bath, while for intermediate attractions it undergoes an effective tunneling. In the case of weak attractive or repulsive couplings the impurity penetrates the bosonic bath and performs a dissipative oscillatory motion. Further increasing the impurity-bath repulsion results in the pinning of the impurity between the density peaks of the bosonic medium, a phenomenon that is associated with a strong impurity-medium entanglement. For strong repulsions, the impurity is totally reflected by the bosonic medium. To unravel the underlying microscopic excitation processes accompanying the dynamics, we employ an effective potential picture. We extend our results to the case of two bosonic impurities and demonstrate the existence of a qualitatively similar impurity dynamics.

DOI: [10.1103/PhysRevResearch.3.023068](https://doi.org/10.1103/PhysRevResearch.3.023068)

I. INTRODUCTION

Due to their extraordinary controllability, ultracold atoms have been used to study various properties of many-body quantum systems. Indeed, they can be confined in arbitrary trapping geometries and dimensions [1–4], the underlying interatomic interactions are tunable via Feshbach resonances [5–9] while mixtures of quantum gases, namely, Bose-Bose [10,11], Bose-Fermi [12,13], and Fermi-Fermi ones [14–17] can be realized. Recently, major attention has been placed on strongly particle imbalanced mixtures where for instance a single impurity is immersed in a many-body environment. Here, the concept of a polaron [18], which has been exhaustively studied in solid-state physics, can be recovered where the impurity plays the role of an effective particle dressed by the excitations of its surroundings. In this context, the existence and characteristics of Fermi [19–23] and Bose polarons [24–31] have been unveiled, mainly focusing on their stationary properties [29,32–37] and more recently on the dynamics [38–41] of these quasiparticles.

The involved confining potentials have a major impact on the dynamical behavior of the impurity. For instance, it has been shown that the impurity-medium interaction quench dynamics in a harmonic trap leads to oscillatory [42], dipole-like, and dissipative impurity [43] motion depending on the

impurity-bath coupling strength or to temporal orthogonality catastrophe events for strong repulsions [28]. Another important aspect of such impurity settings concerns their transport properties through the environment [44]. Indeed, the tunneling dynamics of impurities confined in a double well and coupled to a lattice trapped medium has been studied in the context of an effective potential [45,46]. Additionally, dephasing and clustering processes [47,48] as well as distinct transport pathways [49] were observed for impurities confined in lattice potentials. Furthermore, the collisional dynamics of impurities with a Bose-Einstein condensate (BEC) has been studied experimentally [50,51] and theoretically [52]. In the latter case, the complete reflection of the impurities from a harmonically trapped BEC, their trapping within the bath, as well as the generation of dark and bright solitons have been revealed in the absence of correlations.

Apart from the above-described intriguing collisional channels, certainly a much richer dynamical response is expected to emerge in the presence of a lattice potential. Here, the periodic structure of the medium's density imprinted by the external potential acts as a material multibarrier which enforces specific tunneling pathways for the impurity. A minimal setup of this type consists of a bosonic bath trapped in a double-well potential, where complex dynamical response regimes of the impurity are anticipated. For instance, dephasing dynamics of the impurity associated with enhanced energy redistribution processes can be triggered [43,53] or in the case of attractive impurity-bath coupling strengths bound states can emerge. Moreover, the back-action of the impurity on the bosonic background where the former is expected to induce tunneling of the medium emulating a Josephson junction [54] is certainly of interest. Here, also the intraspecies coupling

Published by the American Physical Society under the terms of the Creative Commons Attribution 4.0 International license. Further distribution of this work must maintain attribution to the author(s) and the published article's title, journal citation, and DOI.

of the bath particles enforcing the latter to configure in a superfluid or Mott state, thus affecting their mobility, is expected to impact the impurity's response. In this context the interplay of the boson-boson interaction with the impurity-impurity induced correlations is also a relevant direction of study. Another interesting aspect is whether the emergent dynamical response regimes, found in the double-well case, remain robust in a setup where the bath is trapped in a multiwell potential. Additionally, due to the collision of the impurities with their environment strong impurity-medium correlations are expected to emerge, giving rise to beyond-mean-field collisional channels. To trace the nonequilibrium quantum dynamics, we employ the multilayer multiconfiguration time-dependent Hartree method for atomic mixtures (ML-MCTDHX) [55–57], which is capable of capturing all relevant interspecies and intraspecies correlations.

To address these aspects we consider a harmonically trapped impurity which is coupled via a contact interaction potential to a bosonic environment confined in a double well. The dynamics is induced by quenching the initially displaced harmonic confinement of the impurity to the center of the double well. By steering the impurity-medium interaction strength from attractive to strongly repulsive values we are able to identify five dynamical response regimes in the case of a single impurity [58]. These regimes range from a bound-state formation between the impurity and its environment for strong attractive impurity-bath interaction strengths to its dissipative oscillatory motion [43,59] within the bosonic background at weak attractive and repulsive couplings and, finally, its total reflection from the medium for strong repulsive interactions. For intermediate attractive or repulsive interaction strengths, the impurity effectively tunnels between the sites of the double-well potential or it is pinned between the later, respectively [45]. In all of the above-mentioned cases we reveal the buildup of a significant impurity-medium entanglement [28] which is mostly pronounced in the dissipative oscillation and the pinning regimes. To unravel the microscopic processes participating in the dynamics, we construct an effective potential [40,43,49,60]. This picture enables us to understand the dynamical behavior of the impurity in all response regimes and, in particular, uncover hidden excitations in the pinning regime. Extending our results to the two-impurity case we identify five qualitatively similar response regimes as compared to the single-impurity scenario. In this case we explicate the involvement of single- and two-particle excitation processes of the impurities within the effective potential [61] and also reveal the interplay of impurity-impurity induced correlations for different intraspecies interactions of the bath. To demonstrate the generalization of the identified dynamical response regimes of the impurity, we additionally consider a bosonic bath trapped in a triple well. In this context, we find that the steady bound state, the dissipative oscillation, and the total reflection regimes remain robust (see in particular Appendix E).

This work is structured as follows. In Sec. II we introduce the system under investigation and specify the used quench protocol. The employed variational method to trace the many-body dynamics is outlined in Sec. III. Section IV provides a detailed classification and analysis of the dynamical response regimes in dependence of the impurity-medium interaction

strength. We extend our results to two impurities in Sec. V and conclude this work in Sec. VI providing a summary and an outlook of possible future research directions. In the Appendices we further elaborate on the features of the identified dynamical response regimes discussing energy redistribution processes (Appendix A), the impurity-medium two-body correlation dynamics at strong attractions (Appendix B), the effective mass of the impurity (Appendix C), and the exposure of hidden excitations revealed for repulsive impurity-medium couplings (Appendix D). Appendix E demonstrates the collisional dynamics when considering a bosonic bath in a triple well.

II. SETUP AND QUENCH PROTOCOL

Our setup consists of two different species of bosons B and I , also referred to as the medium and impurity species, respectively. For the two species we consider N_B and N_I particles of mass m_B and m_I , respectively. We operate in the ultracold regime and thus s -wave scattering is the dominant process allowing us to model the interaction between the atoms with a contact interaction potential [62]. Therefore, we employ for the impurity-bath interaction a contact interaction potential of strength g_{BI} , while particles of the same species interact with a contact interaction potential among each other with strengths g_{BB} for the environment and g_{II} for the impurity species. Each species is confined in a different one-dimensional optical potential V_σ at zero temperature. This can be easily achieved experimentally [11,63–65] especially for the mass-imbalanced case under consideration of, i.e., ^{87}Rb atoms for the bath and ^{133}Cs atoms for the impurity species. The resulting Hamiltonian of the system reads as $\hat{\mathcal{H}} = \hat{\mathcal{H}}^B + \hat{\mathcal{H}}^I + \hat{\mathcal{H}}^{\text{int}}$ where

$$\hat{\mathcal{H}}^\sigma = \sum_{i=1}^{N_\sigma} \left(-\frac{\hbar^2}{2m_\sigma} \frac{\partial^2}{(\partial x_i^\sigma)^2} + V_\sigma(x_i^\sigma) + g_{\sigma\sigma} \sum_{i<j} \delta(x_i^\sigma - x_j^\sigma) \right) \quad (1)$$

is the Hamiltonian of species $\sigma \in \{B, I\}$. The bosonic medium and impurity species are coupled via $\hat{\mathcal{H}}^{\text{int}} = g_{BI} \sum_{i=1}^{N_B} \sum_{j=1}^{N_I} \delta(x_i^B - x_j^I)$. The impurities are confined in a harmonic oscillator potential $V_I(x_i^I) = m_I \omega_I^2 (x_i^I + x_0^I)^2 / 2$, where ω_I is the trapping frequency with x_0^I being the spatial displacement of the trap. The environment is trapped in a double well $V_B(x_i^B) = m_B \omega_B^2 (x_i^B)^2 / 2 + \frac{h_B}{\sqrt{2\pi} w_B} \exp(-\frac{(x_i^B)^2}{2(w_B)^2})$ which is constructed by superimposing a harmonic oscillator potential of frequency ω_B and a Gaussian of width w_B and height h_B [29]. We consider for the bosonic medium $N_B = 20$ ^{87}Rb atoms with mass $m_B = 1$, and for the impurity species $N_I = 1, 2$ ^{133}Cs atoms with mass $m_I = \frac{133}{87}$ [66].

Experimentally, a one-dimensional potential can be realized by employing a strong harmonic confinement along the transverse direction in order to freeze out the relevant degrees of freedom [62,67]. Subsequently, we provide the energy of the Hamiltonian $\hat{\mathcal{H}}$ in terms of $\tilde{E} = \hbar \tilde{\omega}$, where $\tilde{\omega}$ is the frequency of the perpendicular confinement. The length scales and timescales are then expressed in units of $\tilde{x} = \sqrt{\hbar / (m_B \tilde{\omega})}$ and $\tilde{\omega}^{-1} = \hbar \tilde{E}^{-1}$, respectively. Regarding the frequency of the harmonic oscillator potential of the impurities we use

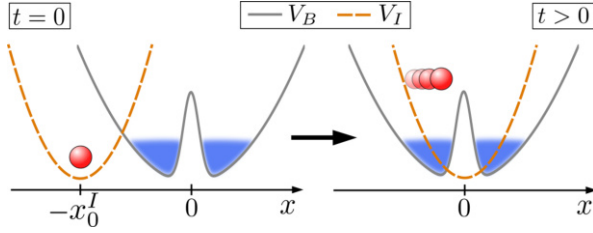


FIG. 1. Sketch of the setup under consideration at $t = 0$ (left panel). The harmonic trap of the impurity (red circle) is initially displaced by x_0^I with respect to the center of the double-well potential of the bosonic medium (blue shaded area). The dynamics is induced by quenching the potential of the impurity to $x_0^I = 0$ (right panel).

$\omega_I/\tilde{\omega} = 0.2$. For the harmonic contribution to the double-well potential we employ a frequency of $\omega_B/\tilde{\omega} = 0.15$ and for the Gaussian a width of $w_B/\tilde{x} = 0.8$ and a height of $h_B/\tilde{E}\tilde{x} = 2.0$ leading to a central barrier of the double well below which the six energetically lowest eigenstates of the corresponding one-body Hamiltonian are located.

We prepare the system in its ground state with the harmonic trap of the impurities displaced by x_0^I . The spatial overlap between the species in the noninteracting case is of about 3.5% for $x_0^I = 8$ and increases (decreases) for attractive (repulsive) impurity-medium interactions. After a g_{BI} -dependent ground state is found the dynamics is induced by quenching, at $t = 0$, the trap center of the impurity's harmonic potential to the center of the bosonic environment, i.e., setting $x_0^I = 0$ (see Fig. 1 for $t > 0$). Thereby, a collision of the initially displaced impurities with the bosonic medium is triggered, a process that strongly depends on the impurity-medium coupling strength g_{BI} as we shall demonstrate below.

III. MANY-BODY WAVE-FUNCTION ANSATZ

To calculate the quantum dynamical behavior of the binary system we employ the *ab initio* multilayer multiconfiguration time-dependent Hartree method for atomic mixtures (ML-MCTDHX) [55–57]. Within this approach we express the many-body wave function $|\Psi^{\text{MB}}(t)\rangle$ of the binary mixture using the Schmidt decomposition [68,69]

$$|\Psi^{\text{MB}}(t)\rangle = \sum_{i=1}^M \sqrt{\lambda_i(t)} |\Psi_i^B\rangle \otimes |\Psi_i^I\rangle. \quad (2)$$

For our purposes we expand each species in $M = 6$ species functions $|\Psi_i^\sigma\rangle$ with $\sigma \in \{B, I\}$. Moreover, the species functions are weighted with the time-dependent Schmidt coefficients λ_i which contain information about the entanglement between the two species. For instance, in the case of only one nonvanishing Schmidt coefficient the species are considered to be not entangled since the system can be described by a single product state (species mean-field ansatz) [69,70]. Next, each species function is expanded in a set of time-dependent number states $|\bar{n}_i^\sigma(t)\rangle$:

$$|\Psi_i^\sigma\rangle = \sum_{\bar{n}_i|N_\sigma} C_{i,\bar{n}}^\sigma(t) |\bar{n}_i^\sigma(t)\rangle, \quad (3)$$

with time-dependent coefficients $C_{i,\bar{n}}^\sigma$. Each number state $|\bar{n}_i^\sigma(t)\rangle$ determines the configurational occupation of N_σ particles on d_σ single-particle functions (SPFs) where, at the same time, the number of occupied SPFs must add up to the total particle number N_σ (indicated by $\bar{n}_i|N_\sigma$). In this work we employed $d_B = d_I = 6$ SPFs. Eventually, the single-particle functions are represented in a time-independent discrete variable representation (DVR) [71]. The propagation in time is performed by employing the Dirac-Frenkel variational principle [72,73] leading to a set of equations of motion for the system (see for more details [57,74]).

The advantage of this method is its underlying multilayering architecture of the total wave function combined with its time-dependent basis set [Eqs. (2) and (3)]. Especially, with the latter a comoving basis set is utilized leading to a significant reduction of required basis functions compared, e.g., to an exact diagonalization approach. On the other hand, the multilayering structure provides access to all relevant interspecies and intraspecies correlations of the system in an efficient manner.

IV. DYNAMICAL RESPONSE REGIMES OF A SINGLE IMPURITY

In the following we analyze the collisional dynamics of a single impurity ($N_I = 1$) trapped in a harmonic oscillator and interacting with a bosonic medium confined in a double well. Initially, the system is prepared in its ground state with the impurity's harmonic trap being spatially shifted by $x_0^I/\tilde{x} = 8$ with respect to the center of the double well. The dynamics is induced by quenching the harmonic oscillator of the impurity to $x_0^I/\tilde{x} = 0$. Varying the impurity-medium interaction strength g_{BI} from the strongly attractive to the strongly repulsive regime we discuss the emergent dynamical response of the impurity and its back-action to the environment. The intraspecies interaction strength between the medium particles is fixed to $g_{BB}/\tilde{E}\tilde{x} = 0.5$.

To reveal the overall dynamical response of the system, we initially inspect the one-body density $\rho_\sigma^{(1)}(x, t) = \langle \Psi^{\text{MB}}(t) | \hat{\Psi}_\sigma^\dagger(x) \hat{\Psi}_\sigma(x) | \Psi^{\text{MB}}(t) \rangle$ of species σ , where $\hat{\Psi}_\sigma(x)$ is the bosonic field operator of the corresponding species. The spectral decomposition of the one-body density [75,76] reads as

$$\rho_\sigma^{(1)}(x, t) = \sum_j n_j^\sigma(t) \Phi_{\sigma,j}^*(x, t) \Phi_{\sigma,j}(x, t), \quad (4)$$

where n_j^σ denote the natural populations and $\Phi_{\sigma,j}$ the natural orbitals of species σ .

Figure 2 presents the time evolution of $\rho_\sigma^{(1)}(x, t)$ for different impurity-medium interaction strengths g_{BI} ranging from strongly attractive to strongly repulsive values. In Figs. 2(a1) and 2(a2) we monitor the one-body density of the impurity $\rho_I^{(1)}(x, t)$ and the bosonic environment $\rho_B^{(1)}(x, t)$ in the course of the evolution for $g_{BI}/\tilde{E}\tilde{x} = -0.9$, namely, for strong attractive couplings. As a result of the quench, the impurity starts to oscillate with a small amplitude which decays during the time evolution. Thereby, the spatial maximum of $\rho_I^{(1)}(x, t)$ remains

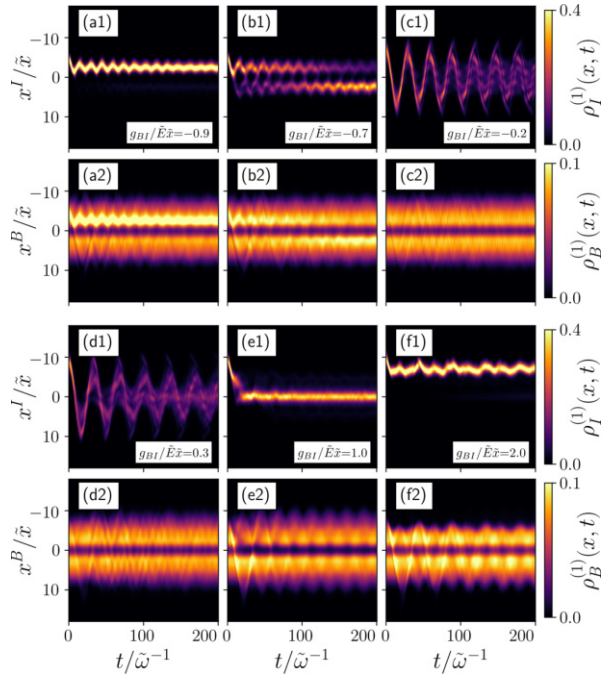


FIG. 2. Temporal evolution of the one-body density of (a1)–(f1) the impurity and (a2)–(f2) the bosonic medium. We induce the dynamics by quenching the initial displacement $x_0^I/\bar{x} = 8$ of the harmonic trap to $x_0^I = 0$. Different dynamical response regimes are realized by steering the impurity-medium interaction strength g_{BI} (see legends). The system consists of a $N_I = 1$ impurity and $N_B = 20$ bath particles with $g_{BB}/\bar{E}\bar{x} = 0.5$.

in the vicinity of the left site of the double-well potential.¹ Also, $\rho_B^{(1)}(x, t)$ exhibits a maximum at the same location [cf. Fig. 2(a2)], a phenomenon that is attributed to the strong impurity-bath attraction [77]. Due to this behavior, i.e., the enhanced spatial localization tendency of the impurity and the medium, and the fact that the impurity dominantly occupies a state with negative eigenenergy [see for details Fig. 5(a1)] we refer to this dynamical response regime as the *steady bound-state regime*. A similar dynamical response where the impurities localize at the maximum of the medium’s one-body density has also been observed in the case of a harmonically trapped bath [52].

For intermediate attractive impurity-medium interactions, $g_{BI}/\bar{E}\bar{x} = -0.7$, corresponding to the one-body densities shown in Figs. 2(b1) and 2(b2) the impurity does not localize exclusively on one site of the double well anymore as in the above discussed case. Rather, we observe a decay of $\rho_I^{(1)}(x, t)$ on the left site and a simultaneous increase at the right site of the double well. This response of the impurity is reminiscent of the tunneling dynamics of a single particle confined in a double well [78]. Later on, we will show that the effective potential encountered by the impurity resembles a double well

since it accounts for the effects of the attractive impurity-medium coupling [cf. Fig. 5(b1)]. In this sense we label this response regime as the (effective) *tunneling regime*. Note that the back-action of the impurity on the bosonic medium leads to a shift of the maximum of $\rho_B^{(1)}(x, t)$ following the impurity’s tunneling behavior. Interestingly, this effective tunneling behavior of the impurity at intermediate attractions resembles the dynamical response of an impurity trapped in a double well and repulsively coupled to a lattice-trapped bosonic bath [45].

The next response regime, which we will refer to as the *dissipative oscillation regime*, emerges at weakly attractive or repulsive impurity-medium interaction strengths, e.g., for $g_{BI}/\bar{E}\bar{x} = -0.2, 0.3$. Here, the impurity-medium coupling is sufficiently small such that the impurity is able to completely penetrate its environment. Consequently, the impurity initiates a tunneling of $\rho_B^{(1)}(x, t)$ from one site of the double well to the other which decays in the course of time. The resulting impurity dynamics turns out to be a decaying oscillatory motion with an initial amplitude as large as the spatial extent of $\rho_B^{(1)}(x, t)$ [cf. Figs. 2(c1), 2(c2) and 2(d1), 2(d2)]. We attribute this decay process to a continuous energy transfer from the impurity to the medium (see Appendix A for details). A more detailed analysis of this dissipative behavior estimating also the effective mass of the emergent quasi-particle can be found in Appendix C. Note that such a dissipative behavior of impurities is a generic feature caused by the buildup of impurity-medium correlations and has been reported, e.g., in [43,52,59].

In the case of intermediate repulsive impurity-bath couplings, e.g., $g_{BI}/\bar{E}\bar{x} = 1.0$, we observe a spatial localization tendency of the impurity at the trap center accompanied by vanishing oscillations [cf. Fig. 2(e1)]. Therefore, we refer to this response regime as the *pinning regime*. During the impurity’s localization process, an intrawell dynamics is induced on the bosonic background. Here, the central barrier of the double well is effectively enlarged due to the material barrier created by the impurity and leading to an oscillatory motion of the bath cloud in each site of the double well. Further increasing g_{BI} to strong impurity-medium interaction strengths, e.g., $g_{BI}/\bar{E}\bar{x} = 2.0$, the underlying repulsion between the impurity and the bath particles in the left site of the double well becomes sufficiently large such that the impurity is totally reflected [see Fig. 2(f1)]. In this sense, we shall address this behavior as the *total reflection regime*. Thereby, the bosonic environment experiences a population imbalance in the double-well potential [cf. Fig. 2(f2)] which is accompanied by the phase separation between the medium and the impurity, a well-known process occurring in the strongly repulsive case [28,52].

In conclusion, we have captured five different dynamical response regimes of the impurity depending on the impurity-medium interaction strength. Remarkably, by tuning the impurity-bath coupling g_{BI} it is possible to control the location of the impurity. Note that, in each of the above-described regimes, Josephson-type oscillations of the bath take place induced by the coupling to the impurity. Furthermore, in all response regimes, apart from the total reflection regime, the impurity exhibits a finite spatial overlap with the bath in the course of the evolution. Thus, it can be dressed by

¹We have checked that also for a longer evolution time $t/\bar{\omega}^{-1} = 1600$ the impurity remains localized at the left site of the double well.

the excitations of the latter, allowing in principle for quasi-particle, in particular Bose polaron, formation [28,79,80]. In the total reflection regime, the impurity phase separates from its environment after the first collision and, therefore, the polaron, even it is formed for very short evolution times, decays. Similar manifestations of a decaying polaron formation at strong repulsive impurity-medium couplings in the course of the evolution have been already reported in the literature, being referred to as temporal orthogonality catastrophe events [28,80,81].

In order to further classify the above-discussed response regimes, we invoke the mean position of the impurity $\langle \hat{x}^I(t) \rangle$ [see Fig. 3(a)] for different impurity-medium interactions corresponding to the aforementioned dynamical regimes. Evidently, $\langle \hat{x}^I(t) \rangle$ exhibits individual characteristics in each regime allowing for their clear distinction. For instance, in the case of weak impurity-bath couplings, e.g., $g_{BI}/\tilde{E}\tilde{x} = -0.2$, an oscillatory behavior of $\langle \hat{x}^I(t) \rangle$ takes place as expected from $\rho_i^{(1)}(x, t)$ [cf. Fig. 2(c1)]. Turning to the total reflection regime, e.g., for $g_{BI}/\tilde{E}\tilde{x} = 2.0$, $\langle \hat{x}^I(t) \rangle$ captures the irregular behavior of the impurity on the left edge of the double well, thus indicating its total reflection from the bosonic environment. The long-time evolution of $\langle \hat{x}^I(t) \rangle$ for $g_{BI}/\tilde{E}\tilde{x} = -0.2$ is illustrated in the inset of Fig. 3(a). As can be seen, the decreasing amplitude of $\langle \hat{x}^I(t) \rangle$ becomes evident which is caused by the continuous energy transfer from the impurity to the bosonic medium (see also Appendix A).

To provide the complete response phase diagram of the impurity we show the behavior of $\langle \hat{x}^I(t) \rangle$ in dependence of the impurity-medium interaction strength g_{BI} , thus capturing the dynamical crossover between the aforementioned regimes [see Fig. 3(b)]. For convenience, the five identified response regimes are labeled from I to V. Regime I corresponds to the steady bound-state formation, see the small amplitude oscillations of $\rho_i^{(1)}(x, t)$ in the vicinity of the left site of the double-well. In regime II we find the expected behavior of $\langle \hat{x}^I(t) \rangle$ represented by its low-frequency oscillations around the trap center as shown in Fig. 3(a). For weak impurity-medium interaction strengths, corresponding to regime III, the dissipative oscillatory motion of $\langle \hat{x}^I(t) \rangle$ occurs characterized by a relatively large amplitude of the underlying oscillations. Increasing g_{BI} to intermediate repulsive values we reach the pinning regime (cf. regime III) where the mean position saturates towards $x^I = 0$. For larger g_{BI} the impurity is not able to penetrate the bath anymore and it is totally reflected at the edge of the latter. This regime corresponds to the total reflection one and it is denoted by V in Fig. 3(b). Finally, we comment on the response regimes in which the mean position obtains values close to zero, viz., the pinning and the tunneling regime. Even though the impurity's mean position within these regimes is well distinguishable [see Fig. 3(a)] in a corresponding experiment a clear distinction might be challenging. To ensure a clear distinction between these regimes, one can use the experimentally accessible position variance $s = \langle \hat{x}^2 \rangle - \langle \hat{x} \rangle^2$ [82,83]. Since in the tunneling regime the impurity is distributed over the double well the respective variance is larger than the one in the pinning regime where the impurity is localized at the trap center (not shown here).

In order to expose the robustness of the impurity dynamics with respect to parametric variations, we present in

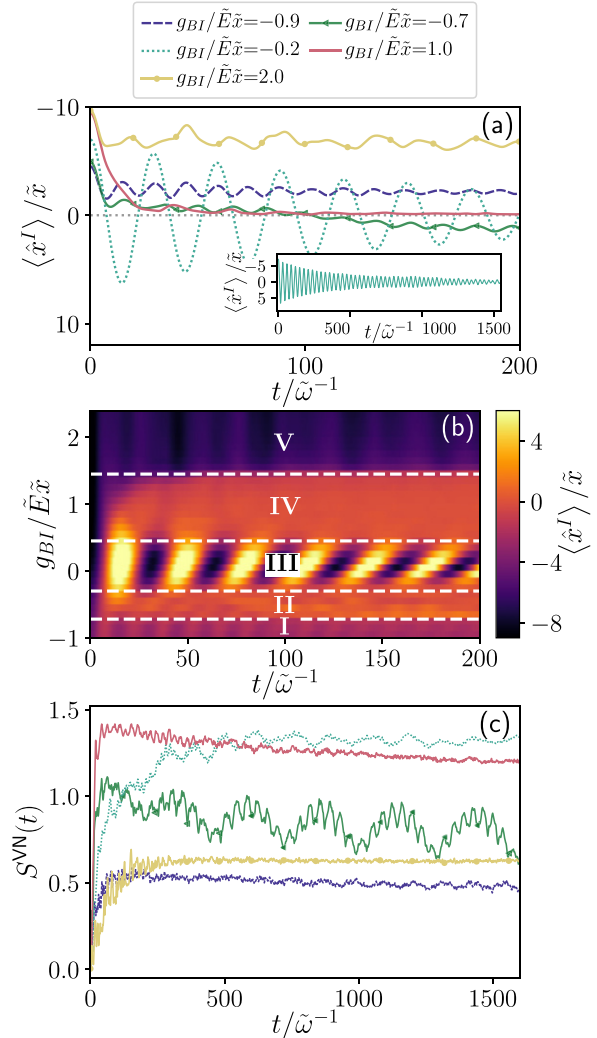


FIG. 3. (a) Time evolution of the mean position of the impurity for different impurity-medium interaction strengths g_{BI} (see legend). Each value of g_{BI} corresponds to one of the five dynamical response regimes of the impurity. The inset of (a) shows the long-time evolution of the mean position obtained for $g_{BI}/\tilde{E}\tilde{x} = -0.2$. (b) Temporal evolution of the mean position as a function of the impurity-medium interaction strength g_{BI} . (c) Long-time evolution of the von Neumann entropy $S^{VN}(t)$ obtained for the same g_{BI} as used in (a).

Fig. 4 $\langle \hat{x}^I(t) \rangle$ for a wide range of system parameters. As we emphasized previously, it is possible to distinguish between the dynamical response regimes by inspecting the behavior of $\langle \hat{x}^I(t) \rangle$. Therefore, we choose the impurity-bath coupling strength g_{BI} such that we obtain a behavior of $\langle \hat{x}^I(t) \rangle$ which can be in turn associated with a specific dynamical response regime. Figures 4(a) and 4(b) show $\langle \hat{x}^I(t) \rangle$ obtained for $x_0^I/\tilde{x} = 5$ and 10, respectively. Here, each mean position exhibits the same behavior as the corresponding one depicted in Fig. 3(a) for $x_0^I/\tilde{x} = 8$. As expected within the dissipative oscillation regime, an amplification of the oscillation amplitude occurs as the initial displacement increases. Based on these

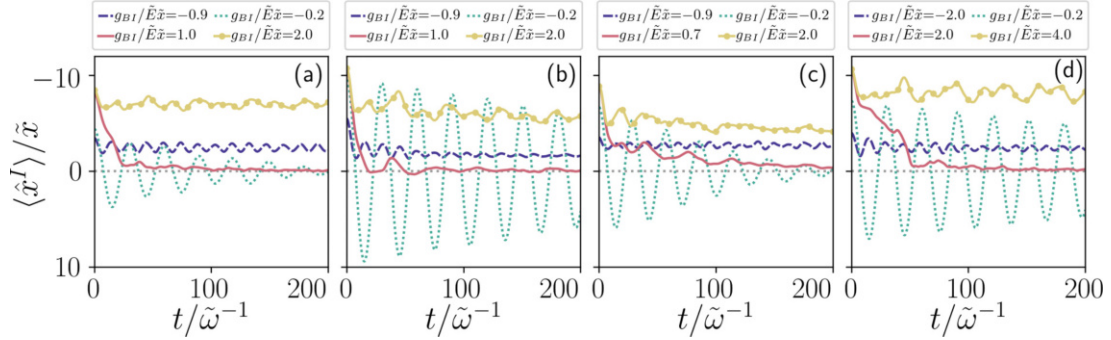


FIG. 4. Time evolution of the impurity's mean position for varying system parameters (see legends). (a) Corresponds to an initial displacement $x'_0/\tilde{x} = 5$ of the impurity's harmonic trap and (b) refers to $x'_0/\tilde{x} = 10$. In both cases $g_{BB}/\tilde{E}\tilde{x} = 0.5$. In (c) and (d) the intraspecies interaction strengths are set to $g_{BB}/\tilde{E}\tilde{x} = 0.2$ and 1.0 , respectively, for fixed $x'_0/\tilde{x} = 8$. The impurity-medium couplings g_{BI} are chosen such that the mean positions exhibit a behavior which can be attributed to the distinct dynamical response regimes.

observations we conclude that the impurity dynamics is robust with respect to the initial displacement and, more precisely, for values from $x'_0 = 5$ to 10 . We remark that in the limit of small displacements x'_0 and intermediate repulsive interaction strengths the ground state is altered, viz., the impurity is initially located between the two one-body density maxima of the bath where it remains in the course of the evolution.

Varying the intraspecies coupling strength g_{BB} between the bath particles we are again able to realize the respective dynamical response regimes but for shifted g_{BI} [see Figs. 4(c) and 4(d)]. For smaller intraspecies interaction strengths, e.g., $g_{BB}/\tilde{E}\tilde{x} = 0.2$, the dynamical regimes are shifted towards smaller absolute values of g_{BI} [cf. Fig. 4(c)] and vice versa in case of a larger g_{BB} , e.g., $g_{BB}/\tilde{E}\tilde{x} = 1.0$ [cf. Fig. 4(d)]. In particular, in order to realize the steady bound-state regime for a larger g_{BB} stronger impurity-medium attractions are necessary than in the case of a weakly interacting medium (small g_{BB}). We attribute this property to the mobility of the bath particles, i.e., the compressibility of the medium, which becomes smaller (larger) for increasing (decreasing) g_{BB} . Therefore, in the case of a strongly interacting bath, larger impurity-medium attractions are needed in order to shift a sufficient amount of the medium's one-body density to the left site of the double well which, eventually, binds the impurity [see also the mean positions corresponding to the steady bound-state regime in Figs. 4(c) and 4(d)]. On the other hand, for strongly repulsive impurity-medium interactions the total reflection regime emerges in the case of a weakly interacting bath at smaller g_{BI} compared to the case of a strongly interacting bath. We attribute this property to the g_{BB} dependence of the spatial extension of the medium's cloud. The latter is broadened for large g_{BB} and becomes narrower at the sites of the double well for small g_{BB} , leading in the latter case to an increased effective potential barrier experienced by the impurity [see also Eq. (6)]. Therefore, it is easier for the impurity to overcome the bosonic medium at the left site of the double well in the case of a larger g_{BB} , i.e., for a broadened background, than in the case of a smaller g_{BB} , e.g., compare the mean positions of $g_{BI}/\tilde{E}\tilde{x} = 2.0$ in Figs. 4(c) and 4(d).

Hence, the intraspecies interaction strength g_{BB} indeed impacts the impurity dynamics. However, the same dynamical regimes can be recaptured by properly adjusting g_{BI} at

least in the considered cases of relatively weak and strong intraspecies interaction strengths, i.e., $g_{BB}/\tilde{E}\tilde{x} = 0.2, 1.0$ considered herein. We remark that for even stronger repulsions where the medium resides in a Mott-type state an altered dynamical response of the impurity is expected, an investigation which is left for future studies.

Subsequently, we aim to quantify the associated impurity-medium entanglement by monitoring the von Neumann entropy [84], which reads as

$$S^{VN}(t) = - \sum_{i=1}^M \lambda_i(t) \ln \lambda_i(t). \quad (5)$$

This expression possesses an upper bound for maximal entanglement between the species, viz., $\lambda_i = 1/M$ leading to $S_{\max}^{VN} = \ln M = 1.79$ in our case ($M = 6$), and vanishes when no entanglement is present, e.g., $\lambda_i = 1$ with $\lambda_{i>1} = 0$. In Fig. 3(c) we provide the long-time evolution of the von Neumann entropy for different values of g_{BI} corresponding to the five dynamical response regimes of the impurity. We find in all regimes a finite impurity-medium entanglement [28,43] which tends to saturate for larger times ($t/\tilde{\omega}^{-1} > 1500$) besides the tunneling regime where $S^{VN}(t)$ performs an oscillatory motion. Among the investigated regimes, the steady bound state and the total reflection regime appearing at large attractive and repulsive g_{BI} couplings experience the smallest amount of entanglement. Indeed, $S^{VN}(t)$ is maximized within the pinning ($g_{BI}/\tilde{E}\tilde{x} = 1.0$) and the dissipative oscillation regime ($g_{BI}/\tilde{E}\tilde{x} = -0.2$). Additionally, in the latter response regime the entanglement increases with time and reaches a plateau at around $t/\tilde{\omega}^{-1} = 300$. During this time interval the impurity penetrates the bosonic medium 20 times, thereby enhancing the entanglement at each penetration. In the pinning regime, the system becomes maximally entangled after the impurity penetrates its environment a single time and, subsequently, becomes pinned between the effective barriers raised by the bosonic medium.

To obtain a better understanding of the underlying microscopic mechanisms appearing in the respective response regimes we analyze, in the following, the impurity dynamics with respect to an effective potential [40,43,45], which reads

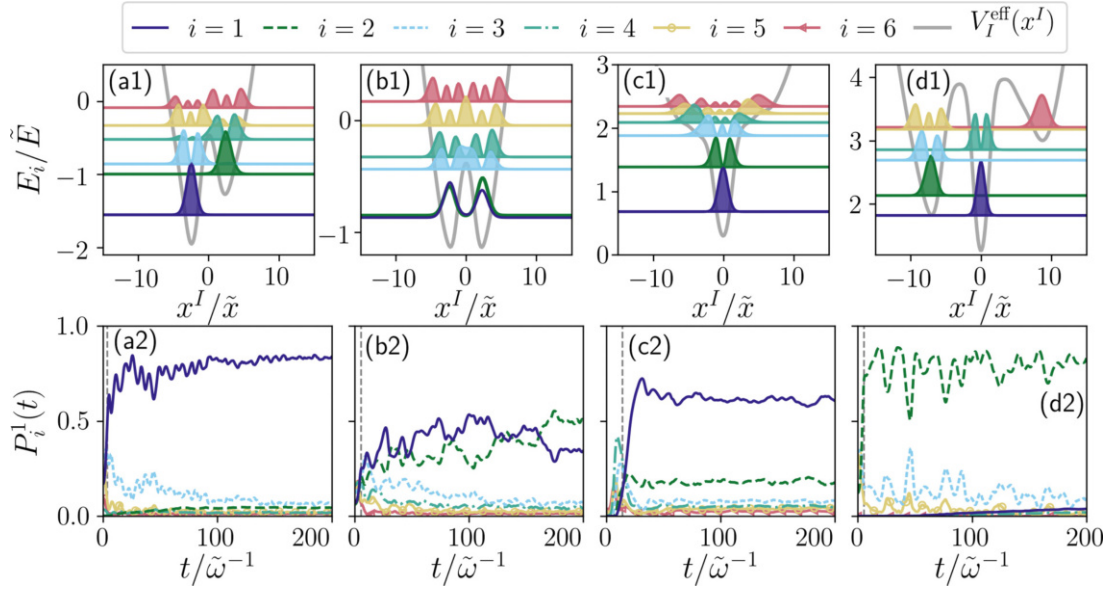


FIG. 5. (a1)–(d1) Time-averaged effective potential of the impurity $V_I^{\text{eff}}(x^I)$ (gray solid lines) together with the first six energetically lowest eigenfunctions (see legend) shifted by the respective eigenenergies obtained from the associated single-particle Hamiltonian $\hat{\mathcal{H}}^{(1)}$ (see text). (a2)–(d2) Time-dependent probabilities for the impurity to occupy one of the eigenfunctions shown in (a1)–(d1), respectively. Each column corresponds to a particular dynamical response regime (with a specific value of g_{BI}) which is sorted from left to right by $g_{BI}/\bar{E}\bar{x} = -0.9, -0.7, 1.0, 2.0$. $\sum_i P_i^1(t) > 0.94$ is fulfilled for times later than the threshold time depicted by the gray dashed lines.

as

$$V_I^{\text{eff}}(x^I) = \frac{1}{T} \int_0^T [N_B g_{BI} \rho_B^{(1)}(x^I, t) + V_I(x^I)] dt. \quad (6)$$

Here, we choose $x_0^I = 0$ for the harmonic confinement $V_I(x^I)$. This effective potential is based on the assumption of a product state ansatz $|\Psi^{\text{MB}}(t)\rangle = |\Psi^B(t)\rangle \otimes |\Psi^I(t)\rangle$ where the degrees of freedom of the bosonic medium are integrated out. Thus, the effective potential is the superposition of the harmonic confinement $V_I(x^I)$ after the quench and the one-body density of the environment weighted with the particle number N_B and the impurity-medium interaction strength g_{BI} [45]. Since the bosonic medium remains to a certain extent well localized at the sites of the double well in the course of the evolution the averaging of the effective potential over the total propagation time $T/\bar{\omega}^{-1} = 200$ is justified. Note that even though we considered a product state ansatz for the construction of $V_I^{\text{eff}}(x^I)$, beyond-mean-field effects are included in the one-body density $\rho_B^{(1)}(x, t)$ which is calculated with a many-body ansatz (see Sec. III).

The time-averaged effective potentials (gray solid lines) for four representative dynamical response regimes corresponding to $g_{BI}/\bar{E}\bar{x} = -0.9, -0.7, 1.0, 2.0$ are demonstrated in Figs. 5(a1)–5(d1). For the steady bound-state regime, at $g_{BI}/\bar{E}\bar{x} = -0.9$ the effective potential $V_I^{\text{eff}}(x^I)$ takes the form of an asymmetric double well [cf. Fig. 5(a1)] with a deeper left site since $\rho_B^{(1)}(x, t)$ is attracted to the impurity and, therefore, it is shifted to the left site of the double well. For intermediate attractions, e.g. $g_{BI}/\bar{E}\bar{x} = -0.7$, $V_I^{\text{eff}}(x^I)$ has the shape of a nearly symmetric double-well potential [see Fig. 5(b1)]. In this case, the symmetry can be ascribed to the fact that the averaging in Eq. (6) is performed over the period $T/\bar{\omega}^{-1} =$

200 during which the maximum of $\rho_B^{(1)}(x, t)$ shifts from one site of the double well to the other, leading on average to the observed nearly symmetric double well. This in turn explains the tunneling behavior of the impurity depicted in Fig. 2(b1).

This picture changes drastically for repulsive impurity-medium interactions. Here, the bosonic medium imprints a potential barrier with two maxima located at the two sites of its actual double well. Therefore, in this case, e.g., for $g_{BI}/\bar{E}\bar{x} = 1.0$, the effective potential $V_I^{\text{eff}}(x^I)$ obtains the shape of a deformed harmonic oscillator having an additional prominent dip at the trap center [Fig. 5(c1)]. As g_{BI} increases to $g_{BI}/\bar{E}\bar{x} = 2.0$, the aforementioned two density maxima of $\rho_B^{(1)}(x, t)$ become visible, giving rise to two potential barriers. Due to the superposition of the latter with the initially considered harmonic confinement $V_I(x^I)$, the effective potential of the impurity $V_I^{\text{eff}}(x^I)$ deforms to an asymmetric triple well [see Fig. 5(d1)].

As a next step, we construct for each $V_I^{\text{eff}}(x^I)$ the single-particle Hamiltonian $\hat{\mathcal{H}}^{(1)} = \frac{\hbar^2}{2m_I} \frac{\partial^2}{\partial x^2} + \hat{V}_I^{\text{eff}}$ and calculate its first six energetically lowest-lying eigenfunctions ψ_i^{eff} . The corresponding absolute squares of the eigenfunctions shifted by their eigenenergies are shown in Figs. 5(a1)–5(d1). In the following, these sets of eigenfunctions ψ_i^{eff} are taken as basis sets in order to analyze the underlying microscopic mechanisms in the course of the impurity dynamics. The time-dependent probability for the impurity to occupy the state ψ_i^{eff} reads as

$$P_i^1(t) = \sum_j |(\Psi^{\text{MB}}(t)|\varphi_j^B) \otimes |\psi_i^{\text{eff}})|^2, \quad (7)$$

where $\{\varphi_j^B\}$ is an arbitrary basis set covering the whole subspace of the bosonic medium. By summing over all basis states of the bath we single out the probability to find the impurity in ψ_i^{eff} . Note that $|\Psi^{\text{MB}}(t)\rangle$ is the full many-body wave function defined via ML-MCTDX [Eq. (2)], while ψ_i^{eff} serves as a basis set to unravel the underlying participating dynamical processes. The occupation probabilities for the respective basis sets [Figs. 5(a1)–5(d1)] are presented in Figs. 5(a2)–5(d2). In order to justify the quality of the basis, we sum up all nonvanishing occupation probabilities $P_i^1(t)$ and determine the time at which the sum exceeds and subsequently remains above 0.94 (dashed gray lines).

For $g_{BI}/\tilde{E}\tilde{x} = -0.9$ the impurity predominantly populates the energetically lowest eigenstate on the left site of the tilted effective double well $V_I^{\text{eff}}(x^I)$, while the probability to occupy energetically higher-lying states is strongly suppressed as time evolves [see Fig. 5(a2)]. Based on this behavior of $P_i^1(t)$, i.e., the spatial localization of the impurity, and the fact that the eigenenergies are negative we associate the bound-state formation with the energetically lowest eigenstate of the effective potential $V_I^{\text{eff}}(x^I)$ [43]. A further analysis of this steady bound state is provided in Appendix B in terms of the involved two-body density. For intermediate attractive impurity-medium couplings corresponding to the tunneling regime $V_I^{\text{eff}}(x^I)$ has, in contrast to the steady bound-state regime, the shape of a nearly symmetric double well. Accordingly, the impurity dynamics is mainly determined by the superposition of the two energetically lowest eigenstates of $V_I^{\text{eff}}(x^I)$ [see Fig. 5(b2)].

In the case of intermediate repulsive interactions, a pinning of the impurity between the density maxima of the bosonic bath is realized [cf. Fig. 5(c2) with $g_{BI}/\tilde{E}\tilde{x} = 1.0$]. Here, the occupation probabilities start to saturate after $t/\tilde{\omega}^{-1} = 50$ which in turn leads to the energetically lowest eigenstate of $V_I^{\text{eff}}(x^I)$ being predominantly populated. However, we observe that the probability to find the impurity in an energetically higher-lying eigenstate is approximately 40%. In this sense, the broadening of $\rho_I^{(1)}(x, t)$ around the trap center [see Fig. 2(e1)] can be interpreted as impurity excitations with respect to the effective potential. We refer to those excitations as *hidden excitations* since they can only be identified by such a microscopic analysis. It is worth noticing that the spatial structure of the first three species functions of the impurity $|\Psi_i^I\rangle$ are in a good agreement with the three energetically lowest eigenfunctions of $V_I^{\text{eff}}(x^I)$ (see Appendix D). For strong repulsive couplings, e.g., $g_{BI}/\tilde{E}\tilde{x} = 2.0$, the effective potential exhibits the shape of a triple well where the two potential barriers stem from the bosonic medium being localized at the sites of the double-well potential. Since these potential barriers are comparatively large, the impurity is totally reflected by the left barrier and predominantly occupies the eigenstates located in the left site of the triple well [see Fig. 5(d2)].

In summary, the analysis of the effective potential enables us to unravel the underlying microscopic mechanisms of the impurity dynamics. In particular, it allows for a deep understanding of the steady bound-state formation and proves to be crucial in order to identify the hidden excitations in the pinning regime. Note that for an analogous analysis of the dissipative oscillation regime, a much larger set of eigenfunctions has to be taken into account to achieve a comparable quality of the employed single-particle basis (similar to a coherent state

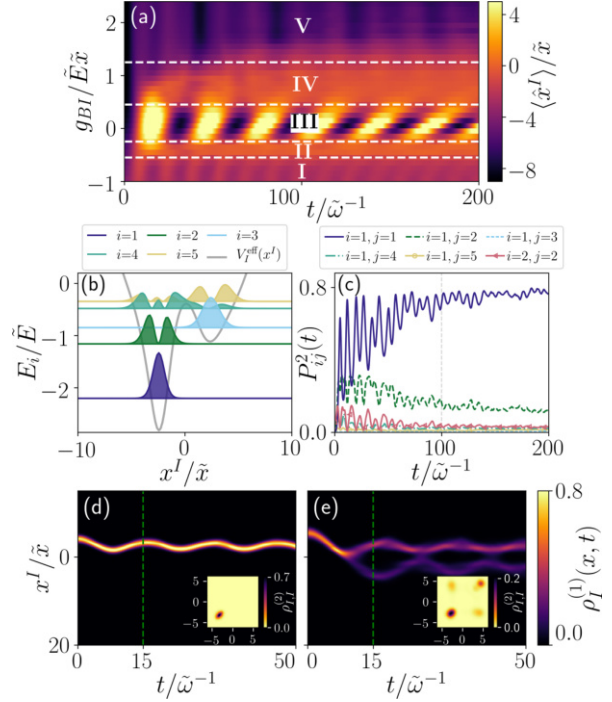


FIG. 6. (a) Temporal evolution of the two impurities’ mean position for various impurity-medium coupling strengths g_{BI} . (b) Time-averaged effective potential calculated for the two-impurity case for $g_{BI}/\tilde{E}\tilde{x} = -0.9$ [see Eq. (6)]. The associated eigenfunctions of the effective potential are shifted with respect to their eigenenergies E_i . (c) Time evolution of the conditional probability $P_{i,j}^2(t)$ to find one impurity in ψ_i^{eff} while at the same time the other impurity occupies the eigenstate ψ_j^{eff} . Panels (d) and (e) showcase the time evolution of the one-body densities $\rho_I^{(1)}(x, t)$ for $g_{BI}/\tilde{E}\tilde{x} = -1.0$ and $g_{BB}/\tilde{E}\tilde{x} = 0.5, 1.0$, respectively. Each inset illustrates a snapshot of the respective two-body density $\rho_{i,j}^{(2)}(x_1^I, x_2^I)$ at $t/\tilde{\omega}^{-1} = 15$ (green dashed line).

in a harmonic oscillator). In Appendix C we provide a discussion of the impurity dynamics in the dissipative oscillation regime where we compare the motion of its mean position to a damped harmonic oscillator.

V. DYNAMICAL RESPONSE REGIMES OF TWO IMPURITIES

To generalize our findings, in the following, we consider two noninteracting impurities ($g_{II} = 0$) coupled to the bosonic environment. Therefore, all interactions between the impurities are induced by their coupling to the bosonic medium [27,40,85]. The quench protocol is the same as described in Sec. II.

In order to characterize the dynamics of the two bosonic impurities, we monitor the time evolution of their mean position, i.e., their center-of-mass position, for different impurity-bath coupling strengths g_{BI} [Fig. 6(a)]. Analogously to the one-impurity case, we identify five dynamical response regimes depending on g_{BI} and appearing for similar

interaction strengths as for $N_I = 1$ [see also Fig. 3(b)]. However, we find in the response regime II [Fig. 6(a)] that the mean position is almost constant with $\langle x^I \rangle = 0$, whereas in the single-impurity case $\langle \hat{x}^I(t) \rangle$ oscillates with a small amplitude around zero. By inspecting the impurity's one-body density $\rho_I^{(1)}(x, t)$ for the corresponding regime II (not shown here) it is observed that $\rho_I^{(1)}(x, t)$ is almost equally distributed over the effective double-well potential (mediated by the bosonic bath) yielding a mean position close to zero. Moreover, the discrepancy between the tunneling and the pinning regime regarding the impurities' mean position can be revoked by inspecting the variance s analogously to the single-impurity case [see also Fig. 3(b)]. Additionally, we observe a broadening of the transition from the pinning to the total reflection regime for increasing g_{BI} with respect to the single-impurity case where we identified a sharper transition [see Fig. 6(a)]. As a case example we shall focus on the steady bound-state regime and unravel the microscopic processes in the case of two impurities.

To provide a qualitative understanding of the dynamics in the steady bound-state response regime we will describe the impurity dynamics within an effective potential picture, similarly to the previously discussed single-impurity case. For this purpose, we calculate the effective potential $V_I^{\text{eff}}(x^I)$ [see Eq. (6)] for $g_{BI}/\tilde{E}\tilde{x} = -0.9$ which we present in Fig. 6(b).² Additionally, we compute the effective single-particle eigenstates ψ_i^{eff} shifted by their eigenenergies E_i [see Fig. 6(b)]. A comparison with the effective potential in Fig. 5(a1) reveals that the left site of $V_I^{\text{eff}}(x^I)$ in the two-impurity case is much deeper. Therefore, the two energetically lowest eigenfunctions ψ_1^{eff} and ψ_2^{eff} in the two-impurity scenario are located at the left site of $V_I^{\text{eff}}(x^I)$.

Next, we unravel the interplay between the impurities by studying the conditional probabilities to occupy specific eigenstates of their effective potential. In particular, we define $P_{ij}^2(t)$ as the probability for one impurity to occupy the effective eigenstate ψ_i^{eff} while at the same time the other impurity populates the eigenstate ψ_j^{eff} .

In Fig. 6(c) we demonstrate $P_{ij}^2(t)$ with respect to the five energetically lowest-lying eigenstates of the effective potential for $g_{BI}/\tilde{E}\tilde{x} = -0.9$ [cf. Fig. 6(b)].³ Interestingly, we can infer that the two impurities predominantly occupy simultaneously the same energetically lowest eigenstate, which is in accordance with the observations made in the single-impurity case [Fig. 5(a2)]. However, also single-particle excitations in the second eigenstate ψ_2^{eff} [$P_{12}^2(t)$] as well as two-particle excitations contribute to the many-body wave function of the impurities [45,49]. For instance, we find a small but nonvanishing probability for observing two impurities in the second eigenstate $P_{22}^2(t)$. Notice that an analogous analysis for the other response regimes, apart from the dissipative oscillation one, leads to similar observations where one or two impurities

occupy simultaneously the same or different excited eigenstates of $V_I^{\text{eff}}(x^I)$ (not shown here).

In the following, we demonstrate that the dynamical response of two impurities can be tuned by changing the intraspecies interactions g_{BB} of the bath, similarly to the single-impurity case (cf. Sec. IV). As a characteristic example, we present in Figs. 6(d) and 6(e) the time evolution of the impurities' one-body densities for strong impurity-medium attractions and two different intraspecies couplings g_{BB} . In the case of a weakly interacting bath [cf. Fig. 6(d)] the major portion of the medium's one-body density is shifted to the left site of the double well (not shown here) such that the impurities are permanently bound to the medium at this site. Therefore, this situation corresponds to the steady bound-state regime [cf. regime I in Fig. 6(a)]. By increasing the intraspecies interaction strength, the compressibility of the bath is reduced and, thus, also the amount of the medium's one-body density accumulated at the left double-well site. In this sense, the impurities cannot be permanently bound at one site of the double well and distribute over the latter performing an effective tunneling dynamics.⁴ In particular, the corresponding one-body density $\rho_I^{(1)}(x, t)$ splits into two branches with each one oscillating at an individual site of the double well [see Fig. 6(e)]. Thereby, this dynamical response of the impurities resembles the dynamics corresponding to regime II in Fig. 6(a) in the case of a weakly interacting medium.

To further shed light on the spatial configuration of the two impurities, we investigate their reduced two-body density $\rho_{I,I}^{(2)}(x_1^I, x_2^I)$, defined as

$$\rho_{I,I}^{(2)}(x_1^I, x_2^I) = \int dx_1^B \dots dx_{N_B}^B |\Psi^{\text{MB}}(x_1^I, x_2^I, x_2^B, \dots, x_{N_B}^B)|^2. \quad (8)$$

In the inset of Fig. 6(d) the reduced two-body density of the impurities is provided for a weakly interacting bath at a specific time instant $t/\tilde{\omega}^{-1} = 15$. It exhibits an elongated peak along the diagonal which is, in particular, located at the left double-well site. This behavior indicates nonvanishing impurity-impurity induced correlations [40]. On the other hand, for a strongly interacting medium and at $t/\tilde{\omega}^{-1} = 15$ (corresponding to the time instance where the one-body density features the splitting) the two-body density reveals two dominant maxima in the diagonal and in terms of the amplitude two smaller ones in the off diagonal [see inset of Fig. 6(e)]. Thereby, the diagonal peaks of $\rho_{I,I}^{(2)}(x_1^I, x_2^I)$ explicate that both impurities move together and reside in either of the double-well sites. Complementarily, the smaller off-diagonal peaks hint at a suppressed probability of finding each impurity at a different site. Thus, a scenario in which one impurity remains at one double-well

²Note that Eq. (6) can be also employed in the case of two impurities.

³The sum of the presented probabilities exceeds 0.94 at $t/\tilde{\omega}^{-1} \approx 100$ (dashed gray line).

⁴In order to realize the dynamics corresponding to the steady bound-state regime occurring for large g_{BB} , the impurity-medium attraction needs to be adjusted accordingly. For instance, we have verified for $g_{BB}/\tilde{E}\tilde{x} = 1.0$ and $g_{BI}/\tilde{E}\tilde{x} = -2.0$ the formation of a steady bound-state response.

site while the other impurity tunnels to the other one is less probable.

In summary, we have deduced that the dynamical response regimes of two noninteracting impurities are similar to the single-impurity case with a small modification regarding the effective tunneling regime. Furthermore, we can gain insights into the time-dependent microscopic configuration of the two impurities by investigating the associated conditional probability to find the impurities in two particular eigenstates of their effective potential. Particularly, we exemplified that for the steady bound-state regime the impurities predominantly occupy simultaneously the lowest-lying eigenstate of $V_I^{\text{eff}}(x^I)$. However, we also observed the occurrence of single- and two-particle excitations in higher-lying eigenstates. Additionally, for strong impurity-medium attractions we varied the compressibility of the bath by considering a weakly and a strongly interacting medium. Thereby, we observed an alteration of the dynamical response of the impurities from a steady bound state (for small g_{BB}) to a distribution of the impurities over the double well (for large g_{BB}). The respective two-body density distributions revealed that in the latter case the impurities tend to move together manifesting the dominant presence of attractive induced interactions during the effective tunneling dynamics of the impurities.

VI. SUMMARY AND OUTLOOK

We have investigated the dynamical behavior of bosonic impurities colliding with a BEC trapped in a double well. The impurities are initially confined in a harmonic oscillator which is spatially displaced with respect to the double well of the bosonic medium. Upon quenching the harmonic potential to the trap center of the double well the quantum dynamics is induced such that the impurities collide with the bosonic environment. The correlated nonequilibrium dynamics is tracked with the variational ML-MCTDHX method which enables us to access the full many-body wave function of the system, thereby, including all relevant interspecies and intraspecies correlations.

By varying the impurity-medium interaction strength g_{BI} from strongly attractive to repulsive values, we are able to control the collisional dynamics of the impurity and identify five distinct dynamical response regimes by inspecting the associated one-body density evolution. These response regimes correspond to the *steady bound-state regime*, the *tunneling regime*, the *dissipative oscillation motion*, the *pinning regime*, and the *total reflection regime*. We demonstrate that they can be easily identified by monitoring the mean position of the impurity. Moreover, by calculating a crossover phase diagram of the impurity's mean position with respect to the impurity-medium coupling strength we obtain an overview of the emergent dynamical response regimes as a function of g_{BI} and identify smooth transitions between two consecutive ones. Additionally, we explicate the robustness of the response regimes for different parametric system variations, i.e., the intraspecies interaction strength of the bath and the initial displacement of the impurity's harmonic trap.

To provide a better understanding of the involved microscopic mechanisms, we employ a time-averaged effective

potential picture. By projecting the total many-body wave function onto the eigenstates associated with this effective potential allows us to gain insights into the underlying excitation processes for different interactions. In particular, we find that the impurity is bound to the bosonic medium for strong attractive impurity-bath interaction strengths corresponding to the steady bound-state regime and unveil hidden excitations in the pinning regime occurring for intermediate repulsive g_{BI} . We extend our study to the two-impurity case where we showcase the emergence of similar dynamical response regimes as in the single-impurity scenario. Furthermore, we unravel the underlying microscopic mechanisms of the impurities' dynamics analogously to the single-impurity case. Here, for the steady bound-state regime the participation of single- as well as two-particle excitations into energetically higher-lying states of the effective potential is demonstrated. Additionally, for strong impurity-medium attractions we show that the dynamical response of the impurities can be altered from a steady bound state (for a weakly interacting medium) to a configuration where the impurities distribute over the double well (for a strongly interacting medium).

The results of this work are beneficial for future ultracold-atom experiments of impurity-medium scattering for investigating the corresponding collisional channels caused exclusively by presence of the impurity-bath entanglement. Furthermore, this setup can be extended by implementing an additional spin degree of freedom for two noninteracting or weakly interacting impurities. In this case it would be interesting to identify the individual spin configurations and related spin-mixing processes in dependence of the impurity-medium coupling and whether the impurities evolve as a "Cooper pair." Certainly, the generalization of our results to higher dimensions is an intriguing perspective.

ACKNOWLEDGMENTS

K.K. gratefully acknowledges a scholarship of the Studienstiftung des deutschen Volkes. S.I.M. gratefully acknowledges financial support in the framework of the Lenz-Ising Award of the University of Hamburg. This work has been funded by the Deutsche Forschungsgemeinschaft (DFG, German Research Foundation), Grant No. SFB-925, project 170620586.

APPENDIX A: IMPURITY-MEDIUM ENERGY TRANSFER PROCESSES

Due to the initial quench of the harmonic oscillator potential, the impurities collide with their bosonic background and, thereby, a transfer of energy to the latter is triggered [28,58,80]. The total energy of the system can be written as $E_{\text{tot}} = E_{\text{tot}}^B + E_{\text{tot}}^I + E_{\text{int}}$ where $E_{\text{tot}}^\sigma = \langle \Psi^{\text{MB}} | \hat{\mathcal{H}}^\sigma | \Psi^{\text{MB}} \rangle$ represents the total energy of species $\sigma \in \{B, I\}$ and $E_{\text{int}} = \langle \Psi^{\text{MB}} | \hat{\mathcal{H}}^{\text{int}} | \Psi^{\text{MB}} \rangle$ the interaction energy between the species.

In order to capture the quench-induced impurity-medium energy transfer, we present in Fig. 7 the relative energy of species σ defined as $E_{\text{rel}}^\sigma(t) = E_{\text{tot}}^\sigma(t) - E_{\text{tot}}^\sigma(0)$. In each dynamical response regime we observe an energy transfer from the impurity to its environment. The smallest energy transfer occurs for attractive impurity-medium interaction strengths where, due to the attraction to the bath, the impurity resides

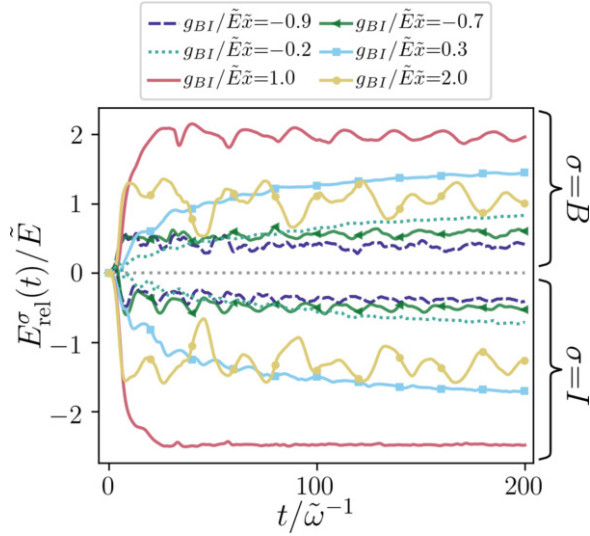


FIG. 7. Time evolution of the relative energy $E_{\text{rel}}^\sigma(t) = E_{\text{tot}}^\sigma(t) - E_{\text{tot}}^\sigma(0)$ of species $\sigma \in \{B, I\}$ for different g_{BI} (see legend). In each dynamical response regime the impurity transfers energy to the bosonic medium.

closer to the trap center, leading to a smaller initial total energy $E_{\text{tot}}^I(0)$ than in the case of repulsive g_{BI} [compare with the mean position in Fig. 3(a)].

For weak impurity-bath coupling strengths of either sign, i.e., $g_{BI}/\tilde{E}\tilde{x} = -0.2, 0.3$, the impurity continuously transmits energy to its environment until the relative energy of both species eventually saturates for longer times [58,80]. This loss of impurity energy essentially causes its dissipative oscillatory behavior [cf. Fig. 3(a)]. The largest energy transfer takes place in the pinning regime. Here, the impurity overcomes the bosonic medium in the left site of the double well only once and, thereby, transfers a large amount of energy to the bosonic medium such that the impurity becomes pinned within the latter.

APPENDIX B: TWO-BODY CORRELATION IN THE STEADY BOUND-STATE REGIME

To elucidate the interplay between the bosonic medium and the impurity in the steady bound-state regime in more detail, we perform an analysis of the impurity-medium reduced two-body density $\rho_{B,I}^{(2)}(x^I, x^B; t)$, defined as

$$\begin{aligned} \rho_{B,I}^{(2)}(x^I, x^B; t) \\ = \int dx_2^B \dots dx_{N_B}^B |\Psi^{\text{MB}}(x^I, x^B, x_2^B, \dots, x_{N_B}^B; t)|^2. \end{aligned} \quad (\text{B1})$$

This quantity provides information about the probability of finding the impurity at position x^I and one particle of the bosonic background located at x^B .

A snapshot of the one-body density $\rho_\sigma^{(1)}(x^\sigma)$ with $\sigma \in \{B, I\}$ and the two-body density $\rho_{B,I}^{(2)}(x^I, x^B)$, respectively, at $t/\tilde{\omega}^{-1} = 150$ and for $g_{BI}/\tilde{E}\tilde{x} = -0.9$ is depicted in Figs. 8(b) and 8(c). Here, we find the impurity to be localized at the left

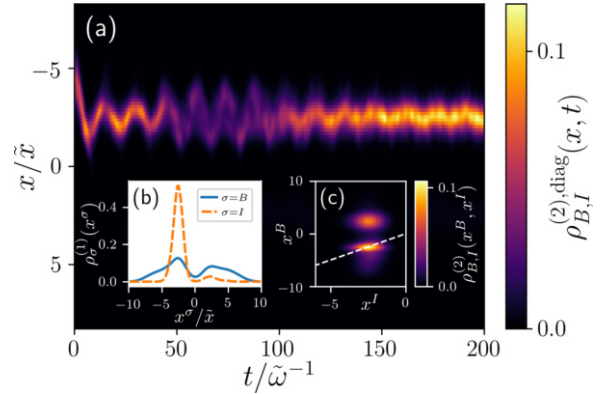


FIG. 8. (a) Time evolution of the diagonal elements of the two-body density $\rho_{B,I}^{(2),\text{diag}}(x, t)$ for $g_{BI}/\tilde{E}\tilde{x} = -0.9$ corresponding to the steady bound-state regime. (b), (c) Snapshot of the one-body density matrix $\rho_\sigma^{(1)}(x^\sigma)$ with $\sigma \in \{B, I\}$ and the two-body density $\rho_{B,I}^{(2)}(x^I, x^B)$, respectively, at $t/\tilde{\omega}^{-1} = 150$.

maximum of the bosonic medium corresponding to the left site of the double well which agrees with the observations made for the single-impurity case in Figs. 5(a1) and 5(a2). Furthermore, the two-body density indicates that the probability to find one particle of the bath at the left site of the double well, i.e., close to the impurity, is enhanced compared to the respective probability for the right site. In particular, the diagonal of $\rho_{B,I}^{(2)}(x^I, x^B)$ [dashed white line in Fig. 8(c)] represents the probability to capture the impurity and one particle of the environment at the same position which we will refer to as $\rho_{B,I}^{(2),\text{diag}}(x, t)$. Figure 8(a) shows the time evolution of $\rho_{B,I}^{(2),\text{diag}}(x, t)$ which strongly resembles the one-body density of the impurity for $t/\tilde{\omega}^{-1} > 100$ [cf. Fig. 2(a1)] and designates a high probability for the impurity and one particle of the bosonic medium to be at the same location [40,43].

APPENDIX C: DISSIPATIVE OSCILLATION RESPONSE REGIME: EFFECTIVE MASS AND DAMPING OF THE BOSE POLARON

Let us also analyze the dissipative oscillation regime in the case of a single impurity in more detail. As observed in Fig. 3(a), the mean position of the impurity for weak impurity-medium couplings exhibits a damped oscillatory behavior. Therefore, in the following we compare the analytical solution of a damped harmonic oscillator with the mean position $\langle \hat{x}^I(t) \rangle$ and mean momentum $\langle \hat{p}^I(t) \rangle$ obtained within the ML-MCTDH method (see Sec. III). The equation of motion of a particle subjected to a damped harmonic oscillator [86] reads as

$$\ddot{x} + \frac{\gamma^{\text{eff}}}{m^{\text{eff}}}\dot{x} + (\omega^{\text{eff}})^2 x = 0, \quad (\text{C1})$$

where γ^{eff} denotes the effective damping constant, ω^{eff} the effective trapping frequency, and m^{eff} refers to the effective mass of the impurity. Here, we interpret the impurity as a quasiparticle, namely, a Bose polaron, which is dressed by the excitations of its surroundings and moves in an effective

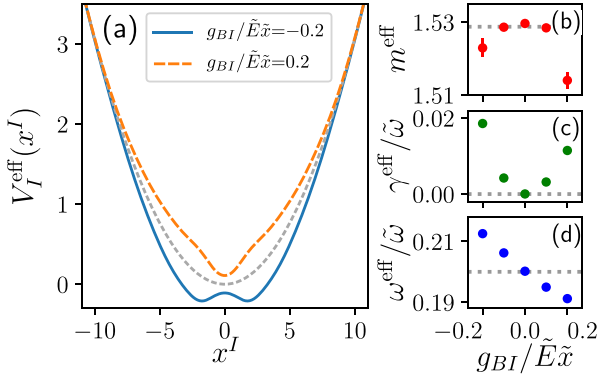


FIG. 9. (a) Time-averaged effective potential $V_I^{\text{eff}}(x^I)$ [see Eq. (6)] for $g_{BI}/\tilde{E}\tilde{x} = -0.2$ and 0.2 together with the harmonic oscillator potential of the impurity (dashed gray line). Equations (C2) and (C3) are fitted to the many-body results of the impurity's mean position and mean momentum with respect to the effective mass m^{eff} , the damping constant γ^{eff} , and the effective frequency ω^{eff} , shown in (b)–(d), respectively.

harmonic oscillator. The mean position for a particle obeying Eq. (C1) reads as

$$\langle \hat{x}_{\text{eff}}(t) \rangle = \exp\left(-\frac{\gamma^{\text{eff}}}{2m^{\text{eff}}}t\right) \times \left[x_0 \cos(\omega_0 t) - \frac{x_0 \gamma^{\text{eff}}}{2\omega_0 (m^{\text{eff}})^2} \sin(\omega_0 t) \right], \quad (\text{C2})$$

with $\omega_0 = \sqrt{(\omega^{\text{eff}})^2 - \left(\frac{\gamma^{\text{eff}}}{2m^{\text{eff}}}\right)^2}$. Additionally, we assume that the particle is initially at rest, i.e., $p_0 = 0$, and shifted by $x_0^{\text{eff}} = \langle \hat{x}^I(0) \rangle$. The corresponding mean momentum of Eq. (C1) is accordingly written as

$$\langle \hat{p}_{\text{eff}}(t) \rangle = -\exp\left(-\frac{\gamma^{\text{eff}}}{2m^{\text{eff}}}t\right) \times \left(m^{\text{eff}} \omega_0 x_0 + \frac{x_0 (\gamma^{\text{eff}})^2}{4\omega_0 (m^{\text{eff}})^2} \right) \sin(\omega_0 t). \quad (\text{C3})$$

Subsequently, we fit the analytical results of Eqs. (C2) and (C3) to the mean position and mean momentum calculated from the ML-MCTDHX approach for the free parameters γ^{eff} , ω^{eff} , and m^{eff} [43,60].

In Figs. 9(b)–9(d) we present the fitted parameters for impurity-medium interactions ranging exemplarily from $g_{BI}/\tilde{E}\tilde{x} = -0.2$ to 0.2 . We find that the effective mass [28,60] of the impurity decreases for larger absolute values of g_{BI} . This property is attributed to the fact that the bath is confined in a double-well potential. Closely inspecting Figs. 2(c1) and 2(d1) one can observe that a large part of the impurity's density performs a damped oscillatory motion while a smaller fraction of its one-body density accumulates either in the center of the double well for repulsive impurity-medium interactions or within the double-well sites for attractive couplings. Consequently, the corresponding dynamics of the mean position and momentum of the impurity capture this damped oscillatory motion. Thereby, the reason of this damping behavior is twofold. First, the nonvanishing impurity-medium coupling and the associated energy transfer

[28,43,44] from the impurity to the medium (cf. Appendix A) enforce a damped oscillatory behavior on the mean position and momentum. Second, the accumulation of the impurity's one-body density around $x^I = 0$ additionally enhances the damping of the mean position's and momentum's oscillation, i.e., the decrease of the mean position's and momentum's amplitude in time. Interestingly, the fitting procedure reveals that this damping is not only caused by a damping constant larger than zero, but is also due to an effective mass smaller than the bare value. Furthermore, this effect (damping) can be enhanced by slightly increasing the attractive or repulsive impurity-medium coupling strength (within a parameter range corresponding to the dissipative oscillation regime) leading to a pronounced energy transfer and an accompanied increase of the amount of density accumulated around the trap center. In this sense, we relate the decrease of the effective mass (in the picture of a damped harmonic oscillator) to the accumulation of density around the trap center which reduces the oscillating fraction of the impurity's one-body density. Therefore, the (unexpected) decrease of the effective mass can be traced back to the particular choice of the double-well potential experienced by the bath atoms. Finally, we remark that in the case of a harmonically trapped bath an increase of the effective mass due to the dressing is anticipated [43].

Moreover, the increase of γ^{eff} for increasing attractive and repulsive couplings can be explained by the corresponding growing influence of the bosonic environment. Additionally, we find an approximately linear decrease of the effective frequency ω^{eff} . In order to intuitively explain this behavior, we show in Fig. 9(a) the time-averaged effective potential for the two considered extrema of g_{BI} (i.e., $g_{BI}/\tilde{E}\tilde{x} = -0.2$ and 0.2). As can be seen, the effective potential is deeper in the case of attractive g_{BI} compared to the one obtained for repulsive g_{BI} leading to a higher effective frequency ω^{eff} in the attractive case than in the repulsive one.

Finally, we calculate the effective mass for the impurity in the steady bound-state regime for $g_{BI}/\tilde{E}\tilde{x} = -0.9$ [cf. Fig. 2(a1)]. Since in this regime the impurity's one-body density exhibits small-amplitude oscillations within the left site of the double-well potential, the above-mentioned procedure can be applied to the mean position and momentum of the impurity. Thereby, we extract an effective mass $m^{\text{eff}} = 1.96 \pm 0.06$ which is significantly heavier than the bare impurity mass. In contrast to the dissipative oscillation regime in which the accumulation of density around the trap center led to a decreased effective mass, in the steady bound-state regime the complete one-body density of the impurity undergoes a damped oscillatory motion which, eventually, leads to the increase of m^{eff} .

APPENDIX D: ANALYZING THE HIDDEN EXCITATIONS OF THE PINNING REGIME

The pinning regime appears at intermediate repulsive impurity-medium interaction strengths where the impurity becomes pinned within the bosonic environment residing in the double well. We attribute the origin of this pinning mechanism to the comparatively large energy transfer of the impurity when it penetrates the bosonic medium for the first time (see Fig. 7). Furthermore, we have verified that the impurity does not solely occupy the energetically lowest eigenstate of the

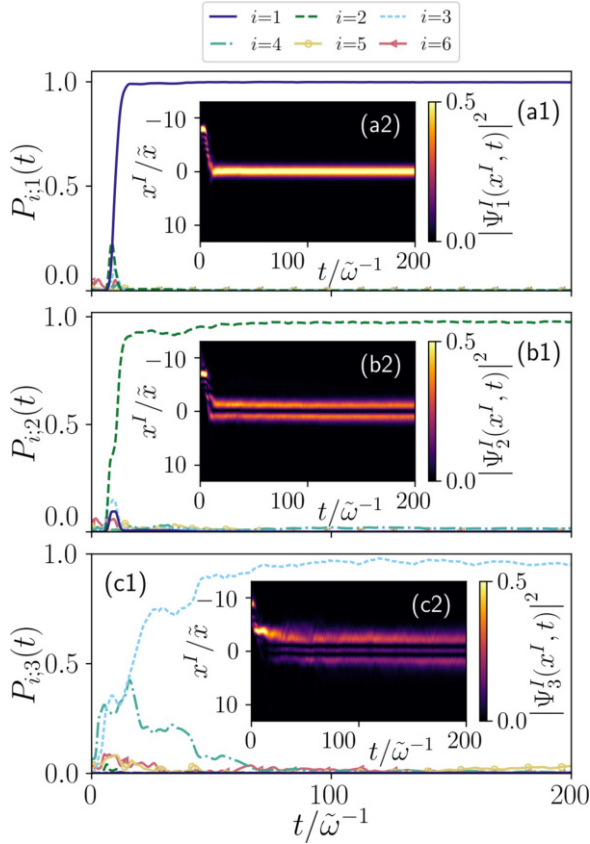


FIG. 10. (a1)–(c1) Overlap $P_{i,j}(t) = |\langle \Psi_j^I(t) | \psi_i^{\text{eff}} \rangle|^2$ of the j th highest occupied species function $|\Psi_j^I\rangle$ of the impurity and the i th eigenfunction of the effective potential [cf. Fig. 5(c1)]. Insets (a2)–(c2) show the time evolution of the respective densities of the species functions. In all panels we set $g_{BI}/\tilde{E}\tilde{x} = 1.0$ which corresponds to the pinning regime.

effective potential, but also populates energetically higher-lying states [Figs. 5(c1) and 5(c2)]. In the main text we referred to these states as hidden excitations since they are not apparent by merely inspecting the evolution of the one-body density $\rho_j^{(1)}(x, t)$ [see Fig. 2(e1)].

In the following we aim at investigating these hidden excitations in more detail. To this end, we monitor the time evolution of the density associated with the individual species functions $|\Psi_j^I\rangle$ for $g_{BI}/\tilde{E}\tilde{x} = 1.0$ [Figs. 10(a2)–10(c2)]. As it can be readily seen, the densities of the species functions remain constant once the impurity is pinned. Moreover, a careful inspection of the densities of the first three species functions reveals an ascending number of nodes which is tantamount to the existence of energetically higher-lying excitations of $|\Psi_j^I\rangle$.

In order to unravel the structure of the aforementioned species functions we project them on the basis set consisting of the eigenfunctions ψ_i^{eff} of the effective potential [cf. Fig. 5(c1)] and take the absolute square of the respective overlap, i.e., $P_{i,j}(t) = |\langle \Psi_j^I(t) | \psi_i^{\text{eff}} \rangle|^2$, where $j = 1, 2, 3$. Indeed, we find that the three dominantly occupied species functions

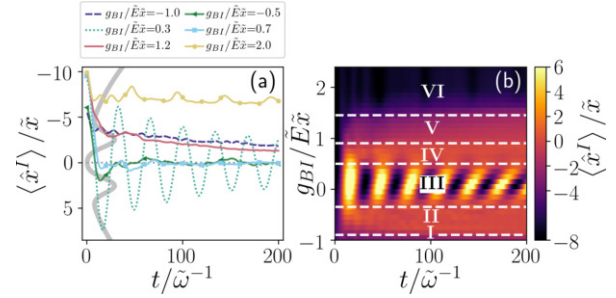


FIG. 11. Dynamical response regimes of the impurity as captured by its mean position for the case that the bosonic medium is confined in a triple well. (a) Time evolution of the impurity's mean position for specific values of g_{BI} (see legend) corresponding to six identified dynamical response regimes. The triple-well potential of the environment (gray line) is also presented. (b) Dynamical crossover phase diagram of the impurity's mean position with respect to g_{BI} .

correspond to the three energetically lowest eigenfunctions of the effective potential [see Figs. 10(a1)–10(c1)]. In particular, $|\Psi_1^I(x^I, t)|^2$ matches with the energetically lowest eigenstate ψ_1^{eff} , whereas $|\Psi_2^I(x^I, t)|^2$ and $|\Psi_3^I(x^I, t)|^2$ correspond to the second and third eigenstates, i.e., ψ_2^{eff} and ψ_3^{eff} .

APPENDIX E: DYNAMICAL RESPONSE FOR A TRIPLE-WELL TRAPPED ENVIRONMENT

To extend our basic conclusions regarding the impurity's response, described in Sec. II, we replace the double well of the bosonic medium with a triple well. However, the harmonic trap of the impurity as well as the employed quench protocol to induce the dynamics remain unchanged. The triple well of the bosonic environment reads as $V_B(x^B) = m_B \omega_B^2 (x^B)^2 / 2 + g_-(x^B) + g_+(x^B)$, where a superimposed harmonic trap with frequency $\omega_B/\tilde{\omega} = 0.15$ and two Gaussians $g_{\pm}(x^B) = \frac{h_B}{\sqrt{2\pi}w_B} \exp(-\frac{(x^B \mp \Delta)^2}{2(w_B)^2})$ shifted by Δ from the trap center are used. Also, the Gaussians have a width of $w_B/\tilde{x} = 0.8$ and a height of $h_B/\tilde{E}\tilde{x} = 1.8$ while the displacement is $\Delta/\tilde{x} = 2.5$. The system consists of $N_B = 20$ bosons for the bosonic medium and a single impurity $N_I = 1$. Additionally, we employ $M = 6$ species and $d_B = d_I = 6$ single-particle functions for the calculations to be presented below.

Figure 11(a) shows the time evolution of the impurity's mean position corresponding to the six identified dynamical response regimes which are labeled as I–VI in the respective crossover diagram in terms of g_{BI} illustrated in Fig. 11(b). As in the double-well case [see Fig. 3(a)], we find that for strong attractive impurity-medium interactions (regime I) a localization of the impurity in the vicinity of the most left site of the triple well occurs. This behavior is attributed to the initial large overlap of the impurity with the bath on the left site.⁵

⁵Note that for larger attractions the overlap of the impurity with the medium is initially larger at the central site of the triple well such that the impurity is initially localized at the trap center, where it remains in the course of the evolution.

By decreasing g_{BI} to intermediate attractive couplings, i.e., $g_{BI}/\tilde{E}\tilde{x} = -0.5$ corresponding to the regime II, we observe that the impurity localizes at the central site of the triple well. Entering the weak attractive and repulsive impurity-medium coupling strengths we identify a dissipative oscillation of the impurity similar to the case in which the bosonic bath is trapped to a double well [Fig. 3(b)]. For stronger repulsive g_{BI} the aforementioned oscillatory character vanishes (regime IV) and the one-body density of the impurity $\rho_I^{(1)}(x, t)$ (not shown) exhibits two humps located at the two maxima of the triple well. Here, $\langle \hat{x}^l(t) \rangle$ tends to zero, e.g., for $g_{BI}/\tilde{E}\tilde{x} = 0.7$. Note that even though the regimes II and IV show a similar behavior in terms of $\langle \hat{x}^l(t) \rangle$ we can distinguish them by evaluating the variance (s) which is in the attractive case smaller than in the repulsive one (not shown here). A further increase of the impurity-bath repulsion to $g_{BI}/\tilde{E}\tilde{x} = 1.2$ leads to a localization of the impurity at the position between the left and

central sites of the well [cf. regime V in Fig. 11(b)]. For strong repulsive impurity-medium interaction strengths we reach the regime VI which corresponds to the total reflection of the impurity as in the double-well case [45].

In summary, similarly to the double-well scenario we observe for a triple well continuous transitions between the emergent dynamical response regimes of the impurity with respect to g_{BI} . Analogously to the double-well case, the setup including a triple well also leads to a bound state and a total reflection regime at strong attractive and repulsive impurity-medium interactions as well as a dissipative oscillation regime at weak g_{BI} . Only at intermediate attractive and repulsive g_{BI} corresponding to the effective tunneling and the pinning regime in the double-well case, the impurity features an altered tunneling dynamics. Still, we find that the behavior of the impurity can be steered and controlled via the impurity-medium coupling strength.

-
- [1] K. Henderson, C. Ryu, C. MacCormick, and M. G. Boshier, Experimental demonstration of painting arbitrary and dynamic potentials for Bose-Einstein condensates, *New J. Phys.* **11**, 043030 (2009).
- [2] W. Ketterle and N. J. van Druten, Bose-Einstein condensation of a finite number of particles trapped in one or three dimensions, *Phys. Rev. A* **54**, 656 (1996).
- [3] A. Görlitz, J. M. Vogels, A. E. Leanhardt, C. Raman, T. L. Gustavson, J. R. Abo-Shaer, A. P. Chikkatur, S. Gupta, S. Inouye, T. Rosenband, and W. Ketterle, Realization of Bose-Einstein Condensates in Lower Dimensions, *Phys. Rev. Lett.* **87**, 130402 (2001).
- [4] D. S. Petrov, D. M. Gangardt, and G. V. Shlyapnikov, Low-dimensional trapped gases, *J. Phys. IV France* **116**, 5 (2004).
- [5] U. Fano, Effects of Configuration Interaction on Intensities and Phase Shifts, *Phys. Rev.* **124**, 1866 (1961).
- [6] T. Köhler, K. Góral, and P. S. Julienne, Production of cold molecules via magnetically tunable Feshbach resonances, *Rev. Mod. Phys.* **78**, 1311 (2006).
- [7] C. Chin, R. Grimm, P. Julienne, and E. Tiesinga, Feshbach resonances in ultracold gases, *Rev. Mod. Phys.* **82**, 1225 (2010).
- [8] P. O. Fedichev, Yu. Kagan, G. V. Shlyapnikov, and J. T. M. Walraven, Influence of Nearly Resonant Light on the Scattering Length in Low-Temperature Atomic Gases, *Phys. Rev. Lett.* **77**, 2913 (1996).
- [9] S. Inouye, M. R. Andrews, J. Stenger, H.-J. Miesner, D. M. Stamper-Kurn, and W. Ketterle, Observation of Feshbach resonances in a Bose-Einstein condensate, *Nature (London)* **392**, 151 (1998).
- [10] A. C. Pflanzner, S. Zöllner, and P. Schmelcher, Material-barrier tunnelling in one-dimensional few-boson mixtures, *J. Phys. B: At., Mol. Opt. Phys.* **42**, 231002 (2009).
- [11] N. B. Jørgensen, L. Wacker, K. T. Skalmstang, M. M. Parish, J. Levinsen, R. S. Christensen, G. M. Bruun, and J. J. Arlt, Observation of Attractive and Repulsive Polarons in a Bose-Einstein Condensate, *Phys. Rev. Lett.* **117**, 055302 (2016).
- [12] C. A. Stan, M. W. Zwierlein, C. H. Schunck, S. M. F. Raupach, and W. Ketterle, Observation of Feshbach Resonances between Two Different Atomic Species, *Phys. Rev. Lett.* **93**, 143001 (2004).
- [13] Y. I. Shin, A. Schirotzek, C. H. Schunck, and W. Ketterle, Realization of a Strongly Interacting Bose-Fermi Mixture from a Two-Component Fermi Gas, *Phys. Rev. Lett.* **101**, 070404 (2008).
- [14] E. Wille, F. M. Spiegelhalder, G. Kerner, D. Naik, A. Trenkwalder, G. Hendl, F. Schreck, R. Grimm, T. G. Tiecke, J. T. M. Walraven, S. J. J. M. F. Kokkelmans, E. Tiesinga, and P. S. Julienne, Exploring an Ultracold Fermi-Fermi Mixture: Interspecies Feshbach Resonances and Scattering Properties of ^6Li and ^{40}K , *Phys. Rev. Lett.* **100**, 053201 (2008).
- [15] C. Kohstall, M. Zaccanti, M. Jag, A. Trenkwalder, P. Massignan, G. M. Bruun, F. Schreck, and R. Grimm, Metastability and coherence of repulsive polarons in a strongly interacting Fermi mixture, *Nature (London)* **485**, 615 (2012).
- [16] M. Koschorreck, D. Pertot, E. Vogt, B. Fröhlich, M. Feld, and M. Köhl, Attractive and repulsive Fermi polarons in two dimensions, *Nature (London)* **485**, 619 (2012).
- [17] F. Scazza, G. Valtolina, P. Massignan, A. Recati, A. Amico, A. Burchianti, C. Fort, M. Inguscio, M. Zaccanti, and G. Roati, Repulsive Fermi Polarons in a Resonant Mixture of Ultracold ^6Li Atoms, *Phys. Rev. Lett.* **118**, 083602 (2017).
- [18] L. D. Landau, Über die Bewegung der Elektronen in Kristallgitter, *Phys. Z. Sowjetunion* **3**, 644 (1933).
- [19] S. Nascimbène, N. Navon, K. J. Jiang, L. Tarruell, M. Teichmann, J. McKeever, F. Chevy, and C. Salomon, Collective Oscillations of an Imbalanced Fermi Gas: Axial Compression Modes and Polaron Effective Mass, *Phys. Rev. Lett.* **103**, 170402 (2009).
- [20] V. Ngampruetikorn, J. Levinsen, and M. M. Parish, Repulsive polarons in two-dimensional Fermi gases, *Europhys. Lett.* **98**, 30005 (2012).
- [21] P. Massignan, M. Zaccanti, and G. M. Bruun, Polarons, dressed molecules and itinerant ferromagnetism in ultracold Fermi gases, *Rep. Prog. Phys.* **77**, 034401 (2014).
- [22] R. Schmidt, M. Knap, D. A. Ivanov, J.-S. You, M. Cetina, and E. Demler, Universal many-body response of heavy impurities coupled to a Fermi sea: A review of recent progress, *Rep. Prog. Phys.* **81**, 024401 (2018).
- [23] O. Gamayun, O. Lychkovskiy, E. Burovski, M. Malcomson, V. V. Cheianov, and M. B. Zvonarev, Impact of the Injection

- Protocol on an Impurity's Stationary State, *Phys. Rev. Lett.* **120**, 220605 (2018).
- [24] S. Palzer, C. Zipkes, C. Sias, and M. Köhl, Quantum Transport through a Tonks-Girardeau Gas, *Phys. Rev. Lett.* **103**, 150601 (2009).
- [25] T. Fukuhara, A. Kantian, M. Endres, M. Cheneau, P. Schauß, S. Hild, D. Bellem, U. Schollwöck, T. Giamarchi, C. Gross, I. Bloch, and S. Kuhr, Quantum dynamics of a mobile spin impurity, *Nat. Phys.* **9**, 235 (2013).
- [26] A. G. Volosniev and H.-W. Hammer, Analytical approach to the Bose-polaron problem in one dimension, *Phys. Rev. A* **96**, 031601(R) (2017).
- [27] A. S. Dehkharghani, A. G. Volosniev, and N. T. Zinner, Coalescence of Two Impurities in a Trapped One-dimensional Bose Gas, *Phys. Rev. Lett.* **121**, 080405 (2018).
- [28] S. I. Mistakidis, G. C. Katsimiga, G. M. Koutentakis, Th. Busch, and P. Schmelcher, Quench Dynamics and Orthogonality Catastrophe of Bose Polarons, *Phys. Rev. Lett.* **122**, 183001 (2019).
- [29] M. Albiez, R. Gati, J. Fölling, S. Hunsmann, M. Cristiani, and M. K. Oberthaler, Direct Observation of Tunneling and Non-linear Self-Trapping in a Single Bosonic Josephson Junction, *Phys. Rev. Lett.* **95**, 010402 (2005).
- [30] L. A. Peña Ardila, N. B. Jörgensen, T. Pohl, S. Giorgini, G. M. Bruun, and J. J. Arlt, Analyzing a Bose polaron across resonant interactions, *Phys. Rev. A* **99**, 063607 (2019).
- [31] Magnus G. Skou, Thomas G. Skov, Nils B. Jörgensen, Kristian K. Nielsen, Arturo Camacho-Guardian, Thomas Pohl, Georg M. Bruun, and Jan J. Arlt, Non-equilibrium quantum dynamics and formation of the Bose polaron, *Nat. Phys.* (2021).
- [32] A. Privitera and W. Hofstetter, Polaronic slowing of fermionic impurities in lattice Bose-Fermi mixtures, *Phys. Rev. A* **82**, 063614 (2010).
- [33] B. Kain and H. Y. Ling, Generalized Hartree-Fock-Bogoliubov description of the Fröhlich polaron, *Phys. Rev. A* **94**, 013621 (2016).
- [34] F. Grusdt, R. Schmidt, Y. E. Shchadilova, and E. Demler, Strong-coupling Bose polarons in a Bose-Einstein condensate, *Phys. Rev. A* **96**, 013607 (2017).
- [35] T. Ichmoukhamedov and J. Tempere, Feynman path-integral treatment of the Bose polaron beyond the Fröhlich model, *Phys. Rev. A* **100**, 043605 (2019).
- [36] L. A. P. Ardila and T. Pohl, Ground-state properties of dipolar Bose polarons, *J. Phys. B: At., Mol. Opt. Phys.* **52**, 015004 (2019).
- [37] L. A. Peña Ardila, G. E. Astrakharchik, and S. Giorgini, Strong coupling Bose polarons in a two-dimensional gas, *Phys. Rev. Res.* **2**, 023405 (2020).
- [38] D. Boyanovsky, D. Jasnow, X.-L. Wu, and R. C. Coalson, Dynamics of relaxation and dressing of a quenched Bose polaron, *Phys. Rev. A* **100**, 043617 (2019).
- [39] N. A. Kamar, A. Kantian, and T. Giamarchi, Dynamics of a mobile impurity in a two-leg bosonic ladder, *Phys. Rev. A* **100**, 023614 (2019).
- [40] S. I. Mistakidis, G. M. Koutentakis, G. C. Katsimiga, Th. Busch, and P. Schmelcher, Many-body quantum dynamics and induced correlations of Bose polarons, *New J. Phys.* **22**, 043007 (2020).
- [41] Q. Bouton, J. Nettersheim, D. Adam, F. Schmidt, D. Mayer, T. Lausch, E. Tiemann, and A. Widera, Single-Atom Quantum Probes for Ultracold Gases Boosted by Nonequilibrium Spin Dynamics, *Phys. Rev. X* **10**, 011018 (2020).
- [42] A. G. Volosniev, H.-W. Hammer, and N. T. Zinner, Real-time dynamics of an impurity in an ideal Bose gas in a trap, *Phys. Rev. A* **92**, 023623 (2015).
- [43] S. I. Mistakidis, F. Grusdt, G. M. Koutentakis, and P. Schmelcher, Dissipative correlated dynamics of a moving impurity immersed in a Bose-Einstein condensate, *New J. Phys.* **21**, 103026 (2019).
- [44] K. K. Nielsen, L. A. P. Ardila, G. M. Bruun, and T. Pohl, Critical slowdown of non-equilibrium polaron dynamics, *New J. Phys.* **21**, 043014 (2019).
- [45] F. Theel, K. Keiler, S. I. Mistakidis, and P. Schmelcher, Entanglement-assisted tunneling dynamics of impurities in a double well immersed in a bath of lattice trapped bosons, *New J. Phys.* **22**, 023027 (2020).
- [46] K. Keiler, S. I. Mistakidis, and P. Schmelcher, Doping a lattice-trapped bosonic species with impurities: From ground state properties to correlated tunneling dynamics, *New J. Phys.* **22**, 083003 (2020).
- [47] A. Klein, M. Bruderer, S. R. Clark, and D. Jaksch, Dynamics, dephasing and clustering of impurity atoms in Bose-Einstein condensates, *New J. Phys.* **9**, 411 (2007).
- [48] K. Keiler and P. Schmelcher, State engineering of impurities in a lattice by coupling to a Bose gas, *New J. Phys.* **20**, 103042 (2018).
- [49] K. Keiler and P. Schmelcher, Interaction-induced single-impurity tunneling in a binary mixture of trapped ultracold bosons, *Phys. Rev. A* **100**, 043616 (2019).
- [50] F. Schmidt, D. Mayer, Q. Bouton, D. Adam, T. Lausch, N. Spethmann, and A. Widera, Quantum Spin Dynamics of Individual Neutral Impurities Coupled to a Bose-Einstein Condensate, *Phys. Rev. Lett.* **121**, 130403 (2018).
- [51] F. Schmidt, D. Mayer, Q. Bouton, D. Adam, T. Lausch, J. Nettersheim, E. Tiemann, and A. Widera, Tailored Single-Atom Collisions at Ultralow Energies, *Phys. Rev. Lett.* **122**, 013401 (2019).
- [52] F. Lingua, L. Lepori, F. Minardi, V. Penna, and L. Salasnich, Collision of impurities with Bose-Einstein condensates, *New J. Phys.* **20**, 045001 (2018).
- [53] S. Krönke, J. Knörzer, and P. Schmelcher, Correlated quantum dynamics of a single atom collisionally coupled to an ultracold finite bosonic ensemble, *New J. Phys.* **17**, 053001 (2015).
- [54] B. Juliá-Díaz, M. Melé-Messeguer, M. Guilleumas, and A. Polls, Spinor Bose-Einstein condensates in a double well: Population transfer and Josephson oscillations, *Phys. Rev. A* **80**, 043622 (2009).
- [55] L. Cao, S. Krönke, O. Vendrell, and P. Schmelcher, The multi-layer multi-configuration time-dependent Hartree method for bosons: Theory, implementation, and applications, *J. Chem. Phys.* **139**, 134103 (2013).
- [56] S. Krönke, L. Cao, O. Vendrell, and P. Schmelcher, Non-equilibrium quantum dynamics of ultra-cold atomic mixtures: The multi-layer multi-configuration time-dependent Hartree method for bosons, *New J. Phys.* **15**, 063018 (2013).
- [57] L. Cao, V. Bolsinger, S. I. Mistakidis, G. M. Koutentakis, S. Krönke, J. M. Schurer, and P. Schmelcher, A unified ab initio approach to the correlated quantum dynamics of ultracold fermionic and bosonic mixtures, *J. Chem. Phys.* **147**, 044106 (2017).

- [58] K. Mukherjee, S. I. Mistakidis, S. Majumder, and P. Schmelcher, Pulse- and continuously driven many-body quantum dynamics of bosonic impurities in a Bose-Einstein condensate, *Phys. Rev. A* **101**, 023615 (2020).
- [59] M. Knap, C. J. M. Mathy, M. Ganahl, M. B. Zvonarev, and E. Demler, Quantum Flutter: Signatures and Robustness, *Phys. Rev. Lett.* **112**, 015302 (2014).
- [60] S. I. Mistakidis, A. G. Volosniev, N. T. Zinner, and P. Schmelcher, Effective approach to impurity dynamics in one-dimensional trapped Bose gases, *Phys. Rev. A* **100**, 013619 (2019).
- [61] J. Erdmann, S. I. Mistakidis, and P. Schmelcher, Phase-separation dynamics induced by an interaction quench of a correlated Fermi-Fermi mixture in a double well, *Phys. Rev. A* **99**, 013605 (2019).
- [62] M. Olshanii, Atomic Scattering in the Presence of an External Confinement and a Gas of Impenetrable Bosons, *Phys. Rev. Lett.* **81**, 938 (1998).
- [63] L. J. LeBlanc and J. H. Thywissen, Species-specific optical lattices, *Phys. Rev. A* **75**, 053612 (2007).
- [64] A. D. Lercher, T. Takekoshi, M. Debatin, B. Schuster, R. Rameshan, F. Ferlaino, R. Grimm, and H.-C. Nägerl, Production of a dual-species Bose-Einstein condensate of Rb and Cs atoms, *Eur. Phys. J. D* **65**, 3 (2011).
- [65] M.-G. Hu, M. J. Van de Graaff, D. Kedar, J. P. Corson, Eric A. Cornell, and Deborah S. Jin, Bose Polarons in the Strongly Interacting Regime, *Phys. Rev. Lett.* **117**, 055301 (2016).
- [66] M. Haas, V. Leung, D. Frese, D. Haubrich, S. John, C. Weber, A. Rauschenbeutel, and D. Meschede, Species-selective microwave cooling of a mixture of rubidium and caesium atoms, *New J. Phys.* **9**, 147 (2007).
- [67] G. C. Katsimiga, S. I. Mistakidis, T. M. Bersano, M. K. H. Ome, S. M. Mossman, K. Mukherjee, P. Schmelcher, P. Engels, and P. G. Kevrekidis, Observation and analysis of multiple dark-antidark solitons in two-component Bose-Einstein condensates, *Phys. Rev. A* **102**, 023301 (2020).
- [68] E. Schmidt, Zur Theorie der linearen und nichtlinearen Integralgleichungen, *Math. Ann.* **63**, 433 (1907).
- [69] R. Horodecki, P. Horodecki, M. Horodecki, and K. Horodecki, Quantum entanglement, *Rev. Mod. Phys.* **81**, 865 (2009).
- [70] M. Roncaglia, A. Montorsi, and M. Genovese, Bipartite entanglement of quantum states in a pair basis, *Phys. Rev. A* **90**, 062303 (2014).
- [71] J. C. Light, I. P. Hamilton, and J. V. Lill, Generalized discrete variable approximation in quantum mechanics, *J. Chem. Phys.* **82**, 1400 (1985).
- [72] P. A. M. Dirac, Note on exchange phenomena in the Thomas atom, *Math. Proc. Cambridge Philos. Soc.* **26**, 376 (1930).
- [73] A. Raab, On the Dirac-Frenkel/McLachlan variational principle, *Chem. Phys. Lett.* **319**, 674 (2000).
- [74] F. Köhler, K. Keiler, S. I. Mistakidis, H.-D. Meyer, and P. Schmelcher, Dynamical pruning of the non-equilibrium quantum dynamics of trapped ultracold bosons, *J. Chem. Phys.* **151**, 054108 (2019).
- [75] K. Sakmann, A. I. Streltsov, O. E. Alon, and L. S. Cederbaum, Reduced density matrices and coherence of trapped interacting bosons, *Phys. Rev. A* **78**, 023615 (2008).
- [76] I. Peschel and V. Eisler, Reduced density matrices and entanglement entropy in free lattice models, *J. Phys. A: Math. Theor.* **42**, 504003 (2009).
- [77] K. Sacha and E. Timmermans, Self-localized impurities embedded in a one-dimensional Bose-Einstein condensate and their quantum fluctuations, *Phys. Rev. A* **73**, 063604 (2006).
- [78] S. Zöllner, H.-D. Meyer, and P. Schmelcher, Few-Boson Dynamics in Double Wells: From Single-Atom to Correlated Pair Tunneling, *Phys. Rev. Lett.* **100**, 040401 (2008).
- [79] S. P. Rath and R. Schmidt, Field-theoretical study of the Bose polaron, *Phys. Rev. A* **88**, 053632 (2013).
- [80] S. I. Mistakidis, G. C. Katsimiga, G. M. Koutentakis, Th. Busch, and P. Schmelcher, Pump-probe spectroscopy of Bose polarons: Dynamical formation and coherence, *Phys. Rev. Res.* **2**, 033380 (2020).
- [81] J. Goold, T. Fogarty, N. Lo Gullo, M. Paternostro, and Th. Busch, Orthogonality catastrophe as a consequence of qubit embedding in an ultracold Fermi gas, *Phys. Rev. A* **84**, 063632 (2011).
- [82] J. Catani, G. Lamporesi, D. Naik, M. Gring, M. Inguscio, F. Minardi, A. Kantian, and T. Giamarchi, Quantum dynamics of impurities in a one-dimensional Bose gas, *Phys. Rev. A* **85**, 023623 (2012).
- [83] J. P. Ronzheimer, M. Schreiber, S. Braun, S. S. Hodgman, S. Langer, I. P. McCulloch, F. Heidrich-Meisner, I. Bloch, and U. Schneider, Expansion Dynamics of Interacting Bosons in Homogeneous Lattices in One and Two Dimensions, *Phys. Rev. Lett.* **110**, 205301 (2013).
- [84] R. Paškauskas and L. You, Quantum correlations in two-boson wave functions, *Phys. Rev. A* **64**, 042310 (2001).
- [85] J. Chen, J. M. Schurer, and P. Schmelcher, Entanglement Induced Interactions in Binary Mixtures, *Phys. Rev. Lett.* **121**, 043401 (2018).
- [86] C.-I. Um, K.-H. Yeon, and T. F. George, The quantum damped harmonic oscillator, *Phys. Rep.* **362**, 63 (2002).

3.7 Polarons and their induced interactions in highly imbalanced triple mixtures

Polarons and their induced interactions in highly imbalanced triple mixtures

Kevin Keiler¹, Simeon I. Mistakidis¹, and Peter Schmelcher^{1,2}

¹*Center for Optical Quantum Technologies, Department of Physics,
University of Hamburg, Luruper Chaussee 149, 22761 Hamburg, Germany and*

²*The Hamburg Centre for Ultrafast Imaging, University of Hamburg,
Luruper Chaussee 149, 22761 Hamburg, Germany*

We unravel the polaronic properties of impurities immersed in a correlated trapped one-dimensional (1D) Bose-Bose mixture. This setup allows for the impurities to couple either attractively or repulsively to a specific host, thus offering a highly flexible platform for steering the emergent polaronic properties. Specifically, the polaronic residue peak and strength of induced interactions can be controlled by varying the coupling of the impurities to the individual bosonic components. In particular, it is possible to maintain the quasiparticle character for larger interaction strengths as compared to the case of impurities immersed in a single bosonic species. We explicate a hierarchy of the polaron binding energies in terms of the impurity-medium interactions, thereby elucidating the identification of the polaronic resonances in recent experimental radiofrequency schemes. For strong attractive impurity-medium couplings bipolaron formation is captured. Our findings pave the way for continuously changing the quasiparticle character, under the impact of trap effects, while exposing the role of correlations in triple mixture settings.

Introduction.- Ultracold atoms provide pristine platforms for probing quantum phenomena in multi-component fermionic and bosonic [1, 2] settings offering an exquisite tunability [1, 3, 4]. Highly particle imbalanced mixtures [5–8] have lately received major attention in terms of the quasiparticle context [9], leading to fundamentally new insights concerning Fermi and Bose polarons [5, 10, 11]. The quasiparticle notion extends far beyond cold atom settings in semiconducting [12] and superconducting devices [13], while interactions among quasiparticles in liquid Helium mixtures [14, 15] and cuprates [16, 17] are a promising candidate for conventional and high- T_c superconductivity [18–24]. Owing to the recent experimental realization of these impurity systems [6–8, 25, 26], an intense theoretical activity has been triggered for the investigation of their stationary properties [27, 28] e.g. unveiling their effective mass [29–31], excitation spectra [7, 11, 32, 33] and induced-interactions [34–39]. These studies considered an impurity immersed in a single component bath. Only very recently, extensions to impurities interacting with a coherently coupled two-component Bose-Einstein condensate (BEC) [40, 41] and Bose-Bose mixtures [42] have been considered. Especially in the intermediate and strong interaction regime the emergent polaronic states are largely unexplored. To adequately describe the latter, approaches that include higher-order correlations [43–45] and thus operate beyond lower order descriptions [42, 46–60], are necessary as it has been demonstrated already in the case of binary systems, i.e. impurities immersed in a single component bath. It is hence an intriguing perspective to explore whether also higher-order correlations play a crucial role in triple mixture setups, where impurities are immersed in a cumulative bath consisting of a Bose-Bose mixture.

The generalization to triple mixture settings allows for the impurities to selectively couple to the individ-

ual hosts, thus offering an efficient platform for tuning the emergent polaronic properties. This includes the longevity of the polarons and the control of their induced interactions. For this reason, in this Letter, we explore the polaronic properties of impurities coupled to a 1D [61, 62] harmonically trapped Bose-Bose mixture spanning a wide range of attractive and repulsive impurity-medium coupling strengths, while including all particle correlations. Commonly polarons are studied in spatially uniform systems, while we account for trap effects which are relevant to typical ultracold atom experiments. We exemplify that for a single impurity, the distribution of the polaronic residue in terms of the impurity-medium couplings can be steered by adjusting the different interactions to the respective bath of the mixture. In particular, when coupling to the one host repulsively and attractively to the other one, the residue peak can be broadened, such that the polaronic character is maintained for larger interaction strengths. For strong repulsive or attractive impurity-medium interactions we capture the catastrophe of the Bose polaron associated with a vanishing residue. These results hold independently of the particle number of the hosts and the impurity-bath atomic mass ratio. The behavior of the dressed impurity can be intuitively interpreted in terms of an effective potential, which provides a good approximation for weak impurity-bath coupling strengths, where interspecies entanglement is suppressed. The location of the attractive and repulsive quasiparticle resonances is captured by monitoring the polaron binding energy. Upon considering two bosonic impurities, we identify the presence of attractive induced interactions whose strength can be steered by the coupling to the respective host of the Bose-Bose mixture. Induced interactions strongly influence the impurities' spatial distribution allowing, for instance, bipolaron formation and lead to a reduction of

the polaron residue.

Model.- We consider a Bose-Bose mixture consisting of two species A and B with equal masses $m_A = m_B = m$ and $N_A = N_B = 10$ particles. We note that our results persist for larger N_A, N_B , see [63]. $N_C = 1, 2$ bosonic impurities of mass m_C are immersed in this 1D harmonically confined [64, 65] mixture of interacting atoms. The trap frequencies are $\omega_A = \omega_B = \omega_C = \omega = 1.0$. The many-body (MB) Hamiltonian of the system reads

$$\hat{H} = \sum_{\sigma \in \{A, B, C\}} \hat{H}_\sigma + \hat{H}_{AB} + \hat{H}_{AC} + \hat{H}_{BC}. \quad (1)$$

Here, $\hat{H}_\sigma = \int dx \hat{\Psi}_\sigma^\dagger(x) \left(-\frac{\hbar^2}{2m_\sigma} \frac{d^2}{dx^2} + \frac{1}{2} m_\sigma \omega_\sigma^2 x^2 \right) \hat{\Psi}_\sigma(x) + g_{\sigma\sigma} \int dx \hat{\Psi}_\sigma^\dagger(x) \hat{\Psi}_\sigma^\dagger(x) \hat{\Psi}_\sigma(x) \hat{\Psi}_\sigma(x)$ describes the Hamiltonian of species $\sigma \in \{A, B, C\}$, with contact intraspecies interaction of $g_{AA} = g_{BB} > 0$ and $g_{CC} = 0$. $\hat{\Psi}_\sigma(x)$ is the σ -species bosonic field operator. $\hat{H}_{\sigma\sigma'} = g_{\sigma\sigma'} \int dx \hat{\Psi}_\sigma^\dagger(x) \hat{\Psi}_\sigma(x) \hat{\Psi}_{\sigma'}^\dagger(x) \hat{\Psi}_{\sigma'}(x)$ denotes the contact interspecies interaction of strength $g_{\sigma\sigma'}$ [66]. In this sense, $\hat{H}_A + \hat{H}_B + \hat{H}_{AB}$ build the Bose-Bose mixture serving as a cumulative bath for the impurity species, described by \hat{H}_C . The impurities couple repulsively or attractively to both A and B hosts via a contact interaction of strength g_{AC} and g_{BC} , as captured by \hat{H}_{AC} and \hat{H}_{BC} . To directly expose the pure effect of impurity-impurity induced interactions we set $g_{CC} = 0$. We focus on the case of equal masses $m = m_C$, which can be experimentally realized to a good approximation by considering a mixture of isotopes, e.g. a ^{87}Rb BEC where the Bose-Bose mixture refers to two hyperfine states [67, 68] and ^{85}Rb for the impurities. The effects of mass-imbalance are discussed in Ref. [63]. Throughout this work, we consider $g_{AA} = g_{BB} = 0.2$ and $g_{AB} = 0.1$ in units of $\sqrt{\hbar^3 \omega / m}$, leading to a miscible mixture of species A and B. Spatial scales are given in harmonic units of $\sqrt{\hbar / m \omega}$ and energies in terms of $\hbar \omega$.

To address the ground state of our three-component system we use the variational Multi-Layer Multi-Configuration Time-Dependent Hartree method for atomic mixtures (ML-MCTDHX) [1-3]. This non-perturbative approach relies on expanding the MB wavefunction with respect to a variationally optimized time-dependent basis. The ground states are determined by using imaginary time propagation. The multilayer structure of the wave function is tailored to account for all the emergent intra- and interspecies correlations which are indeed crucial for describing the emergent polaronic properties [63].

Results and discussion.- As a first step, we vary the individual impurity-medium coupling strengths g_{AC} and g_{BC} of a single impurity to the cumulative bath from attractive to repulsive values and obtain the ground state of the triple mixture. The underlying polaronic residue

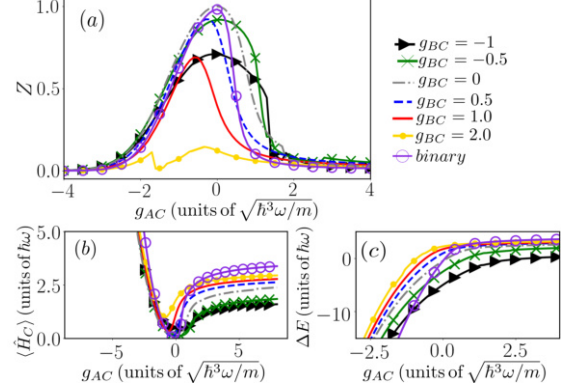


FIG. 1. Polaron (a) residue Z , (b) energy $\langle \hat{H}_C \rangle$ and (c) binding energy ΔE for different impurity-bath couplings g_{AC} and g_{BC} . The violet circles represent the binary mixture with $N = 20$ single species bath atoms and $g = 0.2$.

Z [5] is determined by

$$Z = |\langle \Psi_0 | \Psi \rangle|^2, \quad (2)$$

where $|\Psi_0\rangle$ is the MB wavefunction for a non-interacting impurity with $g_{AC} = g_{BC} = 0$, while $|\Psi\rangle$ denotes the interacting case. Additionally, we determine the residue for a binary mixture, which we define here as an impurity immersed into a bath of $N = 20$ single species bosons interacting repulsively with a strength of $g = 0.2$. Figure 1 (a) illustrates the polaronic residue upon varying the impurity-bath couplings g_{AC} and g_{BC} . In all cases we find that Z exhibits a broad peak with respect to g_{AC} and decreases towards zero for strongly either attractive or repulsive g_{AC} , implying the decay of the polaron [60]. This orthogonality catastrophe of the polaron is caused by the phase-separation of the impurity with its hosts for strong repulsions, thus rendering no dressing possible, see also [63]. In contrast, for strong attractions $g_{AC} \ll 0$ the impurity either lies within both hosts for $g_{BC} < 0$ or solely resides within host A while host B forms a shell structure for $g_{BC} > 0$ [63]. The width of the residue distribution for $g_{BC} = 0$ is larger than for the binary system due to the smaller interspecies coupling strength $g_{AB} = 0.1$, as compared to the intraspecies coupling strength $g = 0.2$. For repulsive g_{BC} we observe a decrease and shift of the polaronic residue peak with increasing g_{BC} as compared to the case of $g_{BC} = 0$ and the binary mixture. These phenomena are again attributed to the presence of the impurity-hosts phase-separation taking place for a larger range of values of g_{AC} with increasing g_{BC} [see Ref. [63]]. Furthermore, the width of the residue distribution decreases for increasingly repulsive values of g_{BC} . However, for attractive g_{BC} a broadening of the residue distribution occurs towards repulsive values of the couplings g_{AC} , while the corresponding value of the maximum. The fact that $Z < 1$ for $g_{AC} = 0$ is attributed to the finite coupling

g_{BC} , leading already to polaron formation by the host B, while for $g_{AC} \neq 0$ the polaron experiences an additional dressing. Importantly, a powerful asset of the binary host is that depending on the combination of attractive and repulsive impurity-bath couplings it is possible to flexibly control and maintain the polaron for larger values of the coupling strength g_{AC} to the medium. This effect can also be retrieved for heavier impurities, e.g. with mass ratios $m/m_C = 87/133$ and $m/m_C = 87/174$, where the baths consist of ^{87}Rb atoms and the impurities are either ^{133}Cs or ^{174}Yb atoms, respectively (see Ref. [63]).

The competition of the impurity-medium coupling strengths also naturally impacts the polaronic energy $\langle \hat{H}_C \rangle = \langle \Psi | \hat{H}_C | \Psi \rangle - \langle \Psi_0 | \hat{H}_C | \Psi_0 \rangle$ [Fig. 1(b)]. While for increasingly attractive g_{AC} an increase of the energy occurs for arbitrary values of g_{BC} , for repulsive g_{AC} the energy tends to saturate towards different values depending on g_{BC} , see also the discussion below. For $g_{BC} > 0$ and $g_{AC} > 0$ we generally encounter larger polaron energies suggesting an increasing effective mass [60] as compared to the case $g_{BC} < 0$. Consequently, it is possible to distinguish between repulsive and attractive impurity-bath coupling strengths g_{BC} based on the corresponding polaron energy. Next, we estimate the polaron binding energy

$$\Delta E = E(N_C, g_{AC}, g_{BC}) - E(N_C = 0, g_{AC} = 0, g_{BC} = 0) \quad (3)$$

being defined as the energy difference due to the injection of the impurity, where $E(N_C, g_{AC}, g_{BC})$ is the total energy of the system with N_C impurities interacting with an effective strength g_{AC} and g_{BC} with the respective species [Fig. 1 (c)]. As expected, ΔE decreases for increasingly attractive g_{AC} and saturates for repulsive values, similarly to the behavior of $\langle \hat{H}_C \rangle$. The former can be associated with a strong binding of the impurity to its hosts, thereby reducing ΔE , while the latter is a consequence of the resultant phase-separation process where the impurity forms a shell structure around the baths [34, 63]. Evidently, we find a clear hierarchy of ΔE depending on g_{BC} , namely decreasing g_{BC} apparently leads to a reduction of ΔE for any fixed g_{AC} . Therefore, experimentally, e.g. utilizing a radiofrequency scheme [72–74], the corresponding polaronic resonances are well distinguishable from each other. We have verified that a similar behavior of ΔE takes place for a larger cumulative bath with $N_A = N_B = 50$ particles [63].

To offer an intuitive understanding into the impurity's state for varying g_{AC} and g_{BC} we construct an effective potential [75] by considering the Bose-Bose mixture as a static potential superimposed to the harmonic confinement of the impurity. It reads

$$V_{eff} = \frac{1}{2} m_C \omega^2 x^2 + g_{AC} \rho_A^{(1)}(x) + g_{BC} \rho_B^{(1)}(x), \quad (4)$$

where $\rho_\sigma^{(1)}(x)$ is the one-body density of $\sigma = A, B$ bath species calculated within the correlated MB approach

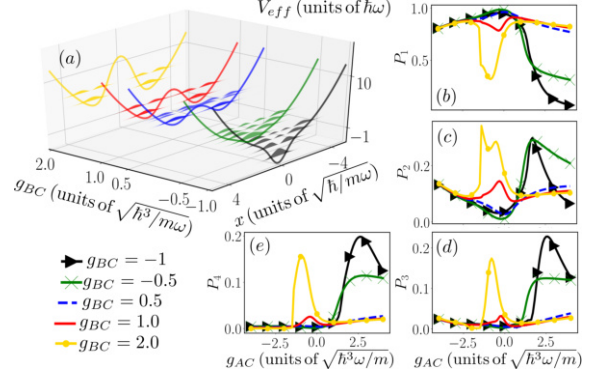


FIG. 2. (a) Effective potential V_{eff} and corresponding eigenvalue distributions $|\phi_i(x)|^2$ for $g_{AC} = 0.5$ and different g_{BC} . (b)-(e) Probability of finding the impurity in the single-particle eigenstate $|\phi_i\rangle$, $i = 1, 2, 3, 4$, of V_{eff} .

and thereby includes all necessary correlations, i.e. it cannot be recovered within a mean-field treatment. Accordingly, the impurity may occupy the eigenstates $|\phi_i\rangle$ of V_{eff} . It is important to note that the simplification in terms of V_{eff} neglects several phenomena that are important for the description of the impurity's state, such as the renormalization of the impurity's mass as well as the possible emergence of induced interactions. Figure 2 (a) shows the deformations of the effective potential and its underlying eigenstates $|\phi_i\rangle$ under variations of g_{BC} for $g_{AC} = 0.5$. For $g_{BC} \ll 0$, specifically $g_{BC} = -1$, the harmonic oscillator potential exhibits an additional dip which becomes more prominent with decreasing g_{BC} , whereas for $g_{BC} > 0$ a double well structure forms. This has an impact on the related eigenstates such that quasi-degeneracies develop. The probability of finding the impurity in the i th eigenstate of V_{eff} irrespectively of the states that are populated by the Bose-Bose mixture is given by

$$P_i = \sum_{kl} |\langle \vec{n}_k^A | \langle \vec{n}_l^B | \langle \phi_i | \Psi \rangle|^2, \quad (5)$$

where $\{|\vec{n}^\sigma\rangle\}$ is an arbitrary complete Fock basis of the $\sigma = A, B$ baths. For all g_{BC} , except for $g_{BC} = 2.0$, the ground state of the impurity is well described, i.e. $P_1 > 0.9$, by the corresponding ground state within the effective potential for weak attractive and weak repulsive g_{AC} [Fig. 2 (b)]. Further decreasing g_{AC} towards attractive couplings the occupation of $|\phi_1\rangle$ is reduced, whereas $|\phi_2\rangle$ starts to contribute [Fig. 2 (c)]. This behavior can still be recovered for $g_{AC} > 0$, while for attractive impurity-bath couplings $g_{BC} < 0$ and $g_{AC} > 0$ we find a drastic decrease of P_1 accompanied by the substantial occupation of the excited states $|\phi_2\rangle$, $|\phi_3\rangle$ and $|\phi_4\rangle$ [Fig. 2 (c)-(e)]. Accordingly, the effective potential picture is no longer valid and does not provide a proper description of the impurity coupled to a cumulative bath. This is in

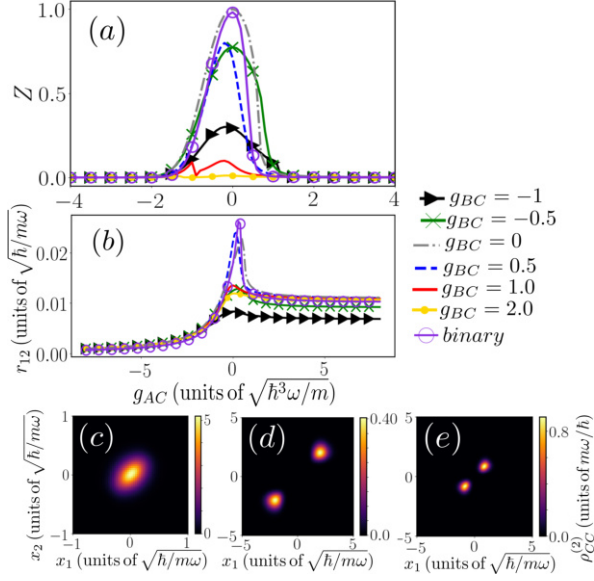


FIG. 3. (a) Polaron residue Z and (b) impurity distance r_{12} for $N_C = 2$ upon varying the impurity-bath couplings g_{AC} and g_{BC} , while $g_{CC} = 0$. The violet circles represent the binary mixture with $N = 20$ bath atoms. Two-body density $\rho_{CC}^{(2)}(x_1, x_2)$ of the two impurities for combinations (g_{AC}, g_{BC}) of (c) $(-2.1, -1)$, (d) $(8, 2)$ and (e) $(8, -1)$.

line with the behavior of the polaronic residue Z which drops to zero in this interaction range [Fig. 1 (a)]. Interestingly, for $g_{BC} > 0$ the prominent decrease of Z does not necessarily lead to an equally strong reduction of P_1 . Thus, in these cases the ground state of the impurity can be well approximated by $|\phi_1\rangle$.

Let us now discuss the behavior of $N_C = 2$ bosonic impurities immersed in a Bose-Bose mixture. Monitoring the polaronic residue [Eq. (2)] in order to extract the impact of the coupling on the impurity, we generally observe a similar behavior [Fig. 3 (a)] as compared to the single impurity case. For $g_{BC} < 0$ the peaks of Z are broadened while being reduced in height, whereas for $g_{BC} > 0$ a smaller width of the residue distribution is encountered compared to $N_C = 1$. The effect of the additional impurity can be evinced in the strong suppression of the peak height of Z for all finite impurity-bath couplings g_{BC} (e.g. a reduction by $\sim 50\%$ for $g_{BC} = -1$), signalling stronger coherence losses when compared to the $N_C = 1$ scenario [73]. Consequently, this leads to a decreasing polaronic residue Z . In the case of $N_C = 2$ the question regarding their effective interactions mediated by the hosts and being naturally related to their relative distance arises. For this reason we analyze the experimentally tractable [76] impurity distance [35, 77, 80]

$$r_{12} = \int \int dx_1 dx_2 |x_1 - x_2| \rho_{CC}^{(2)}(x_1, x_2), \quad (6)$$

with $\rho_{CC}^{(2)}(x_1, x_2)$ being the two-body density of two impurities which is defined as

$$\rho_{CC}^{(2)}(x_1, x_2) = \langle \Psi | \hat{\Psi}_C^\dagger(x_1) \hat{\Psi}_C^\dagger(x_2) \hat{\Psi}_C(x_1) \hat{\Psi}_C(x_2) | \Psi \rangle. \quad (7)$$

This quantity can be interpreted as the probability of finding simultaneously one impurity at position x_1 and the other one at x_2 . Around $g_{AC} = 0$ we find a peak of the impurities' distance, which is most pronounced for $g_{BC} = 0$, $g_{BC} = 0.5$ and the binary system [Fig. 3 (b)]. In all cases the manifestation of attractive induced interactions mediated by the hosts is evident by the decreasing behavior of r_{12} for finite g_{AC} . Accordingly, the strength of the induced interactions in the region of the existence of the polaron becomes stronger when considering two hosts. More precisely r_{12} features a decreasing trend towards zero for $g_{AC} < 0$, while for $g_{AC} > 0$ it saturates to a finite value. These finite values of r_{12} barely differ from each other for $g_{BC} \geq 0$ and in the case of the binary system. In sharp contrast, for $g_{BC} < 0$ a saturation towards smaller distances is observed, indicating that the impurities lie closer with respect to one another.

In order to clarify whether indeed induced interactions are established, we further investigate the impurities' spatial configuration invoking their two-body density [Eq. 7]. Note that the actual profile of the induced interaction has only been recovered for small interspecies entanglement, corresponding to weak impurity-medium couplings, in binary systems [38]. For triple mixture settings the structure and strength of the induced interactions are completely unexplored. Let us first discuss the interaction regime in which r_{12} is independent of $g_{AC} < 0$ [Fig. 3 (b)]. As a characteristic example we present $\rho_{CC}^{(2)}$ for $g_{AC} = -2.1$ and $g_{BC} = -1$ [Fig. 3 (c)]. Here, the two impurities lie together at the trap center and the probability to be located at different positions is reduced, yielding an elongated pattern along $x_1 = x_2$. Hence, the impurities experience an induced interaction due to the cumulative bath. Importantly, this shrinking along the anti-diagonal of $\rho_{CC}^{(2)}$ is indicative of a bound state having formed between the impurities known as a bipolaron state [78–80]. Turning now to the case of $g_{AC} > 0$ for $g_{BC} = 2$ [Fig. 3 (d)] it is possible to infer that the impurities form a shell structure, indicating a phase-separation with their hosts. Moreover, they tend to occupy the same position, residing in a particular side of the appearing shell [39]. A slight elongation as for $g_{BC} = -1$ and $g_{AC} = -2.1$ [Fig. 3 (c)] is also visible. Apart from forming a smaller shell structure for $g_{BC} = -1$ and $g_{AC} = 8$ [Fig. 3 (e)] the off-diagonal contribution is suppressed as compared to $g_{BC} = 2$ and $g_{AC} = 8$ [Fig. 3 (d)], indicating the enhancement of the impurities induced interactions. This explains the saturation of r_{12} towards a smaller value as compared to $g_{BC} = 2$ [Fig. 3 (b)]. In this sense, it is possible to steer the strength of the induced interactions by varying g_{BC} as well as the width

of the shell structure formed by the impurities.

Conclusions.- We have revealed that triple mixtures provide an ideal testbed for emergent polaronic properties with more flexibility as compared to binary systems since they allow for coupling the impurities selectively to the individual hosts. For a single impurity interacting with a correlated Bose-Bose mixture we unravel that the width of the quasiparticle residue distribution and peak can be controlled, such that the polaron state can be maintained for larger impurity-medium couplings as compared to the binary system. In the case of two impurities we exemplify the appearance of induced interactions, which can be changed by tuning the coupling to the respective bosonic host and strongly influences the impurities' spatial distribution. Our results pave the way for controlling the quasiparticle character and induced interactions as well as to expose the role of correlations in triple mixture settings. The latter lays the foundations for studying related quantum phase transitions and pattern formation. Another intriguing step would be to consider the sudden injection of the impurity species [75] into the Bose-Bose mixture for the simulation of spectroscopic techniques [72–74] in order to unravel the polaron dynamics. The generalization of our findings to higher-dimensional settings, where topological effects play an important role, is certainly a valuable perspective.

The authors thank C. Weitenberg for a detailed feedback on the manuscript. P. S. gratefully acknowledges funding by the Deutsche Forschungsgemeinschaft in the framework of the SFB 925 "Light induced dynamics and control of correlated quantum systems". K. K. gratefully acknowledges a scholarship of the Studienstiftung des deutschen Volkes. S. I. M gratefully acknowledges financial support in the framework of the Lenz-Ising Award of the University of Hamburg.

-
- [1] S. Inouye, J. Goldwin, M.L. Olsen, C. Ticknor, J.L. Bohn, and D.S. Jin, *Phys. Rev. Lett.* **93**, 183201 (2004).
- [2] T. Fukuhara, S. Sugawa, Y. Takasu, and Y. Takahashi, *Phys. Rev. A* **79**, 021601 (2009).
- [3] C. Chin, R. Grimm, P. Julienne, and E. Tiesinga, *Rev. Mod. Phys.* **82**, 1225 (2010).
- [4] A. N. Wenz, G. Zürn, S. Murmann, I. Brouzos, T. Lompe, and S. Jochim, *Science* **342**, 457 (2013).
- [5] P. Massignan, M. Zaccanti, and G. M. Bruun, *Rep. Prog. Phys.* **77**, 034401 (2014).
- [6] C. Kohstall, M. Zaccanti, M. Jag, A. Trenkwalder, P. Massignan, G.M. Bruun, F. Schreck, and R. Grimm, *Nature* **485**, 615 (2012).
- [7] M. Koschorreck, D. Pertot, E. Vogt, B. Fröhlich, M. Feld, and M. Köhl, *Nature* **485**, 619 (2012).
- [8] F. Scazza, G. Valtolina, P. Massignan, A. Recati, A. Amico, A. Burchianti, C. Fort, M. Inguscio, M. Zaccanti, and G. Roati, *Phys. Rev. Lett.* **118**, 083602 (2017).
- [9] L. D. Landau, *Phys. Z. Sowjetunion* **3**, 644 (1933).
- [10] F. Grusdt, and E. Demler, *New theoretical approaches to Bose polarons. Quantum Matter at Ultralow Temperatures* **191**, 325 (2015).
- [11] R. Schmidt, M. Knap, D.A. Ivanov, J.S. You, M. Cetina, and E. Demler, *Rep. Progr. Phys.* **81**, 024401 (2018).
- [12] M. E. Gershenson, V. Podzorov, and A. F. Morpurgo, *Rev. Mod. Phys.* **78**, 973 (2006).
- [13] S. T. Ruggiero, and D. A. Rudman, eds., *Superconducting Devices* (Academic, Boston, 1990).
- [14] J. Bardeen, G. Baym, and D. Pines, *Phys. Rev.* **156**, 207 (1967).
- [15] G. Baym, and C. Pethick, *Landau Fermi-Liquid Theory: Concepts and Applications* (Wiley-VCH, 1991).
- [16] D. J. Scalapino, *Phys. Rep.* **250**, 329 (1995).
- [17] J. Sous, M. Chakraborty, R.V. Krems, and M. Berciu, *Phys. Rev. Lett.* **121**, 247001 (2018).
- [18] L. N. Cooper *Phys. Rev.* **104**, 1189 (1956).
- [19] J. R. Schrieffer, *Theory of Superconductivity*, Advanced Book Program Series (Avalon, New York, 1983).
- [20] A. S. Alexandrov, and A. B. Krebs, *Sov. Phys. Usp.*, 35345 (1992).
- [21] N. F. Mott, *J. Phys. Cond. Matt.* **5**, 3487 (1993).
- [22] A. S. Alexandrov, and N. F. Mott, *Rep. Prog. Phys.* **57**, 1197 (1994).
- [23] E. K. Salje, A. S. Alexandrov, and W. Y. Liang, *Polarons and bipolarons in high- T_c superconductors and related materials*, (Cambridge University Press, 2005).
- [24] M. Berciu, I. Elfimov, and G. A. Sawatzky, *Phys. Rev. B* **79**, 214507 (2009).
- [25] J. Catani, G. Lamporesi, D. Naik, M. Gring, M. Inguscio, F. Minardi, A. Kantian, and T. Giamarchi, *Phys. Rev. A* **85**, 023623 (2012).
- [26] T. Fukuhara, A. Kantian, M. Endres, M. Cheneau, P. Schaul, S. Hild, D. Bellem, U. Schollwöck, T. Giamarchi, C. Gross, I. Bloch, and S. Kuhr, *Nat. Phys.* **9**, 235 (2013).
- [27] A. G. Volosniev and H.-W. Hammer, *Phys. Rev. A* **96**, 031601(R) (2017).
- [28] K. Sacha, and E. Timmermans, *Phys. Rev. A* **73**, 063604 (2006)
- [29] F. Grusdt, G. E. Astrakharchik, and E. A. Demler, *New J. Phys.* **19**, 103035 (2017).
- [30] D.C. Khandekar, K.V. Bhagwat, and S.V. Lawande, *Phys. Rev. B* **37**, 3085 (1988).
- [31] L.P. Ardila, and S. Giorgini, *Phys. Rev. A* **92**, 033612 (2015).
- [32] M. Cetina, M. Jag, R.S. Lous, I. Fritsche, J.T. Walraven, R. Grimm, J. Levinsen, M.M. Parish, R. Schmidt, M. Knap, and E. Demler, *Science* **354**, 96 (2016).
- [33] H. Tajima, and S. Uchino, *Phys. Rev. A* **99**, 063606 (2019).
- [34] A. S. Dehkharghani, A. G. Volosniev and N. T. Zinner, *Phys. Rev. A* **92**, 031601(R) (2015).
- [35] S.I. Mistakidis, G.C. Katsimiga, G.M. Koutentakis, and P. Schmelcher, *New J. Phys.* **21**, 043032 (2019).
- [36] K. Keiler, S. Krönke, and P. Schmelcher, *New J. Phys.* **20**, 033030 (2018).
- [37] K. Keiler and P. Schmelcher, *New J. Phys.* **20**, 103042 (2018).
- [38] J. Chen, J. M. Schurer, and P. Schmelcher, *Phys. Rev. Lett.* **121**, 043401 (2018).
- [39] A. S. Dehkharghani, A. G. Volosniev, and N. T. Zinner, *Phys. Rev. Lett.* **121**, 080405 (2018).
- [40] E. Compagno, G. De Chiara, D.G. Angelakis, and G.M. Palma, *Sci. Rep.* **7**, 2355 (2017).

- [41] C. Charalambous, M. A. García-March, Gorka Muñoz-Gil, P. R. Grzybowski, M. Lewenstein, *Quantum* **4**, 232, (2020).
- [42] A. Boudjemâa, N. Guebli, M. Sekmane and S. Khelifa-Karfa, *J. Phys.: Condens. Matter* **32**, 415401, (2020).
- [43] J. Levinsen, M. M. Parish, and G. M. Bruun, *Phys. Rev. Lett.* **115**, 125302 (2015).
- [44] R. S. Christensen, J. Levinsen, and G. M. Bruun, *Phys. Rev. Lett.* **115**, 160401 (2015).
- [45] J. Jäger, R. Barnett, M. Will, and M. Fleischhauer, *Phys. Rev. Research* **2**, 033142 (2020).
- [46] G. E. Astrakharchik, and L. P. Pitaevskii, *Phys. Rev. A* **70**, 013608 (2004).
- [47] F. M. Cucchietti, and E. Timmermans, *Phys. Rev. Lett.* **96**, 210401 (2006).
- [48] R. M. Kalas, and D. Blume, *Phys. Rev. A* **73**, 043608 (2006).
- [49] M. Bruderer, A. Klein, S. R. Clark, and D. Jaksch, *EPL* **82**, 30004 (2008).
- [50] M. Bruderer, A. Klein, S. R. Clark, and D. Jaksch, *Phys. Rev. A* **76**, 011605(R) (2007).
- [51] A. Privitera, and W. Hofstetter, *Phys. Rev. A* **82**, 063614(2010).
- [52] W. Casteels, J. Tempere, and J. T. Devreese, *Phys. Rev. A* **86**, 043614 (2012).
- [53] W. Casteels, J. Tempere, and J. T. Devreese, *Phys. Rev. A* **88**, 013613 (2013).
- [54] B. Kain, and H. Y. Ling, *Phys. Rev. A* **94**, 013621 (2016).
- [55] W. Li, and S. Das Sarma, *Phys. Rev. A* **90**, 013618 (2014).
- [56] Y. E. Shchadilova, R. Schmidt, F. Grusdt, and E. Demler, *Phys. Rev. Lett.* **117**, 113002 (2016).
- [57] S. P. Rath, and R. Schmidt, *Phys. Rev. A* **88**, 053632 (2013).
- [58] X. Li, G. Bighin, E. Yakaboylu, and M. Lemesko, *Mol. Phys.* **117**, 1981 (2019).
- [59] B. Kain, and H. Y. Ling, *Phys. Rev. A* **98**, 033610 (2018).
- [60] F. Grusdt, R. Schmidt, Y. E. Shchadilova, and E. Demler, *Phys. Rev. A* **96**, 013607 (2017).
- [61] F. Serwane, G. Zürn, T. Lompe, T.B. Ottenstein, A.N. Wenz, and S. Jochim, *Science* **332**, 336 (2011).
- [62] A.N. Wenz, G. Zürn, S. Murmann, I. Brouzos, T. Lompe, and S. Jochim, *Science* **342**, 457 (2013).
- [63] See Supplemental Material at [URL] for the description of 1) the ML-MCTDHX method; 2) the impurity correlations and densities; 3) the predictions of the mean-field ansatz; 4) the properties of heavy impurities and the effect of larger baths and 5) homogeneous settings.
- [64] K. Henderson, C. Ryu, C. MacCormick, and M. G. Boshier, *New J. Phys.* **11**, 043030 (2009).
- [65] R. Grimm, M. Weidemüller, and Y.B. Ovchinnikov, *Adv. At. Mol. Opt. Phys.* **42** 95 (2000).
- [66] M. Olshanii, *Phys. Rev. Lett.* **81**, 938 (1998).
- [67] M. Egorov, B. Opanchuk, P. Drummond, B. V. Hall, P.Hannaford, and A. I. Sidorov, *Phys. Rev. A* **87**, 053614 (2013).
- [68] A. Álvarez J. Cuevas, F. R. Romero, C. Hamner, J. J. Chang, P. Engels, P. G. Kevrekidis and D. J. Frantzeskakis, *J. Phys. B: At. Mol. Opt. Phys.* **46**, 065302 (2013)
- [69] S. Krönke, L. Cao, O. Vendrell, and P. Schmelcher, *New J. Phys.* **15**, 063018 (2013).
- [70] L. Cao, S. Krönke, O. Vendrell, and P. Schmelcher, *J. Chem. Phys.* **139**, 134103 (2013).
- [71] L. Cao, V. Bolsinger, S.I. Mistakidis, G. Koutentakis, S. Krönke, J.M. Schurer, and P. Schmelcher, *J. Chem. Phys.* **147**, 044106 (2017).
- [72] A. Amico, F. Scazza, G. Valtolina, P. E. S. Tavares, W.Ketterle, M. Inguscio, G. Roati, and M. Zaccanti, *Phys. Rev. Lett.* **121**, 253602 (2018).
- [73] S.I. Mistakidis, G.C. Katsimiga, G.M. Koutentakis, Th. Busch, and P. Schmelcher, *Phys. Rev. Research* **2**, 033380 (2020).
- [74] D. Dzsojtjan, R. Schmidt, and M. Fleischhauer, *Phys. Rev. Lett.* **124**, 223401 (2020).
- [75] S. I. Mistakidis, G. C. Katsimiga, G. M. Koutentakis, Th. Busch, and P. Schmelcher, *Phys. Rev. Lett.* **122**, 183001 (2019).
- [76] A. Bergschneider, V. M. Klinkhamer, J. H. Becher, R. Klemt, G. Zürn, P. M. Preiss, and S. Jochim, *Phys. Rev. A* **97**, 063613 (2018).
- [77] K. Keiler, S. I. Mistakidis, and P. Schmelcher, *New J. Phys.* **22**, 083003 (2020).
- [78] A. Camacho-Guardian, L. P. Ardila, T. Pohl, and G.M. Bruun, *Phys. Rev. Lett.* **121**, 013401 (2018).
- [79] A. Klein and M. Fleischhauer, *Phys. Rev. A* **71**, 033605 (2005).
- [80] S.I. Mistakidis, G.M. Koutentakis, G.C. Katsimiga, Th. Busch, and P. Schmelcher, *New J. Phys.* **22**, 043007 (2020).

Supplemental Material: Polarons and their induced interactions in highly imbalanced triple mixtures

VARIATIONAL MANY-BODY APPROACH: ML-MCTDHX

Our approach to determine the ground state properties of the triple mixture relies on the *ab-initio* Multi-Layer Multi-Configuration Time-Dependent Hartree method for bosonic (fermionic) mixtures (ML-MCTDHX) [S1–S3], which accounts for all the relevant interparticle correlations [S4–S9]. As a first step, the total many-body (MB) wave function $|\Psi(t)\rangle$ is expanded in M_σ species functions $|\Psi^\sigma(t)\rangle$ of species σ

$$|\Psi(t)\rangle = \sum_{ijk=1}^{M_A, M_B, M_C} A_{ijk} |\Psi_i^A(t)\rangle \otimes |\Psi_j^B(t)\rangle \otimes |\Psi_k^C(t)\rangle, \quad (\text{S1})$$

where the coefficients A_{ijk} account for interspecies correlations [S10]. Furthermore, in order to capture the correlations within each component the species wave functions $|\Psi^\sigma(t)\rangle$ describing an ensemble of N_σ bosons are expanded in a set of permanents

$$|\Psi_i^\sigma(t)\rangle = \sum_{\vec{n}^\sigma | N_\sigma} C_{\sigma\vec{n}}(t) \cdot |\vec{n}^\sigma; t\rangle, \quad (\text{S2})$$

Here, the vector $\vec{n}^\sigma = (n_1^\sigma, n_2^\sigma, \dots)$ denotes the occupations of the time-dependent single-particle functions of the σ species. The notation $\vec{n}^\sigma | N_\sigma$ indicates that for each $|\vec{n}^\sigma; t\rangle$ we require the condition $\sum_i n_i^\sigma = N_\sigma$. The time propagation of the MB wave function is achieved by employing the Dirac-Frenkel variational principle $\langle \delta\Psi | (i\partial_t - \mathcal{H}) | \Psi \rangle$ [S11–S13] with the variation $\delta\Psi$. ML-MCTDHX provides access to the complete MB wave function of the triple mixture which consequently allows us to derive all relevant characteristics of the underlying system. As such we are able, among others, to characterize the system by projecting onto number states with respect to an appropriate single-particle basis [S14, S15]. Besides investigating the quantum dynamics it allows us to determine the ground (or excited) states by using either imaginary time propagation or improved relaxation [S16], thereby being able to uncover also possible degeneracies of the involved MB states. We remark that in commonly used approaches for solving the time-dependent Schrödinger equation, one typically constructs the wave function as a superposition of time-independent Fock states with time-dependent coefficients. Instead, it is important to note that the ML-MCTDHX approach considers a co-moving time-dependent basis on different layers, meaning that in addition to time-dependent coefficients the single particle functions spanning the number states are also time-dependent. This leads to a significantly smaller number of basis states and configurations that are needed to

obtain an accurate description of the system under consideration and thus renders the treatment of mesoscopic systems feasible [S17].

The degree of truncation of the underlying Hilbert space is given by the orbital configuration $C = (M_A, M_B, M_C, d_A, d_B, d_C)$. Here, M_σ refers to the number of species functions in Eq. S1, while d_σ with $\sigma \in \{A, B, C\}$ denote the number of single-particle functions spanning the time-dependent number states $|\vec{n}^\sigma; t\rangle$ (cf. equation S2). The orbital configuration $C = (6, 6, 6, 4, 4, 6)$ has been employed for all MB calculations presented in the main text, yielding a converged behavior of our observables.

CORRELATIONS OF THE TRIPLE MIXTURE AND EMERGENT PHASE-SEPARATION IN THE SPATIAL DISTRIBUTIONS

Further insight into the underlying processes related to the polaron properties can be gained by analyzing the spatial distribution of the three species in terms of the one-body density of the ground state $|\Psi\rangle$ of the species $\sigma = A, B, C$, which is defined as

$$\rho_\sigma^{(1)}(x) = \langle \Psi | \hat{\Psi}_\sigma^\dagger(x) \hat{\Psi}_\sigma(x) | \Psi \rangle. \quad (\text{S3})$$

The spectral decomposition of the one-body density of species σ reads

$$\rho_\sigma^{(1)}(x) = \sum_j n_{\sigma j} \Phi_{\sigma j}^*(x) \Phi_{\sigma j}(x), \quad (\text{S4})$$

where $n_{\sigma j}(t)$ in decreasing order, obeying $\sum_j n_{\sigma j} = 1$, are the so-called natural populations and $\Phi_{\sigma j}(x, t)$ the corresponding natural orbitals. In this sense, the σ -species natural orbitals are the eigenstates, while the natural populations are the corresponding eigenvalues [S16], which are determined by diagonalizing the σ -species one-body reduced density matrix. The natural populations serve as a measure for the correlations in a subsystem. Accordingly, in order to quantify the degree of correlations or fragmentation we resort to the σ -species entropy [S7, S8, S18] defined as

$$S_\sigma(t) = - \sum_j n_{\sigma j}(t) \ln(n_{\sigma j}(t)). \quad (\text{S5})$$

Here, the case of $S_\sigma = 0$ indicates that the subsystem σ is not depleted, implying that all particles occupy the same single particle state, i.e. $n_{\sigma 1} = 1$. Fig. S1 (a)-(c) shows the fragmentation S_σ for the respective species in the case of $N_C = 1$ and $N_A = N_B = 10$. For $g_{BC} > 0$ we observe

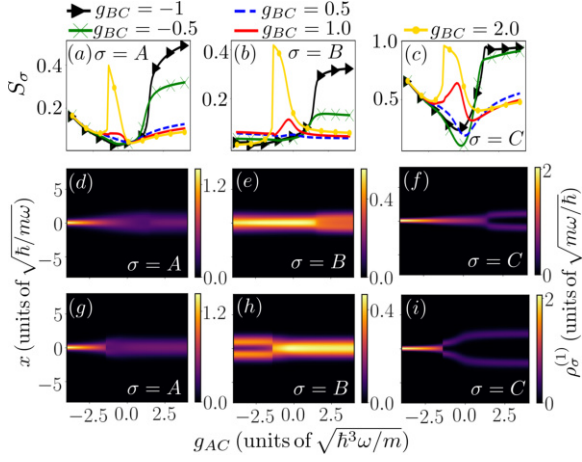


FIG. S1. (a) - (c) Entropy S_σ for varying g_{AC} and g_{BC} quantifying the degree of intraspecies correlations. (d)-(f) One body density $\rho_\sigma^{(1)}(x)$ for $g_{BC} = -1$ (middle row) and $g_{BC} = 2$ (lower row) for different impurity-bath couplings g_{AC} , showcasing that e.g. for $g_{AC} = -3$, $g_{BC} = -1$ the impurity lies in their hosts, while for $g_{AC} = 3$, $g_{BC} = -1$ a phase-separation occurs. Here $g_{AA} = g_{BB} = 0.2$, $g_{AB} = 0.1$, $m_A = m_B = m_C$, $N_A = N_B = 10$ and $N_C = 1$.

a minor increase (decrease) of S_A (S_B) towards repulsive and attractive values of g_{AC} , whereas the impact on S_C is more pronounced. Attractive impurity-host couplings g_{BC} lead to a drastic increase of all S_σ for repulsive g_{AC} . This behavior of the fragmentation can also be observed in the context of the occupation of the states $|\Phi_i\rangle$ in the effective potential V_{eff} [see Fig. 2]. Due to the emergent strong correlations a correlated approach, such as ML-MCTDHX, is needed in order to properly describe the system.

Moreover, the existence of correlations is imprinted in the spatial distribution of the mixture and the impurity. Recall that for a single impurity interspecies correlations (entanglement) between the impurity and the cumulative bath (Bose-Bose mixture) are accounted for by S_C . For strongly repulsive g_{AC} the impurity forms a shell structure [Fig. S1 (f),(i)] and a phase-separation can be observed. The separation of the shell is smaller for attractive g_{BC} as compared to repulsive ones due to the attraction to the B species. This attraction also leads to the formation of a less pronounced shell structure in the B species and thereby enhances the overlap with the impurity. We can interpret this as a weak phase-separation between the A species and the B species as well as the impurity species with both hosts [Fig. S1 (d)-(f)]. As a result the fragmentation is significantly increased. However, for $g_{BC} > 0$ and large repulsive g_{AC} the phase-separation takes place between the impurity and the cumulative bath, while the two hosts remain miscible [Fig. S1 (g)-(i)], a process that leads to a smaller fragmen-

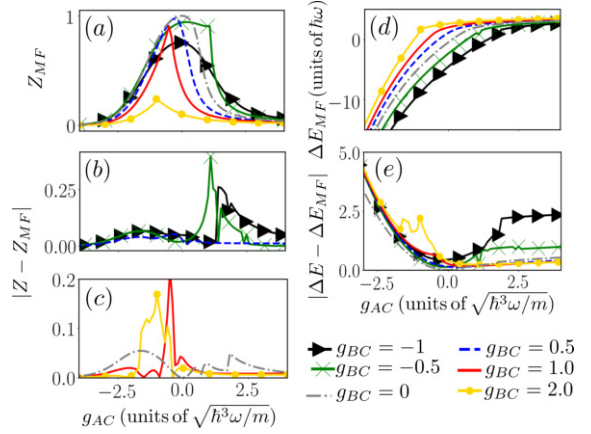


FIG. S2. Polaron (a) residue Z , (d) binding energy ΔE for different impurity-bath couplings g_{AC} and g_{BC} employing a mean-field ansatz. Absolute difference for (b), (c) the residue $|Z - Z_{MF}|$ and (e) the deviation of the binding energy $|\Delta E - \Delta E_{MF}|$ between employing the MF ansatz and the MB treatment for varying g_{AC} and g_{BC} . The same system parameters as in Fig. S1 are used.

tation in all cases. The peak in the relevant entropic measures for $g_{BC} = 2$ and weakly attractive g_{AC} is due to the formation of a shell structure in the A species and the impurity species, similar to the case of $g_{BC} < 0$ and strongly repulsive g_{AC} .

POLARON PROPERTIES IN THE MEAN-FIELD FRAMEWORK

As it becomes evident from Eqs. S1, S2, ML-MCTDHX is able to operate within different approximation orders. For instance, it reduces to the set of coupled mean-field (MF) Gross-Pitaevskii equations of motion when $C = (1, 1, 1, 1, 1)$. Moreover, in case that $A_{111} = 1$ the species A, B and C are not entangled [S10] but intraspecies correlations can be taken into account. As a result the system is described within a species mean-field approximation (SMF) corresponding to a single product state ansatz, characterized by $M_A = M_B = M_C = 1$ [S19]. In the following we aim to reveal the necessity of a fully correlated approach, i.e. accounting for all the emergent intra- and interspecies correlations, for determining the ground state of the polaron. In this sense, as we shall demonstrate a standard MF ansatz is not sufficient for describing the polaronic properties e.g. discussed in Fig 1. To validate this assumption, we subsequently determine the ground state employing a MF ansatz, $C = (1, 1, 1, 1, 1)$, and calculate the polaron residue as well as its binding energy [Fig. S2]. Qualitatively we find a similar behavior of the residue distribution Z_{MF} [Fig. S2 (a)], using a MF

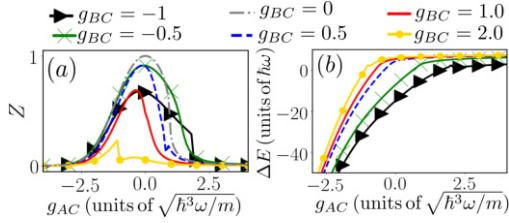


FIG. S3. Polaron (a) residue Z for $m_A/m_C = 87/174$ and $N_A = N_B = 10$, (b) binding energy ΔE for $m_A/m_C = 1$ and $N_A = N_B = 50$ upon varying the impurity-bath couplings g_{AC} and g_{BC} . The other system parameters are the same as in Fig. S1.

ansatz, for the different impurity-medium couplings g_{AC} and g_{BC} as compared to the residue where the underlying MB wavefunction, taking correlations into account, has been considered [see Fig. 1 (a)]. Hence, the broadening of the residue distribution for $g_{BC} < 0$ which effectively leads to a stabilization of the polaronic character for larger interactions can also be predicted using a MF ansatz. However, upon investigating the absolute difference $|Z - Z_{MF}|$ we quantitatively identify strong deviations between the two distributions for various g_{AC} and g_{BC} [Fig. S2 (b),(c)]. Consequently, the MF ansatz over- or underestimates the residue distribution at specific interaction intervals. For strong repulsive or attractive impurity-host couplings g_{AC} a comparison is not adequate since in both cases, i.e. MF and MB, there is a phase-separation of the impurity with their hosts. Turning now to the polaron binding energy, employing a MF ansatz [Fig. S2 (d)] we find a clear hierarchy of the polaronic resonances as already discussed in Fig. 1 (c). Considering the absolute difference $|\Delta E - \Delta E_{MF}|$ with respect to the MB treatment we capture also here a quantitative deviation between the two approaches [Fig. S2 (e)]. In particular, for $g_{AC} < 0$ the deviation $|\Delta E - \Delta E_{MF}|$ increases with decreasing g_{AC} , while for repulsive g_{AC} it saturates towards a finite value with increasing g_{AC} . Only for weak impurity-bath couplings the MF approach is able to reproduce binding energies which are close to the ones using a full MB treatment. In case of a SMF approximation we find deviations $|Z - Z_{SMF}|$ and $|\Delta E - \Delta E_{SMF}|$ which are very similar to the ones observed for a MF ansatz (not shown here for brevity). This evinces that indeed interspecies correlations play a crucial role in the polaron formation.

HEAVY IMPURITIES AND LARGER HOSTS

Our findings regarding e.g. the polaron residue are not limited to the case of a mass-balanced triple mixture, i.e. $m_A = m_B = m_C$ [Fig. 1 (a)], but can also be generalized for heavier impurities, namely ^{133}Cs or ^{174}Yb such

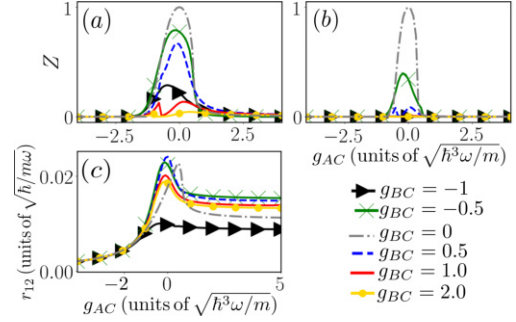


FIG. S4. Polaron residue Z for (a) $N_C = 1$, (b) $N_C = 2$ and (c) impurity distance r_{12} for $N_C = 2$ upon varying the impurity-bath couplings g_{AC} and g_{BC} . All species solely experience a box potential. The other system parameters are the same as in Fig. S1.

that $m/m_C = 87/133$ and $m/m_C = 87/174$, respectively. As an example we will discuss the case of ^{174}Yb and determine the residue according to Eq. 2. Fig. S3 (a) presents Z upon variation of the impurity-medium coupling strengths g_{AC} and g_{BC} . Qualitatively, the residue distribution is similar to the case of equal masses, while exhibiting slightly larger (smaller) widths for $g_{BC} < 0$ ($g_{BC} > 0$). We solely find minor quantitative deviations between a ^{174}Yb and a ^{87}Rb impurity. Importantly, this implies that also for heavier impurities the quasiparticle character can be maintained for larger couplings g_{AC} when $g_{BC} < 0$, while for $g_{BC} > 0$ the width of the residue distribution with respect to g_{AC} is smaller as compared to $g_{BC} = 0$.

State-of-the-art ultracold atom experiments are often of mesoscopic character and consist of $\simeq 100$ particles. For this reason, we compute the polaron binding energy for a larger cumulative bath with $N_A = N_B = 50$ bosons [Fig. S3 (b)]. Similar to the case of $N_A = N_B = 10$ [Fig. 1 (c)], ΔE decreases towards attractive g_{AC} and saturates for repulsive ones. The latter can again be attributed to the phase-separation of the impurity with respect to its hosts, where the impurity forms a shell-structure. The clear hierarchy of ΔE in terms of g_{AC}, g_{BC} can be retrieved for larger hosts, such that the polaronic resonances are well distinguishable from each other e.g. using radiofrequency schemes. Note that the polaron binding energies are strongly reduced, suggesting an increased effective mass, for a large range of impurity-medium couplings g_{AC} as compared to $N_A = N_B = 10$.

POLARONS IN HOMOGENEOUS SETTINGS

In our work we demonstrate the Bose polaron properties in a cumulative bath by explicitly accounting for trap effects in terms of a harmonic confinement. These are almost inevitable in contemporary experiments of cold

atomic settings. To underline the importance of including an external trapping potential we examine its impact on the polaronic properties when considering solely a box potential. Specifically, we omit the terms $\frac{1}{2}m_\sigma\omega_\sigma^2x^2$, $\sigma \in \{A, B, C\}$, in the Hamiltonian [Eq. 1], while keeping the hard wall boundary conditions. The other system parameters remain the same to those utilized in the main text.

As a first step, we determine the polaron residue for a single impurity immersed in a Bose-Bose mixture upon varying the involved impurity-medium coupling strengths [Fig. S4 (a)]. It can be readily seen that the distribution of Z with respect to g_{AC} is significantly reduced as compared to the trap scenario depicted in Fig. 1 (a). Indeed, for all g_{BC} the peak height as well as the width of the residue distribution are strongly reduced. E.g. while in the trapped case [Fig. 1 (a)] for $g_{BC} = 1$ the peak of the Z -distribution is rather pronounced, neglecting the harmonic confinement leads to a drastic decrease such that the peak is barely visible. Moreover, the increased width of the residue distribution for $g_{BC} < 0$ as compared to $g_{BC} = 0$ cannot be recovered. Hence, the polaron state cannot be maintained for larger impurity-medium couplings when considering solely a box potential. The effect on Z is even more dramatic for $N_C = 2$ impurities [Fig. 3 (b)]. Here, only for $g_{BC} = 0$ and $g_{BC} = -0.5$ a polaron state exists when considering weak impurity-bath couplings g_{AC} [Fig. S4 (b)]. Interestingly, the impurity distance r_{12} is less affected by the presence of the external potential [Fig. S4 (c)]. Here, we qualitatively find a similar behavior to the case of a harmonic confinement [Fig. 3 (c)]. Namely, r_{12} features a decreasing trend towards zero for $g_{AC} < 0$, while for $g_{AC} > 0$ it saturates to a finite value for all g_{BC} . For $g_{AC} < 0$ again a shrinking along the anti-diagonal of $\rho_{CC}^{(2)}$ appears, being indicative of bipolaron formation, while for $g_{AC} > 0$

the impurities form a shell structure, indicating a phase separation with their hosts (not shown here for brevity). Nevertheless, we observe a quantitative change of the values of r_{12} when neglecting the harmonic confinement, resulting e.g. in an increase of the impurity distance for large g_{AC} in the case of $g_{BC} = -0.5$.

-
- [S1] S.I. Mistakidis, G.C. Katsimiga, P.G. Kevrekidis, and P. Schmelcher, *New J. Phys.* **20**, 043052 (2018).
 - [S2] J. Erdmann, S. I. Mistakidis, and P. Schmelcher, *Phys. Rev. A* **98**, 053614 (2018).
 - [S3] J. Erdmann, S. I. Mistakidis, and P. Schmelcher, *Phys. Rev. A* **99**, 013605 (2019).
 - [S4] R. Roy, A. Gammal, M. C. Tsatsos, B. Chatterjee, B. Chakrabarti, and A. U. J. Lode, *Phys. Rev. A* **97**, 043625 (2018).
 - [S5] B. Chatterjee, M. C. Tsatsos and A. U. J. Lode, *New J. Phys.* **21**, 033030 (2019).
 - [S6] P. Siegl, S. I. Mistakidis, and P. Schmelcher, *Phys. Rev. A* **97**, 053626 (2018).
 - [S7] R. Horodecki, P. Horodecki, M. Horodecki, and K. Horodecki, *Rev. Mod. Phys.* **81**, 865 (2009).
 - [S8] P. A. M. Dirac, *Proc. Camb. Phil. Soc.* **26**, 376 (1930).
 - [S9] J. Frenkel, *Wave Mechanics; Advanced General Theory Clarendon Press, Oxford* (1934).
 - [S10] A. Raab, *Chem. Phys. Lett.* **319**, 674 (2000).
 - [S11] L. Cao, I. Brouzos, S. Zöllner, and P. Schmelcher, *New J. Phys.* **13**, 033032 (2011).
 - [S12] L. Cao, I. Brouzos, B. Chatterjee, and P. Schmelcher, *New J. Phys.* **14**, 093011 (2012).
 - [S13] H.-D. Meyer, F. Gatti, and G. A. Worth. *Multidimensional Quantum Dynamics: MCTDH Theory and Applications, Wiley-VCH* (2009).
 - [S14] F. Köhler, K. Keiler, S. I. Mistakidis, H.-D. Meyer, P. Schmelcher, *J. Chem. Phys.* **151**, 054108 (2019).
 - [S15] K. Keiler, and P. Schmelcher, *Phys. Rev. A* **100**, 043616 (2019).
 - [S16] F. Theel, K. Keiler, S.I. Mistakidis, and P. Schmelcher, *New J. Phys.* **22**, 023027 (2020).

Conclusions and Outlook

In this cumulative dissertation we have investigated the stationary and dynamical properties of one-dimensional ultracold atomic mixtures at zero temperature. We have focused on highly imbalanced bosonic mixtures and exploited the possibility of choosing different trapping geometries in order to induce a specific response in the system. In particular, we aimed at studying the role of intra- and interspecies correlations for engineering ground states and the non-equilibrium dynamics after performing a corresponding quench. In this sense, we characterized the microscopic origin of the underlying processes and linked this to the respective correlations present in the system. In the following final chapter, we provide the highlights of the projects on which the current thesis is based on and motivate further research directions.

Lattice trapped impurities immersed in a Bose gas

As a starting point we explored the ground state properties of lattice trapped impurities interacting repulsively with a Bose gas. Under variation of the lattice depth and the interspecies interaction strength we found a transition from an uncorrelated to a strongly correlated regime in [1]. By projecting the variationally optimized many-body wave function onto number states spanned by either Bloch or Wannier states we were able to relate the formation of correlations to specific structural changes of the wave function. As such, for small lattice depths and interspecies interaction strengths all impurities essentially occupied the energetically lowest Bloch band, while in the correlated regime all particles clustered in a single lattice site. In the latter case, the ground state is given by a superposition of all possibilities to accumulate the impurities in a single site due to the translational symmetry. For weak coupling strengths we provided an energetic argument for the transition to the correlated state. Hence, we attributed the clustering of the impurities to excitations referring to an occupation of the excited states in the lowest band induced by the interspecies energy per particle. Finally, we introduced an effective Hamiltonian to further understand the clustering of the impurities, thereby identifying an induced hopping and an induced attractive on-site interaction which are responsible for the impurity localization [321].

A natural extension of this study involves impurities trapped in a two-dimensional finite lattice and immersed in a Bose gas. Such a change of dimensionality is likely to alter the transition region as well as the resulting induced interaction thereby favoring localization processes of next-neighbor kind [182]. Moreover, it would be interesting to generate excitations of the impurities into higher bands in order to study the impact on the induced interaction

and resultingly on the clustering process. This could be achieved for example by increasing the number of impurities as well as the intraspecies interaction strength. For a specific filling and interaction among the impurities it might thus be favorable to additionally cluster in excited Wannier states. Beyond that, it is of particular interest to study the dynamical response of such correlated states, e.g. by quenching across the crossover diagram. Moreover, dynamically driven setups offer a lot of potential with respect to the transport of the impurities, for example in terms of persistent currents [329].

A first step towards the control of the clustering process has been made in [[2]]. Here, we added an additional impurity and exploited the intraspecies interaction strength among the impurities as a control parameter. Due to the presence of the impurities' coupling a far richer crossover diagram for the ground state could be recovered as a function of the interspecies interaction strength and the lattice depth. In particular, two additional configurations as compared to the case of non-interacting impurities were found, namely a localization of all impurities in separate wells with the extra particle being delocalized over the lattice geometry as well as a pairwise localization of the impurities in adjacent sites. The latter can be attributed to the interplay between the repulsive intraspecies impurity coupling of contact type and the attractive induced interaction of long-range character [165, 166] emerging due to the coupling to the medium. Fixing the lattice depth as well as the interspecies coupling, it is possible to traverse different ground state impurity configurations by varying solely the intraspecies coupling among the impurities. The intraspecies coupling strength serves as an additional knob to control the range of existence for the pairwise accumulation scenario of the impurities. By varying the boundary conditions of the system we identified yet another steering mechanism for the ground state configurations. Changing these from periodic to hard-wall boundary conditions [322], the initial threefold degeneracy turned into a twofold one or was even completely lifted depending on the impurity configuration. In order to invert the degeneracies with respect to the configurations, a Gaussian barrier has to be implemented in the center of the trap.

Further research directions of this kind involve the investigation of cluster formation for larger lattices and even different lattice geometries which allow for more exotic impurity configurations. As ML-MCTDHX also allows for a treatment of triple mixture setups it would be of immediate interest to consider a binary impurity species in the lattice immersed in a Bose gas, allowing for the formation of multi-atom clusters of different species and even induced interactions of different nature [182]. In case these multi-atom clusters are not of binary type, they could serve as an effective potential for a further investigation of Anderson localization utilizing ultracold atoms as suggested in [330–332]. Lastly, it is an interesting perspective to use the engineered ground states as a starting point for dynamical particle transfer scenarios, employing for example quench protocols relying on optimal control theory [333]. As a showcase this could involve the preparation of the impurities in a state where they accumulate in a single well and dynamically transferring it to a pairwise localized state, and thereby transporting two particles.

In [[3]] we set ourselves on this route by exploring the dynamical response upon a quench of the interspecies interaction strength. For the dynamics we prepare the system such that the ground state exhibits a pairwise accumulation of impurities in a five well lattice. By lowering the interspecies interaction strength we aimed at inducing a tunneling of the impurity species. For small quench amplitudes the impurities remain localized in their initial configuration. The same happens for a quench to zero interaction such that the Bose gas is transparent to the impurities, thus, being reminiscent of repulsively bound pairs [61]. Indeed, it turns out to be crucial to allow for a finite coupling between the impurities and the Bose gas in order for the impurities

to tunnel to adjacent sites. For sufficiently strong quenches a single impurity tunnels to the neighboring site which we uncovered by performing an analysis of the participating number states during the dynamics. Further increasing the quench amplitude it is possible to extend the tunneling of the single impurity to the next-neighboring unpopulated well. The tunneling of the impurity species is accompanied by strong entanglement between the species as well as intraspecies correlations. Finally, we identified the appearing frequencies in the oscillations of the respective one-body densities and related them to excitation processes by constructing an effective Hamiltonian picture.

A natural next step would be to consider a time-dependent quench protocol, e.g. a linear decrease of the interspecies interaction strength or a driving, to further control the transport of the single impurity or even initiate a tunneling of larger impurity clusters. This systematic ejection of impurities may play an important role in the context of atomtronics. As such, we would explicitly exploit the coupling to an environment for the transport process, in the spirit of quantum-reservoir engineering [197–199]. Another interesting approach involves the implementation of a spin degree in the impurity species, such that the impurities would not only be characterized by their localization, but also by the distribution of their spins. During the dynamics the question arises whether it is possible to separately control the distribution of the impurities as well as the spin configuration.

In the previous works we have considered the Bose gas not to be trapped in the lattice potential. In [[4]] both the impurity and the majority species are subject to the lattice geometry. For an increasing strength of the interspecies coupling the entanglement between the species first gradually increases until it suddenly reduces close to zero. For a single impurity this corresponds to an initial delocalization followed by a sudden localization on either outermost lattice site. Simultaneously, the majority species atoms distribute in the remaining unoccupied wells, thereby leading to an interspecies phase separation [261, 277, 323]. Further inspecting the distribution of the majority species, it is found that the atoms form a Mott insulator-like state. This particle-hole pair [324] undergoes transport when subjected to a sudden reduction of the interspecies coupling strength. Its stability, i.e. the probability of measuring the particle-hole pair, strongly depends on the post-quench interspecies interaction strength. It has been shown that the stability during the transport is maximized for sufficiently small quench amplitudes, while for two impurities the stability is strongly reduced.

This work serves as an ideal starting point for more complex scenarios by increasing the number of lattice atoms and sites. A further interesting perspective involves the investigation of the impact of dipolar interactions within and between the species on the ground state phase diagram. Due to the long-range character of such an interaction more phases are expected to appear. Also the notion of an internal degree of freedom, e.g. a spin, is appealing for future studies, allowing for an effective spin transport or the redistribution of the spins in addition to the particle-hole pair dynamics. Another important question arising in this context is whether it is possible to create next-neighbor pairs or even clusters of particle-hole pairs. This might be achieved due to the appearance of an induced interaction by coupling the impurities to the majority species. Based on the potential formation of such clusters one would investigate the transport properties and the stability of the particle-hole pair clusters.

Collisional dynamics of impurities with a lattice trapped bath

In [[5,6]] we have focused on the collisional dynamics of an impurity species with a lattice trapped medium, examining different quench protocols, respectively. In [[5]] the collision was induced by preparing impurities in a tilted double well potential which are interacting repulsively with a majority species in a lattice potential. Quenching the tilt to zero the transport of the impurities to the opposite site of the double well is initiated. We have found qualitatively different dynamical response regimes depending on the interspecies coupling strength. In particular, for moderate coupling strengths a material barrier tunneling [325, 326] of the impurity was identified, where the impurity has to overcome the density maxima of the majority species in addition to the double well barrier. For increasing coupling strengths it was shown that the material barrier tunneling to the opposite site of the double well could be delayed in time, while very large couplings even completely prohibit the transport to the other well [292, 327]. We characterized the underlying microscopic processes employing a time-averaged effective potential, whose associated Wannier states adequately described the material barrier tunneling. We further revealed the necessity of interspecies entanglement for the appearance of the dynamical response regimes and recovered the material barrier tunneling also for the case of two impurities, where the associated transport exhibits single particle as well as pair tunneling processes.

A fruitful direction for further investigations is given by the consideration of quench protocols which additionally include a variation of the interspecies coupling strength. As such it might be possible that a subsequent interaction quench after the transport of the impurity to the opposite site of the double well would allow for a storage of the impurity in that very site. Moreover, it might be of use to employ a dynamical driving of the system parameters in order to enhance the controlled transfer of the impurity species. So far the possible paths of exploration were related to the quench protocol, in particular focusing on the impurity species. On the other hand, it would be intriguing to study the impact of the manipulation of the medium on the transport properties. As such varying the intraspecies coupling strength among the medium atoms will influence the compressibility, leading in the extreme case to the formation of a Mott insulator-like state. Taking this even further, states of the excited band might be occupied by the majority species atoms, which will definitely alter the transport behavior of the impurity species.

The quench protocol has been changed in [[6]] such that impurities are initialized in a displaced harmonic oscillator and are forced to collide with a medium trapped in a double well by quenching the harmonic confinement to the center of the double well [168]. We have recovered a diverse collection of dynamical response regimes depending on the interspecies coupling ranging from strongly attractive to strongly repulsive, namely the steady bound state regime, the tunneling region, the dissipative oscillation motion, the pinning and the total reflection regime. The robustness of the results was explicated by varying the intraspecies interaction strength of the bath and the initial displacement of the impurity's harmonic trap. We have further constructed a time-averaged effective potential in order to gain a better understanding of the microscopic mechanisms, allowing for unraveling the excitation processes which might be hidden when solely monitoring the one-body density. The extension to the case of two impurities exhibits similar dynamical response regimes, while the intraspecies coupling strength among the medium atoms was identified as an additional control parameter influencing the compressibility of the latter and thereby its penetrability. This work is of immediate interest to the ultracold atom community for future investigations of collisional channels solely induced by the presence of impurity-medium interactions.

For future research we see several promising directions. In [[6]] we have considered the unidirectional collisions of impurities with the medium. The study of a bidirectional collisional process is therefore a natural extension and of immediate interest. For this purpose, one would prepare the impurities such that they are displaced separately on either side of the medium. In this context, one might ask how the coupling to the medium influences the collision of the impurities. A further manipulation of the dynamical response could be achieved by the variation of the intraspecies coupling among the impurities. For example, it could be possible to dynamically generate bound impurity clusters through the bidirectional collision and the additional coupling to the medium. Also the implementation of a spin degree of freedom for weakly interacting impurities is indeed an interesting route to consider for future studies as it allows for the identification of individual spin configurations, related spin-mixing processes and the possible formation of Cooper pairs [131] as a function of the impurity-medium coupling. Extending this setup to higher dimensions is certainly of interest, allowing for more complex scattering scenarios and, hence, offering a richer phenomenology.

Highly imbalanced triple mixtures

In [[7]] we have provided the first detailed study of the polaron problem when considering a bath consisting of two hosts. Thus, we have allowed the impurities to couple either attractively or repulsively to the individual components, thus offering an efficient platform for manipulating the polaronic properties. A key result of this study is the possibility to flexibly control the impurity residue [122] and thereby also the polaronic character. In particular, the quasiparticle character can be maintained for larger interactions in case the impurity couples attractively to one medium and repulsively to the other one. This behavior could also be recovered for heavier impurities. Regarding the polaronic resonances we extracted a clear hierarchy of the binding energy due to the immersion of the polaron, a feature that is also present for a larger cumulative bath. Thus, utilizing radiofrequency schemes the respective resonances are well distinguishable from each other. In order to describe the processes which underlie the behavior of the residue we have constructed an effective potential picture which takes into account the density distributions of both hosts. With its aid we were able to get an intuitive understanding of the impurity distribution as well as its motional excitations. Considering an additional impurity led to a strong reduction of the width as well as the height of the associated impurity residue. The presence of two impurities naturally inspires the notion of induced interactions whose impact could be analyzed by invoking the impurities two-body densities. For sufficiently attractive couplings to one of the hosts the formation of a bipolaron was captured [301, 328], while for strongly repulsive couplings the impurity forms a shell structure whose width can be controlled by the coupling strength to the other medium. The results of this work pave the way for steering the quasiparticle character and induced interactions in a systematic manner, thereby also exposing the role of correlations for such triple mixture setups.

In [[7]] the two species in the bath are weakly interacting among each other such that they are in the miscible regime. In the future it is intriguing to exploit the phase of the cumulative bath in order to manipulate the polaronic properties of the impurities. As such the bath can be prepared in any combination of Tonks-Girardeau gases, fermionization, miscible phase as well as in an immiscible phase. Naturally, this has an impact on the impurity species and thereby on the associated quasiparticle character. This will shed light on the polaron problem from a very different perspective and may even lead to fundamentally new concepts. Extending this to higher dimensional settings it is to be expected that topological effects will play a crucial role.

The natural next step would be to investigate the sudden injection of the impurity species into the cumulative bath in order to simulate the respective spectroscopic techniques [184, 185]. Here, the spectral response would provide information about the impurity residue and the involved excited states, consequently, being an immediate realization of our findings. Moreover, this work also serves as a perfect starting point for further investigations of triple mixtures in general [334, 335], which promise to offer a much richer phenomenology as compared to binary mixture settings.

Closing remarks

This cumulative thesis has shown that the field of ultracold atomic mixtures is far from exhausted. Indeed, it offers a lot of potential for future investigations, in particular since the experimental possibilities for the creation and systematic controlled investigations of such systems are growing rapidly. Apart from the well-established in-situ imaging of atomic clouds [336], time-of-flight images [337] and density-density fluctuation measurements [338–341] a new class of experimental advances has been triggered by the quantum gas microscope [342–344] as well as the measurement of dynamical response functions by employing Bragg spectroscopy [345, 346] or radio-frequency protocols [347]. Moreover, the momentum to experimentally realize few-body systems [86–91] will require theoretical descriptions which are able to take into account all necessary inter- and intraspecies correlations, such as ML-MCTDHX. Consequently, it is to be expected that more focus will be placed on the development of such ab-initio methods. A particularly interesting route is given by the possible experimental implementation of triple mixture settings [348–353] which are anticipated to make the relevant phenomenology even more interesting. In this context, highly imbalanced triple mixtures offer the most direct realization of this kind, e.g. in the framework of the polaron problem. As such we believe that [[7]] has opened the door to a significant new research direction which is relevant for the cold atom community.

Bibliography

- [1] Bose, “Plancks Gesetz und Lichtquantenhypothese,” *Z. Physik* **26**, 178 (1924).
- [2] A. Einstein, “Quantentheorie des einatomigen idealen Gases,” in *Albert Einstein: Akademie-Vorträge* (John Wiley & Sons, Ltd, 2005) pp. 237–244.
- [3] A. Einstein, “Quantentheorie des einatomigen idealen Gases. Zweite Abhandlung,” in *Albert Einstein: Akademie-Vorträge* (John Wiley & Sons, Ltd, 2005) pp. 245–257.
- [4] C. J. Pethick and H. Smith, *Bose–Einstein Condensation in Dilute Gases* (Cambridge University Press, Cambridge, 2001).
- [5] L. Pitaevskii and S. Stringari, *Bose-Einstein Condensation and Superfluidity* (Oxford University Press).
- [6] P. G. Kevrekidis, D. J. Frantzeskakis, and R. Carretero-González, eds., *Emergent Nonlinear Phenomena in Bose-Einstein Condensates: Theory and Experiment*, Springer Series on Atomic, Optical, and Plasma Physics (Springer-Verlag, Berlin Heidelberg, 2008).
- [7] M. H. Anderson, J. R. Ensher, M. R. Matthews, C. E. Wieman, and E. A. Cornell, “Observation of Bose-Einstein Condensation in a Dilute Atomic Vapor,” *Science* **269**, 198 (1995).
- [8] K. B. Davis, M. O. Mewes, M. R. Andrews, N. J. van Druten, D. S. Durfee, D. M. Kurn, and W. Ketterle, “Bose-Einstein Condensation in a Gas of Sodium Atoms,” *Phys. Rev. Lett.* **75**, 3969 (1995).
- [9] M. Lewenstein, A. Sanpera, and V. Ahufinger, *Ultracold Atoms in Optical Lattices: Simulating quantum many-body systems* (Oxford University Press).
- [10] K. Henderson, C. Ryu, C. MacCormick, and M. G. Boshier, “Experimental demonstration of painting arbitrary and dynamic potentials for Bose–Einstein condensates,” *New J. Phys.* **11**, 043030 (2009).
- [11] O. Morsch and M. Oberthaler, “Dynamics of Bose-Einstein condensates in optical lattices,” *Rev. Mod. Phys.* **78**, 179 (2006).

- [12] S. Inouye, M. R. Andrews, J. Stenger, H.-J. Miesner, D. M. Stamper-Kurn, and W. Ketterle, “Observation of Feshbach resonances in a Bose–Einstein condensate,” *Nature* **392**, 151 (1998).
- [13] T. Köhler, K. Góral, and P. S. Julienne, “Production of cold molecules via magnetically tunable Feshbach resonances,” *Rev. Mod. Phys.* **78**, 1311 (2006).
- [14] J. I. Kim, V. S. Melezhik, and P. Schmelcher, “Suppression of Quantum Scattering in Strongly Confined Systems,” *Phys. Rev. Lett.* **97**, 193203 (2006).
- [15] C. Chin, R. Grimm, P. Julienne, and E. Tiesinga, “Feshbach resonances in ultracold gases,” *Rev. Mod. Phys.* **82**, 1225 (2010).
- [16] P. Giannakeas, V. S. Melezhik, and P. Schmelcher, “Dipolar Confinement-Induced Resonances of Ultracold Gases in Waveguides,” *Phys. Rev. Lett.* **111**, 183201 (2013).
- [17] M. Lewenstein, A. Sanpera, V. Ahufinger, B. Damski, A. Sen(De), and U. Sen, “Ultracold atomic gases in optical lattices: mimicking condensed matter physics and beyond,” *Advances in Physics* **56**, 243 (2007).
- [18] L. Amico, A. Osterloh, and F. Cataliotti, “Quantum Many Particle Systems in Ring-Shaped Optical Lattices,” *Phys. Rev. Lett.* **95**, 063201 (2005).
- [19] G. Arwas, D. Cohen, F. Hekking, and A. Minguzzi, “Resonant persistent currents for ultracold bosons on a lattice ring,” *Phys. Rev. A* **96**, 063616 (2017).
- [20] B. T. Seaman, M. Krämer, D. Z. Anderson, and M. J. Holland, “Atomtronics: Ultracold-atom analogs of electronic devices,” *Phys. Rev. A* **75**, 023615 (2007).
- [21] K. W. Wilsmann, L. H. Ymai, A. P. Tonel, J. Links, and A. Foerster, “Control of tunneling in an atomtronic switching device,” *Communications Physics* **1**, 1 (2018).
- [22] S. Pandey, H. Mas, G. Drougakis, P. Thekkeppatt, V. Bolpasi, G. Vasilakis, K. Poullos, and W. von Klitzing, “Hypersonic Bose–Einstein condensates in accelerator rings,” *Nature* **570**, 205 (2019).
- [23] M. A. McLain and L. D. Carr, “Quantum phase transition modulation in an atomtronic Mott switch,” *Quantum Sci. Technol.* **3**, 035012 (2018).
- [24] A. C. Mathey and L. Mathey, “Realizing and optimizing an atomtronic SQUID,” *New J. Phys.* **18**, 055016 (2016).
- [25] R. Labouvie, B. Santra, S. Heun, S. Wimberger, and H. Ott, “Negative Differential Conductivity in an Interacting Quantum Gas,” *Phys. Rev. Lett.* **115**, 050601 (2015).
- [26] A. Kumar, S. Eckel, F. Jendrzejewski, and G. K. Campbell, “Temperature-induced decay of persistent currents in a superfluid ultracold gas,” *Phys. Rev. A* **95**, 021602 (2017).
- [27] F. Jendrzejewski, S. Eckel, N. Murray, C. Lanier, M. Edwards, C. Lobb, and G. Campbell, “Resistive Flow in a Weakly Interacting Bose-Einstein Condensate,” *Phys. Rev. Lett.* **113**, 045305 (2014).
- [28] M. Gajdacz, T. Opatrny, and K. K. Das, “An atomtronics transistor for quantum gates,” *Physics Letters A* **378**, 1919 (2014).

-
- [29] S. Eckel, J. G. Lee, F. Jendrzejewski, N. Murray, C. W. Clark, C. J. Lobb, W. D. Phillips, M. Edwards, and G. K. Campbell, “Hysteresis in a quantized superfluid ‘atomtronic’ circuit,” *Nature* **506**, 200 (2014).
- [30] S. C. Caliga, C. J. E. Straatsma, and D. Z. Anderson, “Transport dynamics of ultracold atoms in a triple-well transistor-like potential,” *New J. Phys.* **18**, 025010 (2016).
- [31] S. C. Caliga, C. J. E. Straatsma, A. A. Zozulya, and D. Z. Anderson, “Principles of an atomtronic transistor,” *New J. Phys.* **18**, 015012 (2016).
- [32] S. C. Caliga, C. J. E. Straatsma, and D. Z. Anderson, “Experimental demonstration of an atomtronic battery,” *New J. Phys.* **19**, 013036 (2017).
- [33] I. Bloch, J. Dalibard, and W. Zwerger, “Many-body physics with ultracold gases,” *Rev. Mod. Phys.* **80**, 885 (2008).
- [34] V. I. Yukalov, “Cold bosons in optical lattices,” *Laser Phys.* **19**, 1 (2009).
- [35] J. Hubbard and B. H. Flowers, “Electron correlations in narrow energy bands,” *Proceedings of the Royal Society of London. Series A. Mathematical and Physical Sciences* **276**, 238 (1963).
- [36] V. Bach, E. H. Lieb, and J. P. Solovej, “Generalized Hartree-Fock theory and the Hubbard model,” *J Stat Phys* **76**, 3 (1994).
- [37] E. H. Lieb and F. Y. Wu, “The one-dimensional Hubbard model: a reminiscence,” *Physica A: Statistical Mechanics and its Applications Statphys-Taiwan-2002: Lattice Models and Complex Systems*, **321**, 1 (2003).
- [38] M. P. A. Fisher, P. B. Weichman, G. Grinstein, and D. S. Fisher, “Boson localization and the superfluid-insulator transition,” *Phys. Rev. B* **40**, 546 (1989).
- [39] D. Jaksch, C. Bruder, J. I. Cirac, C. W. Gardiner, and P. Zoller, “Cold Bosonic Atoms in Optical Lattices,” *Phys. Rev. Lett.* **81**, 3108 (1998).
- [40] M. Greiner, O. Mandel, T. Esslinger, T. W. Hänsch, and I. Bloch, “Quantum phase transition from a superfluid to a Mott insulator in a gas of ultracold atoms,” *Nature* **415**, 39 (2002).
- [41] L. Fallani, J. E. Lye, V. Guarrera, C. Fort, and M. Inguscio, “Ultracold Atoms in a Disordered Crystal of Light: Towards a Bose Glass,” *Phys. Rev. Lett.* **98**, 130404 (2007).
- [42] B. Damski, J. Zakrzewski, L. Santos, P. Zoller, and M. Lewenstein, “Atomic Bose and Anderson Glasses in Optical Lattices,” *Phys. Rev. Lett.* **91**, 080403 (2003).
- [43] G. Thalhammer, G. Barontini, L. De Sarlo, J. Catani, F. Minardi, and M. Inguscio, “Double Species Bose-Einstein Condensate with Tunable Interspecies Interactions,” *Phys. Rev. Lett.* **100**, 210402 (2008).
- [44] S. Ospelkaus, C. Ospelkaus, O. Wille, M. Succo, P. Ernst, K. Sengstock, and K. Bongs, “Localization of Bosonic Atoms by Fermionic Impurities in a Three-Dimensional Optical Lattice,” *Phys. Rev. Lett.* **96**, 180403 (2006).
- [45] K. Günter, T. Stöferle, H. Moritz, M. Köhl, and T. Esslinger, “Bose-Fermi Mixtures in a Three-Dimensional Optical Lattice,” *Phys. Rev. Lett.* **96**, 180402 (2006).

- [46] T. Stöferle, H. Moritz, C. Schori, M. Köhl, and T. Esslinger, “Transition from a Strongly Interacting 1D Superfluid to a Mott Insulator,” *Phys. Rev. Lett.* **92**, 130403 (2004).
- [47] M. Köhl, H. Moritz, T. Stöferle, C. Schori, and T. Esslinger, “Superfluid to Mott insulator transition in one, two, and three dimensions,” *J Low Temp Phys* **138**, 635 (2005).
- [48] R. Jördens, N. Strohmaier, K. Günter, H. Moritz, and T. Esslinger, “A Mott insulator of fermionic atoms in an optical lattice,” *Nature* **455**, 204 (2008).
- [49] U. Schneider, L. Hackermüller, S. Will, T. Best, I. Bloch, T. A. Costi, R. W. Helmes, D. Rasch, and A. Rosch, “Metallic and Insulating Phases of Repulsively Interacting Fermions in a 3D Optical Lattice,” *Science* **322**, 1520 (2008).
- [50] B. Paredes, A. Widera, V. Murg, O. Mandel, S. Fölling, I. Cirac, G. V. Shlyapnikov, T. W. Hänsch, and I. Bloch, “Tonks–Girardeau gas of ultracold atoms in an optical lattice,” *Nature* **429**, 277 (2004).
- [51] T. Kinoshita, T. Wenger, and D. S. Weiss, “Observation of a One-Dimensional Tonks-Girardeau Gas,” *Science* **305**, 1125 (2004).
- [52] G. Wirth, M. Ölschläger, and A. Hemmerich, “Evidence for orbital superfluidity in the P -band of a bipartite optical square lattice,” *Nature Physics* **7**, 147 (2011).
- [53] P. Soltan-Panahi, D.-S. Lühmann, J. Struck, P. Windpassinger, and K. Sengstock, “Quantum phase transition to unconventional multi-orbital superfluidity in optical lattices,” *Nature Physics* **8**, 71 (2012).
- [54] S. Choudhury and E. J. Mueller, “Absence of the twisted superfluid state in a mean-field model of bosons on a honeycomb lattice,” *Phys. Rev. A* **87**, 033621 (2013).
- [55] M. Ölschläger, G. Wirth, and A. Hemmerich, “Unconventional Superfluid Order in the $\$F\$$ Band of a Bipartite Optical Square Lattice,” *Phys. Rev. Lett.* **106**, 015302 (2011).
- [56] L. Cao, S. Krönke, J. Stockhofe, J. Simonet, K. Sengstock, D.-S. Lühmann, and P. Schmelcher, “Beyond-mean-field study of a binary bosonic mixture in a state-dependent honeycomb lattice,” *Phys. Rev. A* **91**, 043639 (2015).
- [57] C. Chin, M. Bartenstein, A. Altmeyer, S. Riedl, S. Jochim, J. H. Denschlag, and R. Grimm, “Observation of the Pairing Gap in a Strongly Interacting Fermi Gas,” *Science* **305**, 1128 (2004).
- [58] G. B. Partridge, W. Li, R. I. Kamar, Y.-a. Liao, and R. G. Hulet, “Pairing and Phase Separation in a Polarized Fermi Gas,” *Science* **311**, 503 (2006).
- [59] J. K. Chin, D. E. Miller, Y. Liu, C. Stan, W. Setiawan, C. Sanner, K. Xu, and W. Ketterle, “Evidence for superfluidity of ultracold fermions in an optical lattice,” *Nature* **443**, 961 (2006).
- [60] V. Gurarie and L. Radzihovsky, “Resonantly paired fermionic superfluids,” *Annals of Physics January Special Issue 2007*, **322**, 2 (2007).
- [61] K. Winkler, G. Thalhammer, F. Lang, R. Grimm, J. Hecker Denschlag, A. J. Daley, A. Kantian, H. P. Büchler, and P. Zoller, “Repulsively bound atom pairs in an optical lattice,” *Nature* **441**, 853 (2006).

-
- [62] O. Dutta, M. Gajda, P. Hauke, M. Lewenstein, D.-S. Lühmann, B. A. Malomed, T. Sowinski, and J. Zakrzewski, “Non-standard Hubbard models in optical lattices: a review,” *Rep. Prog. Phys.* **78**, 066001 (2015).
- [63] M. Łacki, D. Delande, and J. Zakrzewski, “Dynamics of cold bosons in optical lattices: effects of higher Bloch bands,” *New J. Phys.* **15**, 013062 (2013).
- [64] T. D. Kühner and H. Monien, “Phases of the one-dimensional Bose-Hubbard model,” *Phys. Rev. B* **58**, R14741 (1998).
- [65] T. D. Kühner, S. R. White, and H. Monien, “One-dimensional Bose-Hubbard model with nearest-neighbor interaction,” *Phys. Rev. B* **61**, 12474 (2000).
- [66] P. Sengupta, L. P. Pryadko, F. Alet, M. Troyer, and G. Schmid, “Supersolids versus Phase Separation in Two-Dimensional Lattice Bosons,” *Phys. Rev. Lett.* **94**, 207202 (2005).
- [67] S. Wessel, “Phase diagram of interacting bosons on the honeycomb lattice,” *Phys. Rev. B* **75**, 174301 (2007).
- [68] J. Y. Gan, Y. C. Wen, J. Ye, T. Li, S.-J. Yang, and Y. Yu, “Extended Bose-Hubbard model on a honeycomb lattice,” *Phys. Rev. B* **75**, 214509 (2007).
- [69] K.-K. Ng, Y. C. Chen, and Y. C. Tzeng, “Quarter-filled supersolid and solid phases in the extended Bose-Hubbard model,” *J. Phys.: Condens. Matter* **22**, 185601 (2010).
- [70] M. Maik, P. Hauke, O. Dutta, M. Lewenstein, and J. Zakrzewski, “Density-dependent tunneling in the extended Bose-Hubbard model,” *New J. Phys.* **15**, 113041 (2013).
- [71] J.-Y. Gan, Y.-C. Wen, and Y. Yu, “Supersolidity and phase diagram of soft-core bosons on a triangular lattice,” *Phys. Rev. B* **75**, 094501 (2007).
- [72] T. Leggett, “Superfluidity in a Crystal?” *Science* **305**, 1921 (2004).
- [73] G. G. Batrouni and R. T. Scalettar, “Phase Separation in Supersolids,” *Phys. Rev. Lett.* **84**, 1599 (2000).
- [74] P. Buonsante, V. Penna, and A. Vezzani, “Fractional-filling loophole insulator domains for ultracold bosons in optical superlattices,” *Phys. Rev. A* **70**, 061603 (2004).
- [75] P. Buonsante and A. Vezzani, “Cell strong-coupling perturbative approach to the phase diagram of ultracold bosons in optical superlattices,” *Phys. Rev. A* **72**, 013614 (2005).
- [76] I. Danshita, J. E. Williams, C. A. R. Sá de Melo, and C. W. Clark, “Quantum phases of bosons in double-well optical lattices,” *Phys. Rev. A* **76**, 043606 (2007).
- [77] D. Muth, A. Mering, and M. Fleischhauer, “Ultracold bosons in disordered superlattices: Mott insulators induced by tunneling,” *Phys. Rev. A* **77**, 043618 (2008).
- [78] O. Jürgensen, J. Heinze, and D.-S. Lühmann, “Large-amplitude superexchange of high-spin fermions in optical lattices,” *New J. Phys.* **15**, 113017 (2013).
- [79] D. Barredo, S. d. Léséleuc, V. Lienhard, T. Lahaye, and A. Browaeys, “An atom-by-atom assembler of defect-free arbitrary 2D atomic arrays,” *Science* (2016).

- [80] M. Endres, H. Bernien, A. Keesling, H. Levine, E. R. Anschuetz, A. Krajenbrink, C. Senko, V. Vuletic, M. Greiner, and M. D. Lukin, “Atom-by-atom assembly of defect-free one-dimensional cold atom arrays,” *Science* **354**, 1024 (2016).
- [81] A. M. Kaufman, B. J. Lester, M. Foss-Feig, M. L. Wall, A. M. Rey, and C. A. Regal, “Entangling two transportable neutral atoms via local spin exchange,” *Nature* **527**, 208 (2015).
- [82] R. Bourgain, J. Pellegrino, A. Fuhrmanek, Y. R. P. Sortais, and A. Browaeys, “Evaporative cooling of a small number of atoms in a single-beam microscopic dipole trap,” *Phys. Rev. A* **88**, 023428 (2013).
- [83] P. Cheinet, S. Trotzky, M. Feld, U. Schnorrberger, M. Moreno-Cardoner, S. Fölling, and I. Bloch, “Counting Atoms Using Interaction Blockade in an Optical Superlattice,” *Phys. Rev. Lett.* **101**, 090404 (2008).
- [84] X. He, P. Xu, J. Wang, and M. Zhan, “High efficient loading of two atoms into a microscopic optical trap by dynamically reshaping the trap with a spatial light modulator,” *Opt. Express*, OE **18**, 13586 (2010).
- [85] S. Will, T. Best, U. Schneider, L. Hackermüller, D.-S. Lühmann, and I. Bloch, “Time-resolved observation of coherent multi-body interactions in quantum phase revivals,” *Nature* **465**, 197 (2010).
- [86] S. Murmann, F. Deuretzbacher, G. Zürn, J. Bjerlin, S. Reimann, L. Santos, T. Lompe, and S. Jochim, “Antiferromagnetic Heisenberg Spin Chain of a Few Cold Atoms in a One-Dimensional Trap,” *Phys. Rev. Lett.* **115**, 215301 (2015).
- [87] S. Murmann, A. Bergschneider, V. M. Klinkhamer, G. Zürn, T. Lompe, and S. Jochim, “Two Fermions in a Double Well: Exploring a Fundamental Building Block of the Hubbard Model,” *Phys. Rev. Lett.* **114**, 080402 (2015).
- [88] G. Zürn, F. Serwane, T. Lompe, A. N. Wenz, M. G. Ries, J. E. Bohn, and S. Jochim, “Fermionization of Two Distinguishable Fermions,” *Phys. Rev. Lett.* **108**, 075303 (2012).
- [89] G. Zürn, A. N. Wenz, S. Murmann, A. Bergschneider, T. Lompe, and S. Jochim, “Pairing in Few-Fermion Systems with Attractive Interactions,” *Phys. Rev. Lett.* **111**, 175302 (2013).
- [90] A. N. Wenz, G. Zürn, S. Murmann, I. Brouzos, T. Lompe, and S. Jochim, “From Few to Many: Observing the Formation of a Fermi Sea One Atom at a Time,” *Science* **342**, 457 (2013).
- [91] F. Serwane, G. Zürn, T. Lompe, T. B. Ottenstein, A. N. Wenz, and S. Jochim, “Deterministic Preparation of a Tunable Few-Fermion System,” *Science* **332**, 336 (2011).
- [92] C. J. Myatt, E. A. Burt, R. W. Ghrist, E. A. Cornell, and C. E. Wieman, “Production of Two Overlapping Bose-Einstein Condensates by Sympathetic Cooling,” *Phys. Rev. Lett.* **78**, 586 (1997).
- [93] D. S. Hall, M. R. Matthews, C. E. Wieman, and E. A. Cornell, “Measurements of Relative Phase in Two-Component Bose-Einstein Condensates,” *Phys. Rev. Lett.* **81**, 1543 (1998).

-
- [94] H.-J. Miesner, D. M. Stamper-Kurn, J. Stenger, S. Inouye, A. P. Chikkatur, and W. Ketterle, "Observation of Metastable States in Spinor Bose-Einstein Condensates," *Phys. Rev. Lett.* **82**, 2228 (1999).
- [95] S. Zöllner, H.-D. Meyer, and P. Schmelcher, "Composite fermionization of one-dimensional Bose-Bose mixtures," *Phys. Rev. A* **78**, 013629 (2008).
- [96] M. D. Girardeau and A. Minguzzi, "Soluble Models of Strongly Interacting Ultracold Gas Mixtures in Tight Waveguides," *Phys. Rev. Lett.* **99**, 230402 (2007).
- [97] F. Deuretzbacher, K. Fredenhagen, D. Becker, K. Bongs, K. Sengstock, and D. Pfannkuche, "Exact Solution of Strongly Interacting Quasi-One-Dimensional Spinor Bose Gases," *Phys. Rev. Lett.* **100**, 160405 (2008).
- [98] B. Fang, P. Vignolo, M. Gattobigio, C. Miniatura, and A. Minguzzi, "Exact solution for the degenerate ground-state manifold of a strongly interacting one-dimensional Bose-Fermi mixture," *Phys. Rev. A* **84**, 023626 (2011).
- [99] S. B. Papp, J. M. Pino, and C. E. Wieman, "Tunable Miscibility in a Dual-Species Bose-Einstein Condensate," *Phys. Rev. Lett.* **101**, 040402 (2008).
- [100] S. Tojo, Y. Taguchi, Y. Masuyama, T. Hayashi, H. Saito, and T. Hirano, "Controlling phase separation of binary Bose-Einstein condensates via mixed-spin-channel Feshbach resonance," *Phys. Rev. A* **82**, 033609 (2010).
- [101] D. J. McCarron, H. W. Cho, D. L. Jenkin, M. P. Köppinger, and S. L. Cornish, "Dual-species Bose-Einstein condensate of ^{87}Rb and ^{133}Cs ," *Phys. Rev. A* **84**, 011603 (2011).
- [102] Y. Kawaguchi and M. Ueda, "Spinor Bose-Einstein condensates," *Physics Reports Spinor Bose-Einstein condensates*, **520**, 253 (2012).
- [103] K. Kasamatsu and M. Tsubota, "Multiple Domain Formation Induced by Modulation Instability in Two-Component Bose-Einstein Condensates," *Phys. Rev. Lett.* **93**, 100402 (2004).
- [104] S. Ronen, J. L. Bohn, L. E. Halmø, and M. Edwards, "Dynamical pattern formation during growth of a dual-species Bose-Einstein condensate," *Phys. Rev. A* **78**, 053613 (2008).
- [105] T. Mishra, R. V. Pai, and B. P. Das, "Phase separation in a two-species Bose mixture," *Phys. Rev. A* **76**, 013604 (2007).
- [106] P. Buonsante, S. M. Giampaolo, F. Illuminati, V. Penna, and A. Vezzani, "Mixtures of Strongly Interacting Bosons in Optical Lattices," *Phys. Rev. Lett.* **100**, 240402 (2008).
- [107] A. B. Kuklov and B. V. Svistunov, "Counterflow Superfluidity of Two-Species Ultracold Atoms in a Commensurate Optical Lattice," *Phys. Rev. Lett.* **90**, 100401 (2003).
- [108] A. Hu, L. Mathey, I. Danshita, E. Tiesinga, C. J. Williams, and C. W. Clark, "Counterflow and paired superfluidity in one-dimensional Bose mixtures in optical lattices," *Phys. Rev. A* **80**, 023619 (2009).
- [109] A. Hu, L. Mathey, C. J. Williams, and C. W. Clark, "Noise correlations of one-dimensional Bose mixtures in optical lattices," *Phys. Rev. A* **81**, 063602 (2010).

- [110] D. Petrov, “Quantum Mechanical Stabilization of a Collapsing Bose-Bose Mixture,” *Phys. Rev. Lett.* **115**, 155302 (2015).
- [111] C. R. Cabrera, L. Tanzi, J. Sanz, B. Naylor, P. Thomas, P. Cheiney, and L. Tarruell, “Quantum liquid droplets in a mixture of Bose-Einstein condensates,” *Science* **359**, 301 (2018).
- [112] P. Cheiney, C. Cabrera, J. Sanz, B. Naylor, L. Tanzi, and L. Tarruell, “Bright Soliton to Quantum Droplet Transition in a Mixture of Bose-Einstein Condensates,” *Phys. Rev. Lett.* **120**, 135301 (2018).
- [113] G. Semeghini, G. Ferioli, L. Masi, C. Mazzinghi, L. Wolswijk, F. Minardi, M. Modugno, G. Modugno, M. Inguscio, and M. Fattori, “Self-Bound Quantum Droplets of Atomic Mixtures in Free Space,” *Phys. Rev. Lett.* **120**, 235301 (2018).
- [114] A. Kleine, C. Kollath, I. P. McCulloch, T. Giamarchi, and U. Schollwöck, “Spin-charge separation in two-component Bose gases,” *Phys. Rev. A* **77**, 013607 (2008).
- [115] E. Nicklas, M. Karl, M. Höfer, A. Johnson, W. Muessel, H. Strobel, J. Tomkovic, T. Gasenzer, and M. Oberthaler, “Observation of Scaling in the Dynamics of a Strongly Quenched Quantum Gas,” *Phys. Rev. Lett.* **115**, 245301 (2015).
- [116] M. Karl, H. Cakir, J. C. Halimeh, M. K. Oberthaler, M. Kastner, and T. Gasenzer, “Universal equilibrium scaling functions at short times after a quench,” *Phys. Rev. E* **96**, 022110 (2017).
- [117] R. N. Bisset, R. M. Wilson, and C. Ticknor, “Scaling of fluctuations in a trapped binary condensate,” *Phys. Rev. A* **91**, 053613 (2015).
- [118] C. Kohstall, M. Zaccanti, M. Jag, A. Trenkwalder, P. Massignan, G. M. Bruun, F. Schreck, and R. Grimm, “Metastability and coherence of repulsive polarons in a strongly interacting Fermi mixture,” *Nature* **485**, 615 (2012).
- [119] M. Koschorreck, D. Pertot, E. Vogt, B. Fröhlich, M. Feld, and M. Köhl, “Attractive and repulsive Fermi polarons in two dimensions,” *Nature* **485**, 619 (2012).
- [120] F. Scazza, G. Valtolina, P. Massignan, A. Recati, A. Amico, A. Burchianti, C. Fort, M. Inguscio, M. Zaccanti, and G. Roati, “Repulsive Fermi Polarons in a Resonant Mixture of Ultracold ^6Li Atoms,” *Phys. Rev. Lett.* **118**, 083602 (2017).
- [121] R. Schmidt, M. Knap, D. A. Ivanov, J.-S. You, M. Cetina, and E. Demler, “Universal many-body response of heavy impurities coupled to a Fermi sea: a review of recent progress,” *Rep. Prog. Phys.* **81**, 024401 (2018).
- [122] P. Massignan, M. Zaccanti, and G. M. Bruun, “Polarons, dressed molecules and itinerant ferromagnetism in ultracold Fermi gases,” *Rep. Prog. Phys.* **77**, 034401 (2014).
- [123] Grusdt F. and Demler E., “New theoretical approaches to Bose polarons,” *ENFI* **191**, 325 (2016).
- [124] F. Grusdt, G. E. Astrakharchik, and E. Demler, “Bose polarons in ultracold atoms in one dimension: beyond the Fröhlich paradigm,” *New J. Phys.* **19**, 103035 (2017).
- [125] J. T. Devreese and A. S. Alexandrov, “Fröhlich polaron and bipolaron: recent developments,” *Rep. Prog. Phys.* **72**, 066501 (2009).

-
- [126] M. E. Gershenson, V. Podzorov, and A. F. Morpurgo, “Colloquium: Electronic transport in single-crystal organic transistors,” *Rev. Mod. Phys.* **78**, 973 (2006).
- [127] S. T. Ruggiero and D. A. Rudman, “Superconducting devices,” (1990).
- [128] J. Bardeen, G. Baym, and D. Pines, “Effective Interaction of He₃ Atoms in Dilute Solutions of He₃ in He₄ at Low Temperatures,” *Phys. Rev.* **156**, 207 (1967).
- [129] D. J. Scalapino, “The case for dx²-y² pairing in the cuprate superconductors,” *Physics Reports* **250**, 329 (1995).
- [130] J. Sous, M. Chakraborty, R. V. Krems, and M. Berciu, “Light Bipolarons Stabilized by Peierls Electron-Phonon Coupling,” *Phys. Rev. Lett.* **121**, 247001 (2018).
- [131] L. N. Cooper, “Bound Electron Pairs in a Degenerate Fermi Gas,” *Phys. Rev.* **104**, 1189 (1956).
- [132] N. F. Mott, “Polaron models of high-temperature superconductors,” *J. Phys.: Condens. Matter* **5**, 3487 (1993).
- [133] A. S. Alexandrov and N. F. Mott, “Bipolarons,” *Rep. Prog. Phys.* **57**, 1197 (1994).
- [134] E. K. H. Salje, A. S. Alexandrov, and W. Y. Liang, “Polarons and Bipolarons in High-Tc Superconductors and Related Materials,” *UK: Cambridge University Press* (2005).
- [135] M. Berciu, I. Elfimov, and G. A. Sawatzky, “Electronic polarons and bipolarons in iron-based superconductors: The role of anions,” *Phys. Rev. B* **79**, 214507 (2009).
- [136] M. G. Skou, T. G. Skov, N. B. Jørgensen, K. K. Nielsen, A. Camacho-Guardian, T. Pohl, G. M. Bruun, and J. J. Arlt, “Non-equilibrium quantum dynamics and formation of the Bose polaron,” *Nature Physics*, 1 (2021).
- [137] J. Catani, G. Lamporesi, D. Naik, M. Gring, M. Inguscio, F. Minardi, A. Kantian, and T. Giamarchi, “Quantum dynamics of impurities in a one-dimensional Bose gas,” *Phys. Rev. A* **85**, 023623 (2012).
- [138] T. Fukuhara, A. Kantian, M. Endres, M. Cheneau, P. Schauß, S. Hild, D. Bellem, U. Schollwöck, T. Giamarchi, C. Gross, I. Bloch, and S. Kuhr, “Quantum dynamics of a mobile spin impurity,” *Nature Physics* **9**, 235 (2013).
- [139] F. Meinert, M. Knap, E. Kirilov, K. Jag-Lauber, M. B. Zvonarev, E. Demler, and H.-C. Nägerl, “Bloch oscillations in the absence of a lattice,” *Science* **356**, 945 (2017).
- [140] D. Mayer, F. Schmidt, D. Adam, S. Haupt, J. Koch, T. Lausch, J. Nettersheim, Q. Bouton, and A. Widera, “Controlled doping of a bosonic quantum gas with single neutral atoms,” *J. Phys. B: At. Mol. Opt. Phys.* **52**, 015301 (2018).
- [141] J. Levinsen, M. M. Parish, and G. M. Bruun, “Impurity in a Bose-Einstein Condensate and the Efimov Effect,” *Phys. Rev. Lett.* **115**, 125302 (2015).
- [142] R. S. Christensen, J. Levinsen, and G. M. Bruun, “Quasiparticle Properties of a Mobile Impurity in a Bose-Einstein Condensate,” *Phys. Rev. Lett.* **115**, 160401 (2015).
- [143] J. Jäger, R. Barnett, M. Will, and M. Fleischhauer, “Strong-coupling Bose polarons in one dimension: Condensate deformation and modified Bogoliubov phonons,” *Phys. Rev. Research* **2**, 033142 (2020).

- [144] A. Bohrdt, Y. Wang, J. Koepsell, M. Kánasz-Nagy, E. Demler, and F. Grusdt, “Dominant Fifth-Order Correlations in Doped Quantum Antiferromagnets,” *Phys. Rev. Lett.* **126**, 026401 (2021).
- [145] G. E. Astrakharchik and L. P. Pitaevskii, “Motion of a heavy impurity through a Bose-Einstein condensate,” *Phys. Rev. A* **70**, 013608 (2004).
- [146] F. M. Cucchietti and E. Timmermans, “Strong-Coupling Polarons in Dilute Gas Bose-Einstein Condensates,” *Phys. Rev. Lett.* **96**, 210401 (2006).
- [147] R. M. Kalas and D. Blume, “Interaction-induced localization of an impurity in a trapped Bose-Einstein condensate,” *Phys. Rev. A* **73**, 043608 (2006).
- [148] A. Privitera and W. Hofstetter, “Polaronic slowing of fermionic impurities in lattice Bose-Fermi mixtures,” *Phys. Rev. A* **82**, 063614 (2010).
- [149] W. Casteels, J. Tempere, and J. T. Devreese, “Polaronic properties of an impurity in a Bose-Einstein condensate in reduced dimensions,” *Phys. Rev. A* **86**, 043614 (2012).
- [150] W. Casteels, J. Tempere, and J. T. Devreese, “Bipolarons and multipolarons consisting of impurity atoms in a Bose-Einstein condensate,” *Phys. Rev. A* **88**, 013613 (2013).
- [151] B. Kain and H. Y. Ling, “Generalized Hartree-Fock-Bogoliubov description of the Fröhlich polaron,” *Phys. Rev. A* **94**, 013621 (2016).
- [152] W. Li and S. Das Sarma, “Variational study of polarons in Bose-Einstein condensates,” *Phys. Rev. A* **90**, 013618 (2014).
- [153] Y. E. Shchadilova, R. Schmidt, F. Grusdt, and E. Demler, “Quantum Dynamics of Ultracold Bose Polarons,” *Phys. Rev. Lett.* **117**, 113002 (2016).
- [154] S. P. Rath and R. Schmidt, “Field-theoretical study of the Bose polaron,” *Phys. Rev. A* **88**, 053632 (2013).
- [155] X. Li, G. Bighin, E. Yakaboylu, and M. Lemesko, “Variational approaches to quantum impurities: from the Fröhlich polaron to the angulon,” *Molecular Physics* **117**, 1981 (2019).
- [156] B. Kain and H. Y. Ling, “Analytical study of static beyond-Fröhlich Bose polarons in one dimension,” *Phys. Rev. A* **98**, 033610 (2018).
- [157] M. J. Edmonds, J. L. Helm, and T. Busch, “Coherent impurity transport in an attractive binary Bose–Einstein condensate,” *New J. Phys.* **21**, 053019 (2019).
- [158] A. G. Volosniev and H.-W. Hammer, “Analytical approach to the Bose-polaron problem in one dimension,” *Phys. Rev. A* **96**, 031601 (2017).
- [159] K. Sacha and E. Timmermans, “Self-localized impurities embedded in a one-dimensional Bose-Einstein condensate and their quantum fluctuations,” *Phys. Rev. A* **73**, 063604 (2006).
- [160] A. S. Dehkarghani, A. G. Volosniev, and N. T. Zinner, “Quantum impurity in a one-dimensional trapped Bose gas,” *Phys. Rev. A* **92**, 031601 (2015).

-
- [161] D. C. Khandekar, K. V. Bhagwat, and S. V. Lawande, “Polaron effective mass,” *Phys. Rev. B* **37**, 3085 (1988).
- [162] L. A. P. Ardila and S. Giorgini, “Impurity in a Bose-Einstein condensate: Study of the attractive and repulsive branch using quantum Monte Carlo methods,” *Phys. Rev. A* **92**, 033612 (2015).
- [163] M. Cetina, M. Jag, R. S. Lous, I. Fritsche, J. T. M. Walraven, R. Grimm, J. Levinsen, M. M. Parish, R. Schmidt, M. Knap, and E. Demler, “Ultrafast many-body interferometry of impurities coupled to a Fermi sea,” *Science* **354**, 96 (2016).
- [164] H. Tajima and S. Uchino, “Thermal crossover, transition, and coexistence in Fermi polaronic spectroscopies,” *Phys. Rev. A* **99**, 063606 (2019).
- [165] A. Dehkharghani, A. Volosniev, and N. Zinner, “Coalescence of Two Impurities in a Trapped One-dimensional Bose Gas,” *Phys. Rev. Lett.* **121**, 080405 (2018).
- [166] J. Chen, J. Schurer, and P. Schmelcher, “Entanglement Induced Interactions in Binary Mixtures,” *Phys. Rev. Lett.* **121**, 043401 (2018).
- [167] P. Naidon, “Two Impurities in a Bose–Einstein Condensate: From Yukawa to Efimov Attracted Polarons,” *J. Phys. Soc. Jpn.* **87**, 043002 (2018).
- [168] F. Lingua, L. Lepori, F. Minardi, V. Penna, and L. Salasnich, “Collision of impurities with Bose–Einstein condensates,” *New J. Phys.* **20**, 045001 (2018).
- [169] S. I. Mistakidis, F. Grusdt, G. M. Koutentakis, and P. Schmelcher, “Dissipative correlated dynamics of a moving impurity immersed in a Bose–Einstein condensate,” *New J. Phys.* **21**, 103026 (2019).
- [170] K. Mukherjee, S. I. Mistakidis, S. Majumder, and P. Schmelcher, “Pulse- and continuously driven many-body quantum dynamics of bosonic impurities in a Bose-Einstein condensate,” *Phys. Rev. A* **101**, 023615 (2020).
- [171] M. Knap, C. J. Mathy, M. Ganahl, M. B. Zvonarev, and E. Demler, “Quantum Flutter: Signatures and Robustness,” *Phys. Rev. Lett.* **112**, 015302 (2014).
- [172] C. J. M. Mathy, M. B. Zvonarev, and E. Demler, “Quantum flutter of supersonic particles in one-dimensional quantum liquids,” *Nature Physics* **8**, 881 (2012).
- [173] O. Gamayun, O. Lychkovskiy, E. Burovski, M. Malcomson, V. V. Cheianov, and M. B. Zvonarev, “Impact of the Injection Protocol on an Impurity’s Stationary State,” *Phys. Rev. Lett.* **120**, 220605 (2018).
- [174] T. H. Johnson, S. R. Clark, M. Bruderer, and D. Jaksch, “Impurity transport through a strongly interacting bosonic quantum gas,” *Phys. Rev. A* **84**, 023617 (2011).
- [175] Z. Cai, L. Wang, X. C. Xie, and Y. Wang, “Interaction-induced anomalous transport behavior in one-dimensional optical lattices,” *Phys. Rev. A* **81**, 043602 (2010).
- [176] S. Palzer, C. Zipkes, C. Sias, and M. Köhl, “Quantum Transport through a Tonks-Girardeau Gas,” *Phys. Rev. Lett.* **103**, 150601 (2009).
- [177] M. Bruderer, A. Klein, S. R. Clark, and D. Jaksch, “Polaron physics in optical lattices,” *Phys. Rev. A* **76**, 011605 (2007).

- [178] M. Bruderer, W. Bao, and D. Jaksch, “Self-trapping of impurities in Bose-Einstein condensates: Strong attractive and repulsive coupling,” *EPL* **82**, 30004 (2008).
- [179] P. Siegl, S. I. Mistakidis, and P. Schmelcher, “Many-body expansion dynamics of a Bose-Fermi mixture confined in an optical lattice,” *Phys. Rev. A* **97**, 053626 (2018).
- [180] F. Grusdt, A. Shashi, D. Abanin, and E. Demler, “Bloch oscillations of bosonic lattice polarons,” *Phys. Rev. A* **90**, 063610 (2014).
- [181] N. A. Kamar, A. Kantian, and T. Giamarchi, “Dynamics of a mobile impurity in a two-leg bosonic ladder,” *Phys. Rev. A* **100**, 023614 (2019).
- [182] A. Klein, M. Bruderer, S. R. Clark, and D. Jaksch, “Dynamics, dephasing and clustering of impurity atoms in Bose-Einstein condensates,” *New J. Phys.* **9**, 411 (2007).
- [183] D. Boyanovsky, D. Jasnow, X.-L. Wu, and R. C. Coalson, “Dynamics of relaxation and dressing of a quenched Bose polaron,” *Phys. Rev. A* **100**, 043617 (2019).
- [184] S. Mistakidis, G. Katsimiga, G. Koutentakis, T. Busch, and P. Schmelcher, “Quench Dynamics and Orthogonality Catastrophe of Bose Polarons,” *Phys. Rev. Lett.* **122**, 183001 (2019).
- [185] S. I. Mistakidis, G. C. Katsimiga, G. M. Koutentakis, T. Busch, and P. Schmelcher, “Pump-probe spectroscopy of Bose polarons: Dynamical formation and coherence,” *Phys. Rev. Research* **2**, 033380 (2020).
- [186] T. Lausch, A. Widera, and M. Fleischhauer, “Role of thermal two-phonon scattering for impurity dynamics in a low-dimensional Bose-Einstein condensate,” *Phys. Rev. A* **97**, 033620 (2018).
- [187] E. Compagno, G. De Chiara, D. G. Angelakis, and G. M. Palma, “Tunable Polarons in Bose-Einstein Condensates,” *Scientific Reports* **7**, 2355 (2017).
- [188] C. Charalambous, M. A. García-March, G. Muñoz-Gil, P. R. Grzybowski, and M. Lewenstein, “Control of anomalous diffusion of a Bose polaron,” *Quantum* **4**, 232 (2020).
- [189] A. Boudjemâa, N. Guebli, M. Sekmane, and S. Khelifa-Karfa, “Breathing modes of repulsive polarons in Bose-Bose mixtures,” *J. Phys.: Condens. Matter* **32**, 415401 (2020).
- [190] C. L. Kane, P. A. Lee, and N. Read, “Motion of a single hole in a quantum antiferromagnet,” *Phys. Rev. B* **39**, 6880 (1989).
- [191] J. Koepsell, J. Vijayan, P. Sompet, F. Grusdt, T. A. Hilker, E. Demler, G. Salomon, I. Bloch, and C. Gross, “Imaging magnetic polarons in the doped Fermi-Hubbard model,” *Nature* **572**, 358 (2019).
- [192] L. J. LeBlanc and J. H. Thywissen, “Species-specific optical lattices,” *Phys. Rev. A* **75**, 053612 (2007).
- [193] A. Rubio-Abadal, J.-y. Choi, J. Zeiher, S. Hollerith, J. Rui, I. Bloch, and C. Gross, “Many-Body Delocalization in the Presence of a Quantum Bath,” *Phys. Rev. X* **9**, 041014 (2019).
- [194] A. Griessner, A. J. Daley, S. R. Clark, D. Jaksch, and P. Zoller, “Dark-State Cooling of Atoms by Superfluid Immersion,” *Phys. Rev. Lett.* **97**, 220403 (2006).

-
- [195] A. J. Daley, P. O. Fedichev, and P. Zoller, “Single-atom cooling by superfluid immersion: A nondestructive method for qubits,” *Phys. Rev. A* **69**, 022306 (2004).
- [196] R. G. Lena and A. J. Daley, “Dissipative dynamics and cooling rates of trapped impurity atoms immersed in a reservoir gas,” *Phys. Rev. A* **101**, 033612 (2020).
- [197] F. Verstraete, M. M. Wolf, and J. Ignacio Cirac, “Quantum computation and quantum-state engineering driven by dissipation,” *Nature Physics* **5**, 633 (2009).
- [198] F. Pastawski, L. Clemente, and J. I. Cirac, “Quantum memories based on engineered dissipation,” *Phys. Rev. A* **83**, 012304 (2011).
- [199] S. Diehl, A. Micheli, A. Kantian, B. Kraus, H. P. Büchler, and P. Zoller, “Quantum states and phases in driven open quantum systems with cold atoms,” *Nature Physics* **4**, 878 (2008).
- [200] M. Bruderer, A. Klein, S. R. Clark, and D. Jaksch, “Transport of strong-coupling polarons in optical lattices,” *New J. Phys.* **10**, 033015 (2008).
- [201] T. Yin, D. Cocks, and W. Hofstetter, “Polaronic effects in one- and two-band quantum systems,” *Phys. Rev. A* **92**, 063635 (2015).
- [202] A. Lampo, S. H. Lim, M. A. García-March, and M. Lewenstein, “Bose polaron as an instance of quantum Brownian motion,” *Quantum* **1**, 30 (2017).
- [203] O. Lychkovskiy, “Perpetual motion of a mobile impurity in a one-dimensional quantum gas,” *Phys. Rev. A* **89**, 033619 (2014).
- [204] J. Akram and A. Pelster, “Numerical study of localized impurity in a Bose-Einstein condensate,” *Phys. Rev. A* **93**, 033610 (2016).
- [205] S. I. Mistakidis, L. Hilbig, and P. Schmelcher, “Correlated quantum dynamics of two quenched fermionic impurities immersed in a Bose-Einstein condensate,” *Phys. Rev. A* **100**, 023620 (2019).
- [206] A.-M. Visuri, T. Giamarchi, and P. Törmä, “Excitations and impurity dynamics in a fermionic Mott insulator with nearest-neighbor interactions,” *Phys. Rev. B* **93**, 125110 (2016).
- [207] F. Massel, A. Kantian, A. J. Daley, T. Giamarchi, and P. Törmä, “Dynamics of an impurity in a one-dimensional lattice,” *New J. Phys.* **15**, 045018 (2013).
- [208] C. W. Duncan, F. F. Bellotti, P. Öhberg, N. T. Zinner, and M. Valiente, “Mobile spin impurity in an optical lattice,” *New J. Phys.* **19**, 075001 (2017).
- [209] S. Sarkar, S. McEndoo, D. Schneble, and A. J. Daley, “Interspecies entanglement with impurity atoms in a lattice gas,” *New J. Phys.* **22**, 083017 (2020).
- [210] F. Schmidt, D. Mayer, Q. Bouton, D. Adam, T. Lausch, N. Spethmann, and A. Widera, “Quantum Spin Dynamics of Individual Neutral Impurities Coupled to a Bose-Einstein Condensate,” *Phys. Rev. Lett.* **121**, 130403 (2018).
- [211] F. Schmidt, D. Mayer, Q. Bouton, D. Adam, T. Lausch, J. Nettersheim, E. Tiemann, and A. Widera, “Tailored Single-Atom Collisions at Ultralow Energies,” *Phys. Rev. Lett.* **122**, 013401 (2019).

- [212] M. Fox, *Quantum Optics: An Introduction*, Oxford Master Series in Physics (Oxford University Press, Oxford, New York, 2006).
- [213] R. Grimm, M. Weidemüller, and Y. B. Ovchinnikov, “Optical Dipole Traps for Neutral Atoms,” in *Advances In Atomic, Molecular, and Optical Physics*, Vol. 42, edited by B. Bederson and H. Walther (Academic Press, 2000) pp. 95–170.
- [214] M. Olshanii, “Atomic Scattering in the Presence of an External Confinement and a Gas of Impenetrable Bosons,” *Phys. Rev. Lett.* **81**, 938 (1998).
- [215] G. H. Wannier, “Dynamics of Band Electrons in Electric and Magnetic Fields,” *Rev. Mod. Phys.* **34**, 645 (1962).
- [216] G. H. Wannier, “The Structure of Electronic Excitation Levels in Insulating Crystals,” *Phys. Rev.* **52**, 191 (1937).
- [217] S. Kivelson and J. R. Schrieffer, “Fractional charge, a sharp quantum observable,” *Phys. Rev. B* **25**, 6447 (1982).
- [218] S. Kivelson, “Wannier functions in one-dimensional disordered systems: Application to fractionally charged solitons,” *Phys. Rev. B* **26**, 4269 (1982).
- [219] W. Kohn, “Analytic Properties of Bloch Waves and Wannier Functions,” *Phys. Rev.* **115**, 809 (1959).
- [220] S. R. White, “Density matrix formulation for quantum renormalization groups,” *Phys. Rev. Lett.* **69**, 2863 (1992).
- [221] S. R. White, “Density-matrix algorithms for quantum renormalization groups,” *Phys. Rev. B* **48**, 10345 (1993).
- [222] U. Schollwöck, “The density-matrix renormalization group,” *Rev. Mod. Phys.* **77**, 259 (2005).
- [223] U. Schollwöck, “The density-matrix renormalization group in the age of matrix product states,” *Annals of Physics January 2011 Special Issue*, **326**, 96 (2011).
- [224] G. E. Astrakharchik and S. Giorgini, “Quantum Monte Carlo study of the three- to one-dimensional crossover for a trapped Bose gas,” *Phys. Rev. A* **66**, 053614 (2002).
- [225] E. P. Gross, “Hydrodynamics of a Superfluid Condensate,” *Journal of Mathematical Physics* **4**, 195 (1963).
- [226] E. P. Gross, “Structure of a quantized vortex in boson systems,” *Nuovo Cim* **20**, 454 (1961).
- [227] M. Girardeau and R. Arnowitt, “Theory of Many-Boson Systems: Pair Theory,” *Phys. Rev.* **113**, 755 (1959).
- [228] C. W. Gardiner, “Particle-number-conserving Bogoliubov method which demonstrates the validity of the time-dependent Gross-Pitaevskii equation for a highly condensed Bose gas,” *Phys. Rev. A* **56**, 1414 (1997).
- [229] M. D. Girardeau, “Comment on “Particle-number-conserving Bogoliubov method which demonstrates the validity of the time-dependent Gross-Pitaevskii equation for a highly condensed Bose gas”,” *Phys. Rev. A* **58**, 775 (1998).

-
- [230] Y. Castin and R. Dum, “Low-temperature Bose-Einstein condensates in time-dependent traps: Beyond the $U(1)$ symmetry-breaking approach,” *Phys. Rev. A* **57**, 3008 (1998).
- [231] J. Dziarmaga and K. Sacha, “Bogoliubov theory of a Bose-Einstein condensate in the particle representation,” *Phys. Rev. A* **67**, 033608 (2003).
- [232] J. Dziarmaga and K. Sacha, “Depletion of the dark soliton: The anomalous mode of the Bogoliubov theory,” *Phys. Rev. A* **66**, 043620 (2002).
- [233] J. Dziarmaga, Z. P. Karkuszewski, and K. Sacha, “Images of the dark soliton in a depleted condensate,” *J. Phys. B: At. Mol. Opt. Phys.* **36**, 1217 (2003).
- [234] J. Dziarmaga and K. Sacha, “Images of a Bose-Einstein condensate: diagonal dynamical Bogoliubov vacuum,” *J. Phys. B: At. Mol. Opt. Phys.* **39**, 57 (2005).
- [235] C. K. Law, P. T. Leung, and M.-C. Chu, “Quantum fluctuations of coupled dark solitons in a trapped Bose-Einstein condensate,” *J. Phys. B: At. Mol. Opt. Phys.* **35**, 3583 (2002).
- [236] C. K. Law, “Dynamic quantum depletion in phase-imprinted generation of dark solitons,” *Phys. Rev. A* **68**, 015602 (2003).
- [237] D. J. Frantzeskakis, “Dark solitons in atomic Bose-Einstein condensates: from theory to experiments,” *J. Phys. A: Math. Theor.* **43**, 213001 (2010).
- [238] A. Weller, J. P. Ronzheimer, C. Gross, J. Esteve, M. K. Oberthaler, D. J. Frantzeskakis, G. Theocharis, and P. G. Kevrekidis, “Experimental Observation of Oscillating and Interacting Matter Wave Dark Solitons,” *Phys. Rev. Lett.* **101**, 130401 (2008).
- [239] G. Theocharis, A. Weller, J. P. Ronzheimer, C. Gross, M. K. Oberthaler, P. G. Kevrekidis, and D. J. Frantzeskakis, “Multiple atomic dark solitons in cigar-shaped Bose-Einstein condensates,” *Phys. Rev. A* **81**, 063604 (2010).
- [240] H. Sakaguchi and B. A. Malomed, “Matter-wave solitons in nonlinear optical lattices,” *Phys. Rev. E* **72**, 046610 (2005).
- [241] O. V. Borovkova, Y. V. Kartashov, L. Torner, and B. A. Malomed, “Bright solitons from defocusing nonlinearities,” *Phys. Rev. E* **84**, 035602 (2011).
- [242] T. Busch and J. R. Anglin, “Dark-Bright Solitons in Inhomogeneous Bose-Einstein Condensates,” *Phys. Rev. Lett.* **87**, 010401 (2001).
- [243] C. Hamner, J. J. Chang, P. Engels, and M. A. Hoefer, “Generation of Dark-Bright Soliton Trains in Superfluid-Superfluid Counterflow,” *Phys. Rev. Lett.* **106**, 065302 (2011).
- [244] D. Yan, J. J. Chang, C. Hamner, P. G. Kevrekidis, P. Engels, V. Achilleos, D. J. Frantzeskakis, R. Carretero-González, and P. Schmelcher, “Multiple dark-bright solitons in atomic Bose-Einstein condensates,” *Phys. Rev. A* **84**, 053630 (2011).
- [245] A. Álvarez, J. Cuevas, F. R. Romero, C. Hamner, J. J. Chang, P. Engels, P. G. Kevrekidis, and D. J. Frantzeskakis, “Scattering of atomic dark-bright solitons from narrow impurities,” *J. Phys. B: At. Mol. Opt. Phys.* **46**, 065302 (2013).
- [246] M. R. Matthews, B. P. Anderson, P. C. Haljan, D. S. Hall, C. E. Wieman, and E. A. Cornell, “Vortices in a Bose-Einstein Condensate,” *Phys. Rev. Lett.* **83**, 2498 (1999).

- [247] K. W. Madison, F. Chevy, W. Wohlleben, and J. Dalibard, “Vortex Formation in a Stirred Bose-Einstein Condensate,” *Phys. Rev. Lett.* **84**, 806 (2000).
- [248] J. R. Abo-Shaeer, C. Raman, J. M. Vogels, and W. Ketterle, “Observation of Vortex Lattices in Bose-Einstein Condensates,” *Science* **292**, 476 (2001).
- [249] T. W. Neely, E. C. Samson, A. S. Bradley, M. J. Davis, and B. P. Anderson, “Observation of Vortex Dipoles in an Oblate Bose-Einstein Condensate,” *Phys. Rev. Lett.* **104**, 160401 (2010).
- [250] S. Donadello, S. Serafini, M. Tylutki, L. P. Pitaevskii, F. Dalfovo, G. Lamporesi, and G. Ferrari, “Observation of Solitonic Vortices in Bose-Einstein Condensates,” *Phys. Rev. Lett.* **113**, 065302 (2014).
- [251] E. C. Samson, K. E. Wilson, Z. L. Newman, and B. P. Anderson, “Deterministic creation, pinning, and manipulation of quantized vortices in a Bose-Einstein condensate,” *Phys. Rev. A* **93**, 023603 (2016).
- [252] L. S. Cederbaum and A. I. Streltsov, “Best mean-field for condensates,” *Physics Letters A* **318**, 564 (2003).
- [253] O. E. Alon, A. I. Streltsov, and L. S. Cederbaum, “Multiorbital mean-field approach for bosons, spinor bosons, and Bose-Bose and Bose-Fermi mixtures in real-space optical lattices,” *Phys. Rev. A* **76**, 013611 (2007).
- [254] O. E. Alon, A. I. Streltsov, and L. S. Cederbaum, “Time-dependent multi-orbital mean-field for fragmented Bose-Einstein condensates,” *Physics Letters A* **362**, 453 (2007).
- [255] R. Horodecki, P. Horodecki, M. Horodecki, and K. Horodecki, “Quantum entanglement,” *Rev. Mod. Phys.* **81**, 865 (2009).
- [256] M. Horodecki, P. Horodecki, and R. Horodecki, “Separability of n-particle mixed states: necessary and sufficient conditions in terms of linear maps,” *Physics Letters A* **283**, 1 (2001).
- [257] M. Roncaglia, A. Montorsi, and M. Genovese, “Bipartite entanglement of quantum states in a pair basis,” *Phys. Rev. A* **90**, 062303 (2014).
- [258] O. Penrose and L. Onsager, “Bose-Einstein Condensation and Liquid Helium,” *Phys. Rev.* **104**, 576 (1956).
- [259] E. J. Mueller, T.-L. Ho, M. Ueda, and G. Baym, “Fragmentation of Bose-Einstein condensates,” *Phys. Rev. A* **74**, 033612 (2006).
- [260] P.-O. Löwdin, “Quantum Theory of Many-Particle Systems. I. Physical Interpretations by Means of Density Matrices, Natural Spin-Orbitals, and Convergence Problems in the Method of Configurational Interaction,” *Phys. Rev.* **97**, 1474 (1955).
- [261] M. A. García-March, B. Juliá-Díaz, G. E. Astrakharchik, J. Boronat, and A. Polls, “Distinguishability, degeneracy, and correlations in three harmonically trapped bosons in one dimension,” *Phys. Rev. A* **90**, 063605 (2014).
- [262] L. Cao, S. Krönke, O. Vendrell, and P. Schmelcher, “The multi-layer multi-configuration time-dependent Hartree method for bosons: Theory, implementation, and applications,” *J. Chem. Phys.* **139**, 134103 (2013).

-
- [263] S. Krönke, L. Cao, O. Vendrell, and P. Schmelcher, “Non-equilibrium quantum dynamics of ultra-cold atomic mixtures: the multi-layer multi-configuration time-dependent Hartree method for bosons,” *New J. Phys.* **15**, 063018 (2013).
- [264] L. Cao, V. Bolsinger, S. I. Mistakidis, G. M. Koutentakis, S. Krönke, J. M. Schurer, and P. Schmelcher, “A unified ab initio approach to the correlated quantum dynamics of ultracold fermionic and bosonic mixtures,” *J. Chem. Phys.* **147**, 044106 (2017).
- [265] H. D. Meyer, U. Manthe, and L. S. Cederbaum, “The multi-configurational time-dependent Hartree approach,” *Chemical Physics Letters* **165**, 73 (1990).
- [266] M. H. Beck, A. Jäckle, G. A. Worth, and H. D. Meyer, “The multiconfiguration time-dependent Hartree (MCTDH) method: a highly efficient algorithm for propagating wavepackets,” *Physics Reports* **324**, 1 (2000).
- [267] U. Manthe, “The multi-configurational time-dependent Hartree approach revisited,” *J. Chem. Phys.* **142**, 244109 (2015).
- [268] C. Bardos, I. Catto, N. Mauser, and S. Trabelsi, “Setting and Analysis of the Multi-configuration Time-dependent Hartree–Fock Equations,” *Arch Rational Mech Anal* **198**, 273 (2010).
- [269] D. J. Haxton, K. V. Lawler, and C. W. McCurdy, “Multiconfiguration time-dependent Hartree-Fock treatment of electronic and nuclear dynamics in diatomic molecules,” *Phys. Rev. A* **83**, 063416 (2011).
- [270] E. Fasshauer and A. U. J. Lode, “Multiconfigurational time-dependent Hartree method for fermions: Implementation, exactness, and few-fermion tunneling to open space,” *Phys. Rev. A* **93**, 033635 (2016).
- [271] A. U. Lode, C. Lévêque, L. B. Madsen, A. I. Streltsov, and O. E. Alon, “Colloquium: Multiconfigurational time-dependent Hartree approaches for indistinguishable particles,” *Rev. Mod. Phys.* **92**, 011001 (2020).
- [272] R. Lin, P. Mognini, L. Papariello, M. C. Tsatsos, C. Lévêque, S. E. Weiner, E. Fasshauer, R. Chitra, and A. U. J. Lode, “MCTDH-X: The multiconfigurational time-dependent Hartree method for indistinguishable particles software,” *Quantum Sci. Technol.* **5**, 024004 (2020).
- [273] O. E. Alon, A. I. Streltsov, and L. S. Cederbaum, “Multiconfigurational time-dependent Hartree method for bosons: Many-body dynamics of bosonic systems,” *Phys. Rev. A* **77**, 033613 (2008).
- [274] O. E. Alon, A. I. Streltsov, and L. S. Cederbaum, “Unified view on multiconfigurational time propagation for systems consisting of identical particles,” *J. Chem. Phys.* **127**, 154103 (2007).
- [275] O. E. Alon, A. I. Streltsov, and L. S. Cederbaum, “Unified view on linear response of interacting identical and distinguishable particles from multiconfigurational time-dependent Hartree methods,” *J. Chem. Phys.* **140**, 034108 (2014).
- [276] O. E. Alon, “Many-body excitation spectra of trapped bosons with general interaction by linear response,” *J. Phys.: Conf. Ser.* **594**, 012039 (2015).

- [277] O. E. Alon, A. I. Streltsov, and L. S. Cederbaum, “Demixing of Bosonic Mixtures in Optical Lattices from Macroscopic to Microscopic Scales,” *Phys. Rev. Lett.* **97**, 230403 (2006).
- [278] A. I. Streltsov, K. Sakmann, O. E. Alon, and L. S. Cederbaum, “Accurate multi-boson long-time dynamics in triple-well periodic traps,” *Phys. Rev. A* **83**, 043604 (2011).
- [279] A. I. Streltsov, O. E. Alon, and L. S. Cederbaum, “Formation and Dynamics of Many-Boson Fragmented States in One-Dimensional Attractive Ultracold Gases,” *Phys. Rev. Lett.* **100**, 130401 (2008).
- [280] A. I. Streltsov, O. E. Alon, and L. S. Cederbaum, “General variational many-body theory with complete self-consistency for trapped bosonic systems,” *Phys. Rev. A* **73**, 063626 (2006).
- [281] A. I. Streltsov, O. E. Alon, and L. S. Cederbaum, “General mapping for bosonic and fermionic operators in Fock space,” *Phys. Rev. A* **81**, 022124 (2010).
- [282] A. I. Streltsov, O. E. Alon, and L. S. Cederbaum, “Role of Excited States in the Splitting of a Trapped Interacting Bose-Einstein Condensate by a Time-Dependent Barrier,” *Phys. Rev. Lett.* **99**, 030402 (2007).
- [283] A. I. Streltsov, O. E. Alon, and L. S. Cederbaum, “Swift Loss of Coherence of Soliton Trains in Attractive Bose-Einstein Condensates,” *Phys. Rev. Lett.* **106**, 240401 (2011).
- [284] K. Sakmann, A. I. Streltsov, O. E. Alon, and L. S. Cederbaum, “Exact Quantum Dynamics of a Bosonic Josephson Junction,” *Phys. Rev. Lett.* **103**, 220601 (2009).
- [285] K. Sakmann, *Many-Body Schrödinger Dynamics of Bose-Einstein Condensates*, Springer Theses (Springer-Verlag, Berlin Heidelberg, 2011).
- [286] K. Sakmann, A. I. Streltsov, O. E. Alon, and L. S. Cederbaum, “Universality of fragmentation in the Schrödinger dynamics of bosonic Josephson junctions,” *Phys. Rev. A* **89**, 023602 (2014).
- [287] B. Chatterjee and A. U. J. Lode, “Order parameter and detection for a finite ensemble of crystallized one-dimensional dipolar bosons in optical lattices,” *Phys. Rev. A* **98**, 053624 (2018).
- [288] S. Dutta, M. C. Tsatsos, S. Basu, and A. U. J. Lode, “Management of the correlations of Ultracold Bosons in triple wells,” *New J. Phys.* **21**, 053044 (2019).
- [289] A. U. Lode and C. Bruder, “Fragmented Superradiance of a Bose-Einstein Condensate in an Optical Cavity,” *Phys. Rev. Lett.* **118**, 013603 (2017).
- [290] S. Zöllner, H.-D. Meyer, and P. Schmelcher, “Correlations in ultracold trapped few-boson systems: Transition from condensation to fermionization,” *Phys. Rev. A* **74**, 063611 (2006).
- [291] S. Zöllner, H.-D. Meyer, and P. Schmelcher, “Excitations of few-boson systems in one-dimensional harmonic and double wells,” *Phys. Rev. A* **75**, 043608 (2007).
- [292] S. Zöllner, H.-D. Meyer, and P. Schmelcher, “Tunneling dynamics of a few bosons in a double well,” *Phys. Rev. A* **78**, 013621 (2008).

-
- [293] U. Manthe, “A multilayer multiconfigurational time-dependent Hartree approach for quantum dynamics on general potential energy surfaces,” *J. Chem. Phys.* **128**, 164116 (2008).
- [294] H. Wang, “Multilayer Multiconfiguration Time-Dependent Hartree Theory,” *J. Phys. Chem. A* **119**, 7951 (2015).
- [295] H. Wang and M. Thoss, “Numerically exact quantum dynamics for indistinguishable particles: The multilayer multiconfiguration time-dependent Hartree theory in second quantization representation,” *J. Chem. Phys.* **131**, 024114 (2009).
- [296] H. Wang and H.-D. Meyer, “On regularizing the ML-MCTDH equations of motion,” *J. Chem. Phys.* **149**, 044119 (2018).
- [297] H. R. Larsson and D. J. Tannor, “Dynamical pruning of the multiconfiguration time-dependent Hartree (DP-MCTDH) method: An efficient approach for multidimensional quantum dynamics,” *J. Chem. Phys.* **147**, 044103 (2017).
- [298] F. Köhler, K. Keiler, S. I. Mistakidis, H.-D. Meyer, and P. Schmelcher, “Dynamical pruning of the non-equilibrium quantum dynamics of trapped ultracold bosons,” *J. Chem. Phys.* **151**, 054108 (2019).
- [299] G. Bougas, S. I. Mistakidis, and P. Schmelcher, “Pattern formation of correlated impurities subjected to an impurity-medium interaction pulse,” *Phys. Rev. A* **103**, 023313 (2021).
- [300] S. I. Mistakidis, A. G. Volosniev, N. T. Zinner, and P. Schmelcher, “Effective approach to impurity dynamics in one-dimensional trapped Bose gases,” *Phys. Rev. A* **100**, 013619 (2019).
- [301] S. I. Mistakidis, G. M. Koutentakis, G. C. Katsimiga, T. Busch, and P. Schmelcher, “Many-body quantum dynamics and induced correlations of Bose polarons,” *New J. Phys.* **22**, 043007 (2020).
- [302] S. I. Mistakidis, G. C. Katsimiga, P. G. Kevrekidis, and P. Schmelcher, “Correlation effects in the quench-induced phase separation dynamics of a two species ultracold quantum gas,” *New J. Phys.* **20**, 043052 (2018).
- [303] S. I. Mistakidis, A. G. Volosniev, and P. Schmelcher, “Induced correlations between impurities in a one-dimensional quenched Bose gas,” *Phys. Rev. Research* **2**, 023154 (2020).
- [304] M. Pyzh, S. Krönke, C. Weitenberg, and P. Schmelcher, “Spectral properties and breathing dynamics of a few-body Bose–Bose mixture in a 1D harmonic trap,” *New J. Phys.* **20**, 015006 (2018).
- [305] S. Krönke, J. Knörzer, and P. Schmelcher, “Correlated quantum dynamics of a single atom collisionally coupled to an ultracold finite bosonic ensemble,” *New J. Phys.* **17**, 053001 (2015).
- [306] K. Mukherjee, S. I. Mistakidis, S. Majumder, and P. Schmelcher, “Induced interactions and quench dynamics of bosonic impurities immersed in a Fermi sea,” *Phys. Rev. A* **102**, 053317 (2020).
- [307] J. Erdmann, S. I. Mistakidis, and P. Schmelcher, “Correlated tunneling dynamics of an ultracold Fermi-Fermi mixture confined in a double well,” *Phys. Rev. A* **98**, 053614 (2018).

- [308] J. Erdmann, S. I. Mistakidis, and P. Schmelcher, “Phase-separation dynamics induced by an interaction quench of a correlated Fermi-Fermi mixture in a double well,” *Phys. Rev. A* **99**, 013605 (2019).
- [309] S. I. Mistakidis, G. C. Katsimiga, G. M. Koutentakis, and P. Schmelcher, “Repulsive Fermi polarons and their induced interactions in binary mixtures of ultracold atoms,” *New J. Phys.* **21**, 043032 (2019).
- [310] J. Kwasniok, S. I. Mistakidis, and P. Schmelcher, “Correlated dynamics of fermionic impurities induced by the counterflow of an ensemble of fermions,” *Phys. Rev. A* **101**, 053619 (2020).
- [311] J. C. Light, I. P. Hamilton, and J. V. Lill, “Generalized discrete variable approximation in quantum mechanics,” *J. Chem. Phys.* **82**, 1400 (1985).
- [312] U. Manthe, “Layered discrete variable representations and their application within the multiconfigurational time-dependent Hartree approach,” *J. Chem. Phys.* **130**, 054109 (2009).
- [313] U. Manthe, “A time-dependent discrete variable representation for (multiconfiguration) Hartree methods,” *J. Chem. Phys.* **105**, 6989 (1996).
- [314] P. a. M. Dirac, “Note on Exchange Phenomena in the Thomas Atom,” *Mathematical Proceedings of the Cambridge Philosophical Society* **26**, 376 (1930).
- [315] I. I. Frenkel, *Wave mechanics; advanced general theory*, (Clarendon Press, Oxford, 1934) oCLC: 857828.
- [316] A. D. McLachlan, “A variational solution of the time-dependent Schrodinger equation,” *Molecular Physics* **8**, 39 (1964).
- [317] J. Broeckhove, L. Lathouwers, E. Kesteloot, and P. Van Leuven, “On the equivalence of time-dependent variational principles,” *Chemical Physics Letters* **149**, 547 (1988).
- [318] E. H. Lieb and W. Liniger, “Exact Analysis of an Interacting Bose Gas. I. The General Solution and the Ground State,” *Phys. Rev.* **130**, 1605 (1963).
- [319] E. H. Lieb, “Exact Analysis of an Interacting Bose Gas. II. The Excitation Spectrum,” *Phys. Rev.* **130**, 1616 (1963).
- [320] F. Meinert, M. Panfil, M. Mark, K. Lauber, J.-S. Caux, and H.-C. Nägerl, “Probing the Excitations of a Lieb-Liniger Gas from Weak to Strong Coupling,” *Phys. Rev. Lett.* **115**, 085301 (2015).
- [321] S. Nakajima, “Perturbation theory in statistical mechanics,” *Advances in Physics* **4**, 363 (1955).
- [322] A. L. Gaunt, T. F. Schmidutz, I. Gotlibovych, R. P. Smith, and Z. Hadzibabic, “Bose-Einstein Condensation of Atoms in a Uniform Potential,” *Phys. Rev. Lett.* **110**, 200406 (2013).
- [323] M. A. Garcia-March and T. Busch, “Quantum gas mixtures in different correlation regimes,” *Phys. Rev. A* **87**, 063633 (2013).

-
- [324] M. Endres, M. Cheneau, T. Fukuhara, C. Weitenberg, P. Schauß, C. Gross, L. Mazza, M. C. Bañuls, L. Pollet, I. Bloch, and S. Kuhr, “Observation of Correlated Particle-Hole Pairs and String Order in Low-Dimensional Mott Insulators,” *Science* **334**, 200 (2011).
- [325] A. C. Pflanzer, S. Zöllner, and P. Schmelcher, “Material-barrier tunnelling in one-dimensional few-boson mixtures,” *J. Phys. B: At. Mol. Opt. Phys.* **42**, 231002 (2009).
- [326] A. C. Pflanzer, S. Zöllner, and P. Schmelcher, “Interspecies tunneling in one-dimensional Bose mixtures,” *Phys. Rev. A* **81**, 023612 (2010).
- [327] S. Zöllner, H.-D. Meyer, and P. Schmelcher, “Few-Boson Dynamics in Double Wells: From Single-Atom to Correlated Pair Tunneling,” *Phys. Rev. Lett.* **100**, 040401 (2008).
- [328] A. Camacho-Guardian, L. Peña Ardila, T. Pohl, and G. Bruun, “Bipolarons in a Bose-Einstein Condensate,” *Phys. Rev. Lett.* **121**, 013401 (2018).
- [329] M. Cominotti, D. Rossini, M. Rizzi, F. Hekking, and A. Minguzzi, “Optimal Persistent Currents for Interacting Bosons on a Ring with a Gauge Field,” *Phys. Rev. Lett.* **113**, 025301 (2014).
- [330] U. Gavish and Y. Castin, “Matter-Wave Localization in Disordered Cold Atom Lattices,” *Phys. Rev. Lett.* **95**, 020401 (2005).
- [331] P. Massignan and Y. Castin, “Three-dimensional strong localization of matter waves by scattering from atoms in a lattice with a confinement-induced resonance,” *Phys. Rev. A* **74**, 013616 (2006).
- [332] B. Gadway, D. Pertot, J. Reeves, M. Vogt, and D. Schneble, “Glassy Behavior in a Binary Atomic Mixture,” *Phys. Rev. Lett.* **107**, 145306 (2011).
- [333] P. Doria, T. Calarco, and S. Montangero, “Optimal Control Technique for Many-Body Quantum Dynamics,” *Phys. Rev. Lett.* **106**, 190501 (2011).
- [334] D. C. Roberts and M. Ueda, “Stability analysis for n -component Bose-Einstein condensate,” *Phys. Rev. A* **73**, 053611 (2006).
- [335] K. Jimbo and H. Saito, “Interface properties in three-component Bose-Einstein condensates,” [arXiv:2104.00313 \[cond-mat\]](https://arxiv.org/abs/2104.00313) (2021).
- [336] N. Gemelke, X. Zhang, C.-L. Hung, and C. Chin, “In situ observation of incompressible Mott-insulating domains in ultracold atomic gases,” *Nature* **460**, 995 (2009).
- [337] M. Greiner, I. Bloch, O. Mandel, T. W. Hänsch, and T. Esslinger, “Exploring Phase Coherence in a 2D Lattice of Bose-Einstein Condensates,” *Phys. Rev. Lett.* **87**, 160405 (2001).
- [338] S. Fölling, F. Gerbier, A. Widera, O. Mandel, T. Gericke, and I. Bloch, “Spatial quantum noise interferometry in expanding ultracold atom clouds,” *Nature* **434**, 481 (2005).
- [339] T. Rom, T. Best, D. van Oosten, U. Schneider, S. Fölling, B. Paredes, and I. Bloch, “Free fermion antibunching in a degenerate atomic Fermi gas released from an optical lattice,” *Nature* **444**, 733 (2006).

- [340] C.-L. Hung, X. Zhang, L.-C. Ha, S.-K. Tung, N. Gemelke, and C. Chin, “Extracting density–density correlations from in situ images of atomic quantum gases,” *New J. Phys.* **13**, 075019 (2011).
- [341] M. Cheneau, P. Barmettler, D. Poletti, M. Endres, P. Schauß, T. Fukuhara, C. Gross, I. Bloch, C. Kollath, and S. Kuhr, “Light-cone-like spreading of correlations in a quantum many-body system,” *Nature* **481**, 484 (2012).
- [342] W. S. Bakr, J. I. Gillen, A. Peng, S. Fölling, and M. Greiner, “A quantum gas microscope for detecting single atoms in a Hubbard-regime optical lattice,” *Nature* **462**, 74 (2009).
- [343] J. F. Sherson, C. Weitenberg, M. Endres, M. Cheneau, I. Bloch, and S. Kuhr, “Single-atom-resolved fluorescence imaging of an atomic Mott insulator,” *Nature* **467**, 68 (2010).
- [344] C. Weitenberg, M. Endres, J. F. Sherson, M. Cheneau, P. Schauß, T. Fukuhara, I. Bloch, and S. Kuhr, “Single-spin addressing in an atomic Mott insulator,” *Nature* **471**, 319 (2011).
- [345] D. Clément, N. Fabbri, L. Fallani, C. Fort, and M. Inguscio, “Exploring Correlated 1D Bose Gases from the Superfluid to the Mott-Insulator State by Inelastic Light Scattering,” *Phys. Rev. Lett.* **102**, 155301 (2009).
- [346] P. T. Ernst, S. Götze, J. S. Krauser, K. Pyka, D.-S. Lühmann, D. Pfannkuche, and K. Sengstock, “Probing superfluids in optical lattices by momentum-resolved Bragg spectroscopy,” *Nature Physics* **6**, 56 (2010).
- [347] S. Gupta, Z. Hadzibabic, M. W. Zwierlein, C. A. Stan, K. Dieckmann, C. H. Schunck, E. G. M. v. Kempen, B. J. Verhaar, and W. Ketterle, “Radio-Frequency Spectroscopy of Ultracold Fermions,” *Science* **300**, 1723 (2003).
- [348] M. Taglieber, A.-C. Voigt, T. Aoki, T. W. Hänsch, and K. Dieckmann, “Quantum Degenerate Two-Species Fermi-Fermi Mixture Coexisting with a Bose-Einstein Condensate,” *Phys. Rev. Lett.* **100**, 010401 (2008).
- [349] X. W. Guan, M. T. Batchelor, C. Lee, and H.-Q. Zhou, “Magnetic Phase Transitions in One-Dimensional Strongly Attractive Three-Component Ultracold Fermions,” *Phys. Rev. Lett.* **100**, 200401 (2008).
- [350] H. Jing, Y. Jiang, W. Zhang, and P. Meystre, “Creation of three-species ^{87}Rb - ^{40}K - ^6Li molecules: interfering for the best,” *New J. Phys.* **10**, 123005 (2008).
- [351] C. K. Chung and C. K. Law, “Pairing and coherence order parameters in a three-component ultracold Fermi gas,” *Phys. Rev. A* **82**, 033620 (2010).
- [352] C.-H. Wu, I. Santiago, J. W. Park, P. Ahmadi, and M. W. Zwierlein, “Strongly interacting isotopic Bose-Fermi mixture immersed in a Fermi sea,” *Phys. Rev. A* **84**, 011601 (2011).
- [353] I. Santiago González, *LiNaK : multi-species apparatus for the study of ultracold quantum degenerate mixtures*, Thesis, Massachusetts Institute of Technology (2012).

Danksagungen

An erster Stelle möchte ich mich bei Prof. Dr. Peter Schmelcher für die Möglichkeit im Anschluss an meine Masterarbeit ebenfalls in seiner Arbeitsgruppe zu promovieren bedanken. Insbesondere die hervorragenden Arbeitsbedingungen und das angenehme Umfeld haben stark dazu beigetragen, dass ich mich wissenschaftlich in größtem Ausmaß entfalten konnte. Auch die Freiheit hinsichtlich der Gestaltung der Projekte hat mir geholfen meine Fähigkeiten weiter auszubauen. Zudem haben mir die zahlreichen außerwissenschaftlichen Aufgaben, bei denen Prof. Dr. Schmelcher mir mit Rat zur Seite stand, ermöglicht einen Blick über den Tellerrand hinaus zu werfen.

Bedanken möchte ich mich auch bei Dr. Simos Mistakidis für die Zusammenarbeit an diversen Projekten. Insbesondere im Zusammenhang des Iterationsprozesses beim Schreiben der Manuskripte war immer Verlass auf ihn. Ebenso in den regelmäßigen Gesprächen habe ich viel dazu gelernt.

Ein weiterer Dank gilt Maxim Pyzh, der sich bereits im Studium mit mir durch zahlreiche Übungsaufgaben gekämpft hat. Nun auch während meiner Promotion hatte er immer ein offenes Ohr für physikalische und nicht ganz so physikalische Problemstellungen. Es war stets eine Freude mit dir das Whiteboard zu verunstalten.

Danke auch an Fabian Köhler, der eine hervorragende Stütze bei IT-Problemen war und sich die Zeit dafür genommen hat, mir so manches Brett von der Stirn zu nehmen.

Ich möchte mich auch bei der gesamten Arbeitsgruppe im Allgemeinen bedanken. Die offene Atmosphäre hat mir das Gefühl gegeben, dass ich nicht alleine an meinen Projekten arbeite, sondern in etwas Größerem eingebettet bin. Egal ob Büro 101, 103, 106, 110, 111, 112 oder 113, überall hat man einen Ansprechpartner für Probleme jeglicher Art finden können. Vor allem das (fast) tägliche Kaffeekränzchen war ein häufiger Lichtblick inmitten eines stressigen Arbeitstages. Hier konnte man Sorgen loswerden, die über Clusterabstürze und Datenverluste hinausgingen. Danke deshalb auch an Frederic, Christian F., Fabian, Friethjof, Andrea, Dan, Christian M., Alejandro und Malte für die sehr unterhaltsamen Gesprächsthemen, die die Mittagspause das eine oder andere Mal in die Länge gezogen haben.

Meiner Familie und insbesondere meinen Eltern danke ich für die Unterstützung, die sie mir in der gesamten Zeit haben zukommen lassen. Durch euch habe ich gelernt, dass es für jedes

Problem eine Lösung gibt und es deshalb keinen Grund gibt aufzugeben.

Ein großes Dankeschön auch an Etienne und Jun für die gemeinsamen Kneipenabende, die mich aus so manchem Loch geholt haben. Danke dafür, dass man mit euch jedes Auf und Ab der Promotion im Detail ausdiskutieren konnte - ihr wisst ja selber, wie es sich anfühlt. In diesem Zusammenhang möchte ich auch Raison danken, der selbst über den großen Teich hinweg immer wieder Ratschläge für mich übrig hatte.

Mein größter Dank gilt meiner Ehefrau Janina. Ich bin froh, dass du schon an meiner Seite warst, als ich mit dem Physikstudium angefangen habe. Du hast mich wieder zurück ins Jetzt geholt, wenn ich wieder einmal mental falsch abgebogen bin oder mich in einem Problem verhasst habe. Danke für dein Verständnis, deine Geduld und deine Bereitschaft sogar manchmal die physikalischen Details zu verstehen.

Eidesstattliche Versicherung

Hiermit erkläre ich an Eides statt, dass ich die vorliegende Dissertationsschrift selbst verfasst und keine anderen als die angegebenen Quellen und Hilfsmittel benutzt habe.

Hamburg, den 26. Mai 2021

A handwritten signature in black ink, appearing to read 'H. Kiefer', with a checkmark-like flourish at the end.